EXTENDING IONOTHERMAL SYNTHESIS

Farida Himeur Aidoudi

A Thesis Submitted for the Degree of PhD
at the
University of St Andrews

2012

Extending Ionothermal Synthesis

A thesis submitted in application for the title of
Doctor of Philosophy
In the Faculty of Science of the University of St. Andrews by

Farida Himeur Aidoudi

University of St Andrews

September 2011

Declaration

I, Farida Himeur Aidoudi, hereby certify that this thesis, which is approximately 42000 words in length, has been written by me, that it is the record of work carried out by me and that it has not been submitted in any previous application for a higher degree.

Date Signature of candidate

I was admitted as a research student in January 2008 and as a candidate for the degree of PhD in January 2009; the higher study for which this is a record was carried out in the University of St Andrews between 2008 and 2011.

Date Signature of candidate

I hereby certify that the candidate has fulfilled the conditions of the Resolution and Regulations appropriate for the degree of Ph.D. in the University of St Andrews and that the candidate is qualified to submit this thesis in application for that degree.

Date Signature of supervisor

In submitting this thesis to the University of St Andrews I understand that I am giving permission for it to be made available for use in accordance with the regulations of the University Library for the time being in force, subject to any copyright vested in the work not being affected thereby. I also understand that the title and the abstract will be published, and that a copy of the work may be made and supplied to any *bona fide* library or research worker, that my thesis will be electronically accessible for personal or research use unless exempt by award of an embargo as requested below, and that the library has the right to migrate my thesis into new electronic forms as required to ensure continued access to the thesis. I have obtained any third party copyright permissions that may be required in order to allow such access and migration, or have requested the appropriate embargo below.

The following is an agreed request by candidate and supervisor regarding the electronic publication of this thesis:

Embargo on both printed copy and electronic copy for the same fixed period of 1 year on the following ground: publication would preclude future publication.

Date Signature of candidate

Signature of supervisor

Publications

An ionothermally-prepared S = ½ vanadium oxyfluoride kagome lattice

Farida H. Aidoudi, David W. Aldous, Richard J. Goff, Alexandra M. Z. Slawin, J. Paul Attfield, Russell E. Morris and Philip Lightfoot, *Nature Chemistry,* (**2011**), http://dx.doi.org/10.1038/NCHEM.1129.

Ionic liquids and deep eutectic solvents as new solvents for the synthesis of vanadium fluorides and oxyfluorides.

Farida H. Aidoudi, Peter J. Byrne, Phoebe K. Allan, Simon J. Teat, Philip Lightfoot and Russell E. Morris, *Dalton Trans.,* (**2011**), 40, 4324-4331

Increasing the dimensionality of hybrid vanadium oxyfluorides using ionothermal synthesis

Farida Himeur, Phoebe K. Allan, Simon J. Teat, Richard J. Goff, Russell E. Morris and Philip Lightfoot, *Dalton Trans.,* (**2010**), 39, 6018-6020

The ionothermal synthesis of metal organic frameworks, $Ln(C_9O_6H_3)((CH_3NH)_2CO)_2$ using deep eutectic solvents

Farida Himeur, Irene Stein, David S. Wragg, Alexandra M. Z. Slawin, Philip Lightfoot and Russell E. Morris, *Solid State Sci.*, (**2010**), 12, 418-421

Acknowledgements

First of all I would like to thank Professor Russell Morris for giving me the opportunity to work in his group, and for his guidance and supervision throughout this Ph.D. I really appreciate his support and patience, without him it would have been very difficult for me to accomplish this work. I also would like to thank Professor Philip Lightfoot for his invaluable advice and help based on his expertise in crystallography and metal fluorides.

I am grateful to many other people who have contributed in some way towards this thesis. I would especially like to thank Professor Alex Slawin for the collection of most of the single crystal data. Professor Paul Attfield and Dr Richard Goff are thanked for their assistance in some of the magnetic data analysis. Thanks also go to Dr Sharon Ashbrook and Mr Daniel Dawson for solid state NMR work (experimental and simulation). Ms Phoebe Allan is also thanked for the collection of some of the single crystal data at the ALS and also for the diffraction pattern figures she provided me with. I am also grateful to all the technical staff at the University of St Andrews. The assistance and discussion offered by my colleagues in the Morris group have been very helpful; a big thank you to all the past and present REM members. Special thanks to Dr Zhouija Lin (Candy) it was a great pleasure to meet her especially in my early days at the University of St Andrews. Thanks must also be given to Dr David Aldous for reading through most chapters of this thesis. Dr Paul Wheatley, Dr Morven Duncan and Ms Phoebe Allan are also thanked for proof reading the remaining parts.

I thank EPSRC for funding this project.

Finally I would like to thank my family; my husband Mourad and my daughters Sara and Nada. A very special thought is devoted to my parents, to whom this thesis is dedicated.

Abstract

An exploration of some organic-inorganic hybrid metal fluorides and lanthanide containing metal organic frameworks (Ln-MOFs) has been carried out under ionothermal conditions. In this synthesis technique an ionic liquid (IL) or deep eutectic mixture (DES) is used as the solvent and in many cases as the provider of the organic structure directing agent.

A wide range of ILs and DESs have been investigated as the reaction solvent for the synthesis of organically templated vanadium fluorides and oxyfluorides (VOFs), and initially this has proved to be successful with the isolation of 13 phases, including eight new materials. In the VOFs synthesis the IL acts as a solvent, however the DES acts as a solvent and also as a template delivery agent, where the expected template is provided by the partial breakdown of the urea derivative component. Interestingly, it has been shown that the same structure can be accessible *via* two different ways; either by using IL with an added templating source, or simply through the use of a DES without any other additive; since the template is provided by the *in situ* breakdown of the DES.

The synthesis of VOFs with extended structures was achieved by the use of the hydrophobic IL 1-ethyl-3-methylimidazolium bis(trifluoromethylsulfonyl)imide (EMIM Tf_2N) as the solvent. $[HNC_5H_5][V_2O_2F_5]$ represents the first VOF with a 2D network that contains exclusively V^{4+}. This material may be considered as arising *via* condensation of the previously known ladder-like chains. Furthermore, using imidazole as an added template has produced another layer material that has significant similarities to the $[HNC_5H_5][V_2O_2F_5]$ structure, but with some key differences. Within

the same system three other phases were also isolated, including two novel materials displaying the known ladder-type building units. Further investigations in the ionothermal synthesis of VOF using EMIM Tf_2N resulted in a successful synthesis of $[NH_4]_2[HNC_7H_{13}][V_7O_6F_{18}]$, a novel material displaying a unique double layered topology featuring a S = ½ kagome type lattice of V^{4+} ions (d^1). Two of the V^{4+} based kagome sheets are pillared by V^{3+} ions to form a double layered structure templated by both ammonium and quinuclidinium cations. This compound exhibits a high degree of magnetic frustration, with significant antiferromagnetic interactions but no long range ordering was observed above 2 K. This material presents an interesting comparison to the famous Herbertsmithite, $ZnCu_3(OH)_6Cl_2$, and may provide an excellent candidate for realising a quantum spin liquid (QSL) ground state. Interestingly, in this system the use of EMIM Tf_2N as a solvent produces mainly V^{4+}-containing materials, despite the high reaction temperature (170 °C). This characteristic is unprecedented in VOFs synthesis, as rising the reaction temperature above 150 °C in other techniques (*i.e.* hydrothermal synthesis) would often result in further reduction of V^{4+} to V^{3+}.

Using the ionothermal technique in the synthesis of hybrid iron fluorides resulted in the isolation of three chain-type materials. Again, the IL acts as the solvent and the DES acts as the solvent and also as the template provider where the expected template is released by the partial breakdown of the urea derivative component of the DES.

The synthesis of Ln-MOF using a choline chloride/ 1,3-dimethylurea deep eutectic mixture has produced three novel isostructural materials. Usually, in ionothermally prepared materials (*i.e.* zeolites) the urea portion of the DES is unstable and breaks down *in situ* to form ammonium or alkylammonium cations. In the ionothermal

synthesis of Ln-MOF, 1,3-dimethyurea (DMU) remains intact and is occluded in the final structure. Using a choline chloride/ethylene glycol deep eutectic solvent led to the isolation of a Ln-MOF with interesting structural properties, however none of the DES components appeared in the final structure.

These results demonstrate once more the usefulness and applicability of the ionothermal synthesis method and emphasise how this synthesis technique can be further extended and applied in the preparation of important structures with unique properties and functionalities.

Table of Contents

Abbreviations

δ	Chemical shift
χ	Magnetic susceptibility
adap	*N*-(3-aminopropyl)-1,3-diaminopropane)
BMIM Br	1-butyl-3-methylimidazolium bromide
BPB	*N*-butylpyridinium bromide
BMIM Asp	1-butyl-3-methyimidazolium aspartate
CTA	1,3,5-cyclohexanetricarboxylate
DES	Deep eutectic mixture
dpe	*Trans*-1,2-bis(4-pyridyl)-ethylene
dap	1,3-diamino propane
DMU	1,3-dimethyurea
DMF	Dimethylformamide
EMIM Br	1-ethyl-3-methylimidazolium bromide
EMIM Tf2N	1-ethyl-3-methylimidazolium bis(trifluoromethylsulfonyl)imide
EMIM BF_4	1-ethyl-3-methylimidazolium tetrafluoroborate
EMIM PF_6	1-ethyl-3-methylimidazolium hexafluorophosphate
en	Ethylenediamine
FCC	Face centred cubic
H_3 TMA	Trimesic acid (benzene-1,3,5-tricarboxylic acid)
H_2 1,3-bdc	Isophtalic acid
HBet Tf_2N	Betainium bis(trifluoromethylsulfonyl)imide
IL	Ionic liquid
Ln-MOF	Lanthanide containing metal organic framework

MIL	Materials of Institut Lavoisier
MOF	Metal organic framework
NCS	Non-centrosymmetric
NMR	Nuclear magnetic resonance
pipz	Piperazine
PBU	Primary building unit
PMIM PF_6	1-methyl-3-propylimidazolium hexafluorophosphate
PXRD	Powder X-ray diffraction
RTIL	Room- temperature ionic liquid
SDA	Structure directing agent
SHG	Second harmonic generation
SIZ	St Andrews ionic liquid zeotype
SQUID	Superconducting quantum interference device
tca	Propane-1,2,3-tricarboxylic acid
THF	Tetrahydrofuran
TSIL	Task specific ionic liquid
tren	Tris(2-aminoethyl)amine
trien	Triethylenetetramine
VOF	Vanadium fluoride and oxyfluoride
XRD	X-ray diffraction

CHAPTER 1
INTRODUCTION

1-1. Overview

The work described in this thesis concerns the use of ionic liquids (ILs) and deep eutectic mixtures (DESs) as the reaction media for the synthesis of two types of organic-inorganic hybrid materials; organically-templated transition metal fluorides and lanthanide containing metal organic frameworks. In this chapter a brief summary of ILs and DESs will be given. The presentation of the properties of these solvents will make it easier to understand why they have received and still receive much interest and rank as a major research topic in fields as diverse as organic synthesis, electrochemistry, and nanotechnology. These are only a few of applications where ILs have been used and widely studied, and it is quite fair to imagine that there are many other potential applications in various domains where ILs can be explored.

Materials scientists also have benefited greatly from the exceptional features of ILs where ILs and DESs have been used as solvents for the synthesis of crystalline materials "ionothermal synthesis".[1] The second section will be devoted to highlight the advantages of ionothermal synthesis compared to the hydrothermal synthesis and outline some recent development in ionothermal synthesis.

The two remaining sections will be reserved to the two types of organic-inorganic hybrid materials that will be investigated in this work under ionothermal conditions, so

the third section will deal with organically-templated metal fluorides and oxyfluorides by briefly presenting their main structural characteristics and how they have been synthesised, along with describing some properties of fluorides. In the fourth section lanthanide organic frameworks will be presented.

1-2. Ionic liquids and deep eutectic solvents

1-2-1. Background

Ionic liquids (ILs) are molten salts consisting of ionic species having a melting point lower than 100 °C.[2,3] ILs that are liquid at or around room temperature are often called "room-temperature ionic liquids" (RTILs). Such a liquid is obtained when combining a bulky asymmetric organic cation and a small anion, which results in a poorly coordinated network.

While the discovery of ILs dates back to more than 100 years ago, it is only since the late 1990's that these solvents have received a lot of attention. The interest in ILs is reflected by the increase of the number of publications related to this topic; 2500 papers were published in 2008, compared with just 37 papers in 1999. A nice and complete history of ILs with the most memorable key dates was reported by Freemantle in his recent book.[4] Broadly speaking, historically, ILs can be classified into three generations. The first generation consists of the haloaluminate, the first pyridinium based ILs with chloroaluminate ions were developed in 1948. One of the first 1,3-dialkylimidazolium RTILs, 1-ethyl-3-methylimidazolium tetrachloroaluminate, which was obtained through the mixing of 1-ethyl-3-methylimidazolium chloride with aluminium trichloride, was reported in 1982. However, these haloaluminate ILs were found to be moisture sensitive and reactive towards various orga nic compounds, consequently limiting their range of application. A few years later this problem was solved when new air and moisture stable anions, such [PF_6^-], [BF_4^-] and

[$CF_3CO_2^-$], were discovered by Wilkes and Zaworotko,[5] this was followed by the synthesis of completely hydrophobic ILs with [$(CF_3SO_2)_2N^-$] anion by Bonhote.[6] Since then, a considerable amount of research has been carried out and a wide selection of different ILs have been synthesised. These ILs are the second generation of ILs. The third generation emerged in the early 2000s and comprises task-specific ILs and chiral ILs. Task-specific ILs have been introduced by incorporating additional functional groups into the cations[7] and/or anions.[8] Numerous ILs with either chiral cations[9] or chiral anions[10] have been also synthesised.

An ionic liquid is formed from an organic cation and an inorganic or organic anion. Commonly used cations are large and asymmetric, *e.g.* derivatives of imidazolium, pyridinium, pyrrolidinium, ammonium, phosphonium and sulfonium (Figure 1-1). Typical anions commonly used include: halides (Cl^-, Br^-, I^-), tetrachloroaluminate ($AlCl_4^-$), hexafluorophosphate (PF_6^-), tetrafluoborate (BF_4^-), bis(trifluoromethylsulfonyl)imide $(CF_3SO_2)_2N^-$.

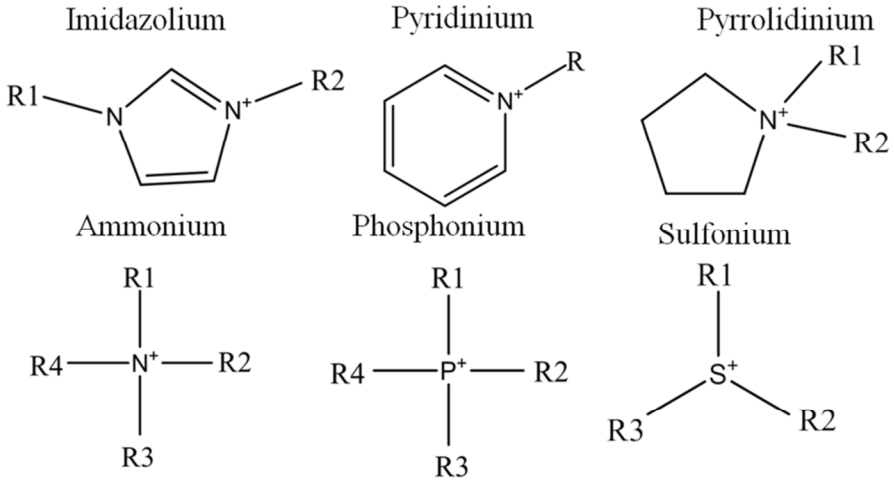

Figure 1-1. Commonly used cations in ionic liquids.

The chemical and physical properties of ionic liquids including solubility, miscibility, solvating ability, viscosity, catalytic activity and melting point can be tuned or tailored by varying the anion and/or the cation.[11,12] In theory ILs can be designed to deliver almost any set of physical and chemical properties for almost any application in the chemical sciences. Hence the term "designer solvent" is often used when describing ILs. However in practice ILs have been actually selected rather than designed for specific applications and this selection has often been based on trial and error. The tailoring or designing of ILs requires a full knowledge of patterns and trends in the characteristics of ILs, which are limited in most types of ILs.[4]

1-2-2. Conventional preparation of ionic liquids

As the number of ILs increases, different methods have been suggested for their synthesis. We will focus in this section on the common methods for preparing ILs of interest in this project, which are mainly imidazolium or pyridinium based ILs.

The general synthetic pathways for preparing ILs from an amine are illustrated in Figure 1-2.[2] The first step is usually a quaternisation reaction, where an amine is alkylated with an appropriate alkylation agent (RX) such as alkyl halide, resulting in the corresponding IL. Since alkyl halides are cheap and easily available they are widely used as alkylation agent in a quaternisation reaction in which the amine and the desired alkyl halide are mixed and the reaction mixture is heated. The reaction temperature and the reaction time depend on the reactivity of the alkyl halide. The reactivity decreases as a function of increasing alkyl chain length. The nature of the halide also influences

the reactivity of the alkyl halide. Iodine is the most reactive, followed by bromine and chlorine.

Many ILs with a desired anion such as (BF_4^-) and $(CF_3SO_2)_2N^-$ cannot be formed *via* this reaction; in these cases an anion exchange reaction is needed. A previously formed IL is used as a precursor, and the anion is changed by a metathesis reaction or with a Lewis acid (MX_y). The metathesis reaction can be performed by using a metal salt (MA), a Bronsted acid (HA) or an ion exchange resin.

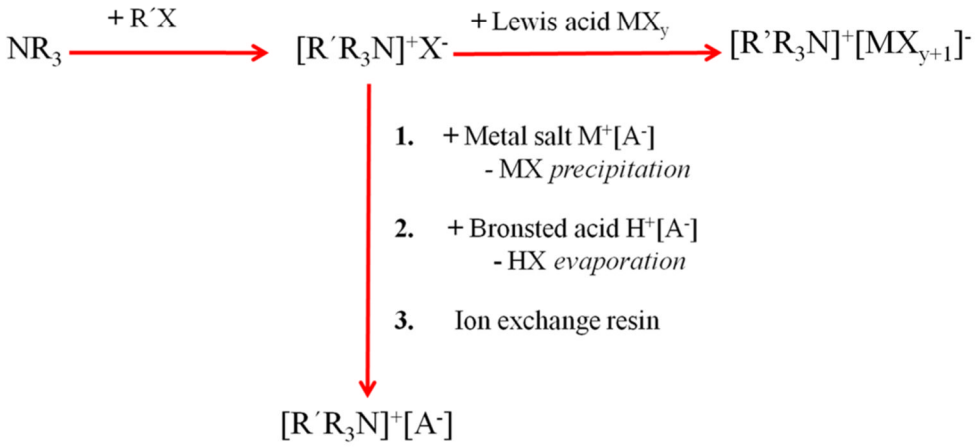

Figure 1-2. Synthetic pathways for preparing ILs from an amine.[2]

As an example, Figure 1-3 presents the widely used synthetic path for preparing the IL EMIM Tf_2N. The preparation requires two steps, the first step is the preparation of EMIM Br through alkylation of *N*-methylimidazole this step usually is carried out under inert atmosphere with reaction temperature around 30 °C for 3 hrs, after that the product is crystallised with ethyl acetate. The next step is the anion exchange with $LiTf_2N$ salt this step is carried out at room temperature for 4 hrs.

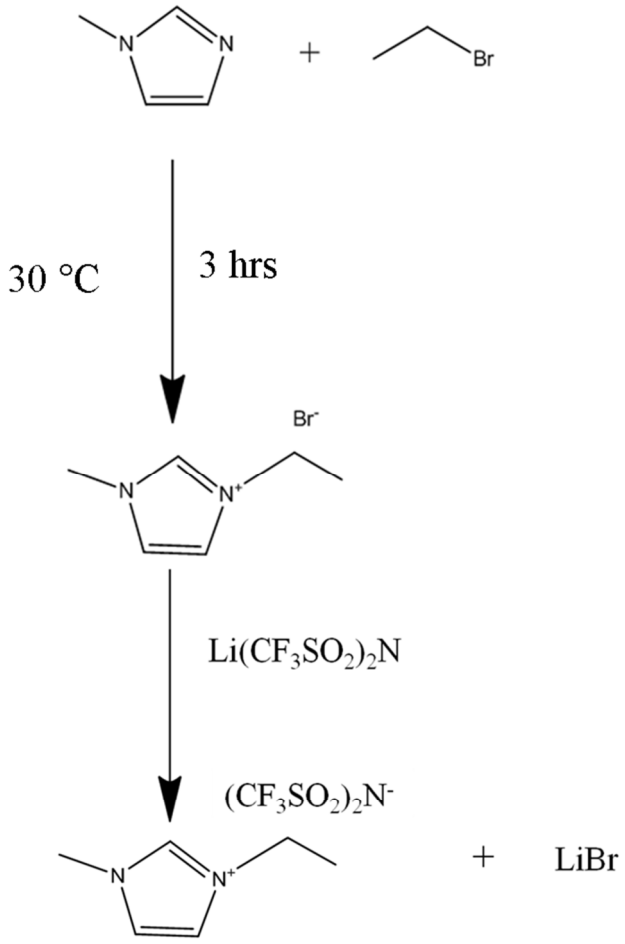

Figure 1-3. Alkylation and anion metathesis reactions used for the synthesis of EMIM Tf_2N.

While the process mentioned above is efficient for the synthesis of many high purity ILs, however for some it is difficult to prevent halide contamination, especially when the resulting IL is miscible with water as it is the case with EMIM BF_4. This could interfere with some applications; for example when the IL is used as a solvent for catalytic reactions, the presence of a halide may result in catalyst poisoning and

deactivation. For this reason many groups were involved in extensive research for the development of halide-free synthesis methods of ILs. As an example the synthesis of dialkylimidazolium alkyl sulphate ILs was achieved by the direct alkylation of alkylimidazole with either dimethyl sulphate or diethyl sulphate.[13]

While the synthesis of the above mentioned ILs is often straight forward, the synthesis of ILs belonging to the third generation is relatively more complicated and tedious, and it seems that even the simplest procedure requires a sequence of steps to obtain the desired IL. As it is the case in the preparation of ILs with chiral anions, and according to Ohno[10] who prepared a series of ILs with chiral anions derived from amino acids, these ILs can be synthesised in three steps; alkylation of the amine followed by anion exchange using an ion exchange resin and the last step is the neutralisation using the corresponding amino acid.

1-2-3. What makes ILs attractive solvents?

There is no doubt that ILs have opened up a new area of chemistry and they have contributed to the development of many areas of chemical science. This is due to their unique properties and impressive features. ILs consist exclusively of cations and anions and therefore the obvious and natural characteristic of ILs is ionic, this will alter the chemistry by providing a unique environment compared to the molecular solvents. Another important feature of ILs that has attracted academic interest is their physical and chemical properties can be dramatically altered by simply varying the anion and cation, by introducing specific functionalities into the cation and/or anion or just mixing two or more simple ILs. In addition to that many ILs display interesting properties *e.g.*:

- Many but not all ILs tend to have good thermal stability and can be liquid over a range of 300 °C. This wide liquid range is a distinct advantage over traditional solvent systems that have a much narrower liquid range.
- Low vapour pressure resulting from the strong ionic interaction; although certain ILs can be distilled at high temperature and low pressure.[14]
- ILs have wide range of solubilities and miscibilities with water and other solvents, for example some ILs are hydrophilic while others are hydrophobic.
- ILs are non-flammable, and recyclable.

1-2-4. Eutectic mixtures

By definition, a deep eutectic solvent (DES) is a type of ionic solvent with special properties composed of a mixture, which forms a eutectic with a melting point much lower than either of the individual components.[15,16] The first generation of eutectic solvents were based on mixtures of quaternary ammonium salts with hydrogen bonds donors such as amides and carboxylic acids. The deep eutectic phenomenon for a 2 to 1 molar ratio of choline chloride (2-hydroxyethyl-trimethylammonium chloride) and urea was first described by Abbot *et al*.[16] Choline chloride has a melting point of 302 °C and that of urea is 133 °C. The eutectic mixture, however, has a melting point of 12 °C. The decrease in the melting point arises from the hydrogen bonding interaction between the urea molecules and the chloride ions. The physical and chemical properties of DESs are dependent on the properties and functionality of its components, and also on the ratio of the mixture. Compared to molecular solvents, eutectic solvents have a very low vapour pressure and are non-flammable. They have the exceptional features of ionic

liquids but are a mixture of an ionic compound with a molecular compound. In addition they exhibit some more significant advantages such as relatively high polarity so they can dissolve many metal salts and metal oxides, their trivial preparation from easily available components and their relative unreactivity towards atmospheric moisture. Also they can be regarded as eco-friendly as they do not need any further purification which is an important step in the preparation of most other types of ionic liquids. This step generally requires a large amount of organic solvents; posing the question of how "green" really they are.

1-3. Ionothermal synthesis

1-3-1. Background

The ionothermal method[1] is the use of an ionic liquid or eutectic mixture as the reaction solvent and, in many cases, also as structure directing agent in the preparation of crystalline solids.

The research published by Morris *et al.*[1] in 2004 can be considered as the pioneering work in this domain. The term of "ionothermal synthesis"[1] was introduced to distinguish it from the hydrothermal or solvothermal synthesis.
ILs and DESs were first used as solvents for the synthesis of zeotype materials.[17-21] Since then much effort has been initially directed towards the use of this technique in the preparation of other porous solids such as metal coordination polymers,[22-25] after which many other solids have been investigated under ionothermal conditions.[26] Research in this field is dramatically growing and the number of publications has exponentially increased in recent years. There are also at least four reviews devoted to "ionothermal synthesis".[27-30]

The most popular ILs and DESs used to date in the ionothermal synthesis of different type of materials are imidazolium based *i.e.* EMIM Br, BMIM Br, EMIM Tf_2N, EMIM PF_6 and BMIM Asp. These ILs have shown great success for the preparation of zeotypes and MOFs. Perhaps the most interesting property of ILs is their relatively low vapour pressure,[2] as they are composed entirely of ions. Ionothermal synthesis takes advantage of this, so the synthesis takes place at nearly ambient pressure, eliminating

safety concerns associated with high hydrothermal pressures. Many reactions can take place using simple containers such as round bottomed flasks or glass vials,[29] which makes using a microwave a safe heating method; as in a system containing a pure stable IL as a solvent no autogenous pressure will develop during the heating even at high temperature. However, it has been shown that even the addition of a very small amount of water to the system can generate significant pressures.[31]

In addition to the advantages of ionothermal sythesis mentioned above, it has been shown that the structural characteristics of the materials prepared by this route can be traced back to the solvent chemistry used and many materials have been synthesised with unusual bonds that are difficult to stabilise under conventional hydrothermal conditions. This can be well illustrated in the unusual cobalt aluminophosphate material (SIZ-13),[32] this compound features Co-Cl bonds that are hydrolytically unstable.

In the ionothermal synthesis of materials, the IL or the DES, in addition to its principal role as a solvent, can play multiple roles. In most syntheses they can template the structure and balance the ionic framework through the organic cation,[24] or through the anion.[33] They also can provide the template to the reaction by the *in situ* breakdown of one part of the DES.[34] One report has shown that the chiral IL BMIM Asp can induce chirality in MOFs[23] even though the chiral anion is not occluded into the structure. In other cases the IL acts only as a solvent; it is actually the case where a hydrophobic IL,[20] or a choline chloride/carboxylic acid deep eutectic solvent[35] is involved in the synthesis.

1-3-2. Recent development in ionothermal synthesis.

The early work on ionothermal synthesis showed that ILs are excellent solvents in the synthesis of porous materials, notably zeotypes where the ILs play two-fold role; solvent and template. Many spectacular structures have been synthesised and a lot of work was devoted to delineate the relationship between the IL used and the structural features of the materials obtained. The influence of other parameters *i.e.* presence of water or HF in the reaction has been moderately studied.[31,36] The association of ionothermal synthesis and microwave heating has proved to be very efficient and often resulted in a purer phase and higher crystallinity.[24]

In very recent years, research in ionothermal synthesis has moved another step forward, as much effort now is directed towards creating materials with different functionalities and properties. In this context, Lin and co-workers introduced an organic amine (1,6-hexanediamine) to act as a co-SDA, resulting in a unique material with extra large pores and high stability. This material may have potential applications in separation, catalysis and gas storage.[37] It has also been shown that ILs can be used in the synthesis of functional materials that are difficult to achieve under other synthetic routes. One example is the ionothermal synthesis of Li-based fluorophophates electrodes, $LiFePO_4F$ and $LiTiPO_4F$[38] at 260 °C, while temperatures of 600 - 700 °C are needed to produce the same materials *via* solid state route. The synthesis of magnetic open frameworks has also proved to be successful in ILs, where a nickel phosphate $5H_3O{\cdot}[Ni_8(HPO_3)_9Cl_3]{\cdot}1.5H_2O$[39] was synthesised using PMIM PF_6. This material has not been prepared using other solvents to date.

1-4. Metal Fluorides

1-4-1. Introduction

Although purely inorganic metal fluorides have been known for a long time,[40] the chemistry of organically-templated metal fluorides and oxyfluorides has flourished only recently. This started with the introduction of fluoride as mineraliser in many microporous materials from zeolites to metal organic frameworks. The F^- ion was first introduced as a new route for the synthesis of zeolites.[41] After that the fluoride route has been extended to the synthesis of other types of organic-inorganic hybrid materials such as: aluminium phosphates and metal organic frameworks where F^- ions can play several roles; framework charge balancing and catalysing the formation of some bonds like Al-O-P in zeotypes. In these systems, F^- can be incorporated into the framework or occluded within small cages.

Later several groups have carried out an intensive investigation into various systems, leading to the synthesis of several organically-templated metal fluoro-phosphates[42] or fluoro-sulphates.[43] This was followed by an exploration of different systems that allow F^- to be the only or predominant ligand, and as a consequence the chemistry of organically-templated metal fluorides and oxyfluorides has been developed further.

The spectacular development in fluoride containing compounds led to numerous applications from their incorporation in polymers (Teflon) to their use as catalysts in organic reactions. Many properties of metal (oxy)fluorides have been documented; the optical properties represent one class of the physical properties which takes advantage of the higher ionicity of the M-F bond.[50] Metal fluorides, and in particular lanthanide-based systems, are thus often excellent materials for applications requiring luminescent behaviour.[51,52]

Interest in hybrid metal fluorides is drawn by the wide range of materials that are accessible and the astonishingly diverse structure architectures, in addition to their potential optical and magnetic properties. Moreover, the difference in the bonding nature between M-O and M-F bonds in metal oxyfluorides can have a great impact on their physical properties, and it would be expected that the physical properties of these materials can be tuned according to their structure.[40] This new interest in metal (oxy)fluorides therefore justifies acquiring better knowledge and increasing the availability of appropriate synthetic techniques and the development of new synthetic routes.

1-4-2. Concepts of building units and out of centre distortion

Metal (oxy)fluorides are built up from MX_n (M is an appropriate metal and X could be O or F) polyhedra, with n is the coordination number and can vary from 4 to 9, the most common being the six coordinated octahedron. These simple primary building units (PBUs) can be assembled by their corners, edges or faces to form more complex units that may serve as secondary building units (SBUs). These complex units can have

different shapes (*e.g.* Y shape, bow-tie); this will be illustrated in more details in the following sub-section. MX_6 polyhedra are frequently observed in transition metal (oxy) fluorides, in particular octahedra having the formula $[MO_xF_{6-x}]$ (x = 1, M = V, Nb, Ta; and x = 2, M = Mo, W) are of great interest as they exhibit the characteristic of out-of-centre distortion. An asymmetric environment around the metal centre will be created as a consequence of this distortion. For example Figure 1-4 illustrates a typical distorted octahedron found in a variety of vanadium based oxyfluorides, which can be as an isolated monomer or can be connected with others to form more extended structures.

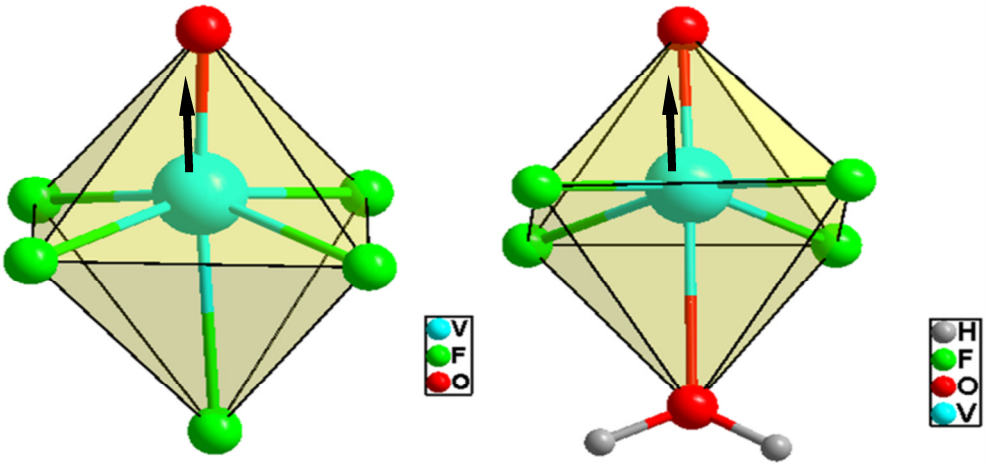

Figure 1- 4. Typical distortion found in VOF_5 octahedron (left) and $VOF_4(H_2O)$ octahedron (right).

In the VOF_5 octahedron (Figure 1-4 (left)) the distortion occurs towards the oxide ligand, this results in one short metal-oxide bond (~ 1.6 Å), one long metal-fluoride bond in *trans* position (~ 2.2 Å) and the remaining four bonds are within the normal range (~ 1.9 Å). In many cases a water molecule can take the place of the *trans* F^- ligand (Figure 1-4 (right)), with the same distortion being preserved.

Octahedra displaying out of centre distortion provide some possibility to disfavour centrosymmetric packing and therefore these types of polyhedra are key constituents of non-centrosymmetric (NCS) materials that exhibit important structure-dependent properties. However, in practice the rational design of NCS materials remains a great challenge for synthetic chemists. To impart a NCS sense in a material, one important factor is to prevent oxide/fluoride ligand disorder around the transition metal. The second is to ensure the individual NCS units combine to form a NCS structure, in order to achieve this, the relationship between the anionic group and the surrounding bond network must be well understood.

Despite several approaches having been followed for designing such materials and some success has been achieved, in particular by Poeppelmeier and co-workers,[44] this field is still far away from being well understood and it appears that different parameters influence the way a structure crystallises. In this context the two compounds $KNaNbOF_5$ and $CsNaNbOF_5$[45] can be compared as both of them contain the acentric $(NbOF_5)^{2-}$ anion. $KNaNbOF_5$ crystallises in the polar orthorhombic space group $Pna2_1$, in contrast to $CsNaNbOF_5$ that crystallises in the centrosymmetric space group *Pbcn*. In this study it was revealed that the small potassium cations play an essential role in the acentric packing of the $(NbOF_5)^{2-}$ anions.

Another interesting example can be found in two vanadium based oxyfluoride compounds, $[H_2en][VOF_4(H_2O)]$[46] and $[H_2pipz][VOF_4(H_2O)]$[47] both based on the acentric $[VOF_4(H_2O)]^{2-}$ octahedron, and both of which display isolated monomeric structures. These monomers are hydrogen bonded through the water molecules and

further connected through the protonated organic amines. However, $[H_2en][VOF_4(H_2O)]$ crystallises in the polar space group $P2_1$ and $[H_2pipz[VOF_4(H_2O)]$ crystallises in a centrosymmetric space group $P\bar{1}$. In this case it was suggested that the polar ordering in $[H_2en][VOF_4(H_2O)]$ is mediated by hydrogen bonding. (This will be discussed further in sub-section 1-4-3).

Materials including metal (oxy)fluorides that crystallise in a non centrosymmetric space groups are predisposed to exhibit useful bulk physical properties such as: optical activity, pyroelectricity, piezoelectricity, ferroelectricity and second-harmonic generation. The relationship between the crystal structures and properties is illustrated in Figure 1-5.[48] From the 21 acentric crystal classes, only compounds found in the class 432 do not posses SHG. It is interesting to note that some properties are inter-related For example, all pyroelectric materials have SHG behaviour but the opposite is not true.

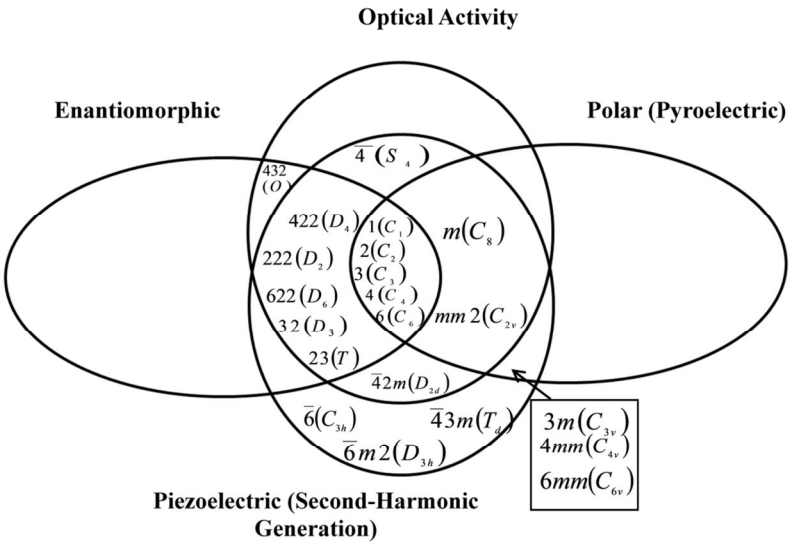

Figure 1-5. Inter-relationships of non-centrosymmetric crystal classes.[48]

1-4-3. Structural features and diversity

Since organically-templated metal (oxy)fluorides have emerged as a new class of organic-inorganic hybrid materials, various structural types of fluorides have been brought forward. It is not intended here to list all the existing structures, but I shall attempt to discuss the main structural features of various crystal structure types that have been reported, giving examples of some interesting structures related to transition metals. Structures based on other metals (*e.g.* main group metals and lanthanides) will be considered where relevant. Structures will be discussed according to their dimensionality, from 0D to 3D. There are now many books[40,49,50] and reviews[51,52] that cover most existing purely inorganic and organic-inorganic hybrid metal (oxy)fluorides. A comprehensive review by Lightfoot *et al.*,[53] was recently devoted exclusively to organically-templated metal fluorides.

1-4-3-1. Zero-dimensional structures

Where the metal-fluoride anions have limited dimensions in all directions and are quasi-isolated from each other, they can be isolated monomers, dimers, trimers, tetramers or polyanions, usually they can be hydrogen bonded to form a continuous network.

Isolated polyhedra:

Several structures have been reported displaying different type of monomers. As an example, the structure of $[H_2en][VOF_4(H_2O)]$[46] was synthesised by a solvothermal technique using a mixture of water and ethylene glycol. It crystallises in the polar space group $P2_1$ and consists of highly anisotropic, *trans*-$[VOF_4(H_2O)]^{2-}$ octahedra involving

all possible H-bond donors in both the water ligand and the ethylenediammonium cation. This material exhibits a significant SHG response which is a property of non-centrosymmetric crystals. It is suggested the polar ordering of this material is traced back to the H-bonding requirements of both the water molecules and the template. It is interesting to note that a similar material $[H_2pipz][VOF_4(H_2O)]$[47] has also been reported displaying the same highly distorted $VOF_4(H_2O)$ and the same hydrogen bonded dimeric chains, however due to different templates used in the synthesis ethylenediamine and piperazine, this has dictated different H-bonding schemes in the two materials as it is illustrated in Figure 1-6. The latter crystallises in a centrosymmetric space group $P\bar{1}$, so it is not SHG active.

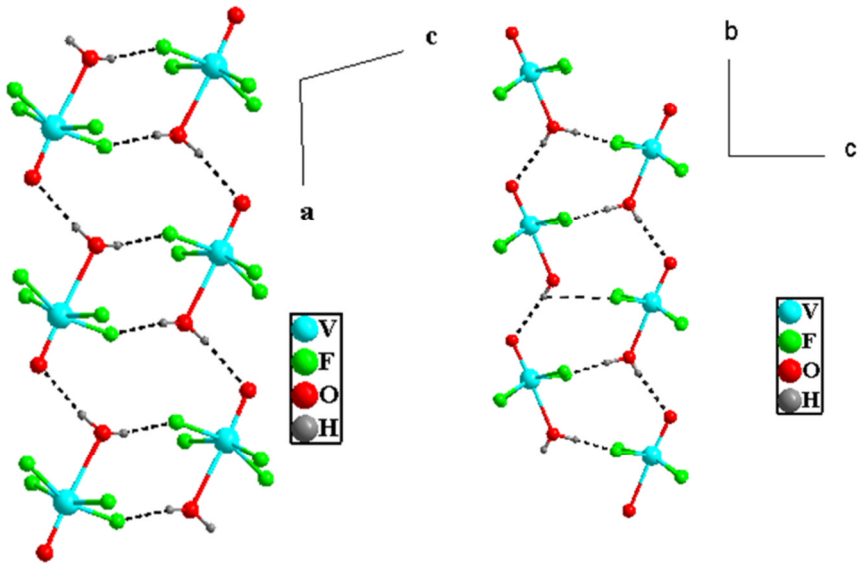

Figure 1-6. The centrosymmetric $[H_2pipz][VOF_4(H_2O)]$[47] (left) and the polar $[H_2en][VOF_4(H_2O)]$[46] (right).

Joined polyhedra (oligomers):

Several structures have been described that exhibit dimeric, trimeric, tetrameric and even larger polyanionic units.

Dimers in metal (oxy)fluorides can be corner-, edge- or face-shared as illustrated in Figure 1-7.

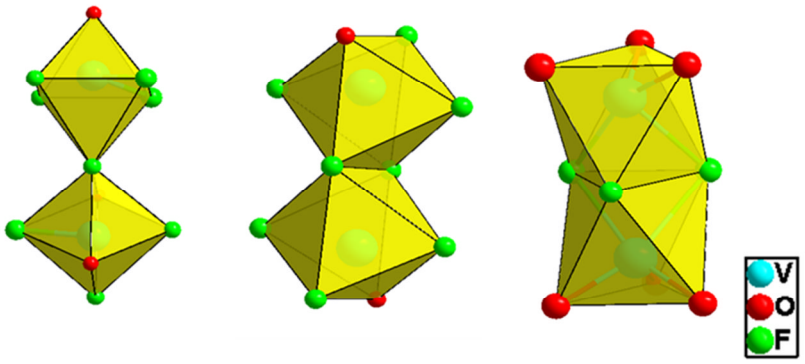

Figure 1-7. Examples of corner-, edge- and face-shared dimers types found in metal (oxy)fluorides.

One example of corner-shared dimers can be found in $Cs[C_4H_{12}N][V_2O_2F_8(H_2O)]$,[54] edge-shared dimers can be found in $[H_4trien][V_2O_2F_8]$[55] and face-shared dimers can be found in $[(NMe_4)_3][V_2O_4F_5]$.[56] There are several other examples of fully fluorinated dimers, such as those in $[NH_3OH]_6[Zr_2F_{14}]$.[57]

Trimeric units are also known in metal (oxy)fluorides, as an example the compound $K[C_4H_{12}N][V_3O_3F_{12}]$.[54] The trimeric unit of this compound is shown in Figure 1-8 and it is built of three corner shared octahedra in a triangular symmetry. The trimeric units are joined together through ionic bonds to the K^+ ions to form chains, which are further hydrogen bonded into a 3D structure through the tetramethylammonium cations.

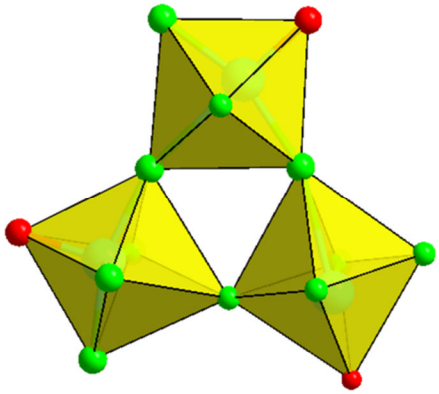

Figure 1-8. Trimeric unit found in $K[C_4H_{12}N][V_3O_3F_{12}]$.[54]

Tetrameric units are very common in metal (oxy)fluorides, they can be formed by octahedra sharing a corner or edge or simultaneously corner and edge. They can be arranged in different modes (*e.g.* square, linear or Y shape).

Square tetramer units (Figure 1-9) can be found in $[H_3tren]_2[V_4O_4F_{14}]\cdot 3H_2O$.[55] The structure is composed of octahedra sharing an edge to form an edge sharing dimer, as described earlier, these dimers are further connected by sharing a corner to form the tetramer.

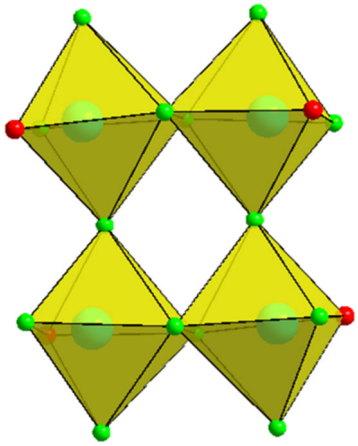

Figure 1-9. Square tetramer found in $[H_3tren]_2[V_4O_4F_{14}]\cdot 3H_2O$.[55]

Figure 1-10 illustrates two other different tetramer types, the tetramer in Figure 1-10(a) is found in $[H_2pipz]_4[V_4O_3F_{17}]\cdot 4H_2O$,[47] and is composed of corner- and edge- sharing octahedra containing V^{4+} and V^{3+} ions, these octahedra are arranged in a Y shape, by two octahedra sharing an edge and only the octahedron composed of a V^{3+} ion will further corner-share two other fluorine atoms with two separated octahedra.

The tetramer in Figure 1-10(b) is found in $[H_3adap]_2[V_4O_4F_{14}]\cdot 2H_2O$[55] and can be described as an edge sharing dimer, with each octahedron of this dimer sharing a further two fluorine atoms with two other different octahedra *via* their corners, in a way that the octahedra forming the central dimer have only one terminal F atom, however the two other surrounding octahedra have three terminal fluorine atoms.

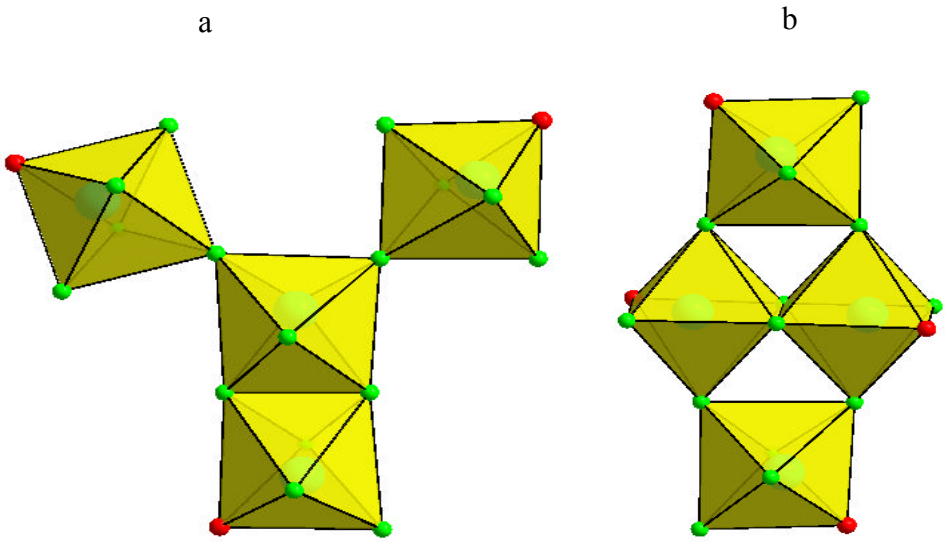

Figure 1-10. (a) Tetramer found in $[H_2pipz]_4[V_4O_3F_{17}]\cdot 4H_2O$,[47] (b) tetramer found in $[H_3adap]_2[V_4O_4F_{14}]\cdot 2H_2O$.[55]

Pairs of polyhedra greater than four are quite rare in transition metal (oxy)fluorides, but frequently observed in main group metal fluorides, *e.g.* the heptameric unit seen in $(H_3O)\cdot[H_3tren]_2[Al_7F_{30}]$[58] and the octameric units in $[(H_3tren)_4][(Al_8F_{35})\cdot(OH)\cdot H_2O]$.[58] The latter is shown in Figure 1-11 and can be considered as the largest known fluorinated polyanion.

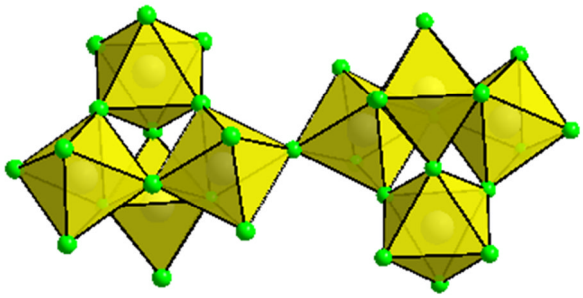

Figure 1-11. Octameric units found in $[(H_3tren)_4][(Al_8F_{35})\cdot(OH)\cdot H_2O]$.[58]

There is also a heptameric unit found in a V/Cu mixed system,[59] Figure 1-12 shows the V heptameric unit only. All fluorines in the central octahedron are bridging, so the central octhedron shared a corner with six neighboring octahedra. It is interesting to note that all the six surrounding octahedra are not connected to each other, they are connected to the central octahedron only.

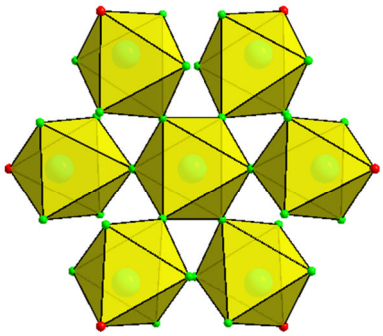

Figure 1-12. Heptameric units found in $[CH_3NH_3]_8[Cu(py)_4]_3[V_7O_6F_{30}]$.[59]

1-4-3-2. One-dimensional structures

When the metal fluoride anions extend infinitely in one dimension and form chains, the individual polyhedra are joined together into a single chain by either sharing corners, edges, faces or simultaneously corners and edges. There are many reports of vanadium or other metal based (oxy)fluorides with chain like structures. These chains range from the simplest corner sharing (*cis* or *trans*) to very complicated arrangements. Mostly the polyhedra are connected through bridging F atoms, however in some cases the bridging atom is oxygen rather than fluorine as it is the case in $[H_2en][TiOF_4]$.[60]

Other chains exhibit more complex and fascinating connectivities, one example being the alternating edge and corner shared octahedra found in $[H_2pipz][V_3O_3F_{20}]\cdot 2H_2O$[47] (Figure 1-13(a)) and in $[H_2dpe][V_2O_2F_6]$[61] (Figure 1-13(b)) displaying a ladder-like type structure, where two octahedra share an edge to form the *rung* of the ladder, and are further connected *via* the corners to form the *rail* of the ladder.

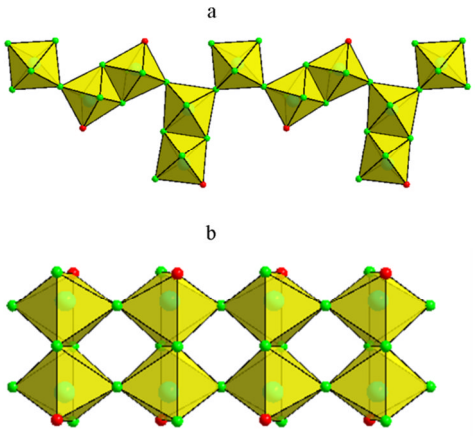

Figure 1-13. Two different types of edge and corner sharing chains; (a) Chains based on the Y shape tetramer,[47] (b) chain displaying a ladder-like type.[61]

A beautiful structure in vanadium based systems displaying an unusual chain type was reported for $[H_2pipz][V_7F_{27}]$.[62] The structure can be regarded as a construction of heptameric pyrochlore-like units that are further linked through bridging F atoms into an infinite chain along the *c*-axis as illustrated in Figure 1-14.

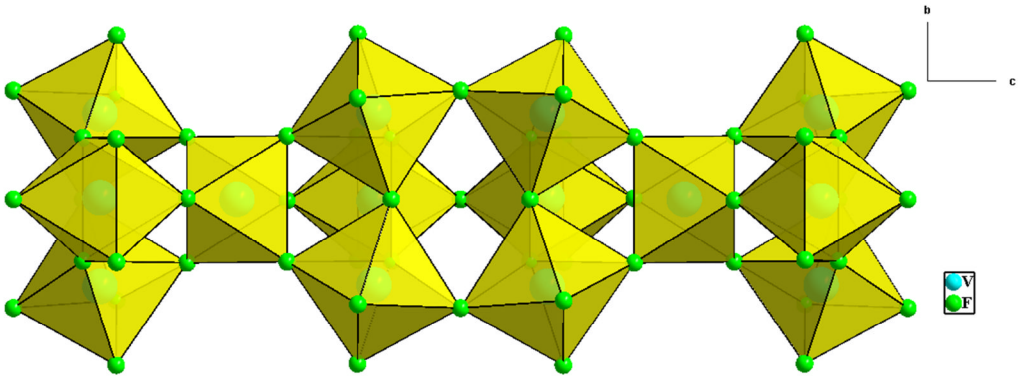

Figure 1-14. Chain type found in $[H_2pipz][V_7F_{27}]$[62] displaying pyrochlore-like heptameric unit.

The inorganic chains are separated by piperazinium moieties as shown in Figure 1-15.

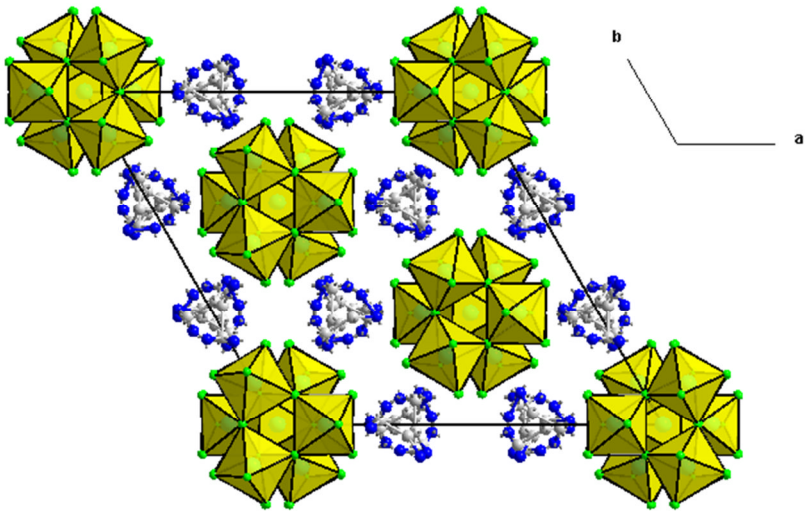

Figure 1-15. The unit cell in $[H_2pipz][V_7F_{27}]$.

This structure is based on a triangular motif, and potentially can present interesting magnetic properties (*e.g.* magnetic frustration) and can be compared with $KCrF_4$.[63] Although $[H_2pipz][V_7F_{27}]$ and $KCrF_4$ are both based on triangular motifs, they present different connection modes, as illustrated in Figure 1-16. In $[H_2pipz][V_7F_{27}]$ two triangular motifs are connected to other two through a monomeric unit to form an alternating trimeric and monomeric chain in a 3-3-1 configuration (Figure 1-16(a)). However the chain $KCrF_4$ can be considered as a trimeric chain formed by repeating the triangular motif in 3-3-3 configuration (Figure 1-16(b)).

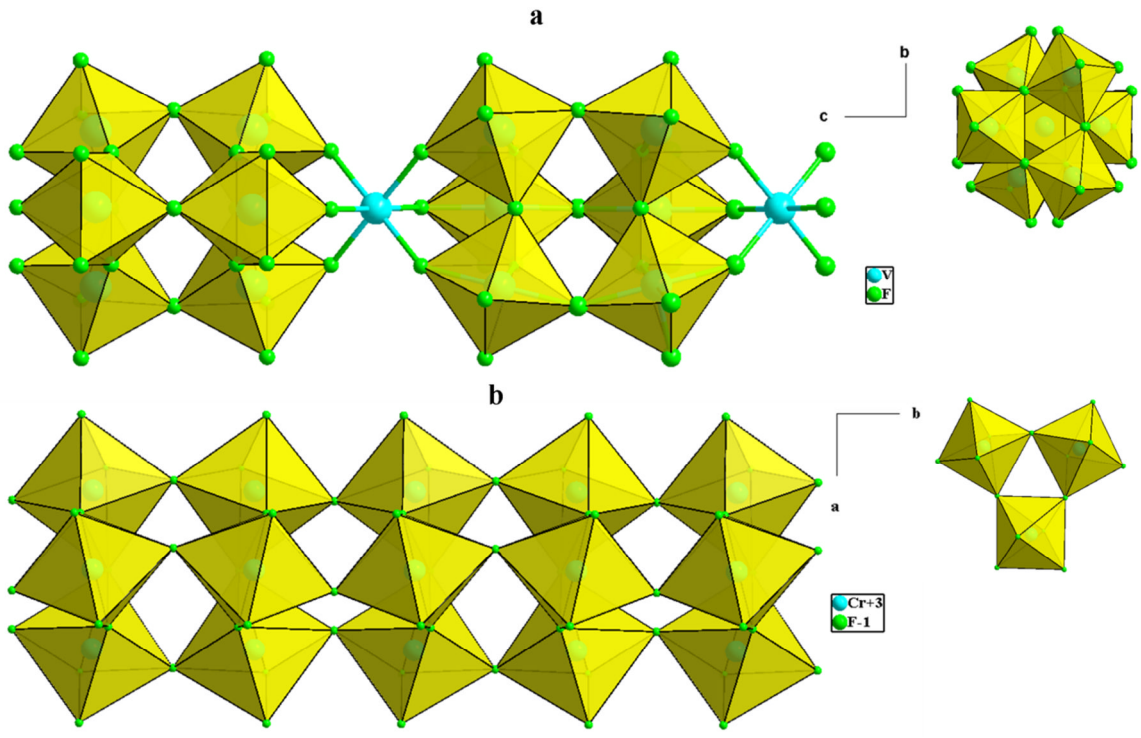

Figure 1-16. (a) The 3-3-1 configuration found in $[H_2pipz][V_7F_{27}]$ (top left) and a projection down the *c* axis (top right), (b) The 3-3-3 configuration found in $KCrF_4$ (bottom left) and a projection down the *c* axis (bottom right).

$KCrF_4$ is known to display magnetic frustration, however in $[H_2pipz][V_7F_{27}]$, and as stated by the authors, the magnetic data were inconclusive. Although the material did not show any magnetic transition down to the lowest measured temperature, there was no clear evidence to prove if the material is a frustrated magnet.

1-4-3-3. Two-dimensional frameworks

Although some structures displaying two-dimensionality were reported for transition metal fluorides, it was noted that layer structures are more frequently observed in main group metals (Al), lanthanides and actinides.[53]

The 2D arrangement can be made by the polyhedra sharing a corner, edge or simultaneously a corner and an edge. Several existing examples can be described as the association of units displaying definite known shapes. For example, the layer in $[H_2en][Sc_2F_8]$[64] is formed from the connection of "bow-tie" shaped units as shown in Figure 1-17. Very recently a Ti based system featuring the same structural motif was reported.[65]

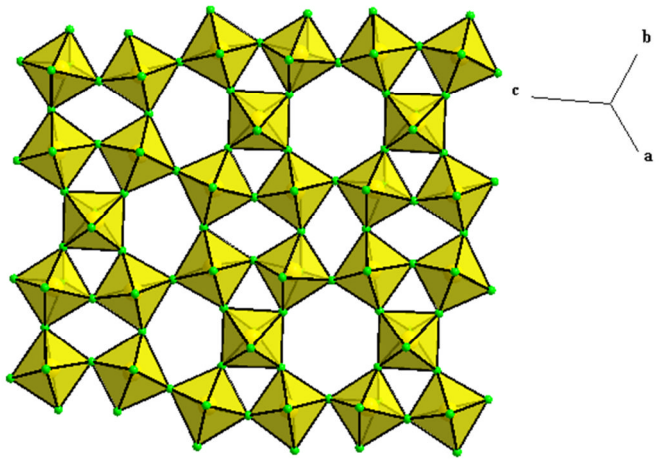

Figure 1-17. Layers found in $[H_2en][Sc_2F_8]$ based on "bow-tie" shape units.[64]

The structure of $[H_2pipz][Mn_4F_{16}]$[66] shown in Figure 1-18 contains layers separated by piperazinium cations. This structure can be described as the association of edge shared dimeric units to form continuous layers. The layer is shown in Figure1-19.

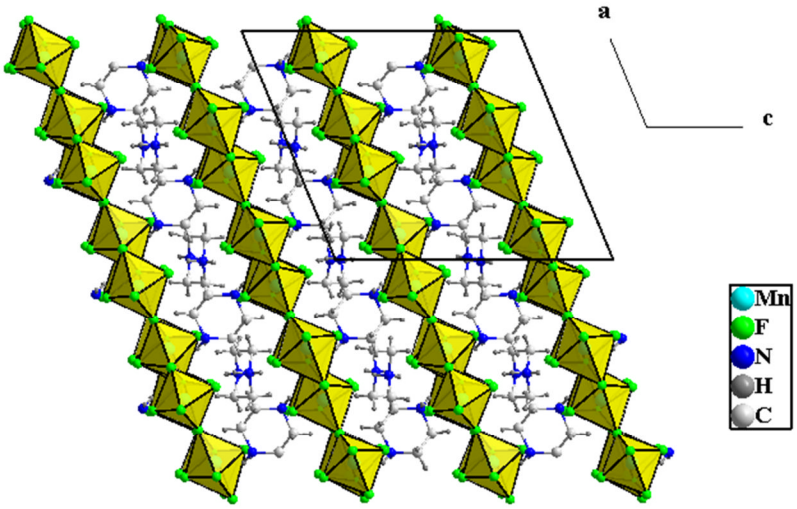

Figure 1-18. Layers found in $[H_2pipz][Mn_4F_{16}]$[66] separated by piperazium moieties viewed down the *b* axis.

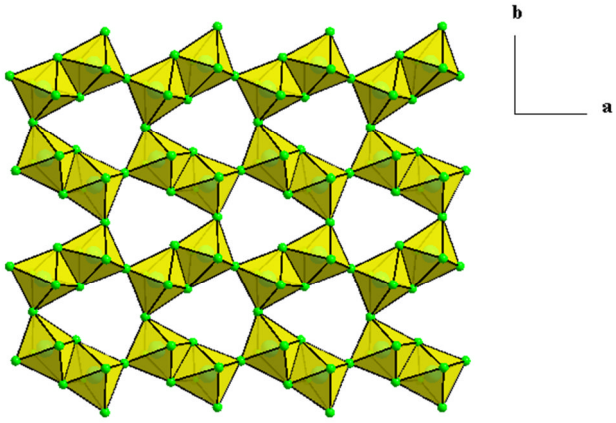

Figure 1-19. The association of edge shared dimers to form a continuous layer $[H_2pipz][Mn_4F_{16}]$.[66]

Very recently an interesting vanadium (oxy)fluoride material was reported, $[H_2pipz]_3[V_4F_{17}O]\cdot 1.5H_2O$,[67] displaying a 2D structure that can be regarded as the association of "Y shaped" units (see Figure 1-20). The most interesting point about this material is it shows direct relation to the tetrameric Y shaped structure $[H_2pipz]_4[V_4O_3F_{17}]\cdot 4H_2O$[47] and the chain structure based on Y shaped tetramers $[H_2pipz][V_3O_3F_{20}]\cdot 2H_2O$.

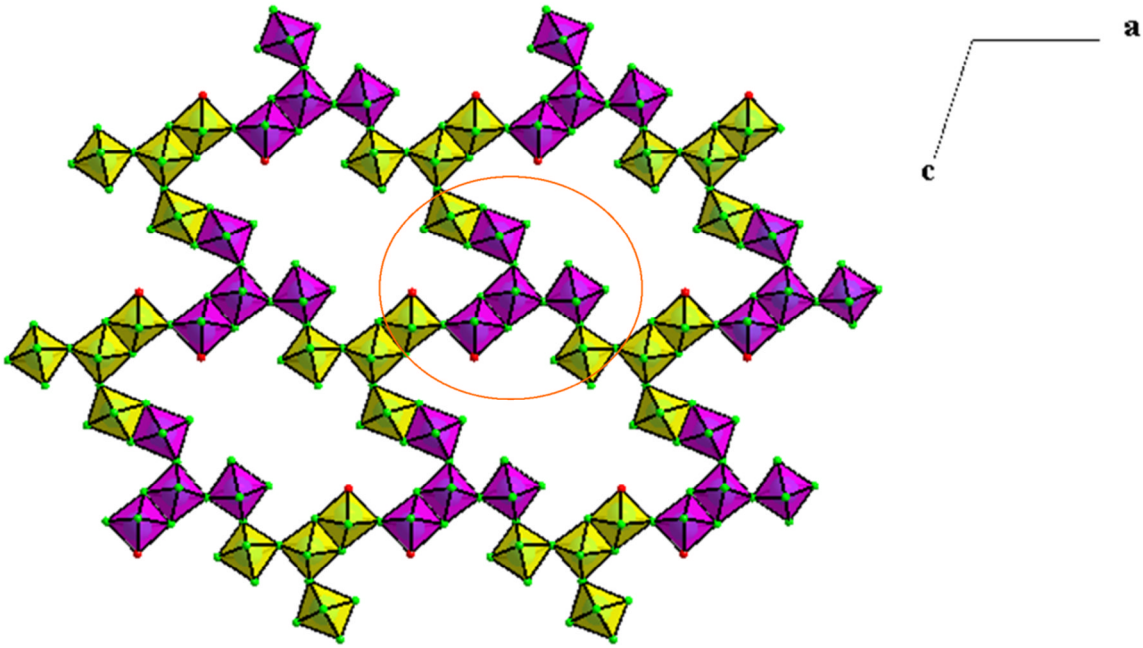

Figure 1-20. Layers found in $[H_2pipz]_3[V_4F_{17}O]\cdot 1.5H_2O$[67], the red circle shows how the Y shaped unit is connected to its three neighbouring.

1-4-3-4. Three-dimensional frameworks

Organically-templated metal fluorides with extended 3D connectivities are fairly rare. Many examples have been reported, all of them concerned metals with high coordination number (n > 6) *i.e.*: Zr, Y, Er, U, Th.

As an example, the U based framework $[H_2pipz][U_2O_4F_6]$,[68] is shown in Figure 1-21. The 3D structure is constructed from corner- and edge-sharing anionic uranium pentagonal bipyramids $[UO_2F_5]^-$, and charge balance is maintained by piperazinium cations. This structure contains three intersecting channels consisting of 10-, 8- and 6-membered rings, as respectively shown in Figure 1-21 and Figure 1-22.

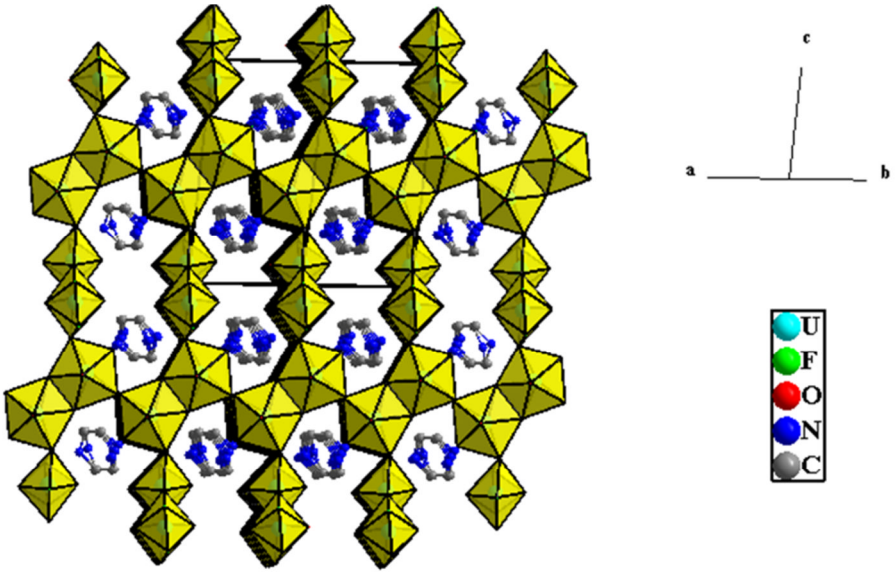

Figure 1-21. A view of $[H_2pipz][U_2O_4F_6]$,[68] showing the 10-membered ring.

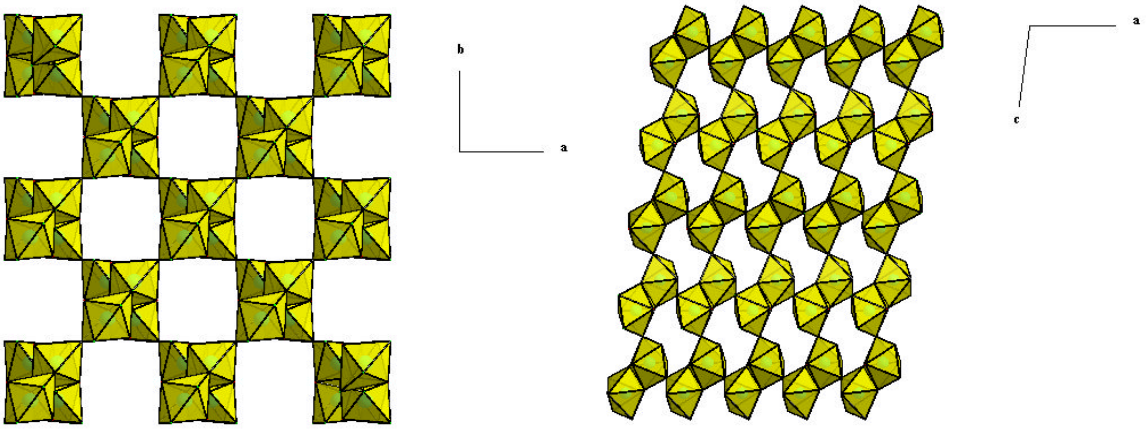

Figure 1-22. A view of $[H_2pipz][U_2O_4F_6]$,[68] showing the 8-membered ring (left) and the 6-membered ring (right).

Another example is $[H_2dap]_{0.5}[Y_3F_{10}]$[69] displaying a 3D connected framework. The structure of $[H_2dap]_{0.5}[Y_3F_{10}]$ is presented in Figure 1-23 and may be described as a 'Super-Diamond' network arising from the cubic arrangement of Y_6F_{32} SBUs, shown in Figure 1-24.

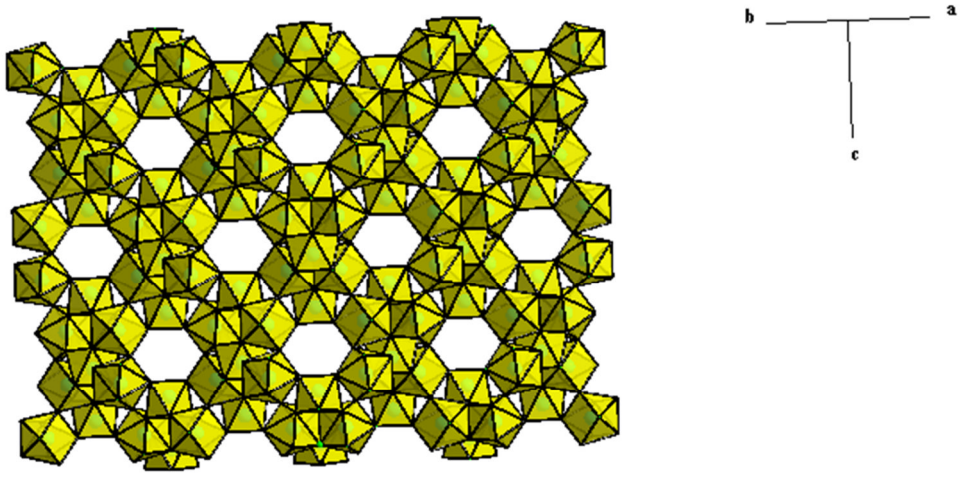

Figure 1.23. Polyhedra representation of the $[Y_3F_{10}]$ framework in $[H_2dap]_{0.5}[Y_3F_{10}]$.[69]

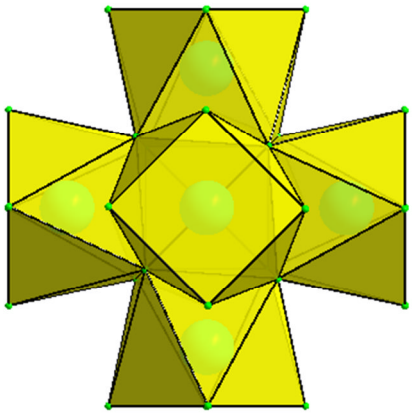

Figure 1-24. TheY_6F_{32} SBU found in $[H_2dap]_{0.5}[Y_3F_{10}]$.

1-4-4. Synthesis aspects: synthesis methods, solvent, template

The most commonly used route to the synthesis of organically-templated metal (oxy)fluorides is hydrothermal synthesis.[70] This involves mixing the reagents in water in the presence of an organic template then heating the resulting solution at the required temperature (< 300 °C) in an autoclave at autogenous pressure (> 1 bar). Other synthetic procedures, *i.e.*, crystallisation from solution has been used for the preparation of organically-templated metal fluorides. Most of the materials synthesised this way consist of isolated [MF_6] octahedra units, with very few extended-connectivity lattices.[51] Solid state reactions and gas-solid reactions have been also widely used in the synthesis of purely inorganic fluorides such : Li_3AlF_6, Li_4ZrF_8.[40]

1-4-4-1. Solvent

Water remains the prefered solvent used in the preparation of organically-templated metal (oxy)fluorides, hence the term “hydrothermal synthesis”, where in many cases it not only acts as a solvent, but it is actually a reactant and can appear in the final structure as a coordinating ligand[55] or as space filling[71] where it plays a role in stabilising the whole structure by providing H-bonding to the inorganic framework. In many cases a mixture of water and other organic co-solvents such as ethanol, ethylene glycol, pyridine, etc. has also been used (solvothermal synthesis). To date, the role that the co-solvent plays in the reaction has not been assessed, and it is not clear if it acts only as a diluent and heat transfer medium or if it can play other positive roles even though in the synthesis of organically-templated vanadium (oxy)fluorides it has been suggested that ethylene glycol may encourage partial

reduction of vanadium.[55] It is worth noting that some ILs have been used as a solvent and/or as a fluoride source for the synthesis of some known metal fluorides but never organically-templated metal (oxy)fluorides.[20,72-75] One example is the synthesis of YF_3 with different phases and morphologies depending on the ratio IL/metal, using 1-butyl-3-methylimidazolium tetrafluoroborate, BMIM BF_4, in H_2O.[75] Another example is the synthesis of β–NH_4AlF_4[20] using 1-ethyl-3-methylimidazolium hexafluorophosphate, EMIM PF_6.

1-4-4-2. Template

Templating can be broadly defined as the use of small organic molecules (or hydrated metal ions) to provide a support about which an inorganic host may crystallise. In general, template molecules may serve several different functions, including framework support and/or charge balance to their hosts. To date, quaternary ammonium cations and a wide range of organic amines have been used as a template for the synthesis of metal (oxy)fluorides. In addition to taking the role of charge balancing to the inorganic frameworks, these play a significant role in structure crystallisation, as a wide range of anionic frameworks with different topologies and dimensionalities have been synthesised within the same system simply by changing the organic amine. One example of this can be found in the thorium based systems[76] where two organically-templated thorium compounds were synthesised under exactly the same conditions (temperature, time, reactant stoichiometry and solvent) just varying the organic template; the use of piperazine afforded a 2D material $[C_4N_2H_{12}]_{0.5}[ThF_5]$, while the use of 2-methylpiperazine resulted in a 1D face shared chain $[C_5N_2H_{14}][ThF_6]\cdot 0.5H_2O$. The structure of these materials is shown in Figure 1-25.

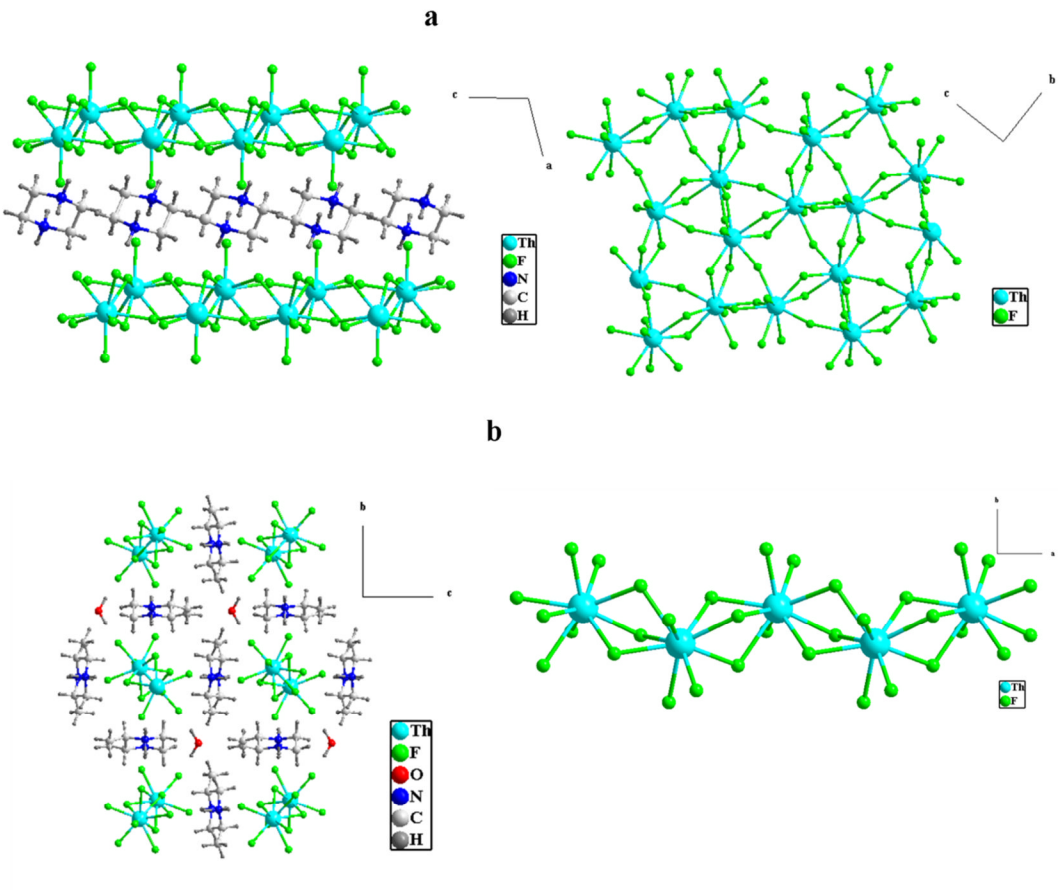

Figure 1-25. (a) Layers found in $[C_4N_2H_{12}]_{0.5}[ThF_5]$, (b) Chains found in $[C_5N_2H_{14}][ThF_6]\cdot 0.5H_2O$.

1-4-4-3. Reactions variables and mechanism

As mentioned earlier, in relatively recent years, hydrothermal synthesis has been shown to be a powerful technique for the synthesis of organically-templated metal (oxy)fluorides. Several groups now are carrying out extensive research in this domain and exploring different systems: Albrecht-Schmitt, O'Hare, Weller, Maisonneuve and Lightfoot have developed the corresponding zirconium,[77] uranium,[78] beryllium,[79] aluminium,[80,81] rare earth,[64,69] early transition metal[62,82] and indium[83] chemistry. This list is by no means exhaustive, and many other groups have

explored organically-templated metal fluorides as part of their research work.[67] This has resulted in different compounds displaying an astonishingly diverse range of structural topologies and novel polyhedral connectivities. It was observed in general, that the synthesis is very sensitive to various reaction conditions, including reagents, pH, water content, organic template, solvent, time, temperature, and even the fill of the autoclave. The chemistry that occurs in such systems is very complicated, making any clear understanding of how these materials form difficult, and it is almost impossible to design or engineer a new material with particular structural features for specific properties. Although it was suggested that it is through the condensation of the PBUs (MX_n), assumed to pre-exist in solution, that the extended solid will form, the crystallisation mechanism is not well understood, and the vast majority of products are unpredictable,.

There have been several attempts to try to identify the mechanism governing the synthesis of metal (oxy)fluorides. One approach is to identify key reaction variables and systematically explore their influence. In this context, composition space diagrams have been developed by varying the reactants composition, while other variables such as temperature, time and solvent are held constant.[71,81,84-86] One example is found in the $Al(OH)_3$/*tren*/HF_{eq}/ethanol system[58] where different phases are accessible, ranging from monomers to 1D structures. Another excellent example that shows the evolution from molecules to frameworks is found in the $UO_2(CH_3COO)_2{\cdot}2H_2O/HF_{aq}$/*pipz* system, where three different materials spaning the range of dimensionalities from 0D through 3D framework have been synthesised by systematically changing the reactant composition.[68]

An alternative approach is to keep all composition variables fixed and vary only an external parameter. A recent example of this second approach is the focussed study of the system V_2O_5/HF/H_2O/ethylene glycol/*pipz*,[47] where it has been observed that there is a clear progression in dimensionality from 0D to 1D structures through a common type-motif (Y shape tetramer) upon increasing the reaction temperature (isolated tetramer has been obtained at 100 °C and 1D chain at 160 °C). In the same system a very recent study shows that a 2D structure displaying the same type-motif can be isolated under different conditions where the molar ratio HF/*pipz* and time of the reaction have been introduced as other variables. This structure can be added to the previous 0D and 1D structures based on Y shaped units to show the progression from 0D to 2D from the same system with variation of the reaction conditions.

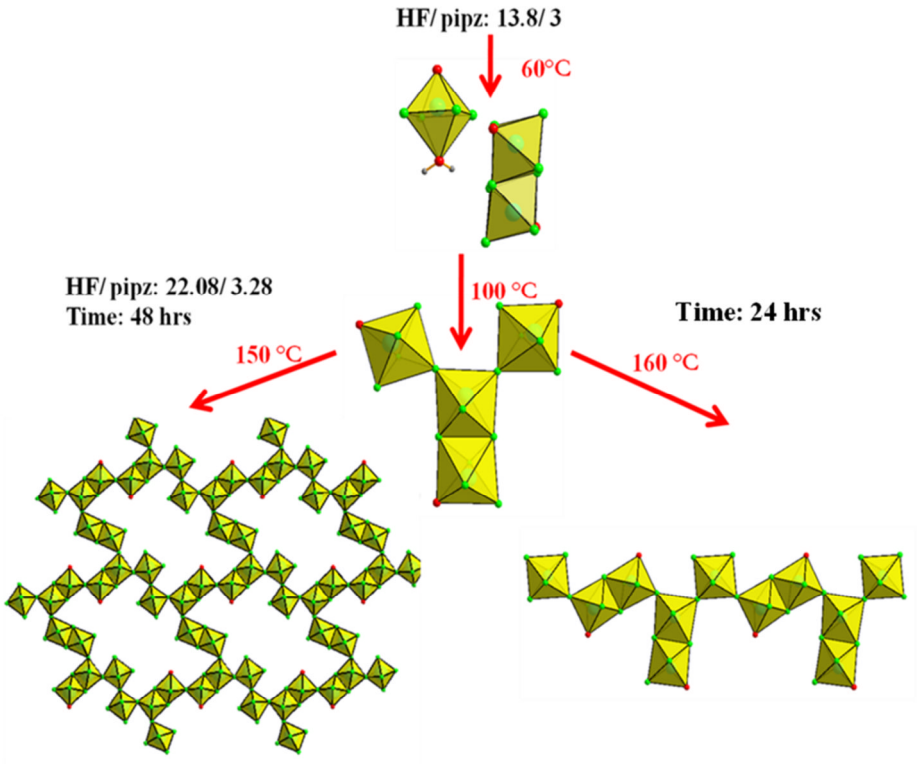

Figure 1-26. Products of the system V_2O_5/HF/*pipz*/H_2O/ethylene glycol under different conditions.

1-5. Lanthanide organic frameworks

1-5-1. Background

Metal-organic frameworks (MOFs), consisting of metal ions coordinated to organic molecules, are one class of organic-inorganic hybrid materials that have attracted much attention in recent years due to their potential applications in a wide variety of domains, most famously in gas adsorption and storage applications.[87] Recently, the potential biological and medical applications of MOFs have also been studied.[88] Among these compounds lanthanide-containing MOFs (Ln-MOF) are of special interest owing to their unique topological structures and fascinating chemical/physical properties.[89] Ln-MOFs have been applied in fields such as gas adsorption, luminescence, magnetism and catalytic activity. Therefore, many spectacular Ln-MOFs have been well documented recently.[90-93]

The higher coordination number of lanthanide ions and the more variable nature of their coordination sphere can induce a versatile structural topology. In particular the structural chemistry of metal carboxylates is quite fascinating, due to the flexibility of the carboxylate groups to adopt different coordination modes. Compared with N-donor ligands, which are intrinsically mono-dentate, carboxylic groups are more complex and less predictable for the framework formation. They have flexible binding behaviour from monodentate and chelating to multi-bridging.

In the vast majority of the reported Ln- MOFs the metal centre is either nine- or eight-

coordinate. One example can be found in the system europium/propane-1,2,3-tricarboxylic acid, $Eu(tca)(H_2O)_3 \cdot nH_2O$,[94] (Figure 1-27) the Eu ion is nine-coordinated by six oxygens from carboxylic acid and three oxygens from the coordinated water molecules. Each carboxylate group in the tca ligand is chelating (bidentate) as shown in Figure 1-27.

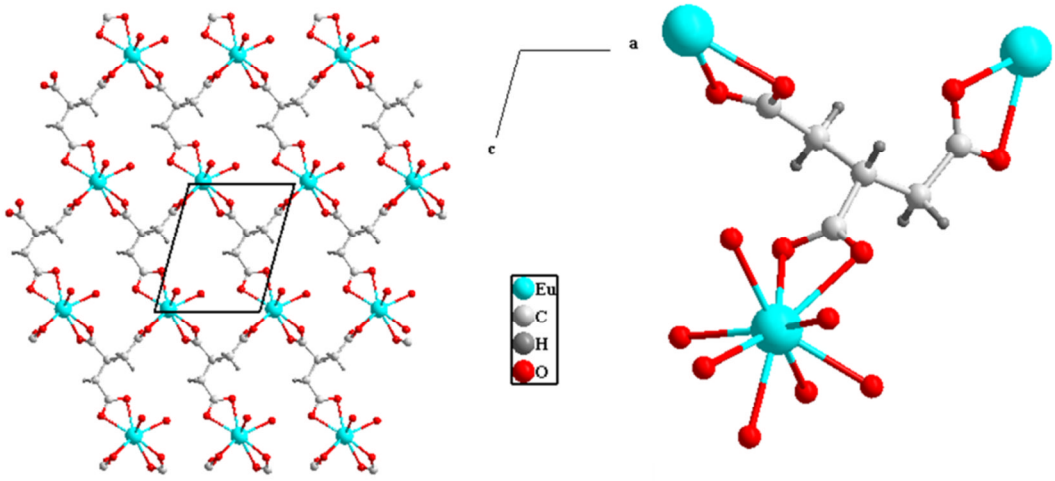

Figure 1-27. Structure of $Eu(tca)(H_2O)_3 \cdot nH_2O$[94] (left), coordination environment of the Eu ion and coordination behaviour of the tca (right).

However a low coordination number (six-coordinate) was reported for: ($Ln(C_6H_9O_6)$: Ln = Er^{3+}, Tb^{3+}).[95] The structure of $Er(C_6H_9O_6)$, as shown in Figure 1-28, consists of a single Er^{3+} metal centre in an octahedral geometry, connected through 1,3,5-cyclohexanetricarboxylate, CTA, ligand into a 3D framework. In this material each carboxylate group of the 1,3,5-CTA exhibits a bridging bidentate connectivity. It was claimed that this material exhibits high thermal stability (stable up to 600 °C).

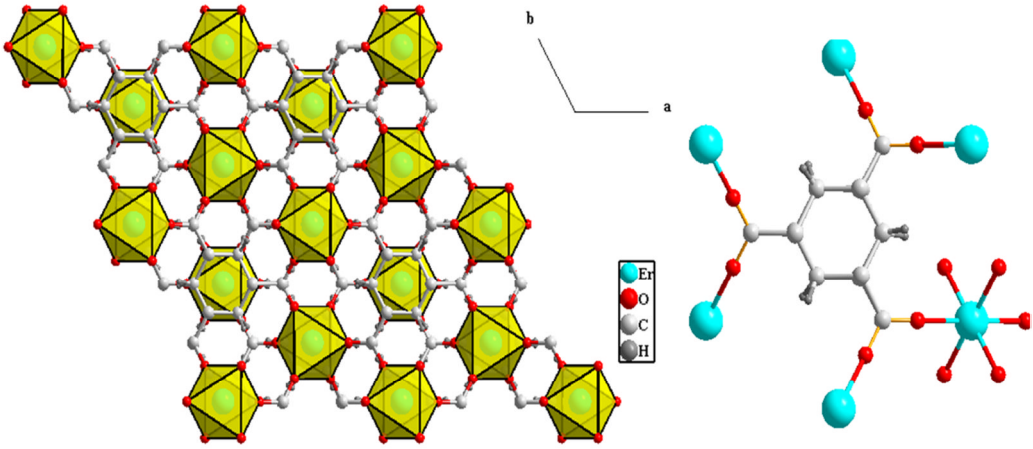

Figure 1-28. Structure of $Er(C_6O_9H_9)$ (left), the coordination environment of the metal centre and connectivity behaviour of 1,3,5-CTA (right).

Lanthanide ions have a strong tendency to form extended inorganic skeletons in the presence of suitable organic linkers, this may generate robust frameworks incorporating a 1D or a 2D inorganic network. MIL-63[96] and MIL-78[97] are good examples. MIL-63, $(Eu_3(H_2O)(OH)_6[C_6H_3(CO_2)_3)]\cdot 3H_2O$, is a 3D porous material obtained using trimesic acid as a ligand, the framework is built up from nine-coordinated Eu^{3+} and trimesate ions. This structure is made from a two-dimensional europium inorganic network connected *via* the carboxylates into a 3D framework. MIL-78 ($M(C_6H_3(CO_2)_3)$, M = Y, Ln) exhibits a 3D framework constructed from eight-coordinated lanthanide ions and trimesate ions. Unlike MIL-63, this material possesses a one-dimensional inorganic chains connected *via* the carboxylates ions creating a 3D open framework. The structure of MIL-78 along with the inorganic chains found in the structure and the coordination behaviour of the trimesic acid are illustrated in Figure 1-29.

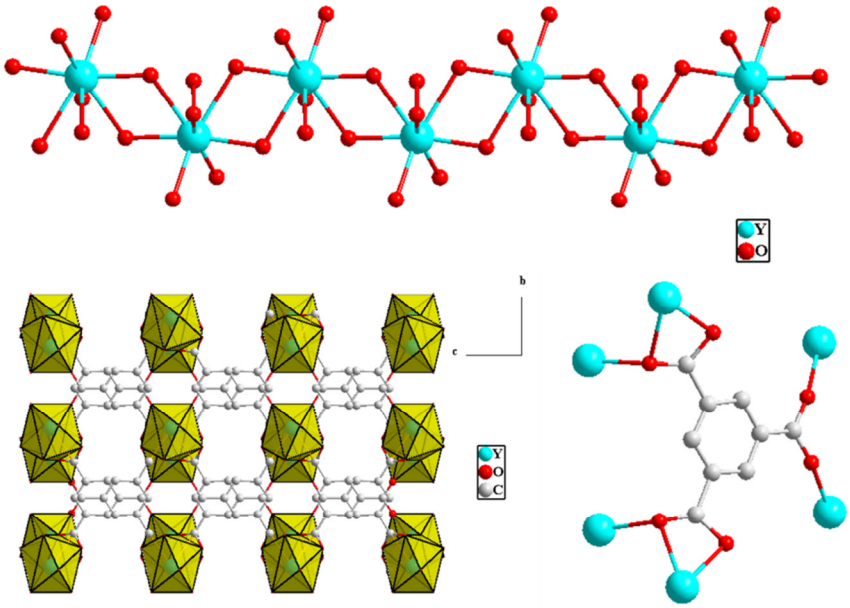

Figure 1-29. The inorganic framework found in MIL-78 (top), a view of MIL-78 along the *a* axis (below left) and the coordination behaviour for trimesic acid (below right).

1-5-2. Synthesis of Ln-MOFs

Ln-MOFs are synthesised in a similar way as any other MOF, typically *via* hydrothermal synthesis in which all chemicals (metal source and an organic linker) are placed into a Teflon-lined autoclave using water as a solvent, and heated statically under autogenous pressure. Alternatively other solvents may be used: ethanol, THF, DMF, hexane, pyridine, or a mix (or mixed with water), more appropriately called "solvothermal synthesis".

The use of an additional organic template or SDA in MOFs is not very popular as it is in the case of the synthesis of zeolites and zeotypes. However SDAs may be used in MOFs synthesis to control the pores sizes.[98,99]

1-6. References

(1) Cooper, E. R.; Andrews, C. D.; Wheatley, P. S.; Webb, P. B.; Wormald, P.; Morris, R. E. *Nature* **2004**, *430*, 1012.

(2) Wasserscheid, P.; Welton, T. *Ionic liquids in synthesis*; Wiley-VCH: Weinbeim, 2003.

(3) Wilkes, J. S. *Green Chem*. **2002**, *4*, 73.

(4) Freemantle, M. *An Introduction to Ionic Liquids*; RSC Publishing: Cambridge, 2010.

(5) Wilkes, J. S.; Zaworotko, M. J. *J. Chem. Soc., Chem. Commun.* **1992**, 965.

(6) Bonhote, P.; Dias, A.P.; Papageorgiou, N.; Kalyanasundaram, K.; Gratzel, M. *Inorg. Chem.* **1996**, *35*, 1168.

(7) Visser, A. E.; Swatloski, R. P.; Reichert, W. M.; Mayton, R.; Sheff, S.; Wierzbicki, A.; Davis, J. J. H.; Rogers, R. D. *Chem. Commun.* **2001**, 135.

(8) Himmler, S.; Hormann, S.; van Hal, R.; Schulz, P. S.; Wasserscheid, P. *Green Chem.* **2006**, *8*, 887.

(9) Clavier, H.; Boulanger, L.; Audic, N.; Toupet, L.; Mauduit, M.; Guillemin, J.-C. *Chem. Commun.* **2004**, 1224.

(10) Fukumoto, K.; Yoshizawa, M.; Ohno, H. *J. Am. Chem. Soc.* **2005**, *127*, 2398.

(11) Tokuda, H.; Hayamizu, K.; Ishii, K.; Susan, M. A. B. H.; Watanabe, M. *J. Phy. Chem. B* **2004**, *108*, 16593.

(12) Tokuda, H.; Ishii, K.; Susan, M. A. B. H.; Tsuzuki, S.; Hayamizu, K.;

Watanabe, M. *J. Phy. Chem. B* **2006**, *110*, 2833.

(13) Holbrey, J. D.; Reichert, W. M.; Swatloski, R. P.; Broker, G. A.; Pitner, W. R.; Seddon, K. R.; Rogers, R. D. *Green Chem*. **2002**, *4*, 407.

(14) Earle, M. J.; Esperanca, J. M. S. S.; Gilea, M. A.; Canongia Lopes, J. N.; Rebelo, L. P. N.; Magee, J. W.; Seddon, K. R.; Widegren, J. A. *Nature* **2006**, *439*, 831.

(15) Abbott, A. P.; Boothby, D.; Capper, G.; Davies, D. L.; Rasheed, R. K. *J. Am. Chem. Soc.* **2004**, *126*, 9142.

(16) Abbott, A. P.; Capper, G.; Davies, D. L.; Rasheed, R. K.; Tambyrajah, V. *Chem. Commun.* **2003**, 70.

(17) Parnham, E. R.; Morris, R. E. *J. Mater. Chem.* **2006**, *16*, 3682.

(18) Parnham, E. R.; Morris, R. E. *Chem. Mater.* **2006**, *18*, 4882.

(19) Parnham, E. R.; Morris, R. E. *J. Am. Chem. Soc.* **2006**, *128*, 2204.

(20) Parnham, E. R.; Slawin, A. M. Z.; Morris, R. E. *J. Solid State Chem.* **2007**, *180*, 49.

(21) Parnham, E. R.; Wheatley, P. S.; Morris, R. E. *Chem. Commun.* **2006**, 380.

(22) Liao, J.-H.; Wu, P.-C.; Bai, Y.-H. *Inorg. Chem. Commun.* **2005**, *8*, 390.

(23) Lin, Z.; Slawin, A. M. Z.; Morris, R. E. *J. Am. Chem. Soc.* **2007**, *129*, 4880.

(24) Lin, Z.; Wragg, D. S.; Morris, R. E. *Chem. Commun.* **2006**, 2021.

(25) Lin, Z.; Wragg, D. S.; Warren, J. E.; Morris, R. E. *J. Am. Chem. Soc.* **2007**, *129*, 10334.

(26) Xie, Z.-L.; White, R. J.; Weber, J.; Taubert, A.; Titirici, M. M. *J. Mater. Chem.* **2011**, *21*, 7434.

(27) Morris, R. E. *Chem. Commun.* **2009**, 2990.

(28) Parnham, E. R.; Morris, R. E. *Acc. Chem. Res.* **2007**, *40*, 1005.

(29) Morris, R. E. *Angew. Chem. Int. Ed.* **2008**, *47*, 442.

(30) Taubert, A.; Li, Z. *Dalton Trans.* **2007**, 723.

(31) Wragg, D. S.; Slawin, A. M. Z.; Morris, R. E. *Solid State Sci.* **2009**, *11*, 411.

(32) Drylie, E. A.; Wragg, D. S.; Parnham, E. R.; Wheatley, P. S.; Slawin, A. M. Z.; Warren, J. E.; Morris, R. E. *Angew. Chem. Int. Ed.* **2007**, *119*, 7985.

(33) Jin, K.; Huang, X.; Pang, L.; Li, J.; Appel, A.; Wherland, S. *Chem. Commun.* **2002**, 2872.

(34) Parnham, E. R.; Drylie, E. A.; Wheatley, P. S.; Slawin, A. M. Z.; Morris, R. E. *Angew. Chem. Int. Ed.* **2006**, *45*, 4962.

(35) Sheu, C.-Y.; Lee, S.-F.; Lii, K.-H. *Inorg. Chem.* **2006**, *45*, 1891.

(36) Wragg, D. S.; Fullerton, G. M.; Byrne, P. J.; Slawin, A. M. Z.; Warren, J. E.; Teat, S. J.; Morris, R. E. *Dalton Trans.* **2011**, *40*, 4926.

(37) Wei, Y.; Tian, Z.; Gies, H.; Xu, R.; Ma, H.; Pei, R.; Zhang, W.; Xu, Y.; Wang, L.; Li, K.; Wang, B.; Wen, G.; Lin, L. *Angew. Chem. Int. Ed.* **2010**, *49*, 5367.

(38) Recham, N.; Chotard, J. N.; Jumas, J. C.; Laffont, L.; Armand, M.; Tarascon, J. M. *Chem. Mater.* **2009**, *22*, 1142.

(39) Xing, H.; Yang, W.; Su, T.; Li, Y.; Xu, J.; Nakano, T.; Yu, J.; Xu, R. *Angew. Chem. Int. Ed.* **2010**, *49*, 2328.

(40) Hagenmuller, P. *Inorganic solid fluorides*; Academic Press: London, 1985.

(41) Flaningen, E. M.; Patton, R. L. U. S. Patent 4073864, 1978.

(42) Ouellette, W.; Yu, M. H.; O'Connor, C. J.; Zubieta, J. *Inorg. Chem.* **2006**, *45*, 7628.

(43) Rao, C. N. R.; Behera, J. N.; Dan, M. *Chem. Soc. Rev.* **2006**, *35*, 375.

(44) Maggard, P. A.; Kopf, A. L.; Stern, C. L.; Poeppelmeier, K. R.; Ok, K. M.; Halasyamani, P. S. *Inorg. Chem.* **2002**, *41*, 4852.

(45) Marvel, M. R.; Lesage, J.; Baek, J.; Halasyamani, P. S.; Stern, C. L.; Poeppelmeier, K. R. *J. Am. Chem. Soc.* **2007**, *129*, 13963.

(46) Stephens, N. F.; Buck, M.; Lightfoot, P. *J. Mater. Chem.* **2005**, *15*, 4298.

(47) Aldous, D. W.; Stephens, N. F.; Lightfoot, P. *Dalton Trans.* **2007**, 4207.

(48) Halasyamani, P. S.; Poeppelmeier, K. R. *Chem. Mater.* **1998**, *10*, 2753.

(49) Nakajima,T.; Žemva, B.; Tressaud, A. *Advanced Inorganic Fluorides, Synthesis, Characterisation and Applications;* Elsevier: Lausanne, 2000.

(50) Tressaud, A. *Functionalized Inorganic Fluorides: Synthesis, Characterization and Properties of Nanostructured Solids*; Wiley: New York, 2010.

(51) Bentrup, U.; Feist, M.; Kemnitz, E. *Prog. Solid State Chem.* **1999**, *27*, 75.

(52) Massa, W.; Babel, D. *Chem. Rev.* **1988**, *88*, 275.

(53) Adil, K.; Leblanc, M.; Maisonneuve, V.; Lightfoot, P. *Dalton. Trans.* **2010**, *39*, 5983.

(54) Hilbers, M.; Leimkuhler, M.; Mattes, R. *Z. Naturforschung. B - Chem. Sci* **1989**, *44*, 383.

(55) Aldous, D. W.; Stephens, N. F.; Lightfoot, P. *Dalton Trans.* **2007**, 2271.

(56) Buchholz, N.; Leimkuehler, M.; Kiriazis, L.; Mattes, R. *Inorg. Chem.*

1988, *27*, 2035.

(57) Ban, I.; Golič, L.; Milićev, S.; Volavšek, B. *Monatshefte für Chemie / Chemical Monthly* **1995**, *126*, 1279.

(58) Adil, K.; Leblanc, M.; Maisonneuve, V. *J. Fluorine Chem.* **2009**, *130*, 1099.

(59) Mahenthirarajah, T.; Lightfoot, P. *Chem. Commun.* **2008**, 1401.

(60) Lhoste, J.; Gervier, R.; Maisonneuve, V.; Leblanc, M.; Adil, K. *Solid State Sci.* **2009**, *11*, 1582.

(61) Aldous, D. W.; Goff, R. J.; Attfield, J. P.; Lightfoot, P. *Inorg. Chem.* **2007**, *46*, 1277.

(62) Aldous, D. W.; Slawin, A. M. Z.; Lightfoot, P. *J. Solid State Chem.* **2008**, *181*, 3033.

(63) Dewan, J. C.; Edwards, A. J. *J. Chem. Soc., Chem. Commun.* **1977**, 533.

(64) Stephens, N. F.; Slawin, A. M. Z.; Lightfoot, P. *Chem. Commun.* **2004**, 614.

(65) Lhoste, J.; Rocquefelte, X.; Adil, K.; Dessapt, R.; Jobic, S.; Leblanc, M.; Maisonneuve, V.; Bujoli-Doeuff, M. *Inorg. Chem.* **2011**, *50,*5671.

(66) Stief, R.; Massa, W. *Z. Anorg. Allg. Chem.* **2006**, *632*, 797.

(67) DeBurgomaster, P.; Ouellette, W.; Liu, H.; O'Connor, C. J.; Yee, G. T.; Zubieta, J. *Inorg. Chim. Acta* **2010**, *363*, 1102.

(68) Walker, S. M.; Halasyamani, P. S.; Allen, S.; O'Hare, D. *J. Am. Chem. Soc.* **1999**, *121*, 10513.

(69) Stephens, N. F.; Lightfoot, P. *J. Solid State Chem.* **2007**, *180*, 260.

(70) Rabenau, A. *Angew. Chem. Int. Ed. Engl.* **1985**, *24*, 1026.

(71) Adil, K.; Saada, M. A.; Ben Ali, A.; Body, M.; Dang, M. T.; Hémon-

Ribaud, A.; Leblanc, M.; Maisonneuve, V. *J. Fluorine Chem.* **2007**, *128*, 404.

(72) Jacob, D. S.; Bitton, L.; Grinblat, J.; Felner, I.; Koltypin, Y.; Gedanken, A. *Chem. Mater.* **2006**, *18*, 3162.

(73) Nuñez, N. O.; Ocaña, M. *Nanotechnology* **2007**, *18*, 455606.

(74) Zhang, C.; Chen, J.; Zhou, Y.; Li, D. *J. Phys. Chem. C* **2008**, *112*, 10083.

(75) Zhong, H.-X.; Hong, J.-M.; Cao, X.-F.; Chen, X.-T.; Xue, Z.-L. *Mater. Res. Bull.* **2009**, *44*, 623.

(76) Kim, J.-Y.; Norquist, A. J.; O'Hare, D. *Chem. Commun.* **2002**, 2198.

(77) Sykora, R. E.; Ruf, M.; Albrecht-Schmitt, T. E. *J. Solid State Chem.* **2001**, *159*, 198.

(78) Francis, R. J.; Halasyamani, P. S.; Bee, J. S.; O'Hare, D. *J. Am. Chem. Soc.* **1999**, *121*, 1609.

(79) Gerrard, L. A.; Weller, M. T. *Chem. Commun.* **2003**, 716.

(80) Adil, K.; Le Bail, A.; Dujardin, G.; Maisonneuve, V. *Polyhedron* **2007**, *26*, 2493.

(81) Adil, K.; Marrot, J.; Leblanc, M.; Maisonneuve, V. *Solid State Sci.* **2007**, *9*, 531.

(82) Aldous, D. W.; Lightfoot, P. *Solid State Sci.* **2009**, *11*, 315.

(83) Jayasundera, A. C. A.; Goff, R. J.; Li, Y.; Finch, A. A.; Lightfoot, P. *J. Solid State Chem.* **2010**, *183*, 356.

(84) Adil, K.; Ben Ali, A.; Leblanc, M.; Maisonneuve, V. *Solid State Sci.* **2006**, *8*, 698.

(85) Norquist, A. J.; Heier, K. R.; Stern, C. L.; Poeppelmeier, K. R. *Inorg. Chem.* **1998**, *37*, 6495.

(86) Walker, S. M.; Halasyamani, P. S.; Allen, S.; O'Hare, D. *J. Am. Chem. Soc.* **1999**, *121*, 10513.

(87) Morris, R. E.; Wheatley, P. S. *Angew. Chem. Int. Ed.* **2008**, *47*, 4966.

(88) McKinlay, A. C.; Morris, R. E.; Horcajada, P.; Férey, G.; Gref, R.; Couvreur, P.; Serre, C. *Angew. Chem. Int. Ed.* **2010**, *49*, 6260.

(89) Bünzli, J.-C. G.; Piguet, C. *Chem. Soc. Rev.* **2005**, *34*, 1048.

(90) Devic, T.; Serre, C.; Audebrand, N.; Marrot, J.; Férey, G. *J. Am. Chem. Soc.* **2005**, *127*, 12788.

(91) Huang, Y.-g.; Wu, B.-l.; Yuan, D.-q.; Xu, Y.-q.; Jiang, F.-l.; Hong, M.-c. *Inorg. Chem.* **2007**, *46*, 1171.

(92) Vitorino, M. J.; Devic, T.; Tromp, M.; Férey, G.; Visseaux, M. *Macromol. Chem. Phys.* **2009**, *210*, 1923.

(93) Zimmermann, M.; Belai, N.; Butcher, R. J.; Pope, M. T.; Chubarova, E. V.; Dickman, M. H.; Kortz, U. *Inorg. Chem.* **2007**, *46*, 1737.

(94) Cañadillas-Delgado, L.; Fabelo, O.; Pasán, J.; Delgado, F. S.; Déniz, M.; Sepúlveda, E.; Laz, M.-M.; Julve, M.; Ruiz-Pérez, C. *Cryst. Growth Des*. **2008**, *8*, 1313.

(95) de Lill, D. T.; Cahill, C. L. *Chem. Commun.* **2006**, 4946.

(96) Serre, C.; Ferey, G. *J. Mater. Chem.* **2002**, *12*, 3053.

(97) Serre, C.; Millange, F.; Thouvenot, C.; Gardant, N.; Pelle, F.; Ferey, G. *J. Mater. Chem.* **2004**, *14*, 1540.

(98) Kitagawa, S.; Uemura, K. *Chem. Soc. Rev.* **2005**, *34*, 109.

(99) Serre, C.; Mellot-Draznieks, C.; Surblé, S.; Audebrand, N.; Filinchuk, Y.; Férey , G. *Science* **2007**, *315*, 1828.

CHAPTER 2

AIMS AND OBJECTIVES

2-1. Synthesis of transition metal fluorides and lanthanide MOFs using ILs and DES

A commonly used preparative method in materials chemistry is hydrothermal synthesis; this method involves mixing the reagents in water or organic solvent, then heating the resulting solution in a sealed autoclave under autogenuous pressure. Recently, the chemistry inside the autoclaves has been altered by replacing the molecular solvent (water/organic solvent) with an ionic solvent (ionic liquid),[1] this has been termed ionothermal synthesis.[2] This synthesis approach has proven to be a versatile route to the preparation of many different type of materials. Moreover, ILs have been shown to play multiple roles:[3-6] they can act as an unusual reaction media, may serve as a template or act in a controlled manner as a template delivery agent. In many cases the materials synthesised *via* this route are unique and cannot be prepared using other standard methods.

The overall aim of this thesis is to explore further this preparative method of ionothermal synthesis in an attempt to extend the range of its applicability to span a wider spectrum of materials chemistry.

This will involve the investigation of organically-templated vanadium fluorides and oxyfluorides using different type of ILs and DESs,[7] mainly those that have shown some success in the ionothermal synthesis of zeotypes and related materials. Organically-templated vanadium (oxy)fluorides (VOFs) have been extensively studied using hydrothermal based media;[7-10] however the dimensionality has been only extended to infinite chains and the only VOF material with a 2D connectivity was reported only very recently.[11] A number of different goals have been set out to exploit this technique of ionothermal synthesis in the preparation of VOFs: initially to investigate whether ILs and DES can replace other solvents in the synthesis of VOFs materials, secondly, whether this technique can be used to synthesise new VOFs materials and thirdly, to try and understand the chemistry behind each step or at least try to identify key factors that may give an indication of how to target materials with more extended networks which could potentially display new and interesting properties. VOFs materials containing reduced vanadium species especially V^{4+} and V^{3+} may display interesting magnetic properties,[12] and hence another aspect of this research is to study the magnetic properties of VOFs synthesised in this work.

The synthesis of organically-templated iron fluorides will also be considered in this thesis. A similar approach to the one described earlier for VOFs materials will be followed. Using ILs and DESs as the solvent may offer new possibilities to develop further iron fluoride chemistry, as the few published studies on the hydrothermal synthesis of hybrid iron fluorides[13,14] revealed poor structural diversity.

The third part of this project comprises an exploration of Ln-MOFs using the ionothermal approach. The combination of the high coordination number of the lanthanide ions with a suitable organic linker in an appropriate IL may lead to the formation of novel materials.

2-2. Characterisation

In order to achieve the goals of this thesis and to ensure continuity and progression of the work, an important part of this project will be to characterise the resulting products. A key technique for characterising these novel materials will be single crystal X-ray diffraction which will be used for the crystal structure determination. Powder X-ray diffraction will also be used for phase identification. Other techniques such as elemental analysis (CHN), thermogravimetric analysis (TGA), and solid state NMR will also be employed when deemed necessary.

2-3. References

(1) Wasserscheid, P.;Welton,T. *Ionic liquids in synthesis*; Wiley-VCH: Weinbeim, 2003.

(2) Cooper, E. R.; Andrews, C. D.; Wheatley, P. S.; Webb, P. B.; Wormald, P.; Morris, R. E. *Nature* **2004**, *430*, 1012.

(3) Drylie, E. A.; Wragg, D. S.; Parnham, E. R.; Wheatley, P. S.; Slawin, A. M. Z.; Warren, J. E.; Morris, R. E. *Angew. Chem. Int. Ed.* **2007**, *119*, 7985.

(4) Lin, Z.; Slawin, A. M. Z.; Morris, R. E. *J. Am. Chem. Soc.* **2007**, *129*, 4880.

(5) Wei, Y.; Tian, Z.; Gies, H.; Xu, R.; Ma, H.; Pei, R.; Zhang, W.; Xu, Y.; Wang, L.; Li, K.; Wang, B.; Wen, G.; Lin, L. *Angew. Chem. Int. Ed.* **2010**, *49*, 5367.

(6) Zhang, J.; Wu, T.; Chen, S.; Feng, P.; Bu, X. *Angew. Chem. Int. Ed. Engl*. **2009**, *48*, 3486.

(7) Abbott, A. P.; Capper, G.; Davies, D. L.; Rasheed, R. K.; Tambyrajah, V. *Chem. Commun.* **2003**, 70.

(8) Aldous, D. W.; Goff, R. J.; Attfield, J. P.; Lightfoot, P. *Inorg. Chem.* **2007**, *46*, 1277.

(9) Aldous, D. W.; Slawin, A. M. Z.; Lightfoot, P. *J. Solid State Chem.* **2008**, *181*, 3033.

(10) Aldous, D. W.; Stephens, N. F.; Lightfoot, P. *Dalton Trans.* **2007**, 2271.

(11) DeBurgomaster, P.; Ouellette, W.; Liu, H.; O'Connor, C. J.; Yee, G. T.; Zubieta, J. *Inorg. Chim. Acta* **2010**, *363*, 1102.

(12) Johnston, D. C.; Johnson, J. W.; Goshorn, D. P.; Jacobson, A. *J. Phys. Rev. B* **1987**, *35*, 219.

(13) Adil, K.; Saada, M. A.; Ben Ali, A.; Body, M.; Dang, M. T.; Hémon-Ribaud, A.; Leblanc, M.; Maisonneuve, V. *J. Fluorine Chem.* **2007**, *128*, 404.

(14) Ben Ali, A.; Grenèche, J.-M.; Leblanc, M.; Maisonneuve, V. *Solid State Sci.* **2009**, *11*, 1631.

CHAPTER 3

EXPERIMENTAL TECHNIQUES

3-1. Introduction

This chapter gives a basic introduction to the experimental techniques used during this work. Each section presents a background to the technique used, followed by a brief explanation of how it was employed in this work.

3-2. Ionothermal synthesis

The background of ionothermal synthesis[1,2] can be found in Chapter One.

All ionothermal reactions were carried out in a Teflon-lined autoclave (15 mL). A typical synthesis procedure involves mixing the appropriate reaction precursors with the IL or DES. The stainless steel autoclave is then sealed and heated in an oven at the required temperature and time.

For comparison purposes some hydrothermal reactions were also carried out following the same reaction procedure but with the IL replaced by other solvents including water, ethylene glycol and pyridine.

3-3. Single-crystal and powder X-ray diffraction[3-6]

X-ray diffraction is one of the key techniques for the investigation of structural properties of various materials. X-ray diffraction can be performed on a single-crystal (single-crystal X-ray diffraction), which can be considered as the most powerful and informative characterisation technique, as it allows the identification of the molecular structure including atom types, bond lengths, angles and intermolecular contacts with great accuracy. In a similar way X-ray diffraction can be performed on a "powder" sample consisting of a large number of tiny, randomly oriented crystallites (powder X-ray diffraction). The background of the two methods and how they have been used for the characterisation of the materials synthesised in this work is given below.

3-3-1. Background

3-3-1-1. Introduction

Understanding function relies on the knowledge of structure at the atomic level. X-ray diffraction can reliably provide information about the structural organisation of crystalline materials. This technique cannot be performed without the correct X-ray source and the appropriate crystalline material. So why are X-rays and crystals essential for this technique?

The use of electromagnetic radiation to visualise objects requires the radiation to have a wavelength comparable to the smallest features that needed to be resolved. X-rays

radiations have a wavelength similar to the distance between atoms (~ 1 Å), so they are useful to explore atomic structure. While we can detect diffraction from molecules using X-rays, the scattering from a single molecule would be incredibly weak and difficult to detect above the noise level. A crystal can act as an "amplifier" because within a crystal a large number of molecules can be arranged in the same orientation, so that scattered waves can add up in phase and raise the signal to a measurable level.[7]

3-3-1-2. Generation of X-rays

X-rays are generated whenever a stream of high-energy electrons strikes a metal target. In an X-ray tube a stream of electrons from the cathode (metal filament) is focused to strike a metal target (anode). If the electrons in the stream possess sufficient energy, the target emits X-rays. This is caused by collisions between the incident electrons and the inner electron shells of the metal atoms. An inner shell (K shell) electron is expelled, the excited atom almost immediately restores its K shell occupancy with an electron of higher energy from its own outer shells (L, M). As this electron drops from a high energy outer shell into a lower energy inner shell, X-rays are emitted. After excitation the atoms in the metal target undergo L-K or M-K transitions and, correspondingly, emit X-rays at different wavelengths (K_α, K_β).

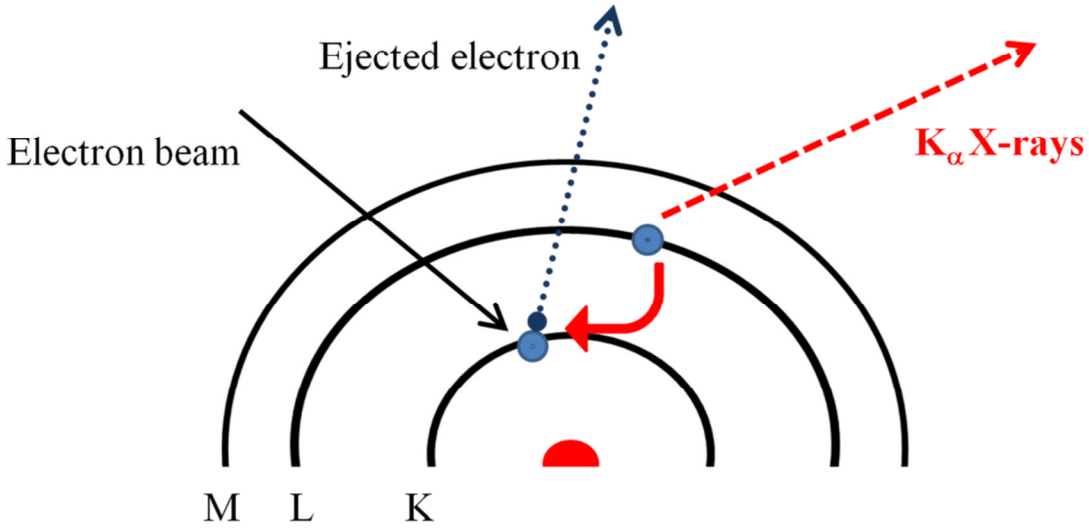

Figure 3-1. Illustration of how K_α X-rays are generated.

K_α exists as a doublet ($K_{\alpha1}$, $K_{\alpha2}$) (as it is illustrated in Figure 3- 2) due to the spin states of the 2p electrons, the wavelength (K_α) used is an average between $K_{\alpha1}$ and $K_{\alpha2}$.

In addition to K_α and K_β an X-ray tube emits radiation with continuous range of wavelengths called Bremsstrahlung as shown in Figure 3-2. For the X-rays to be used, they need to be filtered to produce X-rays of one wavelength (either K_α or K_β).

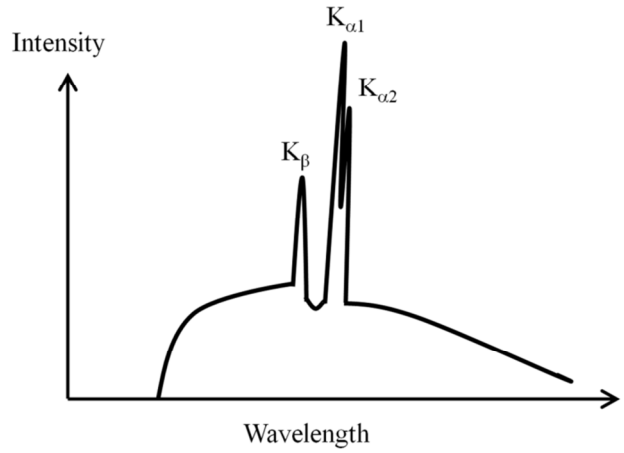

Figure 3-2. A typical X-ray emission spectrum.

X-rays of higher intensity can be obtained from a synchrotron source. Synchrotron radiation is the electromagnetic radiation generated by accelerating relativistic (moving at a speed very close to the speed of light) charged particles through a magnetic field. Figure 3-3 illustrates a typical synchrotron facility, where the charged particles follow a curved trajectory. Electrons are generated in the linear accelerator (linac), and progress into the smaller 'booster' ring, where they are further accelerated up to their final velocity. At this point they are 'injected' into the larger storage ring, where they circulate for a period of hours to days. The electron beam is steered and focused by magnetic fields. At each point where the beam is deflected, electromagnetic radiation is produced tangential to the beam path. These X-rays are focused onto an experimental beamline, where they are used for experiments.

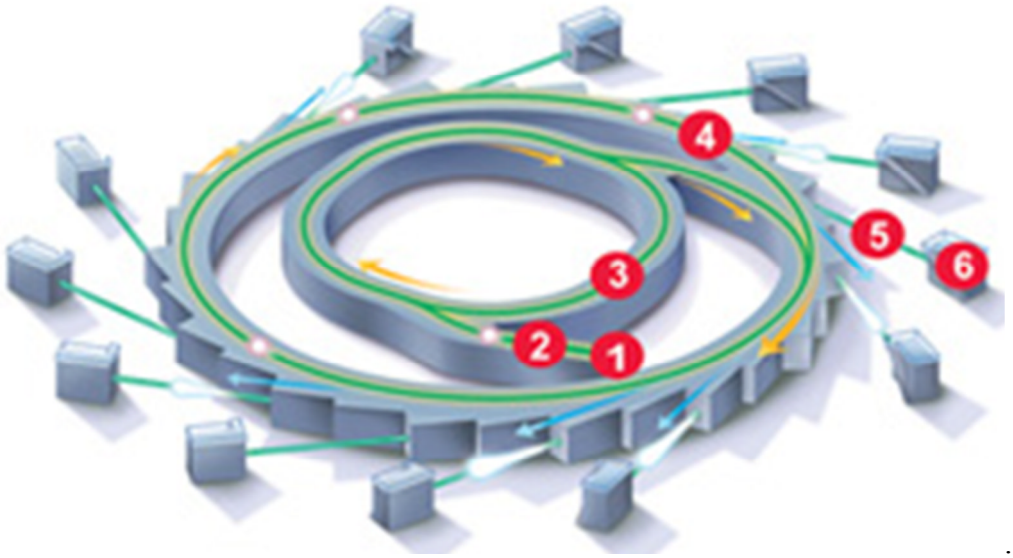

Figure 3-3. Typical components of a synchrotron light source: **(1)** an electron gun, **(2)** a linear accelerator, **(3)** a booster synchrotron, **(4)** a storage ring, **(5)** beamlines, and **(6)** experiment stations.[8]

3-3-1-3. Crystals and crystal chemistry

A crystal consists of atoms arranged in a pattern (single atoms, groups of atoms) that repeats periodically in three dimensions. Crystals are built up from the 3D stacking of unit cells, which are the smallest repeating units that show the full symmetry of the crystal structure.

The unit cell (Figure 3-4) is described by six parameters, the lengths of the unit cell (a, b, c) and the angles between them (α, β, γ).

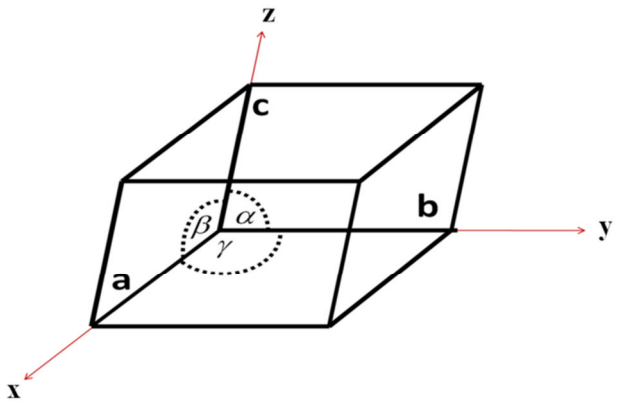

Figure 3-4. Unit cell showing the distances a, b, c along x, y and z and their interaxial angles.

The unit cell can contain one or more repeating motif, called an asymmetric unit, arranged in a pattern characteristic of the set of symmetry operations involved in the crystal structure. Figure 3-5 shows an example of an asymmetric unit that can generate other equivalents units (grey coloured atoms) from which the entire unit cell is built (red box). The unit cell in its turn is repeated or translated indefinitely to produce the whole crystal structure.

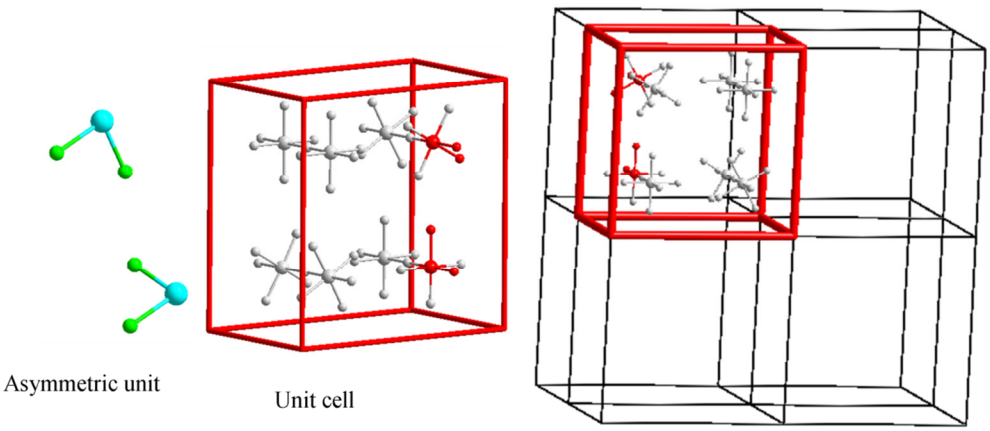

Figure 3-5 . Representation of the asymmetric unit, unit cell and how the unit cell is translated by an integer number to form the whole crystal.

There are seven crystal systems which can be identified by the constraints on the unit cell parameters (a, b, c, α, β, γ) as it is shown in Table 3-1. These seven crystal systems can be expanded into fourteen Bravais lattices by introducing additional centring: face centred (*F*), body centred (*I*) and side centred (*C*).

Crystal systems possess one or more of the ten basic symmetry elements (proper and improper rotation axes); these constitute the 32 point groups. In addition they may present additional translational symmetry elements (lattice centring, screw axes and glide planes) that have no counterpart in molecular symmetry (space symmetry). This combination is called a space group. In total there are 230 space groups and they are fully described in the International Tables for Crystallography.[9]

Table 3-1. The seven different crystal systems

Crystal System	**Bravais Lattice**	**Unit Cell Dimensions**	**Required Symmetry Element**
Triclinic	*P*	$a \neq b \neq c$ $\alpha \neq \beta \neq \gamma$	None
Monoclinic	*P, C*	$a \neq b \neq c$ $\alpha = \gamma = 90° \neq \beta$	Either a mirror plane or a 2-fold axis
Orthorhombic	*P, C, I,* F	$a \neq b \neq c$ $\alpha = \beta = \gamma = 90°$	Any combination of three mutually $\perp$ 2-fold axes or mirror planes
Rhombohedral	*P*	$a = b = c$, $\alpha = \beta = \gamma \neq 90°$	One 3-fold axis
Trigonal	*R*	$a = b \neq c$ $\alpha = \beta = 90°$, $\gamma = 120$	
Hexagonal	*P*	$a = b \neq c$ $\alpha = \beta = 90°$, $\gamma = 120$	One 6-fold axis
Tetragonal	*P, I*	$a = b \neq c$ $\alpha = \beta = \gamma = 90°$	One 4-fold axis
Cubic	*P, I, F*	$a = b = c$ $\alpha = \beta = \gamma = 90°$	Four 3-fold axes

3-3-1-4. Diffraction of X-rays by crystals and Bragg's law

As it was mentioned earlier a crystal is a solid with regular three-dimensional ordering built up of unit cells that contain one or more molecules constructed of atoms. When X-rays interact with a crystal they are scattered by the charged particles (electrons) of the atoms. Because of the orderly arrangement of atoms in a crystal the scattering occurs from what appears to be planes of atoms. The diffraction pattern can only be seen when the scattered waves interfere constructively (in phase). The condition for constructive interference to occur is the path length difference between scatterings from successive atomic planes (xyz = 2d sinθ) must be an integer number of the wavelengths (nλ). This is expressed in Bragg's:

$$n\lambda = 2d \sin\theta \qquad (3\text{-}1)$$

where: θ is the scattering angle (which is also the incident angle), λ is the wavelength and d is the spacing between two atomic planes (A and B) as illustrated in Figure 3-6.

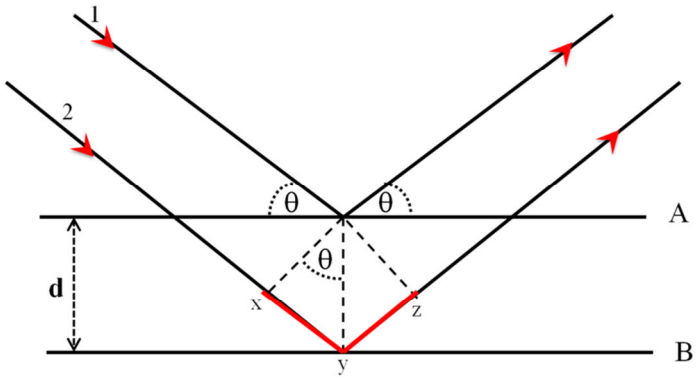

Figure 3-6. The derivation of Bragg's Law.

The interaction of X-rays with electrons in a crystal gives rise to a diffraction pattern (spots), which mathematically is the Fourier transform of the electron density distribution. The structure factor for a reflection can be expressed as a sum of waves scattering from the atomic centres. If the atom locations are known, the structure factor vectors with amplitudes and relative phases for each reflection can be calculated using the following equation:

$$F(hkl) = \sum_{j=1}^{N} f_j \; exp2\pi i(hx_j + ky_j + lz_j) \qquad (3\text{-}2)$$

Similarly the electron density distribution can be expressed by the reverse Fourier transform of the diffraction pattern:

$$\rho(xyz) = \frac{1}{V}\sum_{h,k,l}|F(hkl)|.\, exp[i\varphi(hkl)]\,.\exp[-2\pi i(hx + ky + lz)] \qquad (3\text{-}3)$$

Given the magnitudes of the diffracted waves from a crystal in the form of the structure factor amplitudes $|F_{hkl}|$ and their relative phases (φ_{hkl}), the electron density distribution in the unit cell can be calculated. However, in an X-ray diffraction experiment only the amplitude of the diffracted X-rays is measured, the phase shifts, which are required to use the Fourier transform and find the electron density distribution, are not measurable directly and this is called 'the phase problem'.

There are various approaches that provide a solution to the phase problem, which can be considered as the fundamental problem in crystal structure determination using X-ray diffraction. These approaches have been divided into those that make use of the

effects of atomic scattering on experimental relationships between observed intensities and those that are based on statistical relationships between them. Among these methods, the Patterson function and the direct methods are the most commonly used.

In Patterson function the structure factors represented by their amplitudes $|F(hkl)|$ and phases φ(hkl) are replaced by the squared amplitudes whose values are proportional to the diffraction intensities, with all phases set to zero. This is presented in the following equation:

$$\rho(uvw) = \frac{1}{V}\sum_{h,k,l}|F(hkl)|^2 \cos[2\pi(hx + ky + lz)] \qquad (3\text{-}4)$$

With these modifications the Patterson function can be directly calculated from the experimental data from the diffraction experiment. The information provided by Patterson function corresponds to a map of position vectors (relative position) between each pair of atoms in the structure. These methods are very often successful for the determination of structures containing heavy atoms.

Direct methods retrieve the lost phases from the corresponding diffraction amplitudes. The underlying principle upon which they are based is that the phases of reflections are not independent of one another; in other words the relationships among them are constrained to provide physically meaningful electron density. The correct set of phases must produce a positive electron density, which is localised (atoms occur at discrete points). This leads to statistical relationships among phases of different reflections, and a small set of reliable phases is selected. The most promising phase combinations are

used to generate the structure factors, and hence an electron density map is created by Fourier synthesis.

The Patterson and direct methods described earlier result in the determination of the locations of some or all of the atoms in the unit cell. These locations are determined from maxima in the Fourier map, and are only approximate. A model of the structure (or a portion of the structure) is created by placing spherical atoms at these locations, allowing for the determination of the calculated reflection intensities from the squares of the magnitudes. The parameters of the model that determine the calculated structure factor magnitudes are the atom locations (x,y,z) and the temperature factors or the atomic displacement parameters (ADP's). In order to complete the structure with as much accuracy as possible, the parameters need to be refined to generate calculated intensities that are as close as possible to those observed experimentally. This is accomplished by employing the method of least squares refinement, in which the calculated intensities are compared with the measured intensities. The quality of the model can be judged with the help of various residual factors or (R-factors). These factors should converge to a minimum during the refinement and are to be quoted when a structure is published. The three most commonly used are:

The weighted R-factor based on F^2 (*w*R or *w*R2) given by the following formula:

$$wR = \left[\frac{\sum w\left(F_o{}^2 - F_c{}^2\right)^2}{w\left(F_o{}^2\right)^2}\right]^{1/2} \qquad (3\text{-}5)$$

where F_o and F_c are, respectively, the observed and calculated structure factor, *w* is a weighting factor.

There is also the unweighted residual factor based on F (R or R1) given by the formula:

$$R = \frac{\sum||F_o|-|F_c||}{\sum|F_o|} \quad (3\text{-}6)$$

Goodness of fit (GooF, GOF or S) given by the formula:

$$S = \left[\frac{\sum w\left(F_o{}^2-F_c{}^2\right)^2}{N_R-N_P}\right]^{1/2} \quad (3\text{-}7)$$

where N_R and N_P are, respectively, the number of independent reflections and refined parameters.

Finally, once the refinement is completed with satisfactory R-factors, chemical intuition is required to discern any anomalies in the structure, as the crystal structure must be chemically sensible (otherwise it is wrong).

Nowadays the availability of software packages such as SHELX[10] and SIR,[11] makes the crystal structure solution and refinement routine, provided that the data are collected at a resolution limit that will allow the determination of the location of individual atoms. The major factor affecting crystal structure data is the single-crystal quality, in many cases even if the crystal looks single; it has internal imperfections such as cracks or twinning and sometimes the nice looking crystal is not single and it is actually an aggregate of tiny crystals.

Data quality can be evaluated at the beginning of data collection by collecting a few frames. Diffraction patterns of good quality will feature sharp and unsplit spots (reflections) at a good distance from each other, the spots also go out quite far to the right meaning the crystal diffracts out to high angles (as it is illustrated in Figure 3-7 (left)). In Figure 3-7 (right) there is only low angle diffraction, the spots are very close to each other and the diffraction pattern is smeared this is an indication of poor resolution.

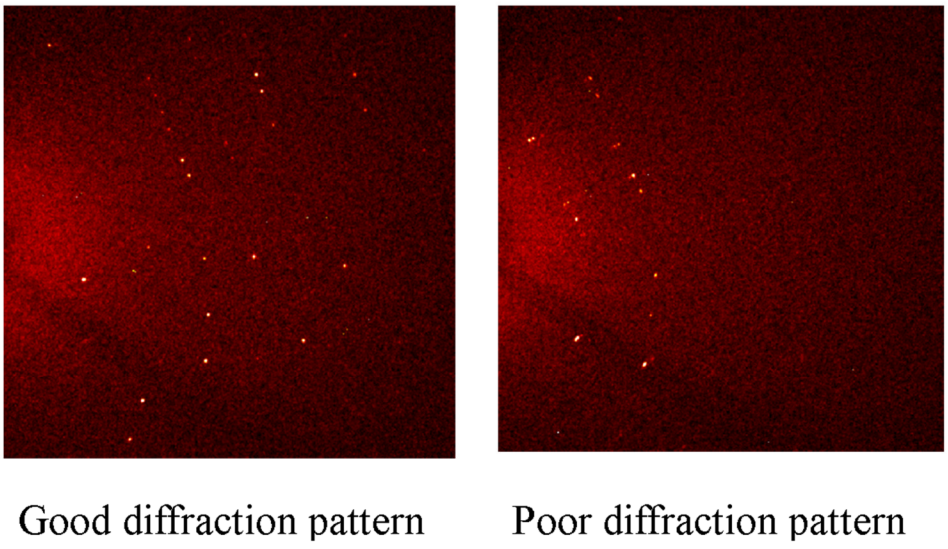

Picture 3-7. An example of a good and poor diffraction pattern.

Once a final model is established, the next step is to confirm that the bulk material is phase pure and can be represented by the single crystal; this can be achieved using powder X-ray diffraction.

3-3-1-5. Powder X-ray diffraction

The powder method is traditionally used to check the sample crystallinity and for phase identification. It can be used for the identification of known phases and also as a complementary technique to single-crystal X-ray diffraction to establish the phase purity of the bulk sample, by comparison the experimental PXRD with the simulated XRD pattern from an individual crystal.

In many cases it is really hard to obtain a single crystal suitable for single crystal XRD and the material is available only in a polycrystalline form, in this case, it is necessary to determine the crystal structure from PXRD. However, solving structures from PXRD data is not a routine yet, and is much more difficult and time consuming than from single-crystal data. The difficulty is arising from peaks overlapping and the loss of information because the available data are a projection of a three dimensional diffraction pattern onto one dimension (radial distance from the reciprocal space origin).

As it stated earlier if a crystal is put in a beam of X-rays it diffracts the X-ray beam and produce a pattern of spots which conform exactly with the internal symmetry of the crystal (Figure 3-8 (left)). If a powder sample consisting of many tiny crystals randomly arranged interacts with the X-ray beam, for every set of crystal planes, there will be one or more crystals that satisfy the Bragg condition. Hence the pattern will be a continuous large number of small spots each from a separate crystal, to give the appearance of a continuous ring (Figure 3-8 (right)).

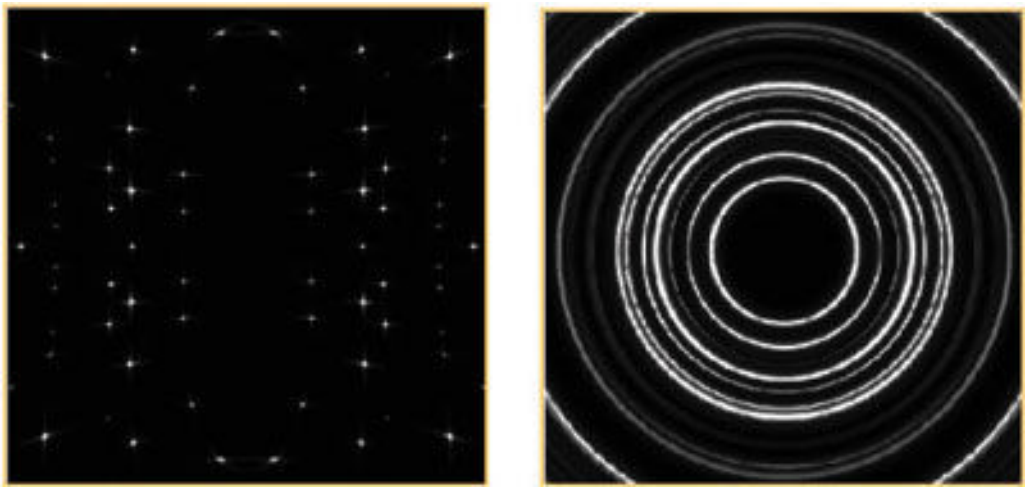

Figure 3-8. X-ray diffraction pattern for single crystal (left) and powder (right).[12]

A typical powder X-ray diffractometer provides a diffraction spectrum consists of a plot of the reflected intensities *versus* the detector angle (2 theta); which is the angle between the incident beam and the reflected beam, from which the d-spacing corresponding to the (h k l) planes that caused the reflection can be calculated (this can be done by the computer associated with the diffractometer).

While crystal determination from PXRD data is still a great challenge, great progress has been achieved in recent years, due to the rapid development of computing facilities and the excellent experimental data with very high resolution that can be obtained using synchrotron radiation. Many published structures have now been solved from powder data. Solving a structure from powder data, in general, starts with indexing the PXRD, then getting the correct space group from the systematic absences, after that the determination of an initial model. Once an initial model is established the Rietveld refinement method[13] can be used to refine the model chosen against the experimental PXRD. The Rietveld method was introduced by Rietveld in 1969. It is not a method

that provides a structure solution, but if a suitable model is available then a powder pattern can be modelled or calculated and the fit between the experimental and the calculated patterns can be optimised. It is based on linear least-squares minimisation on the residual (S) given by the formula:

$$S = \sum w_i |y_{io} - y_{ic}|^2 \qquad (3\text{-}8)$$

where: y_{io}, y_{ic} and w_i are the observed and calculated intensities, and a suitable weight parameter respectively at the *i*th step.

The refinement involves several parameters (*e.g.* background shape, peak shape). Once the model is as close as possible to the experimental, other parameters can also be refined, including the atomic positions and thermal parameters. The reliability of the refinement can be judged by the calculation of several R-factors, the profile R_p and the weighted profile R*wp:*

$$R_p = \frac{\sum |y_{io} - y_{ic}|}{\sum y_{io}} \qquad (3\text{-}9)$$

$$R_{wp} = \left[\frac{\sum w_i (y_{io} - y_{ic})^2}{\sum w_i (y_{io})^2} \right]^{1/2} \qquad (3\text{-}10)$$

R_{exp} is a measure of the data quality, this factor should be close to the refined R_{wp}.

$$R_{exp} = \left[\frac{N-P}{\sum_i^N wi(y_{io})^2}\right]^{1/2} \quad (3\text{-}11)$$

where N and P are, respectively, the number of profile points and refined parameters. This can be illustrated in the goodness of fit function χ. This is a measure of how well the structural model fits the observed data. A value that converges to unity indicates a good refinement.

$$\chi = \left[\frac{R_{wp}}{R_{exp}}\right]^{1/2} \quad (3\text{-}12)$$

Sometimes these factors can be misleading, so it is convenient during the refinement to examine the plot of observed and calculated profiles and the difference between them.

3-3-2. Experimental

Single-crystal X-ray diffraction is the prime technique used in this work for structure determination. Data have been collected either at the University of St Andrews utilising a Rigaku Mercury CCD diffractometer, or for small crystals data have been collected at station 11.3.1 of the Advanced Light Source at Lawrence Berkeley National Laboratory using a Bruker APEX II CCD diffractometer. Structures were solved using direct methods with the program SHELXS and refined on F^2 using full-matrix least-squares with SHELXL-97[10] under WINGX package.[14] CIF files are available for all structures on the accompanying CD.

Powder X-ray diffraction is also an important technique in this work. PXRD has mainly been used to assess the crystallinity of the material and for phase identification, it was used as a complementary technique to single-crystal X-ray diffraction to confirm if the material is phase pure. To confirm the purity of a material, a simulated PXRD pattern is generated by the STOE WinXPOW program using data from the single-crystal refinement and then it is compared to the experimental pattern. In the few cases where the final R-factors from the single-crystal refinement are relatively high, the experimental PXRD is refined using the model from single-crystal X-ray diffraction utilising the Rietveld method within GSAS package.[15] PXRD patterns have been collected using a STOE STADIP diffractometer at the University of St Andrews using monochromated Cu $K_{\alpha 1}$.

3-4. Bond valence sum calculation[16]

In order to confirm the oxidation states of metal centres, the bond valence sum (S_{ij}) was calculated after the determination of each crystal structure. This can confirm the structural model (*e.g.* bond distances and coordination environment around the metal centres), and is also used to discern any disorder in the structure.

The relationship between the bond length (R_{ij}) and the valence (S_{ij}) is given by the following formula:

$$S_{ij} = exp\left(\frac{R_0 - R_{ij}}{B}\right) \qquad (3\text{-}13)$$

where: R_o is a parameter characteristic of the two atoms forming the bond, B is usually take a constant value (0.37 Å). In this work the bond valence sums were calculated using the program Valist.[17]

3-5. Magnetic properties[18]

3-5-1. Background

Charged particles create magnetic fields when in motion. The magnetic moment of an atom may arise from the spin and rotation of the nucleus, from the orbital motion of the electron about the nucleus, or from the spin of the electrons. The nuclear magnetic moments, while they are important in other applications (*e.g.* nuclear magnetic resonance), are negligible in the context of the magnetisation of materials. The magnetic moment of two paired electrons would be effectively cancelled (Pauli exclusion principle). Hence atoms or ions possess an effective magnetic moment, μ_{eff}, proportional to the number of unpaired electrons in their outer shell. The effective magnetic moment is expressed in Bohr Magnetons (given the symbol B.M or μ_B). In the case of first row transition metal ions μ_{eff} is given by the formula:

$$\mu_{eff} = g\sqrt{S(S+1)} \qquad (3\text{-}14)$$

where: g is the Landé factor (for spin only system g ~ 2), and S is the total spin quantum number.

The bulk magnetic properties of materials are usually studied by the measurement of the magnetisation, M, in an applied magnetic field, H. There are various parameters that affect the magnetisation of a material including the strength of the applied magnetic field, H, the temperature, T, the atomic moments and the coupling between moments, J. The magnetic susceptibility, χ, defines the sensitivity of the magnetisation to the magnetic field and is given by the formula:

$$\chi = M/H \qquad (3\text{-}15)$$

The magnetic susceptibility is independent of the magnetic field, and often the molar magnetic susceptibility, χ_M, is preferred in the chemistry community. χ_M is easily calculated when the weight and the formula of the sample are known. The magnetic susceptibility of a sample is composed of two parts; diamagnetic and paramagnetic susceptibility.

$$\chi_M = \chi_{dia} + \chi_{para} \qquad (3\text{-}16)$$

Diamagnetism is a property of all atoms or ions with completely filled orbitals. However, even atoms or ions with unpaired electrons, which are referred as paramagnetic, exhibit some diamagnetism arising from core electrons. Despite the diamagnetic susceptibility being usually small compared to the paramagnetic, it is essential to carry out a diamagnetic correction when the magnetic properties of materials are studied. Diamagnetic corrections can be carried out using Pascals' constants.[19] This technique assumes that the diamagnetic susceptibility can be estimated from atomic or group susceptibilities.

In a paramagnetic material the magnetic susceptibility is inversely proportional to the temperature and can be expressed by the Curie law:

$$\chi = C/T \tag{3-17}$$

where C is the Curie constant and it is given by the formula:

$$C = \frac{Ng^2\mu_B^2}{3k}S(S+1) \tag{3-18}$$

where: N is the Avogadro number, g is the Landé factor (for spin only system g ~ 2), μ_B is the Bohr magneton and k is the Boltzmann constant.

In a paramagnetic material the spins are randomly arranged. However, sometimes in the presence of magnetic field the unpaired electrons can interact with each other, resulting in a particular alignment. If the spins align parallel to one another the material is ferromagnetic, and if the alignment is anti-parallel the material is antiferromagnetic (Figure 3-9).

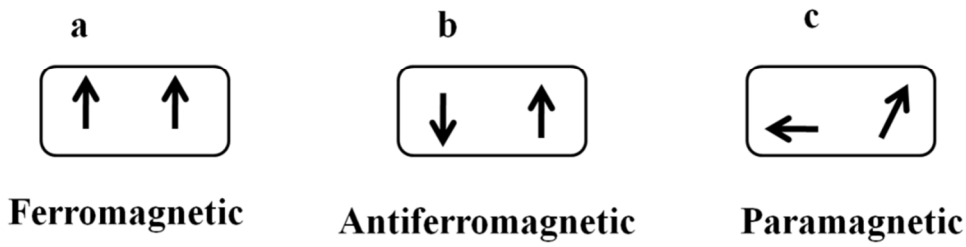

Figure 3-9. Schematic representation of two spins: (a) aligned coparallel (ferromagnetic), (b) aligned anti-parallel (antiferromagnetic), (c) randomly arranged (paramagnetic).

For ferromagnetic or antiferromagnetic materials the ordering occurs below an obvious point which is the transition temperature called, respectively, the Curie temperature (T_C) and the Néel temperature (T_N). Above the transition temperature the material is paramagnetic as it is illustrated in Figure 3-10 below.

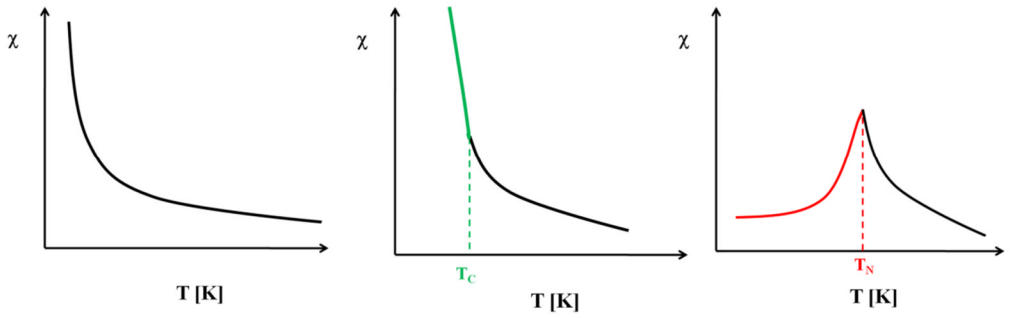

Figure 3-10. Variation of the magnetic susceptibility as a function of temperature for: paramagnetic (left), ferromagnetic (centre) and antiferromagnetic material (right).

In these cases and in the paramagnetic region, above T_C or T_N, the magnetic susceptibility will deviate from the Curie law. Hence the Curie-Weiss law was introduced in order to study the behaviour of the magnetic susceptibility at high temperatures (paramagnetic domain). The Curie-Weiss law is given by:

$$\chi = C/(T - \theta) \qquad (3\text{-}19)$$

Where: θ is the Weiss constant and C is the Curie constant

The value of θ is very important as it reveals the nature of interactions in the material; a positive value indicates ferromagnetic ordering, while a negative value indicates antiferromagnetic ordering. The absolute value, $|\theta|$, gives an indication of the strength of the interactions. From the plot of the inverse of the magnetic susceptibility *versus* the temperature, the Curie and the Weiss constants can be easily extracted as shown in Figure 3-11.

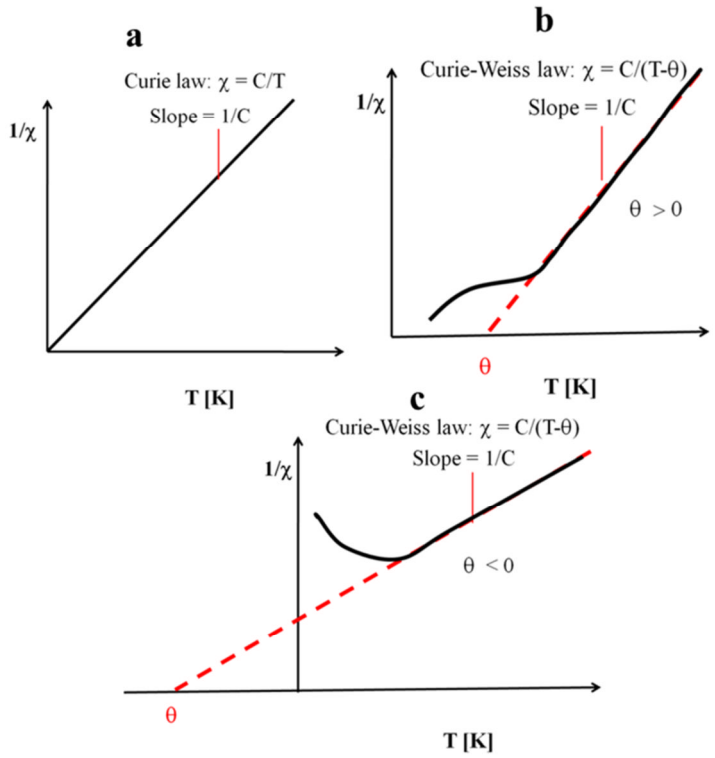

Figure 3-11. Schematic representation of how the Curie and Weiss constants can be extracted from the plot of 1/χ versus T; (**a**): paramagnetic, **b**: ferromagnetic and (**c**): antiferromagnetic.

3-5-2. Experimental

The magnetic properties of some selected materials that have been synthesised in this work have been studied. Magnetic data were collected on a Quantum Design MPMS SQUID using St Andrews University or Edinburgh University facilities. Data were recorded either in a 5000 Oe or 10000 Oe field while warming the sample from 2 to 300 K in 4 K steps, following consecutive zero-field cooling (ZFC) and field cooling (FC) cycles. Data were normalized to the molar quantity of the sample, and corrected for any diamagnetic contributions using Pascal tables.

3-6. Elemental analysis (CHN analysis)

Elemental analysis is based on oxidative combustion of samples and provides the weight percentage of carbon, hydrogen and nitrogen (CHN) or other elements such as sulphur. It is a useful tool to confirm the phase purity of samples. If there is any ambiguity whether the organic template is present in the structure or not, CHN can be used in this case to confirm this.

CHN analysis was carried out using a Carlo Erba 1106 CHN Elemental Analyser at the University of St Andrews.

3-7. Nuclear Magnetic Resonance (NMR) Spectroscopy

NMR is an important technique for the characterisation of compounds in the solution or solid phase. NMR is performed on the nucleus of atoms. Like electrons protons and neutrons can be imagined as spinning on their axes. To be an NMR active a nucleus must possess an overall spin. The overall spin of a nucleus can be determined according to the number of protons (P) and neutrons (N). If N and P are both even they cancel each other and the nucleus has no spin, if N+P is odd the nucleus will have a half integer spin (1/2, 3/2, 5/2) and if N and P are both odd, the nucleus has an integer spin (1, 2, 3). A nucleus with overall spin I will have 2I+1 possible orientations of the magnetic moment. In the case of a nucleus of overall spin, ½, will have two possible orientations of the magnetic moment. If an external magnetic field is applied the spin can align either with or against the field. The distribution between these orientations or energy levels is very small, so they are exposed to energy in the radio frequency (RF) region, which causes a transition from a lower to a higher energy level. After the pulse of RF, the nuclei return to their ground energy state, the nuclei precess back to their start position. This precessing induces a current that is detected using an NMR spectrometer, and by Fourier transform this then will be represented as the frequency spectrum or the chemical shift of the nucleus. The chemical shift is shown in parts per million (ppm). It depends on the fact that electrons in a molecule can deshield the nucleus from the external magnetic field to different degrees causing different nuclei to absorb energy at slightly different frequencies.

Solid state NMR is an important technique for the characterisation of materials, as it is not always possible to dissolve some materials in the typical solvents used for solution NMR. The dominant interactions in solid state NMR are anisotropic in nature, this includes the chemical shift anisotropy and the nuclear dipole-dipole interactions. Unfortunately, these interactions broader the lines and thus causing depletion of the spectral resolution and sensitivity. Various techniques are used to reduce this effect including magic-angle spinning (MAS); this technique involves rotating the sample at high speeds about an axis orientation set at 54.74 ° with respect to the external magnetic field. Cross polarisation (CP) is particularly useful in less abundant spins, *e.g.* ^{13}C and ^{15}N. In this method an abundant spin (^{1}H, ^{19}F) is excited and its energy is transferred to the less abundant spin (^{13}C, ^{15}N). Often this method gives much stronger signal than direct excitation.

^{1}H solution state NMR was a routine method used to characterise the ILs and assess their purity. Measurements were carried out using Bruker Avance 300 and Bruker Avance II 400 spectrometers.

^{13}C Solid state NMR was used in the last chapter to confirm the presence of the organic ligand in Ln-MOFs. ^{13}C CP MAS NMR spectrum was acquired using a Bruker Avance III spectrometer at the University of St Andrews.

A simulated NMR spectrum was obtained using the structural model from single-crystal X-ray diffraction after optimisation of H atomic positions. Calculations were carried out using the EaStCHEM Research Computing Facility.

3-8. Thermogravimetric analysis (TGA)

TGA data are used to investigate the thermal stability of a material. They provide information about the temperatures, T_1 and T_2, at which guest removal and framework decomposition occur. In a typical TGA experiment, under a controlled atmosphere, the weight change of a solid sample is recorded as a function of temperature. The temperature dependent weight loss curves can provide information on the degree of dehydration or desolvation of the studied material, as well as the thermal stability of the guest molecules and the whole material.

TGA has been used in this work to assess the stability of Ln-MOFs. TGA experiments were carried out at the University of St Andrews using a TA Instruments NETZSCH TG 209 Analyser. Samples were heated under argon up to 600 °C at a rate of 10 °C/min.

3-9. References

(1) Morris, R. E. *Chem. Commun.* **2009**, 2990.

(2) Parnham, E. R.; Morris, R. E. *Acc. Chem. Res.* **2007**, *40*, 1005.

(3) Giacovazzo, C. *Fundamentals of crystallography*; Oxford University Press: Oxford, 2002.

(4) Clegg, W. *Crystal Structure determination;* Oxford University Press: Oxford, 1998.

(5) Muller, P. *Crystal Strucrure Refinement: A Crystallographer's Guide to SHELXL*; Oxford University Press: New York, 2006.

(6) Bennet, D. W. *Understanding Single-Crystal X-ray Crystallography*; Wiley-VCH: Weinheim, 2010.

(7) http://www-structmed.cimr.cam.ac.uk/Course/

(8) *Lightsources.org, used with kind permission*

(9) Hahn, T. *International Tables for Crystallography;* Kluwer Academic Publishers: Boston, 1996.

(10) Sheldrick, G. *Acta Crystallographica Section A* **2008**, *64*, 112.

(11) Altomare, A.; Giacovazzo, G. C.; Guagliardi, C. A.; Moliterni, A.G.G.; Burla, M.C.; Polidori G.; Camalli, M.; Spagna, R. *SIR 97 A Package for Crystal Structure Solution by Direct Methods and Refinement*, 1997.

(12) *Polycrystallography.com, used with kind permission*.

(13) Rietveld, H. *J. Appl. Crystallogr.* **1969**, *2*, 65.

(14) *Version 1.80 of WinGX for MS-Windows. Programs for the solution, refinement and analysis of single crystal diffraction data for small*

molecules.

(15) Larson, A.C. ; Von Dreele, R.B. *General Structure Analysis System (GSAS), Los Alamos National Laboratory Report LAUR 86-748* 2000.

(16) Brese, N. E.; O'Keefe, M. *Acta Crystallogr. Sect. B,* **1991**, *47*, 192.

(17) Wills, A. S; *VaList - Bond valence calculation and listing, Version 4.0.6*.

(18) Spaldin, N. A. *Magnetic Materials: Fundamentals and Applications*; Cambridge University Press: Cambridge, 2010.

(19) Bain, G. A.; Berry, J. F. *J. Chem. Educ.* **2008**, *85*, 532.

CHAPTER 4

ILs AND DESs AS NOVEL SOLVENTS FOR THE SYNTHESIS OF VOFs

4-1. Introduction

It is true that the number of ionothermally prepared materials has increased considerably since the first published work on this topic.[1] However there is still much scope for developing this technique for many areas of materials chemistry. Metal fluorides have been recently explored under hydrothermal based media,[2] which has shown some advantages compared to room temperature crystallisation,[3] this points out that different synthesis methods would potentially lead to different materials. Consequently it has been decided to explore the ionothermal synthesis of transition-metal fluorides.

Vanadium is an interesting candidate in that numerous recent reports have demonstrated that vanadium has a rich chemistry owing to its ability to adopt different oxidation states and different coordination behaviour.[4,5] There is great interest in vanadium fluoride compounds owing to their novel structural features and attractive magnetic properties. Vanadium fluorides that crystallise in a non-centrosymmetric space group may exhibit second harmonic generation properties. In this chapter, we will explore thoroughly ionothermal synthesis in order to, initially, test the feasibility of ILs as new solvents for the synthesis of VOFs and then examine the range of products as a function

of different synthesis conditions. Different systems have been investigated by varying the metal source and the fluoride source.

The structures in this chapter are given the codes **VF-1** to **VF-13** in the order they will be discussed here, the symbol **a, b** or **c** is added to the code to differentiate between compounds displaying the same structures but synthesised in different ways. Three ammonium templated structures displaying a 1D type motif (**VF-1a, VF-2a** and **VF-3**) have been isolated from the system V_2O_5/NH_4F. The system V_2O_5/HF in ILs gave the non templated material (**VF-4**), the addition of an organic amine to act as structure directing agent gave three different materials (**VF-5**, **VF-6** and **VF-7a**). After that DESs have been used, and different materials are accessible under different synthesis conditions (**VF-8**, **VF-9**, **VF-10**, **VF-11**, **VF-7b**, **VF-12, VF-1b** and **VF-2b**). The DESs breakdown *in situ* and provide the template for the reaction. **VF-13** and **VF-1c** have been isolated from the system V_2O_5/HF, where the IL BMIM $asp_{1/3}Br_{2/3}$ decomposes to ammonium ions. This exploration allowed us to make some correlations between the synthesis using ILs and DESs. The influence of the reaction conditions will also be discussed. The crystal structures for the new materials will be discussed in detail, however the detailed crystal structures for the known structures included here can be found in the appropriate citations. Magnetic properties of some materials have been studied.

4-2. Synthesis of the ILs

Nowadays, commonly used ionic liquids can be purchased from several commercial sources (Sigma-Aldrich, Fluka, Solvent Innovation) but they are relatively expensive considering the large number of reactions to be carried out. Thus the ILs used in this work have been synthesised in our laboratory from known literature procedures except the IL *N*-butyl phosphonium bromide which was purchased from Solvent Innovation.

4-2-1. Synthesis of 1-ethyl-3-methylimidazolium bromide (EMIM Br, mp = 81 °C)

Under inert atmosphere conditions, degassed ethylbromide (68.43 g, 0.62 mol, Sigma Aldrich) was added to the redistilled *N*-methylimidazole (42.06 g, 0.51 mol, Sigma Aldrich) with constant stirring. This was refluxed initially at 30 °C for 1 hr, then at 40 °C for a further 2 hrs and then cooled to room temperature. Ethyl acetate was added, and the product is crystallised from the solution. It was filtered, washed with ethyl acetate, and dried under vacuum for 24 hrs yielding a white solid. The product was stored under an inert atmosphere. ^{1}H-NMR (400 MHz, D_2O): δ (ppm) 1.40 (t, 3H, CH_3, J = 7.3 Hz), 3.80 (s, 3H, NCH_3), 4.15 (q, 2H, NCH_2, J = 7.3 Hz), 7.38 (d, 2H, NC(H)C(H)N, J = 21.0 Hz), 8.66 (s,1H, NC(H)N). NMR is comparable with literature values.[6]

4-2-2. Synthesis of 1-butyl-3-methylimidazolium bromide (BMIM Br, mp = 78 °C)

Under inert atmosphere conditions, degassed butylbromide (77.64 g, 0.566 mol, Sigma Aldrich) was added to the redistilled *N*-methylimidazole (39.64 g, 0.482 mol, Sigma Aldrich) with constant stirring. This was refluxed at 40 °C for 3 hrs and then cooled to room temperature. Ethyl acetate was added, and the product is crystallised from the solution. It was filtered, washed with ethyl acetate, and dried under vacuum for 24 hrs yielding a white solid. The product was stored under an inert atmosphere. ^{1}H-NMR (400 MHz, D_2O): δ (ppm) 0.9 (t, 3H, CH_3, J = 7.3Hz), 1.2 (m, 2H, CH_2), 1.81 (m, 2H, CH_2), 3.80 (s, 3H, NCH_3), 4.09 (m, NCH_2), 7.38 (d, 2H, NC(H)C(H)N, J = 21.0 Hz), 8.71 (s,1H, NC(H)N). NMR is comparable with literature values. [7]

4-2-3. Synthesis of 1-ethyl-3-methylimidazolium bis(trifluoromethylsulfonyl)imide (EMIM Tf_2N, mp = –3 °C)

EMIM Tf_2N was synthesised according to the literature procedure.[6] EMIM Br (25.33 g, 0.132 mol) was prepared and dried as described in section 4-2-1, then was dissolved in 40 ml of H_2O, after that lithium bis(trifluoromethylsulfonyl)imide (38.07 g, 0.132 mol, Fisher) was added. The mixture was stirred at room temperature for 3 hrs. The aqueous phase was separated from the ionic liquid. After separation of the phases, the ionic liquid was washed several times with small amounts of water until no bromide was detected when testing with silver nitrate. The product was dried under vacuum at 60 °C for 24 hrs yielding a white yellowish liquid.

4-2-4. Synthesis of the IL betainium bis(trifluoromethylsulfonyl)imide (HBet Tf_2N, mp = 57 °C)

HBet Tf2N was synthesised according to the literature procedure.[8] Betaine hydrochloride (51.023 g, 0.332 mol, Sigma Aldrich) was dissolved in 40 mL of H_2O, then lithium bis(trifluoromethylsulfonyl)imide (95.693 g, 0.333 mol, Fisher) was dissolved in 50 mL of H_2O and added to the betaine hydrochloride solution. The mixture was stirred at room temperature for 3 hrs. The aqueous phase was separated from the ionic liquid. After separation of the phases, the ionic liquid was washed several times with small amounts of water until no bromide was detected when testing with silver nitrate. The product was dried under vacuum at 60 °C for 24 hrs yielding a white solid. ^{1}H-NMR (400 MHz, DMSO): δ (ppm) 3.20 (s, 3H, CH_3), 4.30 (s, 2H, CH_2). NMR is comparable with literature values.[8]

4-2-5. Synthesis of the IL *N*-butylpyridinium bromide (BPB, mp = 105 °C)

BPB was synthesised according to the literature procedure.[9] Under inert atmosphere conditions, degassed *N*-butyl bromide (68.43 g, 0.50 mol) was added to pyridine (40.06 g, 0.50 mol) with constant stirring. This was refluxed at 30 °C for 24 hrs. The product was then washed with ethyl acetate and dried under vacuum for 10 hrs yielding a white solid. The product was stored under an inert atmosphere. ^{1}H-NMR (400 MHz, D_2O): δ (ppm) 0.96 (t, 3H, J = 7.2 Hz, CH_3), 1.19-1.3 (m, 2H, CH_2), 1.85-1.93 (m, 2H, CH_2), 4.51 (t, 2H, J = 7.6 Hz, NCH_2), 7.96 (t, 1H, J = 6.6 Hz), 8.44 (t, 2H, J = 7.5 Hz), 8.74(d, 2H, J = 6.8 Hz). NMR is comparable with literature values.[9]

4-2-6. Synthesis of the chiral IL 1-butyl-3-methylimidazolium aspartate (BMIM Asp)

BMIM Asp was synthesised according to the literature procedure,[10] in two steps. The first step consists of exchanging Br^- with OH^- using ion exchange resin and this was followed by neutralisation with aspartic acid.

BMIM Br (40 g, 0.182 mol) was prepared and dried as described in section 4-2-2, then was dissolved in 40 ml of H_2O, after which 40 g of ion exchange resin AMBERSEP 900 OH was added and the mixture was stirred for 24 hrs. The mixture was filtered and the resulting solution was tested with silver nitrate, this step was repeated until no bromide was detected (four times). After that (25 g, 0.187 mol, Sigma Aldrich) of L-aspartic acid was added, this was stirred at RT for another 24 hrs. The solution was filtered to remove the salts, and then excess L-aspartic acid was removed by adding 90 mL of acetonitrile and 10 mL of methanol. The resulting solution was filtered, solvents were evaporated and after that the resulting IL was dried in a high vacuum at 50 °C for 24 hrs.

^{1}H-NMR (400 MHz, DMSO): δ (ppm) 0.9 (t, 3H, CH_3, J = 7.3Hz), 1.2 (m, 2H, CH_2), 1.81 (m, 2H, CH_2), 2.03 (d, 1H, J =11.8Hz), 2.25(d, 1H, J = 8.8Hz), 3.16 (t, 1H, J = 7 Hz),3.80 (s, 3H, NCH_3), 4.09 (m, NCH_2), 7.38 (d, 2H, NC(H)C(H)N, J = 21.0 Hz), 8.71 (s,1H, NC(H)N). NMR is comparable with literature values.[10]

4-2-7. Synthesis of the eutectic mixtures:

The DES choline chloride/urea derivatives was prepared by mixing 5×10^{-3} mol of choline chloride and 10^{-2} mol of the urea derivative in a flask and then heating it until a colourless homogenous liquid formed. This mixture was cooled to RT, forming a white solid in the case of choline chloride/1,3-dimethylurea and choline chloride/ethylene urea (2-imidazolidinone),[11] while a colourless liquid was obtained in the case of choline chloride/2,2,2-trifluoroacetamide.[12] Table 4-1 summarises the three eutectic mixtures used with their corresponding melting points.

Table 4-1. Eutectic mixtures used.

	Amide	Mp (°C)	Quaternary ammonium salt	Mp (°C)	Eutectic mixture mp (°C)
1	1,3-dimethylurea	101-105	Choline chloride	298-305	69 - 71
2	Ethylene urea	129-132	Choline chloride	298-305	69 - 73
3	2,2,2-trifluoroacetamide	72-75	Choline chloride	298-305	~ –30

4-3. ILs as solvents in the synthesis of VOFs

4-3-1. The system V_2O_5/NH_4F in ILs

The idea was to test the feasibility of ILs as solvent for the synthesis of VOFs. Preliminary reactions in this work were carried out in the system V_2O_5/NH_4F.

A typical synthesis procedure was as follows: a Teflon-lined autoclave (volume 15 mL) was charged with V_2O_5 (Sigma Aldrich) and NH_4F (BDH) and then the appropriate IL was added. The stainless steel autoclave was then sealed and heated in an oven to the required temperature and time. The reagents masses, IL used, temperatures and length of time left in the oven are as detailed in Table 4-2. After the autoclave had been cooled to room temperature, the product was filtered, washed with methanol and dried in air for 24 hrs.

Table 4-2. Synthesis details for the preparation of **VF-1a**, **VF-2a** and **VF-3**.

Product	V_2O_5 (g) (mmol)	NH_4F (g) (mmol)	IL: g (mmol)	T (°C)	Time (hrs)
VF-1a	0.182 (1.0)	0.185 (5.0)	EMIM Br : 1.91 (10)	180	72
VF-2a	0.182 (1.0)	0.185 (5.0)	HBet Tf_2N : 3.98 (10)	170	72
VF-3	0.182 (1.0)	0.185 (5.0)	EMIM Tf_2N: 3.91 (10)	170	120

Single-crystal X-ray diffraction data for **VF-1a, VF-2a and V-F3** were collected using Mo-Kα (0.7107 Å) radiation utilising a Rigaku rotating anode single-crystal X-ray diffractometer at the University of St Andrews. The structures were solved with standard direct methods using SHELXS and refined with least-squares minimisation

techniques against F^2 using SHELXL under WinGX packages. All non-hydrogen atoms have been anisotropically refined. The hydrogen atoms for the ammonium cations could be found from the electron density map and refined with N-H distances fixed at 0.86 Å, the H-N-H angles fixed to be as close to tetrahedral as possible.

VF-1a exhibits infinite *trans*-connected chains of corner-sharing $[VF_4F_{2/2}]$ octahedra, the chains are interspersed by ammonium cations, it is the same as the previously reported $(NH_4)_2VF_5$.[13]

VF-2a exhibits infinite *cis*-connected chains of corner sharing $[VOF_3F_{2/2}]$ octahedra, the chains are interspersed by ammonium cations, it is the same as the previously reported $(NH_4)_2VOF_4$.[14]

VF-3 exhibits infinite *trans*-connected chains of corner sharing $[VO_2O_{2/2}]$ tetrahedra, the chains are interspersed by ammonium cations, it is the same as the previously reported NH_4VO_3.[15]

Full details of the three structures can be found in the appropriate citation.

4-3-2. The system V_2O_5/HF in ILs

A typical synthesis procedure was as follows: a Teflon-lined autoclave (volume 15 mL) was charged with V_2O_5 (0.181 g, 1 mmol, Sigma Aldrich) and HF (1 mL, 26.7 mmol, 48% in H_2O, Sigma Aldrich) and then the IL BPB (2.16 g, 10 mmol) was added. The stainless steel autoclave was then sealed and heated in an oven at 150 °C for 5 days. After the autoclave had been cooled to room temperature, the product was filtered, washed with methanol and dried in air for 24 hrs. Brown needle shape crystals were collected (CHN analysis: Calc: %H: 2.77; Found: %H: 2.55).

X-ray diffraction data were collected at station 11.3.1 of the Advanced Light Source at Lawrence Berkeley National Laboratory using a Bruker APEX II CCD diffractometer. The structure was solved using direct methods with the program SHELXS and refined on F^2 using full-matrix least-squares with SHELXL-97 under WINGX package. All non-hydrogen atoms were refined anisotropically. Crystal data and structure refinement datails for **VF-4** are given in Table 4-3. Selected bond lengths and bond valence sums for **VF-4** are tabulated in Table 4-4.

The asymmetric unit in **VF-4** contains two independent V^{3+} cations on special positions, three fluoride ions and two water molecules. The metal cations consist of slightly distorted octahedra made of 4 F^- in plane (similar V-F distances 1.8947(9) - 1.9403(6) and two O atoms in *trans* positions (V-O distances 2.0347(11) - 2.0393(11) Å) as shown in Figure 4-1.

Table 4-3. Crystal data and structure refinement details for **VF-4.**

Compound	**VF-4**
Formula	$VF_3(H_2O)_2$
Fw (g/mol)	143.97
Space group	$P2_1/c$
a /Å	5.5473(5)
b /Å	9.9914(9)
c /Å	7.2050(6)
α /°	90
β /°	107.822(2)
γ /°	90
V / Å^3	380.18(6)
Z	4
Crystal size /mm	0.19 × 0.1 × 0.1
Crystal shape and colour	Brown block
Data collection T/ K	100(2)
F(000)	280
R_{int}	0.0466
Obsd data (I >2σ(I))	985
Data/restraints/parameters	1143/0/74
GOOF on F^2	1.103
R1, *w*R2 (I >2σ(I))	0.0372, 0.1181
R1, *w*R2 (all data)	0.0401, 0.1220
Largest diff. peak / hole	0.817/ –0.839
Oxidation state of V ion	3+

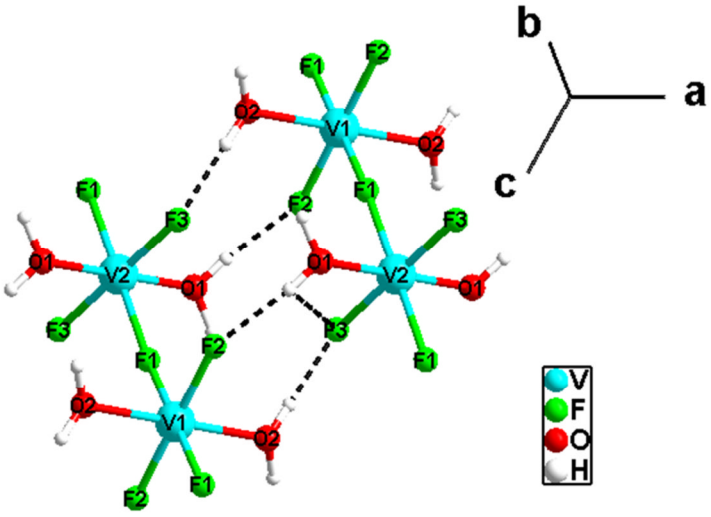

Figure 4-1. *Trans*-connected chains found in **VF-4** viewed in the ac plane.

Short H-bonds (2.6369(17) - 2.6637(17) Å) connect the chains together into a 3D structure; a hexagonal rod packing of these chains along [101] can be found as illustrated in Figure 4-2. Vanadium is in the 3+ oxidation state, as confirmed by the bond valence sum calculations ($\sum V_1 = 3.17$, $\sum V_2 = 3.15$) (see Table 4-4).

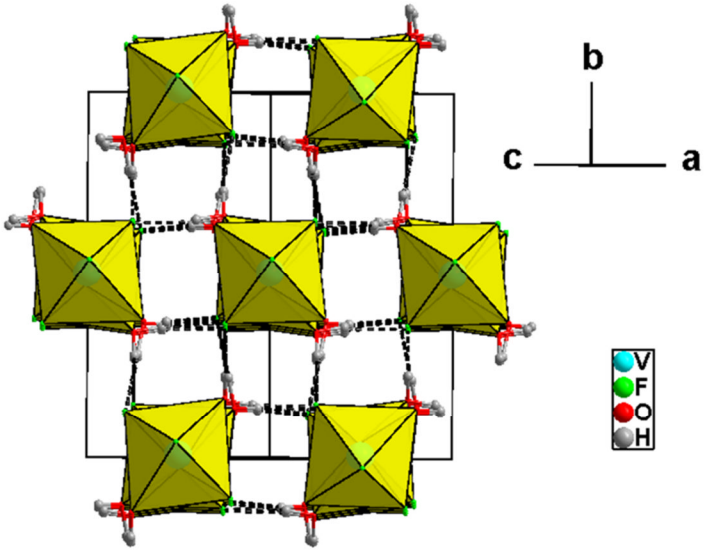

Figure 4-2. A view of **VF-4** illustrating the hydrogen bonds (dotted lines).

Table 4-4. Selected bond lengths and bond valence sums for **VF-4**.

Bond	**Bond Length (Å)**	S_{ij}
V1—F2^{ii}	1.8947 (9)	0.594
V1—F2	1.8947 (9)	0.594
V1—F1	1.9378 (6)	0.529
V1—F1^{ii}	1.9378 (6)	0.529
V1—O2	2.0347 (11)	0.462
V1—O2^{ii}	2.0347 (11)	0.462
		∑V1= 3.170
V2—F3^{i}	1.8947 (9)	0.456
V2—F3	1.8947 (9)	0.456
V2—F1^{i}	1.9403 (6)	0.525
V2—F1	1.9403 (6)	0.525
V2—O1^{i}	2.0393 (11)	0.594
V2—O1	2.0393 (11)	0.594
		∑V2= 3.150
(i) 1–x, –y, 2–z; (ii) –x, –y, 1–z.		

VF-4 shows some interesting magnetic properties. The plot of the magnetic susceptibility, as shown in Figure 4-3, presents two distinct phase transitions, one at low temperature (around 4 K) followed by another one at approximately 40 K, the former is indicating antiferromagnetic interactions, however more low temperature measurements are needed to explain the behaviour of **VF-4**. One suggestion is this is due to small ferromagnetic impurity in the sample, however the data have been collected twice on the same sample and a third time on a newly prepared sample. The question which cannot be answered, unless other measurements or theoretical studies are carried out, is whether this is due to the sample itself or it is due to a reproducible impurity.

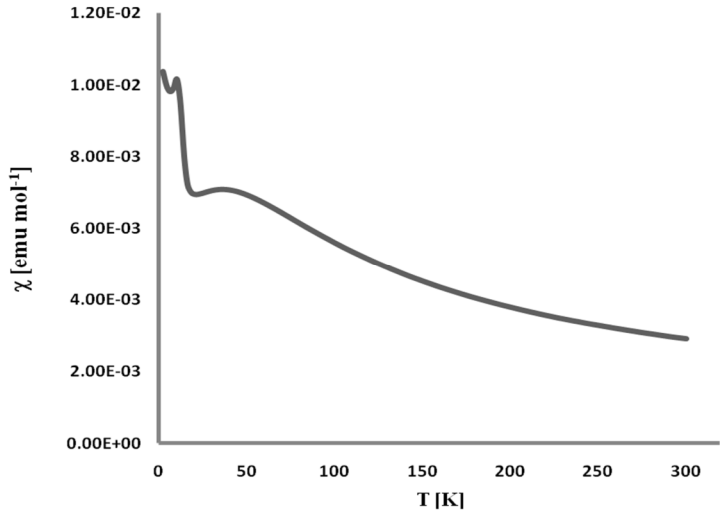

Figure 4-3. A plot of χ *vs* T for **VF-4**.

The chains in **VF-4** are similar to $CuF_2(H_2O)_2pyz$,[16] except the chains in **VF-4** are bridged by F atoms and in $CuF_2(H_2O)_2pyz$ are bridged by the pyrazine ligand. The study of this material has been carried out at various temperatures and supported by electronic structure calculations. It was found that this material exhibits a two dimensional quantum magnet through hydrogen bonded paths as shown in Figure 4-4.

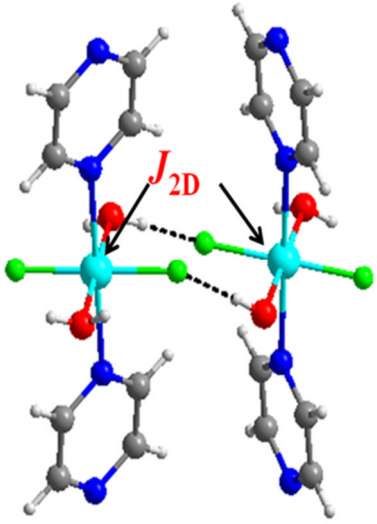

Figure 4-4. The interactions between two Cu sites in $CuF_2(H_2O)_2pyz$.[16]

Another similar example can be found in the system $CuF_2(H_2O)_2$ which has been widely studied in the past. The work of Abrahams,[17] where neutron diffraction at 4.2 K has been undertaken to ascertain the magnetic ordering of $CuF_2(H_2O)_2$ below the Néel temperature, revealed there are antiferromagnetic sheets, which are stacked to give infinite ferromagnetic chains as illustrated in Figure 4-5. The antiferromagnetic Cu-Cu interactions within the sheets are through the paths Cu-O-H.....F-Cu (distance: 5.346 Å), while the ferromagnetic Cu-Cu interaction along the chains is through Cu-F-Cu with a much shorter distance (3.244 Å).

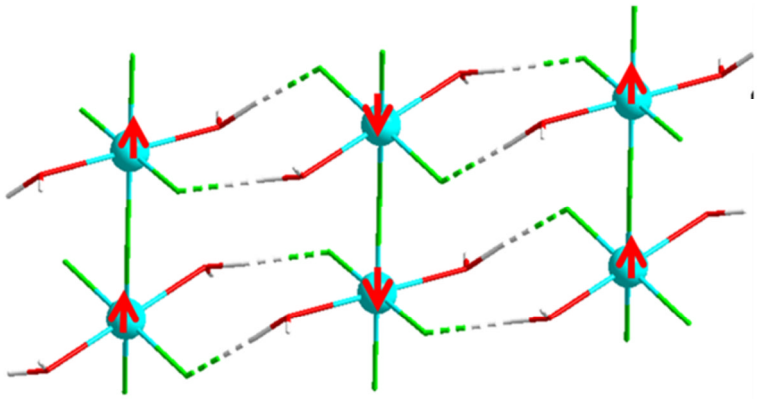

Figure 4-5. Illustration of the magnetic interactions in $CuF_2(H_2O)_2$ at 4.2 K according to Abrahams.[17]

The same pathway must occur in **VF-4** where the antiferromagnetic interactions are mediated by water molecules, however complete low temperature studies of the material would be useful to fully understand and confirm the magnetic properties of **VF-4.**

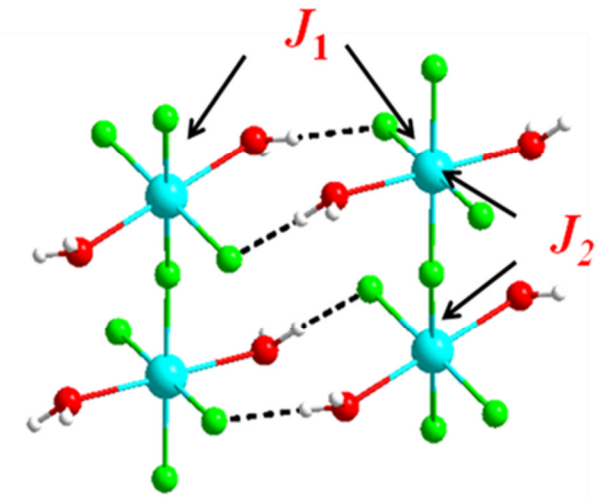

Figure 4-6. Possible V-V interactions at low temperature for **VF-4**.

Above 150 K 1/χ fits well to the Curie-Weiss law (Figure 4-7) with a Weiss constant of –124 K indicating strong antiferromagnetic interactions, this also can be seen in the plot of χT versus T (Figure 4-8) where it does not show any saturation even at 300 K. The experimental effective magnetic moment (μ_{eff} = 3.13 μ_B) is in good agreement with the ideal system of one isolated spin 1 (μ_{ideal} = 2.83 μ_B). This also confirms the BVS of the V atom sites to be 3+.

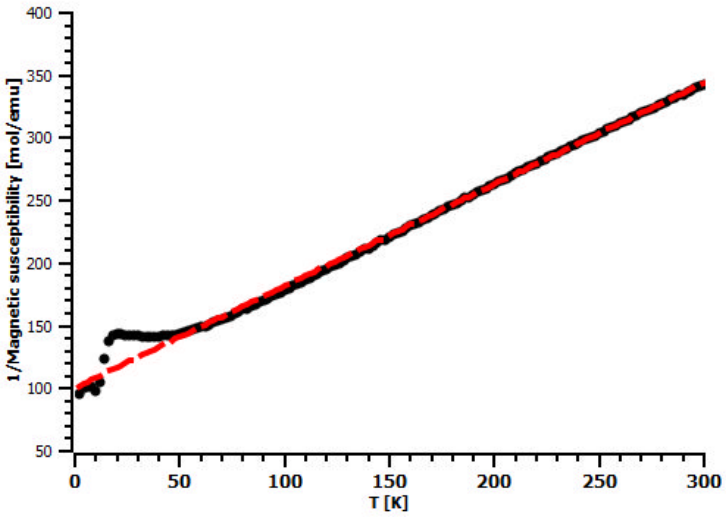

Figure 4-7. Curie-Weiss fit above 150 K for **VF-4.**

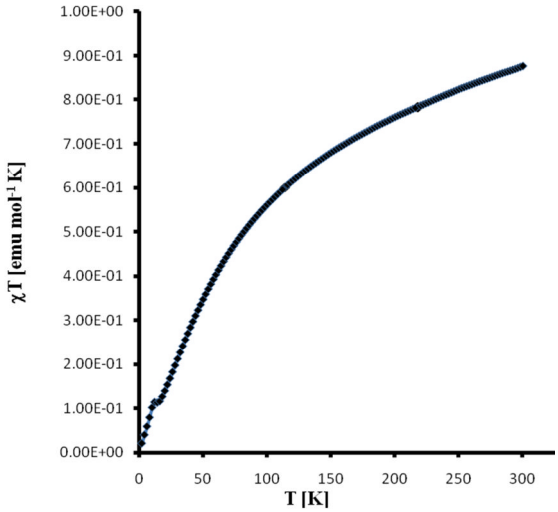

Figure 4-8. Plot of χT *vs* T for **VF-4**.

4-3-3. Adding organic amine to the system V_2O_5/HF/IL

VF-5, **VF-6** and **VF-7a** were synthesised in a similar way, using V_2O_5 (0.182 g, 1 mmol, Sigma Aldrich) and HF (48% in H_2O) (1 mL, 27.6 mmol, Sigma Aldrich). **VF-5** was prepared at 110 °C for 24 hrs using the IL EMIM Br (1.92 g, 10 mmol) as a solvent and (0.168 g, 1 mmol) of tri-(2-aminoethy)amine (*tren*) as an added template, while **VF-6** and **VF-7a** were obtained as mixed phases by heating at 150 °C for 24 hrs using the IL BPB (2.16 g, 10 mmol) and (0.120 g, 2 mmol) of ethylenediamine (*en*) as an added template. After the autoclaves had been cooled to room temperature, the products were filtered, washed with methanol and dried in air for 24 hrs.

Crystal structures for **VF-5**, **VF-6** and **VF-7a** were collected using Mo-Kα (0.7107 Å) radiation utilising a Rigaku rotating anode single-crystal X-ray diffractometer at the University of St Andrews. The structures were solved with standard direct methods

using SHELXS and refined with least-squares minimisation techniques against F^2 using SHELXL under WinGX packages. Crystallographic data and structural refinements for **VF-6** are summarised in Table 4-5, selected bond lengths and bond valences are tabulated in Table 4-6.

Table 4-5. Crystallographic data for **VF-6**.

Compound	**VF-6**
Formula	$[H_2NH_2(CH_2)_2NH_2][V_2O_2F_6]$
Fw (g/mol)	310
Space group	$P2_1/m$
a /Å	8.8060(3)
b /Å	12.1000(5)
c /Å	9.2060(4)
α /°	90
β /°	106.301(2)
γ /°	90
V / Å^3	941.49 (6)
Z	4
Crystal size /mm	0.2 × 0.2 × 0.2
Crystal shape and colour	Blue prism
Data collection T/ K	93(2)
F(000)	608
R_{int}	0.0601
Obsd data (I >2σ(I))	1711
Data/restraints/parameters	1821/0/159
GOOF on F^2	1.181
R1, *w*R2 (I >2σ(I))	0.1077, 0.2376
R1, *w*R2 (all data)	0.1137, 0.2415
Largest diff. peak / hole	1.312/ –1.530
Oxidation state of V ion	4+

Tetramer $[H_3tren]_2[V_4O_4F_{14}]\cdot 3H_2O$ (VF-5):

VF-5 exhibits tetramers units of corner and edge sharing $[VOF_3F_{2/2}]$ octahedra, the tetramers are interspersed by protonated *tren* moieties. The same structure has been previously reported.[18] Full description of the structure can be found in the relevant citation.

Alternating ladder-type $[H_2NH_2(CH_2)_2NH_2][V_2O_2F_6]$ (VF-6):

The building unit in **VF-6 (**solved in $P2_1/m$) is illustrated in Figure 4-9. The asymmetric unit contains two V atoms, seven fluorides, two oxygens one and half of the protonated *en* moieties. The C atom (C3) is disordered over two positions. The two configurations of *en* are as illustrated in Figure 4-10. Both vanadium sites are in a distorted octahedral geometry and show a similar degree of lengthening of the V-F bond (2.226(9) to 2.273(7) Å) caused by the *trans* effect from the vanadyl bond (1.591(12) to 1.617(12) Å).

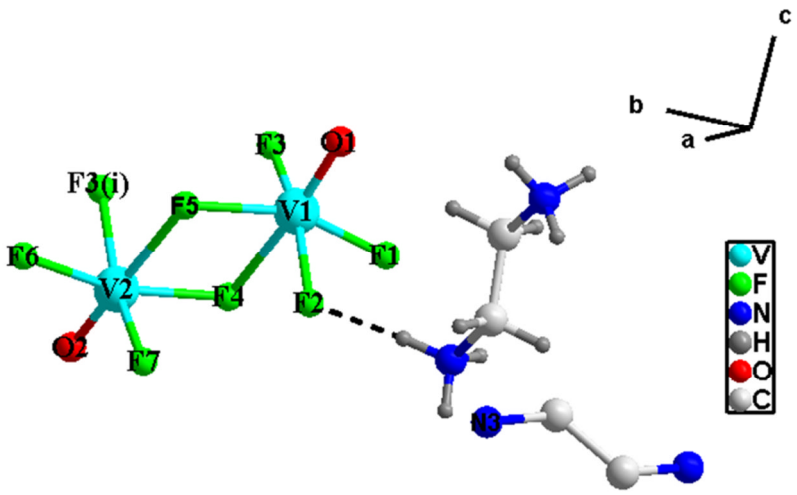

Figure 4-9. The Building unit in **VF-6**. Symmetry operator (i): 1–x, 2–y, 1–z. Note only one configuration of the disordered *en* is shown here.

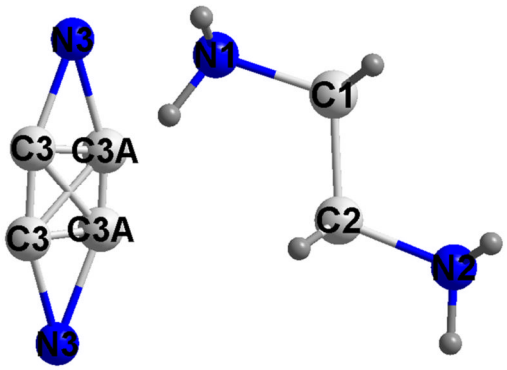

Figure 4-10. Disordered ethylendiammonium cations (left), and ordered (right).

The bond valence sum calculations ($\sum V_1 = 3.69$ amd $\sum V_2 = 3.77$) indicate that both vanadium sites are in the 4+ oxidation state. (see Table 4-6).

Table 4-6. Selected bond lengths and bond valence for **VF-6**.

Bond	**Bond Length (Å)**	***S*$_{ij}$**
V1—F3	1.955(8)	0.502
V1—F4	1.959(8)	0.497
V1—F1	1.988(9)	0.459
V1—F5	1.998 (3)	0.447
V1—F2	2.273 (7)	0.213
V1—O1	1.617 (12)	1.570
		$\sum$V1= 3.688
V2—F7	1.946(9)	0.514
V2—F2	1.987(7)	0.460
V2—F1^{i}	1.987 (9)	0.460
V2—F6	2.031 (4)	0.409
V2—F4	2.226 (9)	0.241
V2—O2	1.591 (12)	1.685
		$\sum$V2= 3.769

(i) 1–x, 2–y, 1–z.

The crystal structure of **VF-6** shows an interesting variation of the typical ladder type previously known for $V_2O_2P_2O_7$[19] and $CsVOF_3$.[2] The octahedra in the ladder in $CsVOF_3$ as shown in Figure 4-11 (right) shared an edge to form the *rung* of the ladder and further shared a corner to form the *rails*. In **VF-6** the octahera shared a corner to form the *rung* and then alternating shared a corner and edge to form that new type of ladder Figure 4-11 (left).

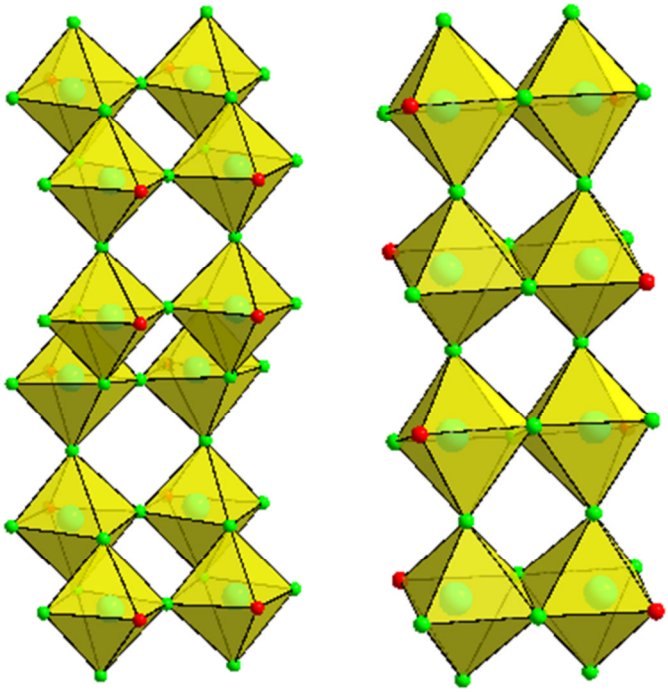

4-11. Alternative ladder type found in **VF-6** (left), and ladder type found in $CsVOF_3$[2] (right).

The protonated *en* cations connect the ladders through H-bonds to the F atoms (2.702(17) - 2.976(17) Å) as illustrated in Figure 4-12.

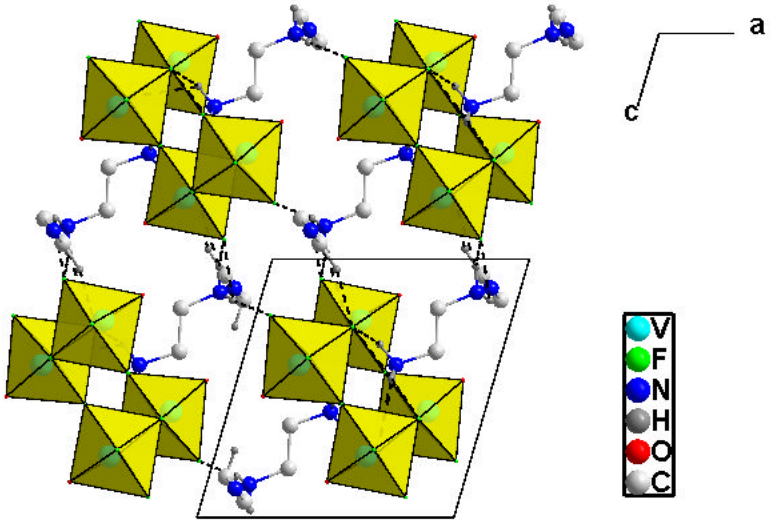

Figure 4-12. VF-6 viewed down the *b* axis, showing how the alternating ladders are connected through hydrogen bonds from the *en* moieties.

While the structure could be solved in the space group $P2_1/m$, however the crystal solution in the polar space group $P2_1$ would lead to a significant improvement in the R-factors (R1 = 0.068, *w*R2 (I >2σ(I) = 0.185) compared to the solution in $P2_1/m$ (R1 = 0.107, *w*R2 (I >2σ(I) = 0.236), moreover the protonated *en* moities do not show any disorder. However this does not confirm that the space group $P2_1$ is correct. The crystal structure has been solved from data collected in house using a standard laboratory X-ray diffractometer, therefore high flux synchrotron radiation is required to obtain better data, for the accurate space group assignment.

Chains $[H_2NH_2(CH_2)_2NH_2][VF_5]$ (VF-7a):

VF-7a exhibits chains of corner sharing $[VF_4F_{2/2}]$ octahera. The chains are interspersed by protonated *en* moieties, and the same structure has been previously reported.[13] Full description of the structure can be found in the relevant citation.

4-4. VOFs synthesis using DESs as solvents and template delivery Agents

The DESs used in this work are a mixture of choline chloride and three different urea derivatives. The DESs were prepared as described in section 4-2. The reactions were carried out at low temperature (110 °C) using different urea sources. The amount of HF was changed until well crystalline materials can be obtained, this was then fixed and the other parameters were varied.

A typical synthesis procedure was as follows: a Teflon-lined autoclave (volume 15 mL) was charged with the appropriate vanadium source, HF, and then the DES was added. The stainless steel autoclave was then sealed and heated in an oven to the required temperature and time (the reagents used and the exact amounts, temperature and time are as detailed in Table 4-7). After the autoclave had been cooled to room temperature, the product was filtered, washed with methanol and dried in air for 24 hrs.

CHN analysis:

$[(HNH_2CH_3)_2][VOF_4(H_2O)]$ (**VF-8**): Calc: %C: 10.66, % H: 6.22, % N: 12.44.
Found: %C: 10.80, %H: 6.96, % N: 12.26.

$[(HNH_2CH_3)_4][V_2O_2F_8]$ (**VF-9**): Calc: %C: 11.59, % H: 5.79, % N: 13.53.
Found: %C: 11.53, %H : 5.69, % N: 12.95.

$[(HNH_2CH_3)_2][VF_5]$ **(VF-10)**: Calc: %C: 11.42, % H: 5.71, % N: 13.33.
Found: %C: 11.49, %H: 6.66, % N: 13.12.

α-$[(H_2NH_2(CH_2)_2NH_2)][VOF_4]$ **(VF-11)**: Calc: %C: 11.70, %H: 4.87, % N: 13.65.
Found: %C: 11.86, %H: 5.16, % N: 13.24.

X-ray diffraction data for **VF-9**, **VF-7b** and **VF-11** were collected at station 11.3.1 of the Advanced Light Source using a Bruker APEX II CCD diffractometer. Structures were solved using direct methods with the program SHELXS and refined on F^2 using full-matrix least-squares with SHELXL-97. All non-hydrogen atoms were refined anisotropically. Hydrogen atoms were placed geometrically on the template molecule where possible.

Single crystal X-ray diffraction data for **VF-8, VF-10**, **VF-12**, **VF-2b** and **VF-1b** were collected using Mo-Kα (0.7107 Å) radiation utilising a Rigaku rotating anode single-crystal X-ray diffractometer at the University of St Andrews. The structures were solved with standard direct methods using SHELXS and refined with least-squares minimisation techniques against F^2 using SHELXL under WinGX packages.

Crystallographic data and structural refinements for **VF-8, VF-9, VF-10, VF-11** and **VF-12** are summarised, respectively, in Table 4-8, Table 4-9 and Table 4-10.

Table 4-7. Synthesis details and conditions for the preparation of the VOF materials.

Product	Reagent used : mass (g) (mol × 10^{-3})			T (°C)	Time (hrs)
	Vanadium source	HF	DES		
VF-8	V_2O_5 : 0.182 (1.0)	1.15 (27.6)	Choline chloride : 0.70 (5) 1,3-dimethylurea : 0.88 (10)	110	48
VF-9	V_2O_5 : 0.182 (1.0)	1.15 (27.6)	Choline chloride : 0.70 (5) 1,3-dimethylurea : 0.88 (10)	110	72
VF-10	$(C_5H_8O_2)_3V$: 0.335(1.0)	1.15 (27.6)	Choline chloride : 0.70 (5) 1,3-dimethylurea : 0.88 (10)	110	72
VF-11	V_2O_5 : 0.182 (1.0)	1.15 (27.6)	Choline chloride : 0.70 (5) 2-imidazolidinone : 0.86 (10)	110	24
VF-7b	V_2O_5 : 0.182 (1.0)	1.15 (27.6)	Choline chloride : 0.70 (5) 2-imidazolidinone : 0.86 (10)	150	24
VF-2b	V_2O_5 : 0.182 (1.0)	1.15 (27.6)	Choline chloride : 0.7 (5) Trifluoroacetamide : 1.13 (10)	110	24
VF-1b	V_2O_5 : 0.182 (1.0)	1.15 (27.6)	Choline chloride : 0.7 (5) Trifluoroacetamide : 1.13 (10)	150	24
VF-12	VOF_3 : 0.124 (1.0)	0.15 (2.76)	Choline chloride : 0.70 (5) 2-imidazolidinone : 0.86 (10)	110	24

Table 4-8. Crystallographic data for compounds **VF-8** and **VF-9.**

Compound	**VF-8**	**VF-9**
Formula	$[(HNH_2CH_3)_2][VOF_4(H_2O)]$	$[(HNH_2CH_3)_4][V_2O_2F_8]$
Fw (g/mol)	225.09	414.15
Space group	$P\bar{1}$	$P\bar{1}$
a /Å	6.932(6)	7.236(6)
b /Å	7.822(6)	9.073(7)
c /Å	8.129(1)	12.154(9)
α /°	110.32(3)	74.189(13)
β /°	90.12(3)	85.589(11)
γ /°	90.95(2)	86.022(11)
V / Å^3	413.3(5)	764.5(10)
Z	2	2
Crystal size /mm	0.21 × 0.09 × 0.09	0.2 × 0.06 × 0.03
Crystal shape and colour	Blue prism	Blue prism
Data collection T/ K	125(2)	150(2)
F(000)	230	420
R_{int}	0.0724	0.0738
Obsd data ($I > 2\sigma(I)$)	1536	2248
Data/restraints/parameters	1629/2/110	3210/3/255
GOOF on F^2	1.193	1.029
R1, *w*R2 ($I > 2\sigma(I)$)	0.0897, 0.1916	0.0634, 0.1467
R1, *w*R2 (all data)	0.0949, 0.1972	0.0994, 0.1612
Largest diff. peak / hole	1.675/–1.051	0.762 /–0.801
Oxidation state of V ion	4+	4+

Table 4-9. Crystallographic data for compounds **VF-10**, **VF-11.**

Compound	**VF-10**	**VF-11**
Formula	$[(HNH_2CH_3)_2][VF_5]$	α-$[H_2NH_2(CH_2)_2NH_2][VOF_4]$
Fw (g/mol)	210.08	205.06
Space group	*Pnma*	$P2_1/n$
a /Å	10.256(3)	14.6312(8)
b /Å	7.899(4)	5.7257(3)
c /Å	9.157(5)	14.6306(8)
α /°	90	90
β /°	90	92.2160(10)
γ /°	90	90
V / Å^3	741.8(6)	1224.75(11)
Z	4	8
Crystal size /mm	0.3 × 0.09 × 0.09	0.2 × 0.02 × 0.02
Crystal shape and colour	Green prism	Blue block
Data collection T/ K	125(2)	150(2)
F(000)	424	824
R_{int}	0.1625	0.0376
Obsd data ($I > 2\sigma(I)$)	734	3358
Data/restraints/parameters	784/0/59	3675/0/182
GOOF on F^2	1.168	1.046
R1, *w*R2 ($I > 2\sigma(I)$)	0.1164, 0.3419	0.0306, 0.0812
R1, *w*R2 (all data)	0.1226, 0.3474	0.0344, 0.0833
Largest diff. peak / hole	0.966/–0.981	0.483 /–0.674
Oxidation state of V ion	3+	4+

Table 4-10. Crystallographic data for compound **VF-12.**

Compound	**VF-12**
Formula	β-$[H_2NH_2(CH_2)_2NH_2][VOF_4]$
Fw (g/mol)	205.06
Space group	*P*4/*ncc*
a /Å	12.7330(5)
b /Å	12.7330(5)
c /Å	8.0300(4)
α /°	90
β /°	90
γ /°	90
V / Å^3	1301.90(10)
Z	8
Crystal size /mm	0.1 × 0.03 × 0.03
Crystal shape and colour	Blue prism
Data collection T/ K	93(2)
F(000)	824
R_{int}	0.0703
Obsd data (I >2σ(I))	491
Data/restraints/parameters	595/0/50
GOOF on F^2	1.263
R1, *w*R2 (I >2σ(I))	0.0541, 0.1305
R1, *w*R2 (all data)	0.0665, 0.1354
Largest diff. peak / hole	0.574 /–0.454
Oxidation state of V ion	4+

Monomer $(HNH_2CH_3)_2VOF_4(H_2O)$ (VF-8):

VF-8 is constructed from one unique vanadium atom, three fluoride ions, one oxygen, one water molecule and two methylammonium cations. **VF-8** consists of pseudo octahedrally coordinated vanadium with one short V=O bond (1.601(5) Å) *trans* to the V-OH_2 bond (2.266(6) Å) with four V-F bonds taking up the remainder of the V coordination sphere (V-F bonds ranging from 1.919(5) to 1.959(4) Å) (see Table 4-11). The V atom is displaced from the centre of $VOF_4(H_2O)$ octahedron towards the vanadyl bond. The bond valence sum calculation ($\sum V_1 = 3.78$) indicates that the oxidation state of the vanadium atom has changed from 5+ to 4+ during the synthesis (see Table 4-11). The monomeric $[VOF_4(H_2O)]^{2-}$ anions form strong hydrogen bonds from the water molecules to F atoms on neighbouring octahedral units (2.655(7) to 2.689(7) Å) to make an infinite chains parallel to the *b* axis. These hydrogen bonded chains are further linked together *via* hydrogen bonds from the methylammonium cations generated *in situ* by the partial breakdown of 1,3-dimethylurea[11] with distances ranging from (2.713(8) to 3.025(8) Å) as shown in Figures 4-13 and 4-14.

This type of unit has been seen in $[H_2en][VOF_4(H_2O)]$[20] but with a different template and a different hydrogen bonding scheme.

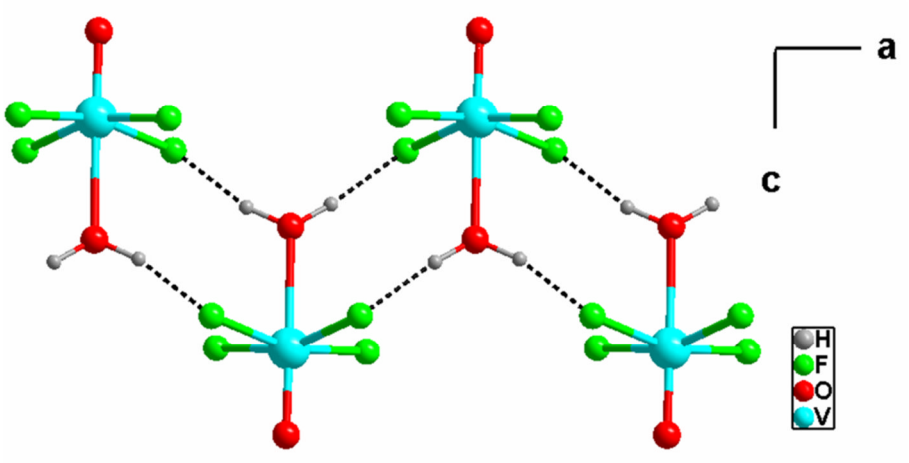

Figure 4-13. The hydrogen bonded chain in **VF-8,** viewed along the *b* axis.

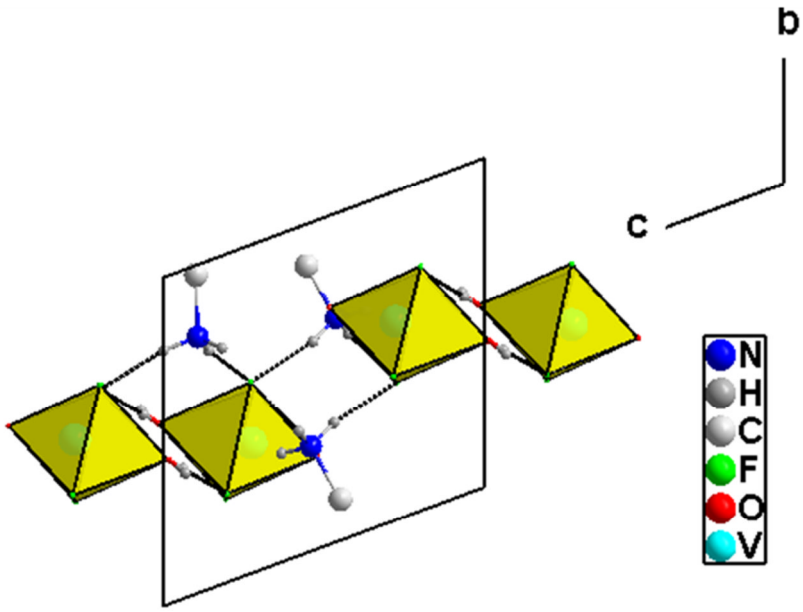

Figure 4-14. Polyhedral view of **VF-8** showing the location of the methylammonium cations and how they are hydrogen bonded (dotted lines) to the polyhedra, viewed down the *a* axis.

Table 4-11. Selected bond lengths and bond valence for **VF-8**.

Bond	**Bond Length (Å)**	S_{ij}
V1—O1	1.601(5)	1.436
V1—F2	1.919(5)	0.553
V1—F4	1.952(5)	0.506
V1—F1	1.944(5)	0.517
V1—F3	1.959(4)	0.497
V1— OW	2.266(6)	0.269
		$\sum$V1 = 3.778

Dimer $[(HNH_2CH_3)_4][V_2O_2F_8]$ (VF-9):

The framework structure of **VF-9** is composed of two distinct vanadium sites, two oxygen atoms, 8 fluorides and four methylammonium cations in the asymmetric unit. **VF-9** is based on a $[V_2O_2F_8]^{4-}$ dimer previously reported for $[C_6N_4H_{22}][V_2O_2F_8]$[18] constructed from $[VOF_3F_{2/2}]$ octahedra in which each octahedron shares a common edge with another (Figure 4-15). The dimer shows a similar degree of lengthening of the V-F bond (2.179(3) to 2.225(4) Å) caused by the *trans* effect from the vanadyl bond (1.588(4) to 1.563(4) Å). The bond valence sum calculations ($\sum V_1 = 4.00$ amd $\sum V_2 = 3.92$) indicate that both vanadium sites are in the 4+ oxidation state (Table 4-13). The protonated methylamine cations, which have been generated *in situ* by the partial breakdown of 1,3-dimethylurea, connect the dimers through hydrogen bonding (2.634(5) - 3.016(6) Å) as it is illustrated in Figure 4-16.

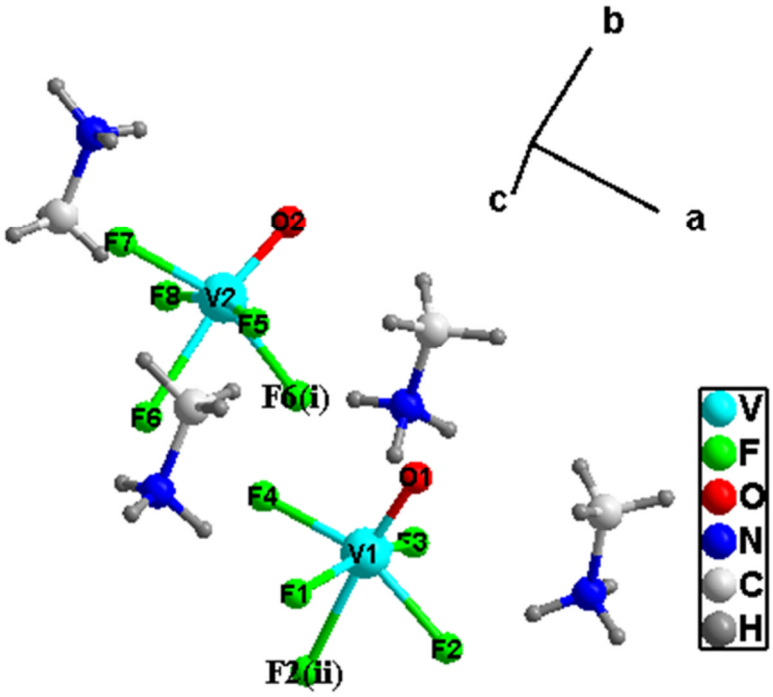

Figure 4-15. The building unit in **VF-9**. Symmetry operators (i): 1–x, 1–y, 2–z; (ii): 2–x, 1–y, 3–z.

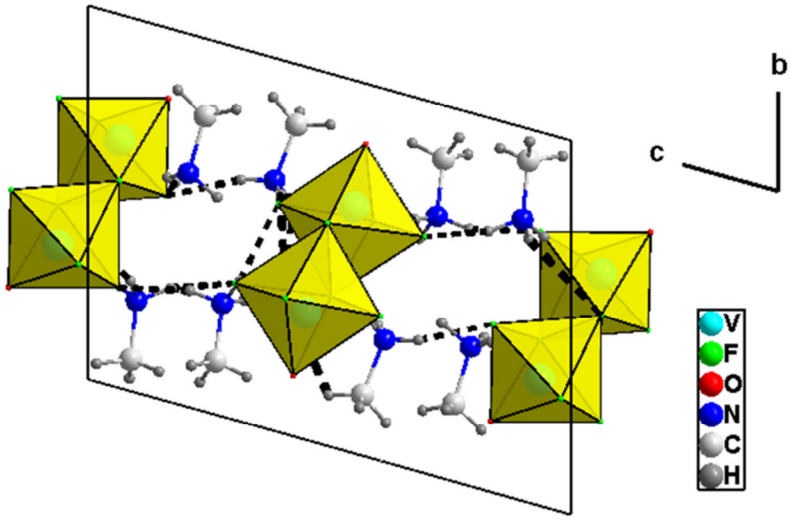

Figure 4-16. The edge sharing dimers in **VF-9** connected through hydrogen bonds *via* methylammonium cations, viewed down the *b* axis.

Table 4-12. Selected bond lengths and bond valence for **VF-9.**

Bond	**Bond Length (Å)**	S_{ij}
V1—O1	1.563(4)	1.592
V1—F2	1.951(3)	0.507
V1—F2^{ii}	2.225(4)	0.242
V1—F1	1.928(3)	0.539
V1—F4	1.907(3)	0.572
V1—F3	1.925(3)	0.544
		∑V1= 3.996
V2—O2	1.588(4)	1.488
V2—F7	1.896(3)	0.587
V2—F5	1.913(3)	0.562
V2—F8	1.939(3)	0.524
V2—F6^{i}	1.971(3)	0.481
V2—F6	2.178(3)	0.274
(i) 1–x, 1–y, 2–z; (ii) 2–x, 1–y, 3–z.		**∑V2= 3.916**

Chains $(HNH_2CH_3)_2VF_5$ (VF-10)

The asymmetric unit of **VF-10** contains one vanadium atom, 3 fluoride ions and two methylammonium cations in the asymmetric unit. The structure consists of infinite zigzag chains of corner-sharing $[VF_4F_{2/2}]$ octahedra (V-F bonds ranging from 1.794(5) to 2.082(6) Å (Figure 4-17). The bond valence sum calculation ($\sum V_1$ = 3.17) indicating that vanadium is in the 3+ oxidation state (Table 4-13). Methylammonium cations, generated *in situ* by the partial breakdown of 1,3-dimethylurea, hold the chains together by an extensive hydrogen bonding (2.648(8) to 3.277(12) Å) (Figure 4-18). This type of chain has been seen in $[C_2N_2H_{10}][VF_5]$[13]

but with a different template and a different hydrogen bonding scheme.

As the R- factors from single crystal diffraction refinement are quite high (this is due to the quality of the single-crystal data), a Rietveld refinement of the experimental PXRD using the model from single-crystal data was carried out, a good refinement was obtained with agreement factors; wRp = 0.0687, Rp = 0.0518, Chi^2 = 1.888). The plot of the Rietvield refinement is illustated in Figure 4-19.

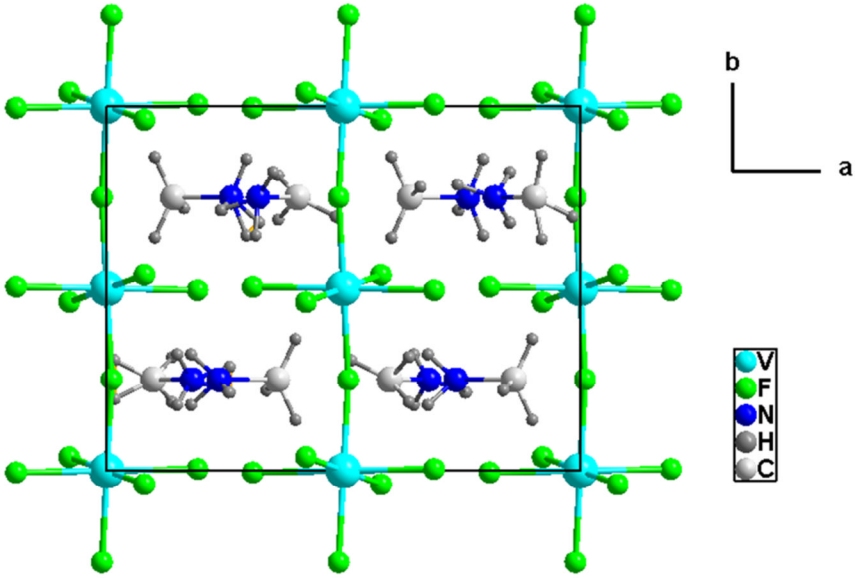

Figure 4-17. The structure of **VF-10** showing isolated chains of corner sharing octahedra running parallel to the crystallographic *b* axis.

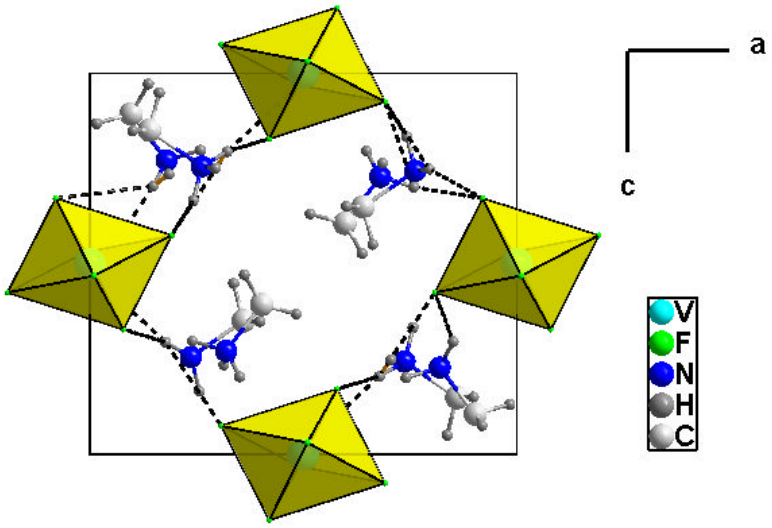

Figure 4-18. The structure of **VF-10** viewed parallel to *b* showing how the methylammonium cations hydrogen bond to the chains.

Table 4-13. Selected bond lengths and bond valence for **VF-10.**

Bond	**Bond Length (Å)**	S_{ij}
V1—F3	1.794(5)	0.780
V1—F3i	1.794(5)	0.780
V1—F1i	1.998(2)	0.449
V1—F1	1.998(2)	0.449
V1—F2	2.082(6)	0.358
V1—F2i	2.082(6)	0.358
(i) –x, 1–y, 1–z		**∑V1 = 3.174**

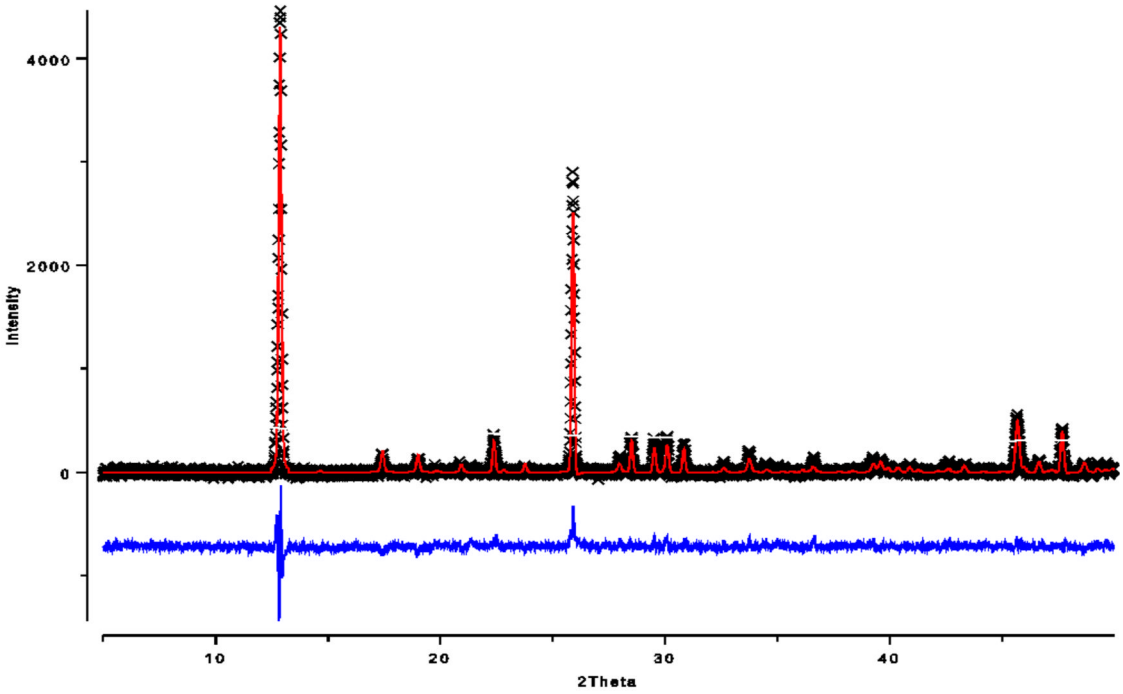

Figure 4-19. The Rietveld refinement of $[(HNH_2CH_3)_2][VF_5]$ (**VF-10**), black crosses indicate experimental data, the red line is the calculated data and the blue line is the difference profile between them.

Chain α-$(H_2NH_2(CH_2)_2NH_2)VOF_4$ (VF-11)

The structure of **VF-11** consists of two vanadium atoms on general positions, two oxygen atoms, eight fluorine atoms and two ethylenediammonium cations in the asymmetric unit. Figure 4-20 shows the building unit in **VF-11**.

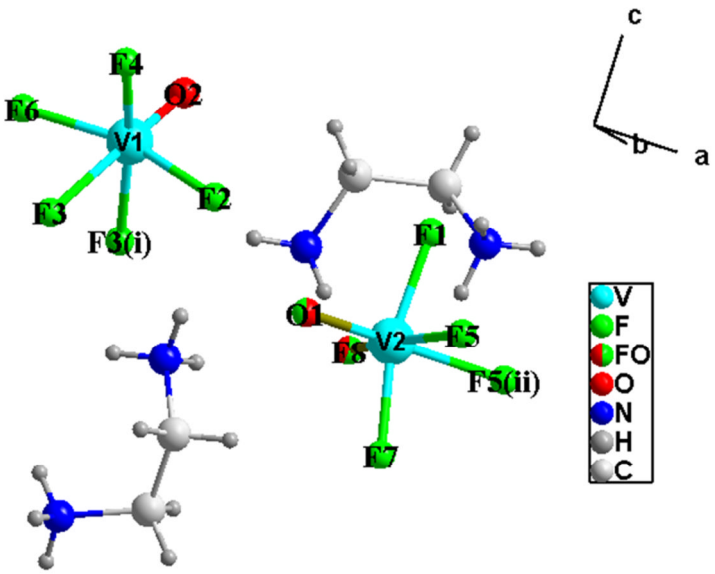

Figure 4-20. The building unit in **VF-11**. Symmetry operators (i): 1.5–x, 0.5+y, 0.5–z; (ii) 2.5–x, 0.5+y, 0.5–z.

Vanadium is in a distorted octahedron due to the presence of the V=O bond. The corner sharing $VOF_3F_{2/2}$ octahedra (via F atoms) are *cis*-connected to form chains (V1 and V2 build separate chains), which are standing almost orthogonal to each other (Figure 4-21), as previously seen in $CsVOF_4$.[21] These chains are different from the one seen in **VF-2a** ($(NH_4)_2VOF_4$), as both are *cis*-connected, however in the former they run anti parallel to each other while in the latter they are running parallel. The non-bonding fluorine and oxygen atoms F8 and O1 which lie in the plane of the chain built by V2 are disordered, having an average length of 1.7442(18) Å on the O1 site (which corresponds to 56% O and 44% F) and an average length of 1.7816(18) Å on F8 site (which corresponds to 44% O and 56% F).

Ethylenediammonium moieties generated by the decomposition of the urea derivative bind the chains together *via* H-bonds to F and O atoms (Figure 4-22).

Vanadium is in the 4+ oxidation state as confirmed by the bond valence sum calculations ($\sum V_1 = 3.88$, $\sum V_2 = 3.64$) (Table 4-14).

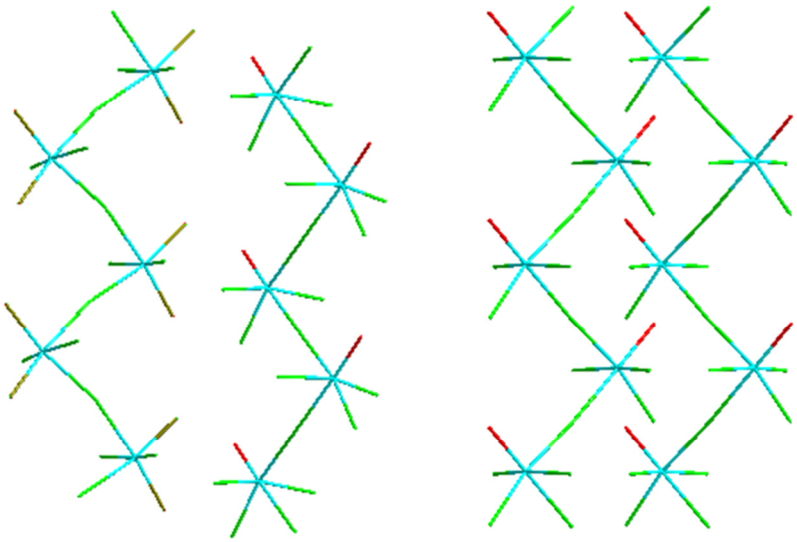

Figure 4-21. *Cis*-connected chains found in **VF-11** in antiparallel fashion (left), *cis*-connected chains found in **VF-2a** in parallel fashion (right).

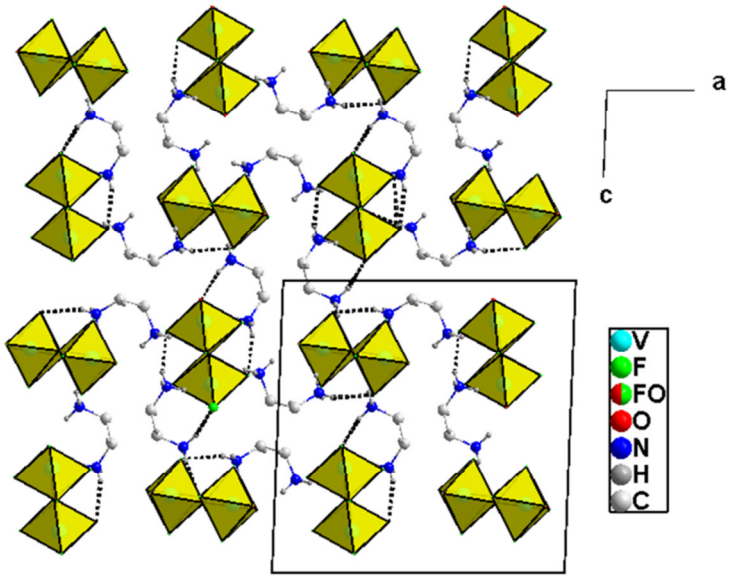

Figure 4-22. Structure of **VF-11** viewed along the *b* axis.

Table 4-14. Selected bond lengths and bond valence for **VF-11.**

Bond	**Bond Length (Å)**	S_{ij}
V1—O2	1.6087(17)	1.599
V1—F4	1.9158(14)	0.561
V1—F6	1.9333(19)	0.533
V1—F2	1.9393(16)	0.523
V1—F3^{i}	1.9894(13)	0.459
V1—F3	2.2858(13)	0.204
		∑V1 = 3.879
V2—O1	1.7442(18)	1.114
V2—F8	1.7806(18)	0.803
V2—F1	1.9180(19)	0.555
V2—F7	1.9180(18)	0.555
V2—F5	2.1165(15)	0.325
V2—F5^{ii}	2.1646(14)	0.285
(i) 1.5–x, 0.5+y, 0.5–z;		**∑V2 = 3.637**
(ii) 2.5–x, 0.5+y, 0.5–z;		
(iii) 1.5–x, -0.5+y, 0.5–z; (iv) 2.5–x, -0.5+y, 0.5–z.		

Magnetic measurements for VF-11.

Above 150 K 1/χ fits well to the Curie-Weiss law (Figure 4-23) with a Weiss constant of +9.32 K indicating ferromagnetic interactions. The experimental effective magnetic moment μ_{eff} = 1.66 μ_B is in good agreement with the ideal system of one isolated spin ½ (μ_{ideal} = 1.73 μ_B). This also helps to confirm the BVS of the vanadium sites as 4+.

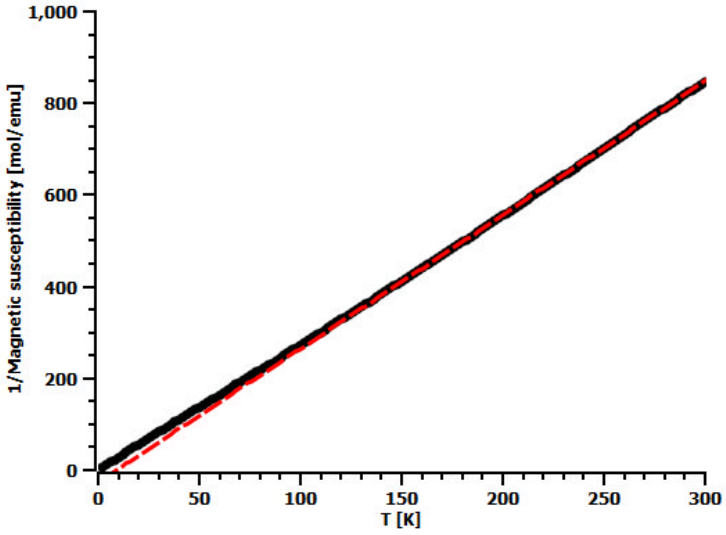

Figure 4-23. Curie-Weiss fit above 150 K for **VF-11.**

Chains β-$[H_2NH_2(CH_2)_2NH_2][VOF_4]$ (VF-12):

Although **VF-12** has the same formula as **VF-11,** it is isostructural with **VF-7a** ($[H_2NH_2(CH_2)_2NH_2][VF_5]$. The same structure type has also been reported for $[H_2en]\cdot[TiOF_4]$[22] and $[H_2en]\cdot[ScF_5]$.[23] It is built up from two types of infinite *trans*-connected chains of corner sharing (*via* O atoms) $[VO_{2/2}F_4]$ octahedra. There are two vanadium atoms, two oxygen atoms, two fluorine atoms and half of the ethylenediammonium cation in the asymmetric unit.

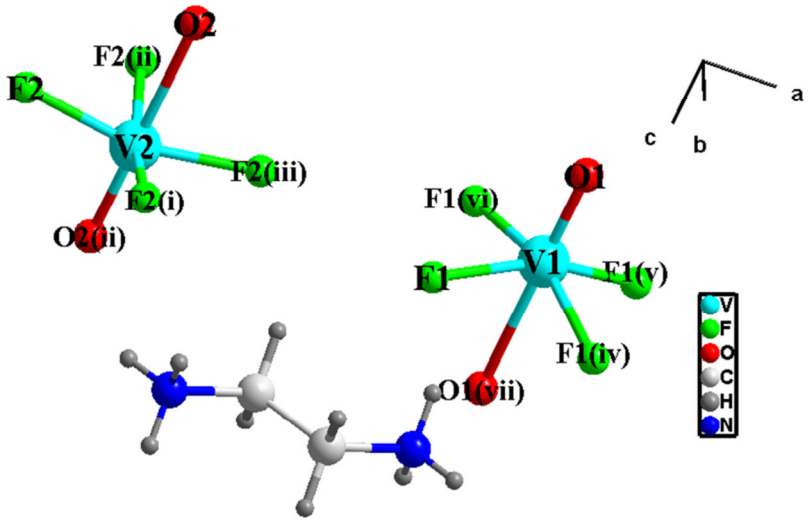

Figure 4-23. The building unit in **VF-12**. Symmetry operators (i) –y, –x, 0.5–z; (ii) –0.5+y, 0.5+x, 0.5–z; (iii) –0.5–x, 0.5–y, z; (iv) y, 0.5–x, z; (v) 0.5–x, 0.5–y, z; (vi) 0.5–y, x, z; (vii) 0.5–x, y, 0.5+z. Note Only one position of V2 is shown here.

Both vanadiums are shifted from the centre of their coordination octahedra due to the "vanadyl" V=O bond. The O atoms bridge the neighbouring octahedra creating chains (V-O distances : 1.703(2) – 2.388(6) Å), while all the F atoms are terminal, having similar V-F bond lengths (around 1.91 Å) (Figure 4-23). It is worth noting that V2 is disordered over two equivalent alternative positions (Figure 4-24). One chain is in an eclipsed conformation, and the other is in a staggered conformation (Figure 4-25) as occurs in **VF-7a**. F atoms are engaged in an extensive H-bond network (2.654(4) – 3.130(5)Å). The bond valence sum calculations ($\sum V_1 = 3.73$, $\sum V_2 = 3.59$) (Table 4-15) indicate possible F/O disorder in the structure.

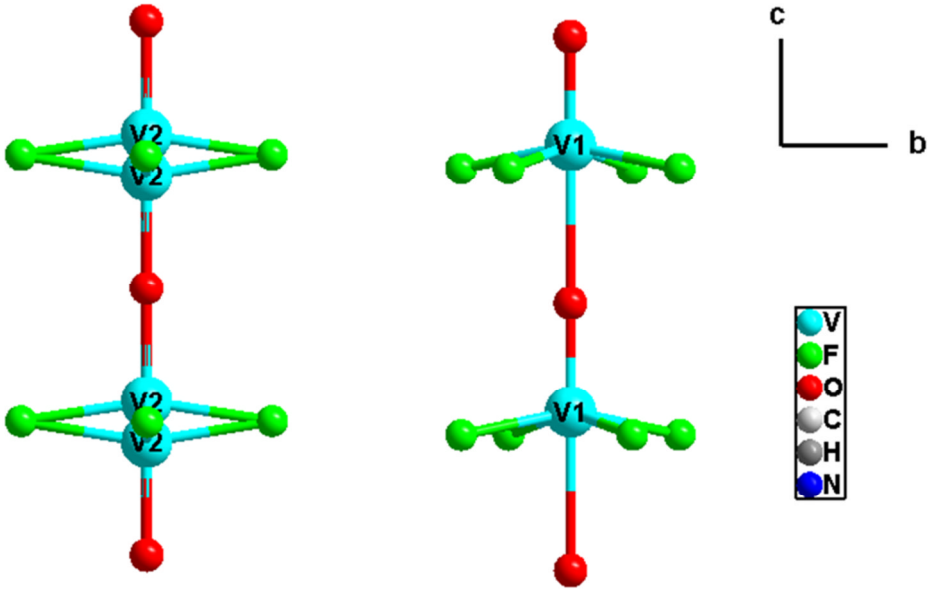

Figure 4-24. A view of **VF-12** showing the disordered chain (left) and the ordered chain (right).

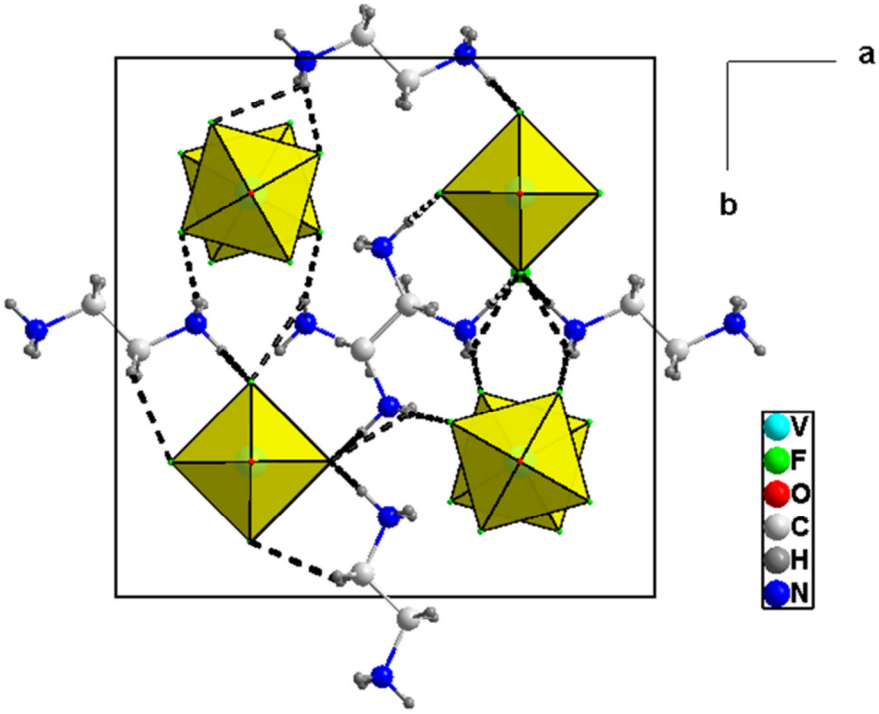

Figure 4-25. The packing of **VF-12** as viewed down the *c* axis showing the eclipsed and staggered chains and how they are hydrogen bonded to the ethylenediammonium cations.

Table 4-15. Selected bond lengths and bond valence for **VF-12.**

Bond	**Bond Length (Å)**	S_{ij}
V1—O1	1.627(6)	1.338
V1—F1^{iv}	1.917(3)	0.556
V1—F^{v}	1.917(3)	0.556
V1—F1	1.917(3)	0.556
V1—F1^{vi}	1.917(3)	0.556
V1—O1^{vii}	2.388(6)	0.171
		∑V1 = 3.733
V2—O2^{ii}	1.703(2)	1.090
V2—F2^{ii}	1.909(3)	0.568
V2—F2^{i}	1.909(3)	0.568
V2—F2	1.912(3)	0.564
V2—F2^{iii}	1.912(3)	0.564
V2—O2	2.312(2)	0.240
		∑V2 = 3.594
(i) –y, –x, 0.5–z; (ii) –0.5+y, 0.5+x, 0.5–z; (iii) –0.5–x, 0.5–y, z; (iv) y, 0.5–x, z; (v) 0.5–x, 0.5–y, z; (vi) 0.5–y, x, z; (vii) 0.5–x, y, 0.5+z.		

Synthesis of $(NH_4)_2VOF_4$ (VF-2b) and $(NH_4)_2VF_5$ (VF-1b) using the eutectic mixture choline chloride/2,2,2-trifluoroacetamide

The two previously reported compounds $(NH_4)_2VOF_4$ and $(NH_4)_2VF_5$ named, respectively, **VF-2b** and **VF-1b**, can be synthesised using the same DES (choline chloride/2,2,2-trifluoroacetamide) at two different temperatures. **VF-2b** was synthesised at 110 °C while **VF-1b** was synthesised at 150 °C. In both cases the DES decompose to ammonium cations.

4-5. Synthesis of NH_4VF_4 (VF-13) using a chiral IL

The IL BMIM Asp was synthesised as described in section 4-2.

VF-13 was synthesised in a 15 mL autoclave by mixing (0.182 g, 1 mmol, Sigma Aldrich) of V_2O_5 and (1 mL, 26.7 mmol, 48% in H_2O, Sigma Aldrich) of HF in a mixture containing ~30% of BMIM Asp (1.49 g, ~ 7 mmol of BMIM Br; 0.95 g, ~ 3 mmol of BMIM Asp. The autoclave was sealed and heated in 110 °C oven for 7 days. After cooling to RT the product was washed with methanol, then water to eliminate any unreacted aspartic acid and allowed to dry at RT for 24 hrs, to give brown crystals. CHN analysis: (Calc: % H: 2.78, % N: 9.68; Found: %H: 2.17, % N: 9.09).

Single crystal X-ray diffraction data for **VF-13** was collected using Mo-Kα (0.7107 Å) radiation utilising a Rigaku rotating anode single-crystal X-ray diffractometer at the University of St Andrews. The structure was solved with standard direct methods using SHELXS and refined with least-squares minimisation techniques against F^2 using SHELXL under WinGX packages. Crystallographic data and structural refinements for **VF-13** are summarised in Table 4-16. Selected bond lengths and bond valences are summarised in Table 4-17.

Table 4-16. Crystallographic information for **VF-13**.

Compound	**VF-13**
Formula	NH_4VF_4
Fw (g/mol)	144.98
Space group	*P*4/*nmm*
a /Å	7.5560(5)
b /Å	7.5560(5)
c /Å	6.3290(3)
α /°	90
β /°	90
γ /°	90
V / Å^3	361.34(4)
Z	4
Crystal size /mm	0.03 × 0.03 × 0.03
Crystal shape and colour	Brown prism
Data collection T/ K	93(2)
F(000)	210
R_{int}	0.0457
Obsd data (I >2σ(I))	214
Data/restraints/parameters	253/0/22
GOOF on F^2	1.336
R1, *w*R2 (I >2σ(I))	0.1531, 0.3113
R1, *w*R2 (all data)	0.1737, 0.3219
Largest diff. peak / hole	1.980/ –2.979
Oxidation state of V ion	3+

Table 4-17. Selected bond lengths for **VF-13**.

Bond	**Bond Length (Å)**	S_{ij}
V1—F1	1.869(13)	0.637
V1—F1^{i}	1.869(13)	0.638
V1—F2	1.994(7)	0.454
V1—F2^{i}	1.994(7)	0.454
V1—F2^{ii}	1.994(7)	0.454
V1—F2^{iii}	1.994(7)	0.454
		$\sum$V1 = 3.091

(i) 1–x, –y, 1–z; (ii) 0.5–y, 0.5–x, z; (iii) 0.5+y, -0.5+x, 1–z.

VF-13 contains one vanadium atom, two fluoride ions and two ammonium cations in the asymmetric unit. The vanadium environment is a fairly regular octahedron (V-F bonds ranging from 1.869(13) to 1.994(7) Å), constructed from two equivalent ordered terminal F atoms (F1), and four equivalent bridging F atoms (F2) in a disordered manner. **VF-13** adopts a layer perovskite-like structure (Figure 4-26), consisting of VF_4^- sheets as illustrated in Figure 4-27, these sheets are separated by ammonium cations. Vanadium is in the 3+ oxidation state as confirmed by bond valence sum calculations ($\sum$V1 = 3.09), see Table 4-17.

Related structures to **VF-13** can be found in $CsFeF_4$,[24] $RbFeF_4$,[25] NH_4FeF_4[26] and also in KVF_4.[27] Selected crystal parameters for $CsFeF_4$, NH_4FeF_4, KVF_4 and **VF-13** are highlighted in Table 4-18. $CsFeF_4$ has a very close unit cell to **VF-13** and it has been solved in the same space group (P4/nmm (129)). However in the case of NH_4FeF_4 and KVF_4 both adopt an orthorhombic unit cell with the *c* axis doubled compared to $CsFeF_4$ and **VF-13**.

Table 4-18. Selected crystal parameters for $CsFeF_4$, NH_4FeF_4, KVF_4 and **VF-13**.

	$CsFeF_4$	NH_4FeF_4	KVF_4	**VF-13 (NH_4VF_4)**
Crystal system	Tetragonal	Orthorhombic	Orthorhombic	Tetragonal
Space group	*P4/nmm*	*Pnma*	*Pmcn*	*P4/nmm*
a (Å)	7.7874(10)	7.559(4)	7.591(1)	7.556(5)
b (Å)	7.7874(10)	7.575(4)	7.744(1)	7.556(5)
c (Å)	6.5402(26)	12.754(8)	12.283(2)	6.329(3)

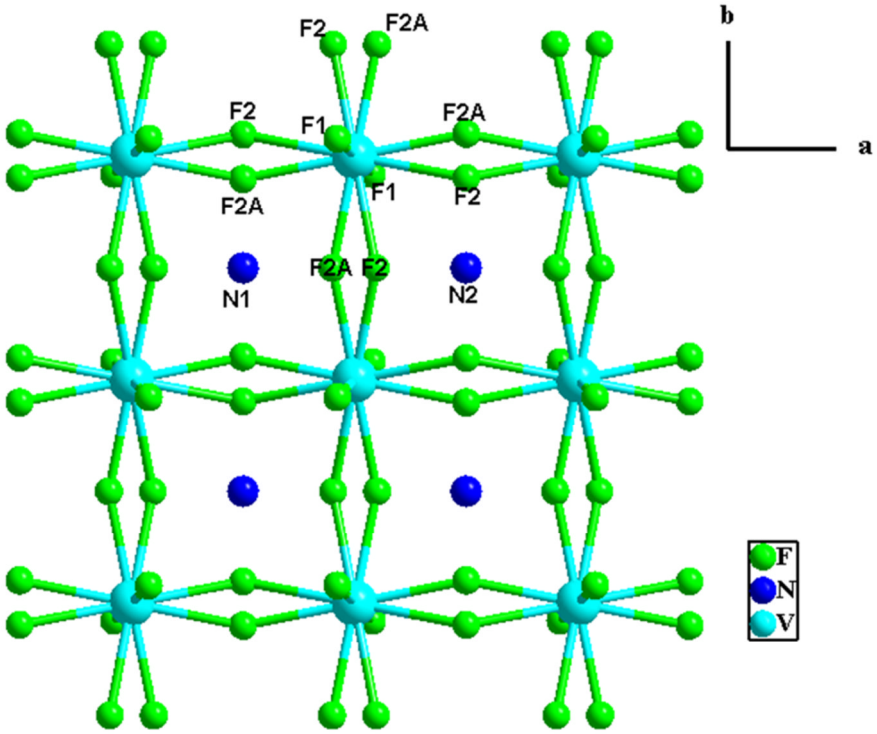

Figure 4-26. A view of **VF-13** showing the disordered bridging F atoms (F2, F2A) and the ordered terminal F1.

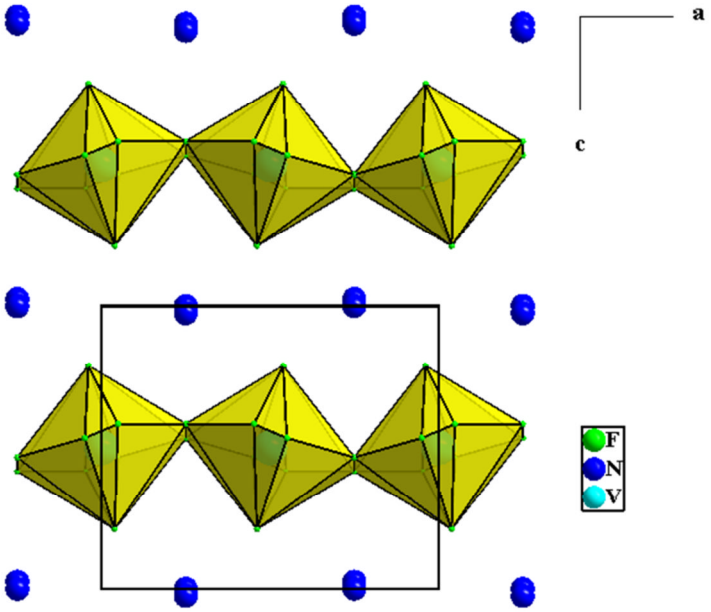

Figure 4-27. Structure of **VF-13** viewed along the *b* axis showing the VF_4^- layers separated by ammonium cations.

While a resonable refinement was obtained in the tetragonal space group *P*4/*nmm*. The disordered fluorine atoms (F2, F2A) are refined isotropically and the hydrogen atoms for the ammonium cations have not been added. In order to get a better refinement, data have been collected several times at low temperature, and also at room temperature to see any phase transitions, all the data sets show the same unit cell, unfortunatly none of them gave a better refinement, and the structure could not be solved from the room temperature data, therefore we could not see if there is any phase transition in the material.

The R-factors are quite high, so a Rietveld refinement of the experimental PXRD (collected at a standard laboratory X-ray diffractometer) using the model from single crystal data was carried out, a good refinement was obtained with agreement factors; wRp = 0.0460, Rp = 0.0350, Chi^2 = 1.305). The Rietveld refinement plot for **VF-13** is illustrated in Figure 4-28.

Further studies of this material using high resolution synchrotron radiations both for single-crystal and powder X ray diffractions at different temperatures, would be very useful in order to confirm the space group assignment and to see the phase transitions, if any, at different temperatures.

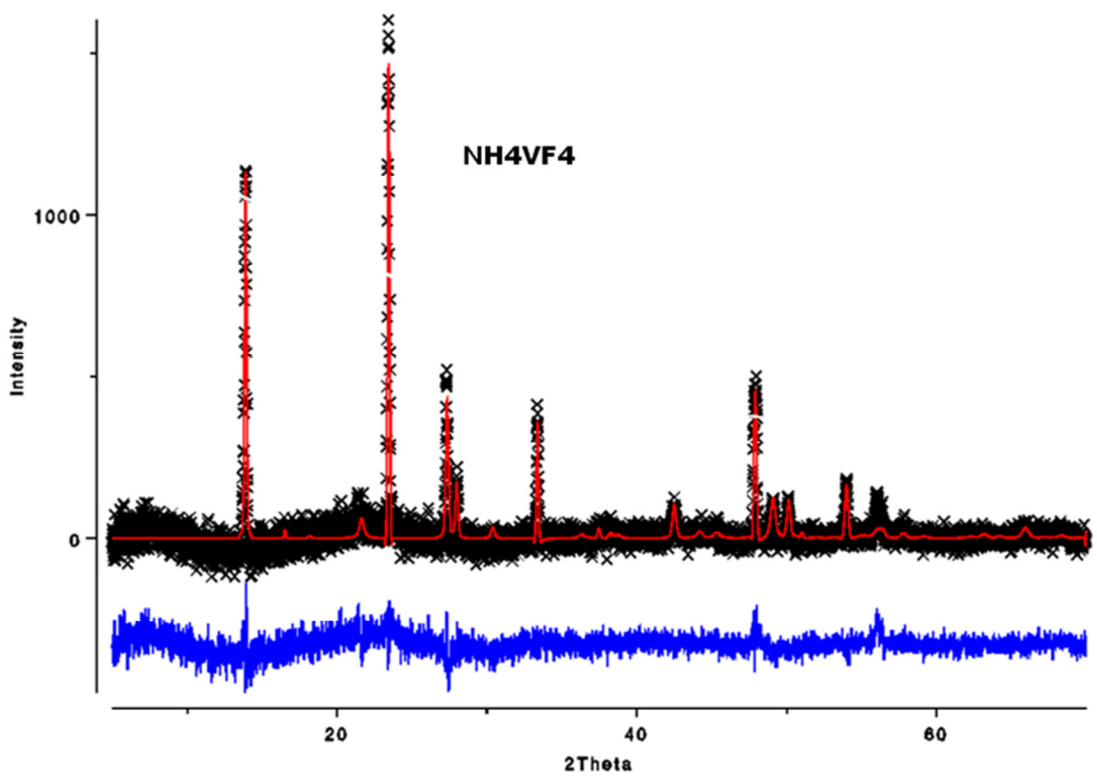

Figure 4-28. The Rietveld refinement of NH_4VF_4 in the tetragonal space group *P*4/*nmm* (black crosses indicate experimental data, the red line is the calculated data and the blue line is the difference profile between them).

Synthetic considerations for VF-13

VF-13 was synthesised from the system V_2O_5/HF using the ionic liquid with the composition BMIM $Asp_{1/3}/Br_{2/3}$ (~30% BMIM Asp/~70% BMIM Br), at low temperature (110 °C) for 7 days. This IL has been used as a solvent for the synthesis of SIMOF-1[28], where it induced chirality in the resulting MOF. For the synthesis of VOFs materials, the IL BMIM $Asp_{1/3}Br_{2/3}$, under the synthesis condition, decomposes to ammonium and therefore does not induce any chirality.

At higher temperature **VF-1c** resulted with the formula $(NH_4)_2VF_5$, this was confirmed by PXRD (see appendix), and CHN analysis; for **VF-1c** (Calc: %H: 4.39, % N: 15.38; Found: %H: 3.93, % N: 14.88) is consistent with two ammonium cations per formula unit, in contrast to **VF-13** (Calc: % H: 2.78, % N: 9.68; Found: %H: 2.17, % N: 9.09) is consistent with only one ammonium cation per formula unit.

This can be explained by the amount of ammonium cations generated *in situ*, by the partial breakdown of the IL, at low temperature the IL will decompose slowly, until we get the right amount to form the layer structure, as no solid product forms if the autoclave is removed before 7 days. However at high temperature the chain type **VF-1c** will form in just 1 day, due to the large amount of ammonium cations formed.

4-6. Concluding remarks

Despite the fact that **VF-1a**, **VF-2a** and **VF-3** are known, one important conclusion from this preliminary work is that ILs can replace other organic solvents for the synthesis of VOFs materials. In order to expand the range of materials accessible in a similar way, we need to finely adjust the chemical environment and rationalise the reaction conditions. These three materials have been synthesised at high temperature (170 °C - 180 °C) and are only templated by ammonium cations. Neither the IL cation nor the anion appeared in the final structure.

By changing NH_4F to HF and using different vanadium sources, a rich phase chemistry which is condition dependent has been observed by the isolation of a series of materials with completely new inorganic frameworks and others with known inorganic frameworks but with a novel template. In this system crystalline materials can be obtained at a temperature as low as 110 °C, more importantly the templating effect could easily be controlled by the selective choice of ILs or DESs.

Using the IL BPB afforded the non templated novel vanadium fluoride hydrate **VF-4,** this material has been isolated using other ILs (BMIM Br, tetrabutyl phosphonium bromide). It is clear that these ILs in the system V_2O_5/HF favour the formation of a non templated material. Although, water is obviously essential for the formation of this material, several reactions have been carried out at the same temperature (150 °C) by replacing the IL with water, varying the reaction time from 1 day to 8 days, but these did not lead to any precipitate.

The ILs used in this study are less likely to be included within the structure, due to the lack of interactions (*e.g.* H- bonds), or due to the amount of water present in the reaction (water arises from HF solution, no water has been added to the reaction) which could disturb the templating effect of the ILs as previously seen in the ionothermal synthesis of zeolites.[11,29] However this is less likely in this case; this is evidenced by the results obtained from the system V_2O_5/NH_4F where no water is present in the reaction (except a very small amount present in the IL even after drying it under high vacuum). These structures are templated only by ammonium cations. This opens up the option of using other type of ILs, the so-called functional ILs, which are ILs with functional groups in the alkyl chain. In this system we believe ILs with the amino functional group could be a good alternative to exhibit this H-bonding.

The addition of an organic template (*tren*, *en*), indeed gave the corresponding organically templated vanadium fluoride or oxyfluoride (compounds **VF-5**, **VF-6** and **VF-7a).**

In the synthesis of VOFs, the DESs serve as template-delivery agents in a controlled manner (Figure 4-29), where the urea portion of the DES breaks down and releases the expected template to the reaction as it is the case in the synthesis of zeolites[11].

Using the DES choline chloride/1,3-dimethylurea (DMU) in which the DMU molecules decompose and provide methylammonium cations to produce the monomeric compound **VF-8** in 2 days, and the dimeric compound **VF-9** in 3 days in which the monomers join together into dimers with F bridging and the exclusion of water molecules. Changing the metal source from V_2O_5 to $V(C_5H_8O_2)_3$ under the same conditions resulted in compound **VF-10** exhbiting chain type structure

templated by methylammonium cations.

Using other DES (choline chloride/2-imidazolidinone) provides compound **VF-11**, exhibiting a chain type motif which has been formed during 1 day at 110 ºC. Changing the urea derivative did actually change the chemistry, with two nitrogen sites in the ethylammonium cation, generated by the decomposition of 2-imidazolidinone, condensing the inorganic framework into chains. At higher temperature (150 °C) the same DES produces **VF-7b**. This structure illustrates in a beautiful way the versatility of the synthesis using ILs and DES, notably to control whether a templated material is produced or not. Using only ILs we can get the non templated material or, if a templated material is needed, we have just to add a templating source in addition to the IL, or simply by using DES instead of IL without adding any other template as illustrated in Figure 4-30.

Fluorinated urea has been used which shows the same pattern as the other non fluorinated urea derivatives and decompose to ammonium to produce the ammonium templated chains **VF-2b** at 110 ºC or **VF-1b** at higher temperature.

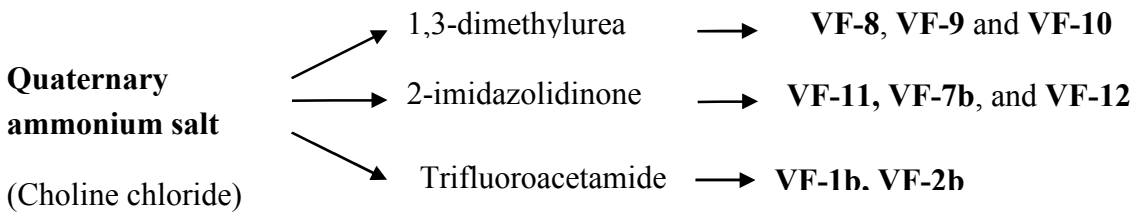

Figure 4-29. The synthesis of VOFs using choline chloride and three different urea derivatives.

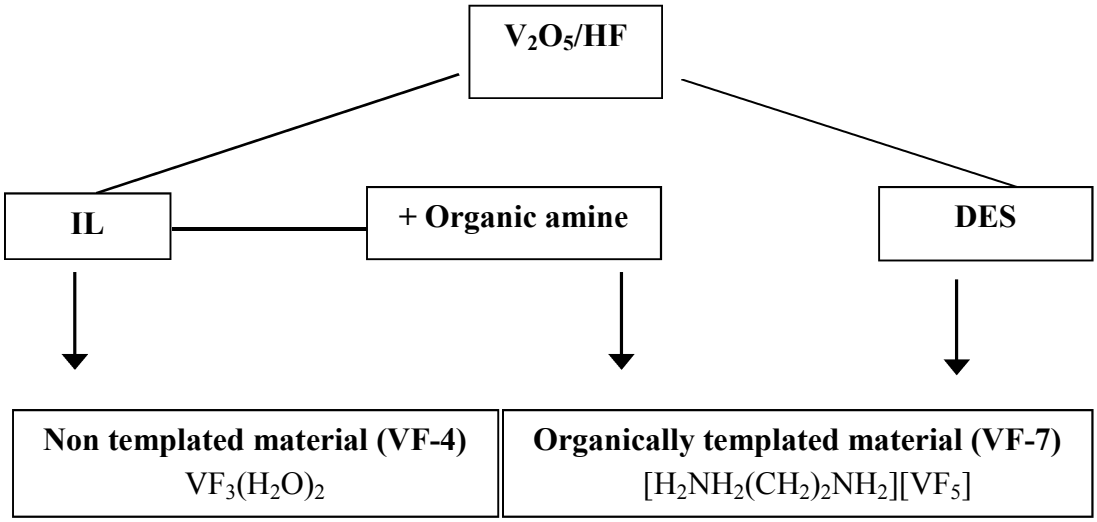

Figure 4-30. Template control in the ionothermal synthesis of VOFs.

In the system V_2O_5/HF/DES, and as reported in the solvothermal synthesis of VOFs and especially in the system V_2O_5/HF/ethylene glycol/piperazine, the temperature does affect the oxidation state of vanadium (as it has been reduced from 4+ to 3+), but does not have any effect on the dimensionality of the material as both materials (**VF-11** and **VF-7b**) are chain types. Water is present in the reaction from the HF solution. In order to understand how this amount of water affects the outcome of the reaction, similar reactions have been carried out by replacing V_2O_5 by VOF_3 and reducing the amount of HF (0.1 mL instead of 1 mL) (thus reducing the amount of water). At 110 ºC this resulted in compound **VF-12**; the amount of water and HF did not affect the oxidation state of vanadium nor the dimensionality but did affect the overall features of the structure. If the amount of HF is increased to 0.5 mL, **VF-11** results. At higher temperature (150 ºC) compound **VF-7b** is obtained. Figure 4-31 shows the three chain type found in **VF-11**, **VF-7b** and **VF-12**.

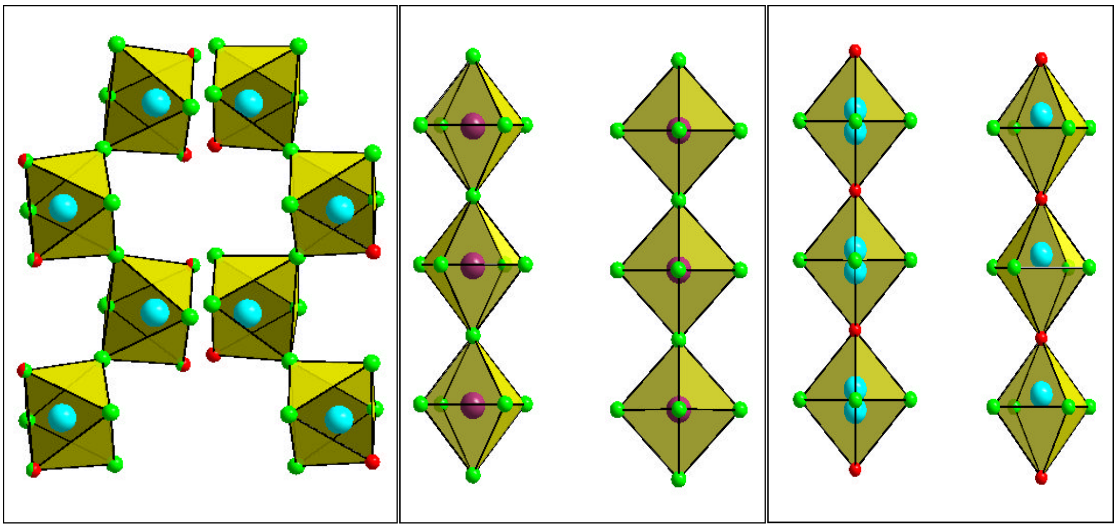

Figure 4-31. Chains type found in **VF-11** (left), **VF-7b** (middle) and **VF-12** (right). (O: red, F: green, V(4+): turquois, V(3+): Brown.

Chiral IL used in this work did not induce any chirality in the resulting VOFs, as it is not stable under the reaction conditions. It decomposes to ammonium to form either the ammoniun templated layer perovskite-like type structure **VF-13**, or the ammonium templated chain type structure **VF-1c**, under different reaction conditions.

The structures presented in this chapter are summarised in Table 4-19, along with their formula, dimentionality and the oxidation state of vanadium ions. References for the known structures are also given.

Table 4-19. Selected structural characteristics of VOFs structures in this chapter.

Identification code	Chemical formula/Ref	Dimensionality	Structural unit	Ox. State
VF-1a **VF-1b** **VF-1c**	$(NH_4)_2VF_5$[13]	1D	*Trans*-connected chains (F bridges)	3+
VF-2a **VF-2b**	$(NH_4)_2VOF_4$[14]	1D	*Cis*-connected chains (F bridges)	4+
VF-3	NH_4VO_3[15]	1D	*Trans*-connected chains (O bridges)	5+
VF-4	$VF_3(H_2O)_2$	1D	*Trans*-connected chains (F bridges)	3+
VF-5	$[C_6N_4H_{21}]_2[V_4O_4F_{14}\cdot 3H_2O$[18]	0D	Tetramers, edge- and corner-sharing octahedra (F bridges)	4+
VF-6	$[H_2NH_2(CH_2)_2NH_2][V_2O_2F_6]$	1D	Alternating-ladder of corner- and edge- sharing octahedra (F bridges)	4+
VF-7a **VF-7b**	$[H_2NH(CH_2)_2NH_2][VF_5]$[13]	1D	*Trans*-connected chains (F bridges)	3+
VF-8	$[HNH_2CH_3]_2[VOF_4]\cdot H_2O$	0D	monomer	4+
VF-9	$[HNH_2CH_3]_4[V_2O_2F_8]$	0D	Dimer, edge-sharing octahedra	4+
VF-10	$[HNH_2CH_3]_2[VF_5]$	1D	*Trans*-connected chains (F bridges)	3+
VF-11	α-$[H_2NH_2(CH_2)_2NH_2][VOF_4]$	1D	*Cis*-connected chains (F bridges)	4+
VF-12	β-$[H_2NH_2(CH_2)_2NH_2][VOF_4]$	1D	*Trans*-connected chains (O bridges)	4+
VF-13	NH_4VF_4	2D	Perovskite type structure	3+

3-7. References

(1) Cooper, E. R.; Andrews, C. D.; Wheatley, P. S.; Webb, P. B.; Wormald, P.; Morris, R. E. *Nature* **2004**, *430*, 1012.

(2) Aldous, D. W.; Goff, R. J.; Attfield, J. P.; Lightfoot, P. *Inorg. Chem.* **2007**, *46*, 1277.

(3) Bentrup, U.; Feist, M.; Kemnitz, E. *Prog. Solid State Chem.* **1999**, *27*, 75.

(4) Aldous, D. W.; Stephens, N. F.; Lightfoot, P. *Dalton Trans.* **2007**, 4207.

(5) Chirayil, T.; Zavalij, P. Y.; Whittingham, M. S. *Chem. Mater.* **1998**, *10*, 2629.

(6) Bonhote, P.; Dias, A.-P.; Papageorgiou, N.; Kalyanasundaram, K.; Gratzel, M. *Inorg. Chem.* **1996**, *35*, 1168.

(7) Varma, R. S.; Namboodiri, V. V. *Pure Appl. Chem* **2001**, *73*, 1309.

(8) Nockemann, P.; Thijs, B.; Pittois, S.; Thoen, J.; Glorieux, C.; Van Hecke, K.; Van Meervelt, L.; Kirchner, B.; Binnemans, K. *J. Phys. Chem. B* **2006**, *110*, 20978.

(9) Owens, G. S.; Abu-Omar, M. M. *J. Mol. Catal. A: Chem.* **2002**, *187*, 215.

(10) Fukumoto, K.; Yoshizawa, M.; Ohno, H. *J. Am. Chem. Soc.* **2005**, *127*, 2398.

(11) Parnham, E. R.; Drylie, E. A.; Wheatley, P. S.; Slawin, A. M. Z.; Morris, R. E. *Angew. Chem. Int. Ed.* **2006**, *45*, 4962.

(12) Nkuku, C. A.; LeSuer, R. J. *J. Phys. Chem. B* **2007**, *111*, 13271.

(13) Aldous, D. W.; Stephens, N. F.; Lightfoot, P. *Inorg. Chem.* **2007**, *46*, 3996.

(14) Bukovec, P.; Golic, L. *Acta Crystallogr., Sect. B* **1980**, *36*, 1925.

(15) Lukesh, J. *Acta Crystallog.* **1950**, *3*, 476.

(16) Manson, J. L.; Conner, M. M.; Schlueter, J. A.; McConnell, A. C.; Southerland, H. I.; Malfant, I.; Lancaster, T.; Blundell, S. J.; Brooks, M. L.; Pratt, F. L.; Singleton, J.; McDonald, R. D.; Lee, C.; Whangbo, M.-H. *Chem. Mater.* **2008**, *20*, 7408.

(17) Abrahams, S. C. *J. Chem. Phys.* **1962**, *36*, 56

(18) Aldous, D. W.; Stephens, N. F.; Lightfoot, P. *Dalton Trans.* **2007**, 2271.

(19) Johnston, D. C.; Johnson, J. W.; Goshorn, D. P.; Jacobson, A. *J. Phys. Rev. B* **1987**, *35*, 219.

(20) Stephens, N. F.; Buck, M.; Lightfoot, P. *J. Mater. Chem.* **2005**, *15*, 4298.

(21) Bushnell, G. W.; Moss, K. C. *Can. J. Chem* **1972**, *50,*, 3700.

(22) Lhoste, J.; Gervier, R.; Maisonneuve, V.; Leblanc, M.; Adil, K. *Solid State Sci.* **2009**, *11*, 1582.

(23) Stephens, N. F.; Lightfoot, P. *Solid State Sci.* **2006**, *8*, 197.

(24) Hidaka, M.; Fujii, H.; Garrard, B. J.; Wanklyn, B. M. *phys. status solidi A* **1986**, *95*, 413.

(25) Hidaka, M.; Akiyama, H.; Wanklyn, B. M. *phys. status solidi A* **1986**, *97*, 387.

(26) Leblanc, M.; Ferey, G.; De Pape, R.; Teillet, J. *Acta Crystallogr., Sect. C* **1985**, *41*, 657.

(27) Aldous, D. W.; Lightfoot, P. *Solid State Sci.* **2009**, *11*, 315.

(28) Lin, Z.; Slawin, A. M. Z.; Morris, R. E. *J. Am. Chem. Soc.* **2007**, *129*, 4880.

(29) Wragg, D. S.; Slawin, A. M. Z.; Morris, R. E. *Solid State Sci.* **2009**, *11*, 411.

CHAPTER 5

VOFs SYNTHESIS USING EMIM TF_2N

5-1. Introduction

In Chapter IV, we have carried out in-depth research on VOFs synthesis using ILs and DESs. Indeed, different types of structures have been isolated; however the dimensionality at this stage is still limited to 1D, when vanadium is in the 4+ oxidation state, and to 2D, when vanadium is in the 3+ oxidation state. This is also frequently observed in the widely explored hydrothermal based systems[1,2] with structure directing organic amines. So far, the only organically-templated VOF displaying a 2D structure, was recently reported by DeBurgomaster *et al*[3], this material with the formula $[H_2NC_4H_8NH_2]_3[V_4F_{17}O]\cdot 1.5H_2O$, consists of four vanadium atoms three of which are in the 3+ oxidation state. The VF_6 and VF_5O ocathedra are edge- and corner-shared to form $V_4F_{17}O_n^{2n-}$ layers as shown in Figure 5-1. These layers are separated by protonated piperazine moieties. As it is clear from Figure 5-1 this compound contains predominantly vanadium in the 3+ oxidation state (yellow polyhedra).

In an attempt to further increase the dimensionality of VOFs towards 2D or 3D frameworks a second metal can be included,[4,5] or phosphate[6] groups can also be introduced within the same system. A beautiful covalently connected 3D structure was reported recently[5] (Figure 5-2), this structure has the formula

$[HNH_2CH_3]_8[Cu(py)_4]_3[V_7O_6F_{30}]$ and consists of $[V_7O_6F_{30}]^{14-}$ polyanion linked *via* $[Cu(py)_4]^{2+}$ moieties.

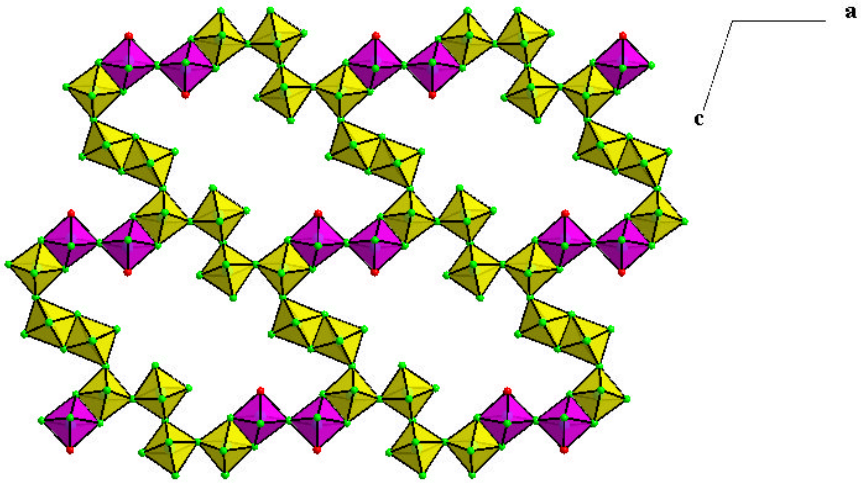

Figure 5-1. The $V_4F_{17}O_n^{2n-}$ layer found in $[H_2NC_4H_8NH_2]_3[V_4F_{17}O].1.5\ H_2O$[3] viewed down the *b* axis, yellow polyhedra present V^{3+} and pink polyhedra present V^{4+}.

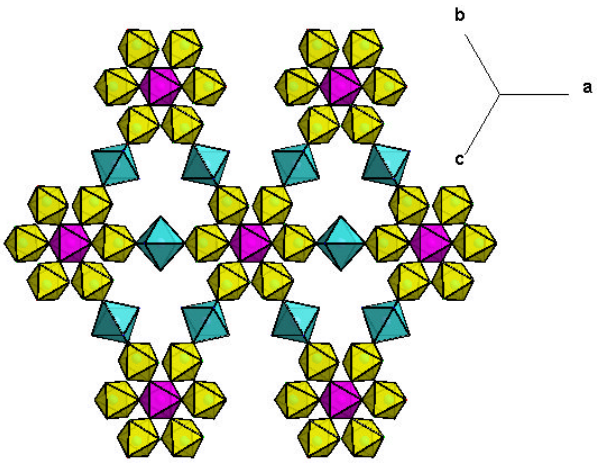

Figure 5-2. Polyhedra representation of the inorganic framework for $[HNH_2CH_3]_8[Cu(Py)_4]_3[V_7O_6F_{30}]$.[5]

In this chapter we will show how careful choice of the appropriate system environment leads to the preparation of organically-templated vanadium oxyfluorides with more extended networks without recourse to the introduction of a second metal centre or adding any other groups (*i.e*. phosphates).

It is apparent that high temperature will enable the preparation of more extended VOFs materials, however in the hydrothermal based media it was observed that with increasing reaction temperature, vanadium would be further reduced to V^{3+}. In the course of the investigations we carried out in the previous chapter, we have encountered numerous signs that suggest the hydrophobic IL EMIM Tf_2N to, potentially, be key in enabling the synthesis of VOFs with extended frameworks. NH_4VO_3 (**VF-3**) has been prepared (as mentioned in section 4-3-1) at 170 °C. This compound contains vanadium in the 5+ oxidation state; despite the high reaction temperature, vanadium did not undergo any reduction and remains in its original oxidation state. In addition, that the examination of the colour of various products obtained when EMIM Tf_2N is the solvent, may indicate (although not confirm) that vanadium is still in a higher oxidation state. Unfortunately, these products could not be identified due to their poor crystallinity. EMIM Tf_2N, by potentially stabilising vanadium ions at higher oxidation states even at elevated temperatures, is an excellent solvent system in order to achieve the synthesis of extended frameworks. This prompts an investigation of the synthesis of VOFs materials using the ionic liquid EMIM Tf_2N as the solvent at a high reaction temperature (170 °C).

To enable the IL to be the predominant solvent in the reaction, we need to reduce the amount of water (water arises from HF solution). Initially, the complex HF·pyridine has been used with V_2O_5, this yielded the first 2D VOF material (**VF-14**) containing exclusively V^{4+} ions. This material can also be prepared by using VOF_3 instead of V_2O_5 and reducing the amount of HF·Pyridine ten times or by using VOF_3 and a small amount of HF (ten times less than the amount used in the previous chapter) with the addition of pyridine as structure directing agent. Once this proved successesful, similar work was carried out by using VOF_3 and other cyclic organic amines (imidazole and quinuclidine).

The reaction of VOF_3 and HF with imidazole as an added structure directing agent yielded four type of materials (**VF-15**, **VF-16, VF-17** and **VF-18)**. **VF-15** represents the second 2D VOF, while **VF-16** and **VF-17** are two new structures based on the ladder-type structure previously reported. **VF-18** can also be prepared, a known material displaying ladder type-motif.

Using quinuclidine as a structure directing agent within the same system yielded a unique material displaying a kagome type lattice (**VF-19)**, which exhibits interesting magnetic properties. The crystal structure of these materials will be discussed in detail along with the magnetic properties for **VF-14** and **VF-19**.

5-2. Synthesis of the IL EMIM Tf_2N

EMIM Tf_2N was synthesised as described in section 4-2.

5-3. Increasing the dimensionality of VOFs using the hydrophobic IL EMIM Tf_2N

A typical synthesis procedure was as follows: A Teflon-lined autoclave (volume 15 mL) was charged with V_2O_5 (0.182 g, 1 mmol, Sigma Aldrich) and HF·Pyridine (70 wt% HF) (0.3 mL, 11.5 mmol HF/1.25 mmol pyridine, Sigma Aldrich) and then the IL EMIM Tf_2N (4 g, ~10 mmol) was added. The stainless steel autoclave was then sealed and heated in an oven at 170 °C for 24 hrs. After the autoclave had been cooled to room temperature, the product was filtered, washed with methanol and dried in air for 24 hrs. Blue crystals were collected (CHN analysis: Calc: %C: 19.43, %H: 1.95, %N: 4.53; Found: %C: 19.18, %H: 1.60, %N: 3.90).

X-ray diffraction data were collected at station 11.3.1 of the Advanced Light Source at Lawrence Berkeley National Laboratory using a Bruker APEX II CCD diffractometer. Structure was solved using direct methods with the program SHELXS and refined on F^2 using full-matrix least-squares with SHELXL-97 under WINGX packages. All non-hydrogen atoms were refined anisotropically. Hydrogen atoms were placed geometrically on the template molecule where possible.

Crystallographic data for **VF-14** are as summarised in Table 5-1. Selected bond lengths and bond valence sums for **VF-14** are tabulated in Table 5-2.

Table 5-1. Crystallographic data and structure refinement for **VF-14.**

Compound	**VF-14**
Formula	$[HNC_5H_5][V_2O_2F_5]$
Fw (g/mol)	308.99
Space group	$P2_1/n$
a /Å	7.5691(7)
b /Å	19.912(2)
c /Å	11.9888(12)
α /°	90
β /°	91.436(2)
γ /°	90
V / Å^3	1806.4
Z	8
Crystal size /mm	0.1 × 0.06 × 0.04
Crystal shape and colour	Blue block
Data collection T/ K	150 (2)
F(000)	1200
R_{int}	0.0397
Obsd data (I >2σ(I))	3447
Data/restraints/parameters	5354/0/279
GOOF on F^2	0.994
R1, wR2 (I >2σ(I))	0.0349, 0.0765
R1, wR2 (all data)	0.0689, 0.0881
Largest diff. peak / hole	0.529, –0.657
Oxidation state of V ions	4+

The crystal structure of **VF-14** consists of an infinite anionic layer of composition $[V_2O_2F_5]_n^{n-}$ separated *via* hydrogen-bonded protonated pyridine moieties (Figure 5-3). There are four crystallographically distinct vanadium sites, ten fluorine atoms, four oxygen and two pyridinium moieties in the asymmetric. All vanadium atoms are in octahedral geometry and exhibit a characteristic short V=O bond (~ 1.59 Å) and elongated *trans* V-F bond (~ 2.12 – 2.19 Å) (see Figure 5-4). The bond valence sum calculations (∑V1= 3.97, ∑V2 = 3.98, ∑V3 = 3.95, ∑V4 = 3.96), (Table 5-2) indicate that the four vanadium atoms are in the 4+ oxidation state.

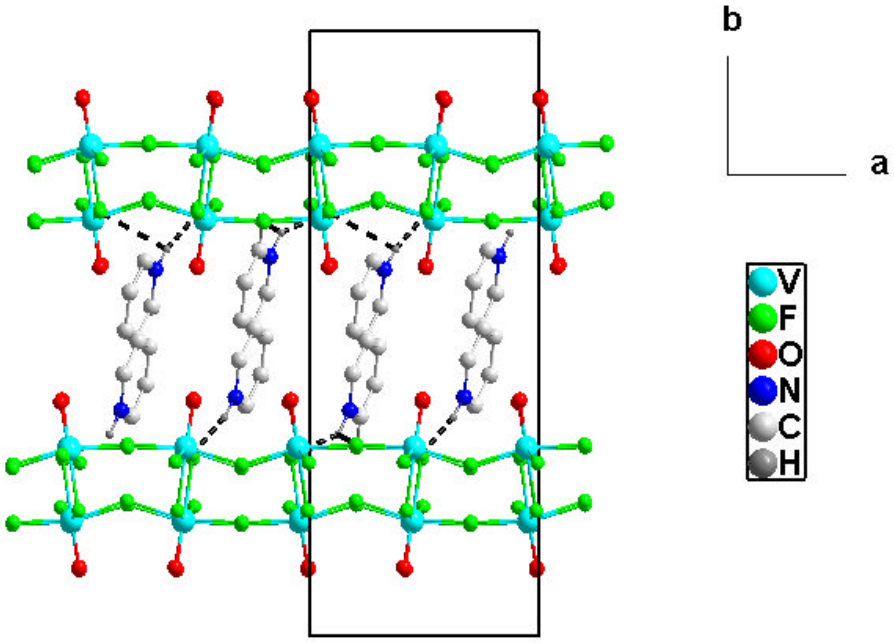

Figure 5-3. A view of **VF-14**, showing the $[V_2O_2F_5]$ layers and how they are hydrogen bonded to the pyridinium moieties.

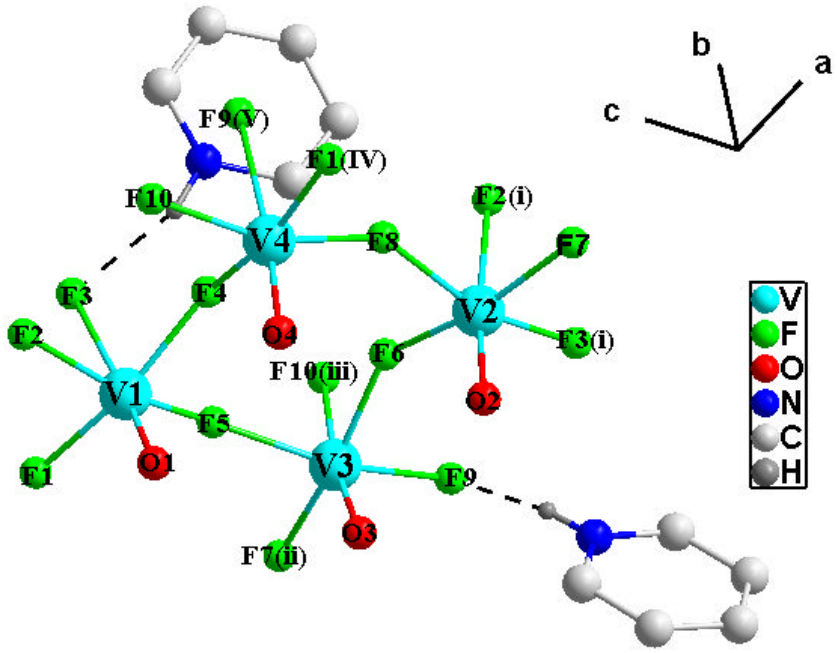

Figure 5-4. The building unit in **VF-14**. Symmetry operators (i) 0.5+x, 0.5-y, -0.5+z; (ii) -1+x, y, z; (iii) -0.5+x, 0.5-y, -0.5+z; (iv) 1+x, y, z; (v) 0.5+x, 0.5–y, 0.5+z.

The VOF layer has a highly distorted square-net topology which may be regarded as derived from the 'ladder-like' $[VOF_3]_n^{n-}$ chains previously reported for $CsVOF_3$ and $[bpeH_2]_{1/2}[VOF_3]$[7] (bpe = *trans*-1,2-bis(4-pyridyl)-ethylene). These ladders consist of $[VO_1F_1F_{4/2}]$ octahedra edge-shared into dimers, and further linked into chains through F bridges, leaving terminal F and O atoms (Figure 5-5 (top)). The VOF layer in **VF-14** arises from fusion of adjacent ladders through pendant fluoride ligands (F5 and F8), leaving only O atoms terminal, as highlighted in Figure 5-5 (below). The resultant layer has a rather corrugated appearance when viewed in a perpendicular direction (Figure 5-6).

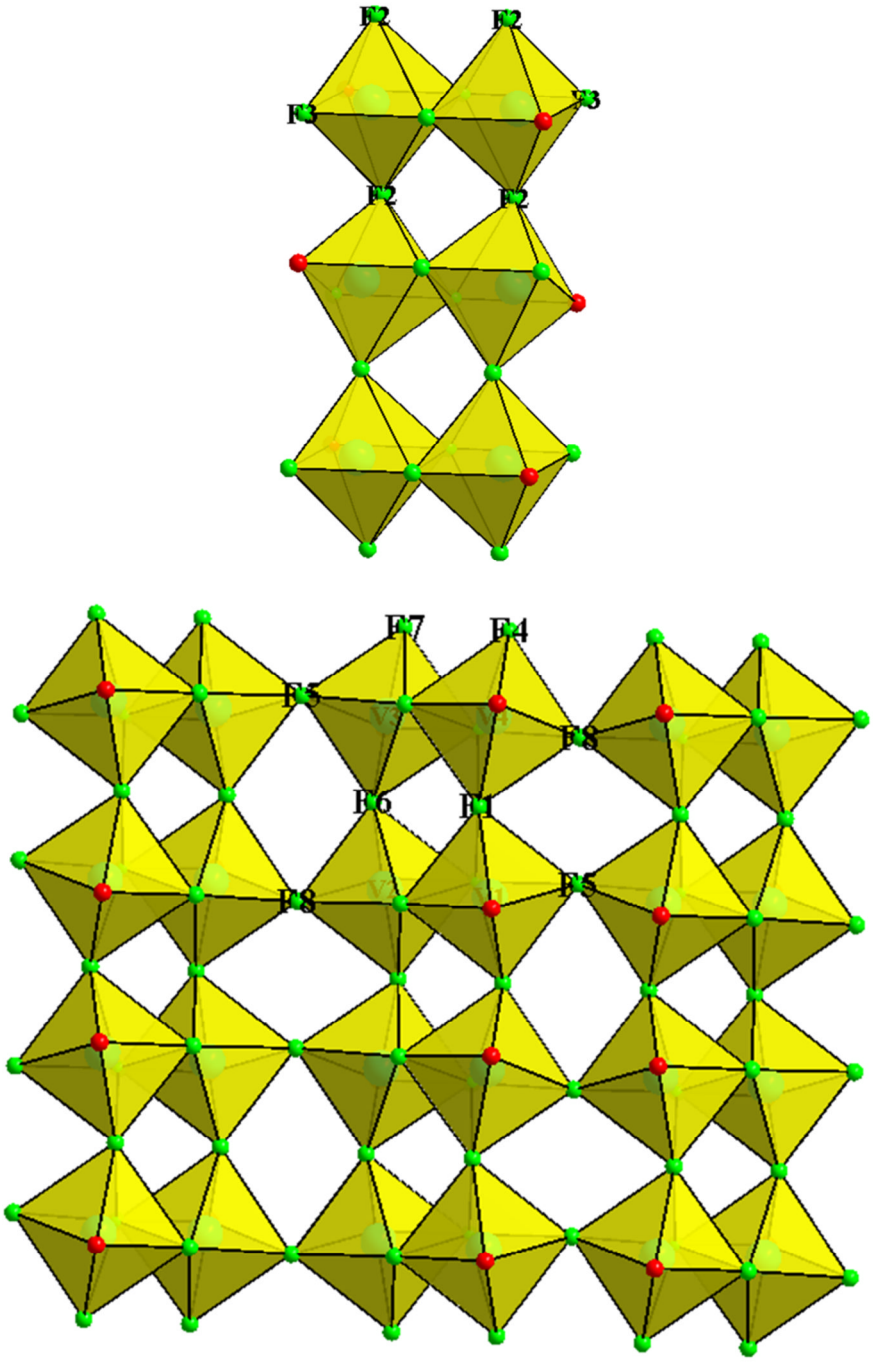

Figure 5-4. Ladder type found in $CsVOF_3$[7] (above), Layer found in **VF-14** (below).

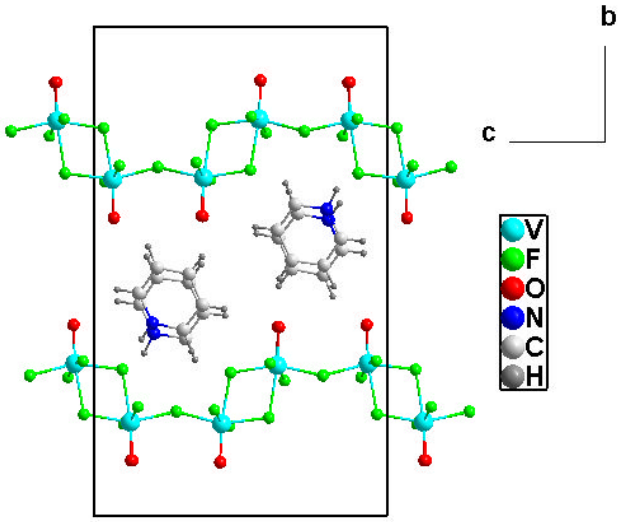

Figure 5-6. Crystal structure of **VF-14** viewed down the *a*-axis, showing corrugated $[V_2O_2F_5]_n^{n-}$ layers.

Table 5-2. Selected bond lenghts and bond valence sums for **VF-14**.

Bond	Bond Length (Å)	S_{ij}	Bond	Bond Length (Å)	S_{ij}
V1—O1	1.588 (2)	1.698	V3—O3	1.5990(19)	1.649
V1—F1	1.9588 (13)	0.497	V3—F5	1.9439(14)	0.517
V1—F2	1.9434 (14)	0.519	V3—F7^{ii}	1.9552(14)	0.502
V1—F3	2.1762 (15)	0.276	V3—F6	1.9593(14)	0.497
V1—F4	1.9729 (14)	0.478	V3—F9	1.9769(14)	0.473
V1—F5	1.9544 (14)	0.503	V3—F10^{iii}	2.1288(15)	0.314
		∑V1= 3.971			**∑V3= 3.952**
V2—O2	1.592 (2)	1.68	V4—O4	1.589(2)	1.694
V2—F2^{i}	2.1253 (15)	0.317	V4—F10	1.9409(14)	0.521
V2—F3^{i}	1.9655 (14)	0.487	V4—F8	1.9510(14)	0.507
V2—F6	1.9589(14)	0.497	V4—F1^{iv}	1.9560(14)	0.501
V2—F7	1.9623 (14)	0.493	V4—F4	1.9770(14)	0.473
V2—F8	1.9501 (14)	0.509	V4—F9^{v}	2.1930(15)	0.264
		∑V2= 3.983			**∑V4= 3.960**

(i) 0.5+x, 0.5–y, –0.5+z; (ii) –1+x, y, z; (iii) –0.5+x, 0.5–y, 0.5+z; (iv) 1+x, y, z; (v) 0.5+x, 0.5–y, 0.5+z;

As shown in Figure 5-7, magnetic susceptibility data for **VF-14** show evidence for low-dimensional antiferromagnetic order, with a broad maximum in the plot of χ *versus* T near 80 K. Above 150 K the data fit well to a Curie-Weiss law (Figure 5-8), with a Weiss constant θ = –189 K indicating strong antiferromagnetic interactions, this also can be seen in the plot of χT versus T (Figure 5-9) where it does not show any saturation even at 300 K. The experimental effective magnetic moment μ_{eff} = 2.65 μ_B; this is slightly higher than the spin-only value of 2.45 μ_B per formula unit, suggestive of a small orbital contribution.

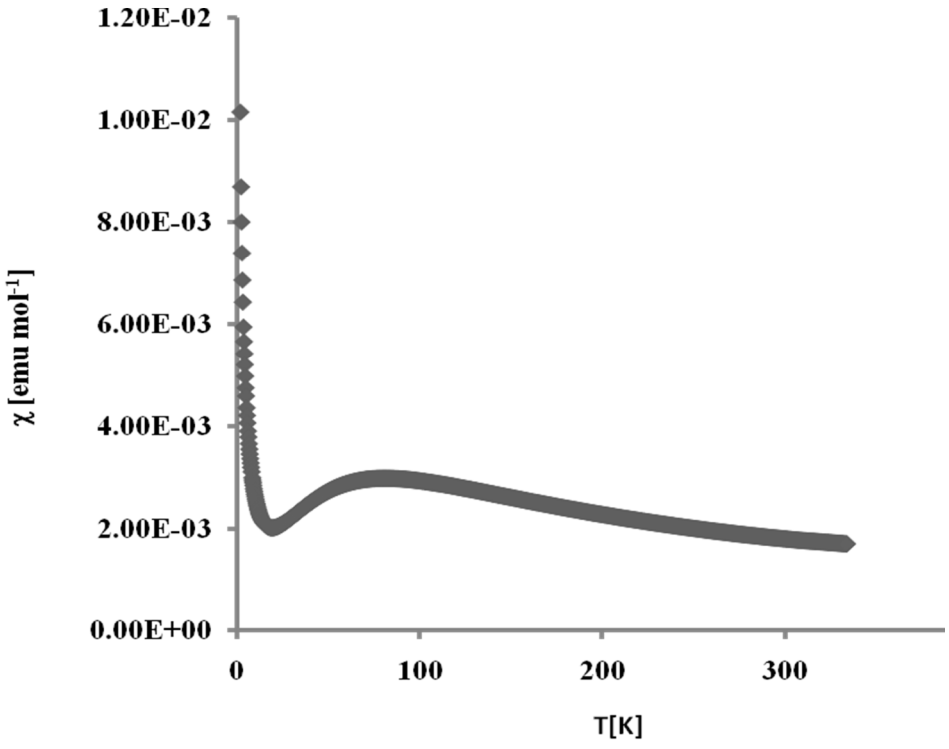

Figure 5-7. Plot of χ *versus* T for **VF-14.**

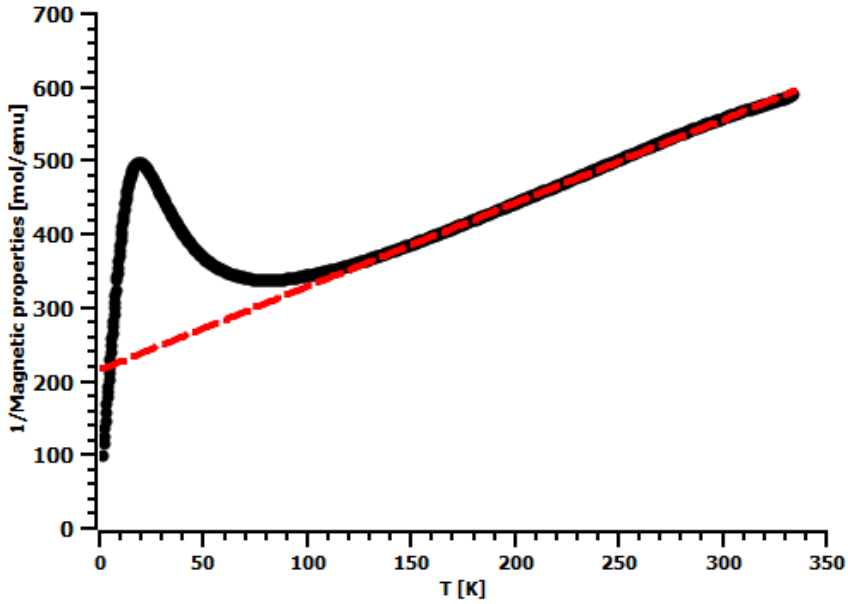

Figure 5-8. Curie-Weiss fit for 1/χ above 150 K.

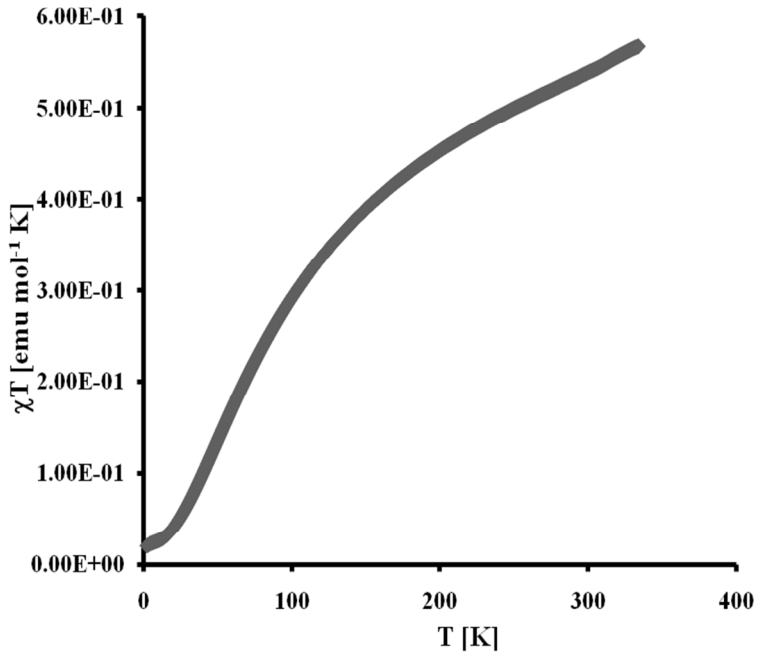

Figure 5-9. Plot of χT *versus* T for **VF-14**.

Looking at the vanadium sublattice of the structure only (Figure 5-10) reveals several different possible V---V interaction pathways within the layer, with 'short' contacts (V---V ~ 3.28 – 3.30 Å) within the edge-shared dimers (the 'rungs' of the ladders) and longer (V---V ~ 3.70 – 3.87 Å) along the 'rails' of the ladder, and across the *inter*-ladder links.

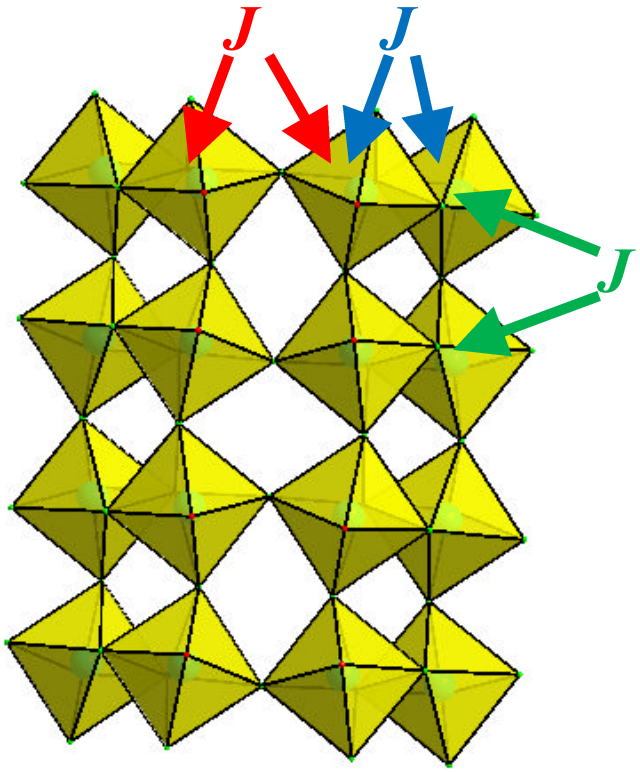

Figure 5-10. Possible V-V interaction pathways in **VF-14**.

Various simple models were used to attempt to fit the χ(T) data, including Bleaney-Bowers dimer,[8] 1D Ising or Heisenberg chains[9,10] and spin ladder[11] models. The best fit was produced from a 1D S = ½ Ising chain model (Figure 5-11), rather the Heisenberg chain (in contrast to the ladder compound $CsVOF_3$). The difference between Ising and Heisenberg spins is related to their anisotropy; Heisenberg spins are isotropic whereas

Ising spins give a differing response to a magnetic field parallel and perpendicular to direction of their magnetic spin.

However in both cases dominant interactions occur along the *rails* of the ladder (*ie*. crystallographic *a*-axis) with negligible interactions along the *rungs*.

The complexity of the structure (*ie*. four distinct V sites, the fusion of the ladders into continuous sheets, and the corrugated nature of both the *intra*-ladder and *inter*-ladder interactions) precludes any further analysis of the magnetic behaviour; and making the *a priori* prediction of magnetic behaviour very difficult.

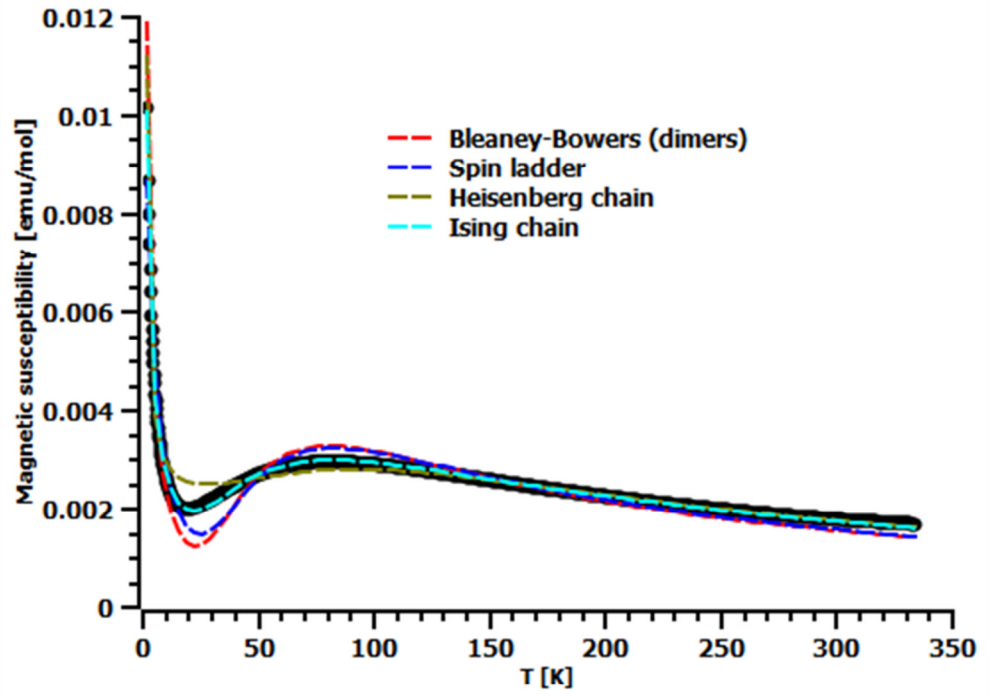

Figure 5-11. Bleaney-Bowers, Heinserberg/ Ising chains and Spin ladder fits to χ (T) for **VF-14**.

5-4. Imidazole as an added template

VF-15, **VF-16** were synthesised following a typical synthesis procedure: a Teflon-lined autoclave (volume 15 mL) was charged with VOF_3 (0.124 g, 1 mmol, Fluorochem) and HF (48 wt% in H_2O) (0.1 mL, 2.76 mmol, Sigma Aldrich) and then the IL EMIM Tf_2N (4 g, ~10 mmol) was added along with (0.068 g, 1 mmol, Sigma aldrich) of imidazole. The stainless steel autoclave was then sealed and heated in an oven at 170 °C for 24 hrs. **VF-15** is the major phase and **VF-16** is the minor phase as shown in the PXRD (see appendix).

VF-17 and **VF-18** were synthesised in a similar way to **VF-15** and **VF-16** except that, (0.101 g, 1 mmol, Fluka) of KNO_3 and (0.195 g, 1 mmol, Sigma Aldrich) of $CsNO_3$ were added, respectively in addition to the imidazole. After the autoclave had been cooled to room temperature, the product was filtered, washed with methanol and dried in air for 24 hrs.

X-ray diffraction data for **VF-15** were collected at station 11.3.1 of the Advanced Light Source at Lawrence Berkeley National Laboratory using a Bruker APEX II CCD diffractometer. Structure was solved using direct methods with the program SHELXS and refined on F^2 using full-matrix least-squares with SHELXL-97 under WINGX packages. All non-hydrogen atoms were refined anisotropically. Hydrogen atoms were placed geometrically on the template molecule where possible.

Single crystal X-ray diffraction data for **VF-16, VF-17** and **VF-18** were collected using Mo-Kα (0.7107 Å) radiation utilising a Rigaku rotating anode single-crystal X-ray diffractometer at the University of St Andrews. The structures were solved with standard direct methods using SHELXS and refined with least-squares minimisation techniques against F^2 using SHELXL under WinGX packages. All non-hydrogen atoms have been anisotropically refined.

Crystallographic data for **VF-15**, **VF-16** and **VF-17** are as summarised in Table 5-3 and Table 5-4 respectively. Selected bond lengths and bond valence sums are tabulated, respectively, in Table 5-5, Table 5-6 and Table 5-7.

Table 5-3. Crystallographic data for compounds **VF-15** and **VF-16.**

Compound	**VF-15**	**VF-16**
Formula	$[HNC_3NH_4][V_2O_2F_5]$	$[HNC_3NH_4][NH_4][(VOF_3)_2]$
Fw (g/mol)	297.97	335.01
Space group	$P2_1$	$P222_1$
a /Å	7.164(5)	3.8610(3)
b /Å	17.359(5)	6.6640(4)
c /Å	7.357(5)	19.8400(13)
α /°	90	90
β /°	117.962(5)	90
γ /°	90	90
V / Å^3	808.1(8)	510.48(6)
Z	4	2
Crystal size /mm	0.04 × 0.02 × 0.02	0.2 × 0.08 × 0.02
Crystal shape and colour	Blue prism	Blue platelet
Data collection T/ K	150(2)	93(2)
F(000)	576	328
R_{int}	0.0494	0.0665
Obsd data (I>2σ(I))	4314	892
Data/restraints/parameters	4875/1/253	940/1/92
GOOF on F^2	1.034	1.165
R1, wR2 (I >2σ(I))	0.0397, 0.1010	0.0386, 0.0825
R1, wR2 (all data)	0.0450, 0.1044	0.0436, 0.0836
Largest diff. peak / hole	0.934/–0.538	0.722 /–0.757
Oxidation state of V ions	4+	4+

Table 5-4. Crystallographic data for compounds **VF-17.**

Compound	**VF-17**
Formula	$[HNC_3NH_4]K[(VOF_3)_2]$
Fw (g/mol)	356.07
Space group	$P222_1$
a /Å	3.8572(13)
b /Å	6.4795(2)
c /Å	20.0510(6)
α /°	90
β /°	90
γ /°	90
V / Å^3	501.13(17)
Z	2
Crystal size /mm	0.3 × 0.02 × 0.02
Crystal shape and colour	Blue needle
Data collection T/ K	93(2)
F(000)	344
R_{int}	0.0370
Obsd data (I>2σ(I))	868
Data/restraints/parameters	906/0/74
GOOF on F^2	1.263
R1, wR2 (I >2σ(I))	0.0528, 0.1421
R1, wR2 (all data)	0.0528, 0.1746
Largest diff. peak / hole	1.071/–1.058
Oxidation state of V ions	4+

Layer $[HNC_3NH_4][V_2O_2F_5]$ (VF-15):

The crystal structure of **VF-15** consists of an infinite anionic layer of composition $[V_2O_2F_5]_n^{n-}$ (similar to the one seen in **VF-14**) separated *via* hydrogen-bonded protonated imidazolium moieties (Figure 5-12). There are four crystallographically distinct vanadium sites, ten fluorine atoms, four oxygen and two imidazolium moieties in the asymmetric unit. All vanadium atoms are in octahedral geometry and exhibit the characteristic short V=O bond (~ 1.60 Å) and elongated *trans* V-F bond (~ 2.13 Å) (see Figure 5-13). The bond valence sum calculations (∑V1= 3.97, ∑V2 = 3.94, ∑V3 = 4.00, ∑V4 = 4.02) (Table 5-5) indicate that the four vanadium atoms are in the 4+ oxidation state.

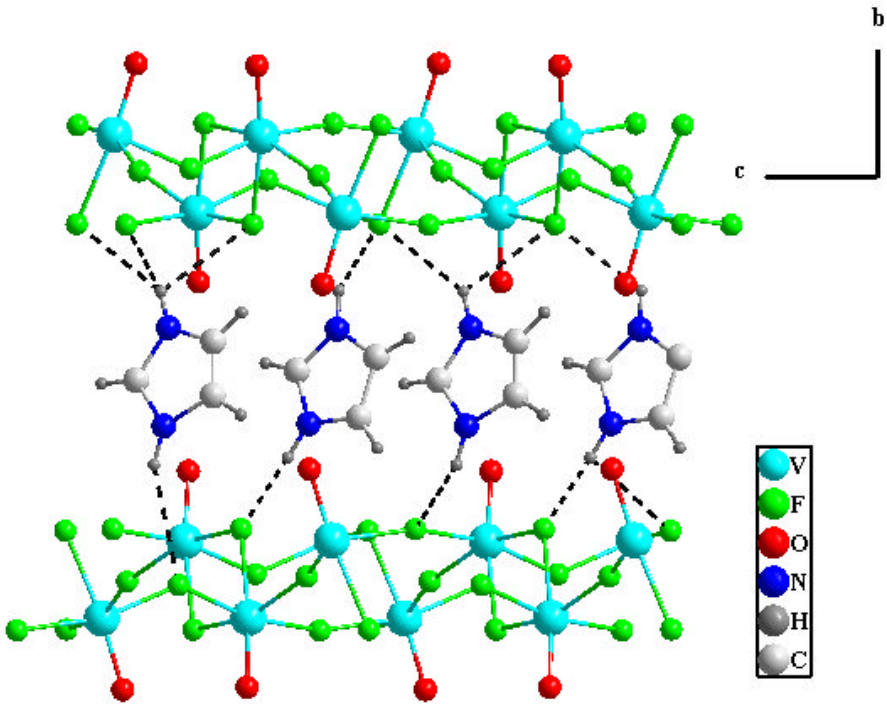

Figure 5-12. A view of **VF-15**, showing the $[V_2O_2F_5]$ layers and how they are hydrogen bonded to the imidazolium moieties.

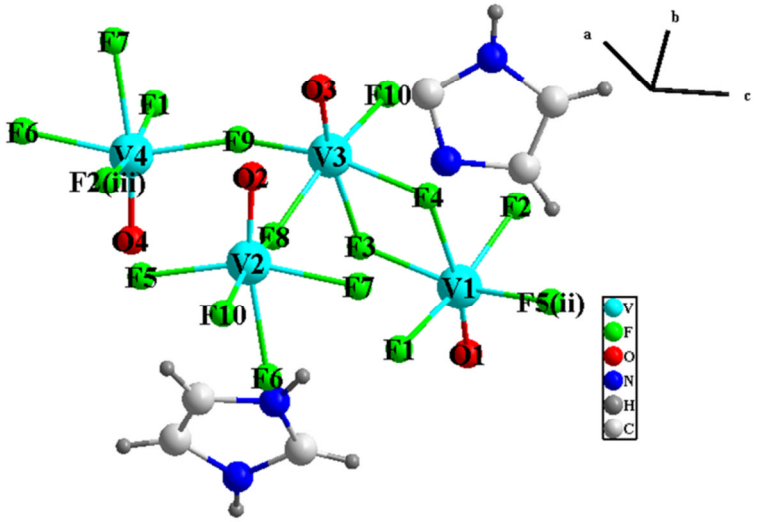

Figure 5-13. Building unit for **VF-15**, some hydrogen atoms are omitted for clarity. Symmetry operators: (i) –1+x, y, –1+z; (ii) x, y, 1+z; (iii) x, y, –1+z; (iv) 1+x, y, z.

The vanadium sublatice in **VF-15** presents the same pattern seen in **VF-14**; the bridging modes, the bond lengths and the bond angles are very similar. **VF-15** also presents a highly distorted square-net topology consists of [VOF_5] octahedra edge-shared into dimers, and further linked into a 2D structure through F bridges (similar to the one seen in **VF-14**) as illustrated in Figure 5-14 (top).

However, it is notable that the two different templates involved in the synthesis of **VF-14** and **VF-15** (pyridine and imidazole), have a great impact on the overall structural features of the resulting materials and direct the structures to crystallise in different space groups $P2_1$ for **VF-15** rather than $P2_1/n$ for **VF-14**. We can also see that the arrangement of the ladders within two different layers are quite different, they are

parallel to each other in **VF-14**, and in contrast they are aligned in a nearly anti-parallel fashion in **VF-15** as highlighted in Figure 5-14 (below).

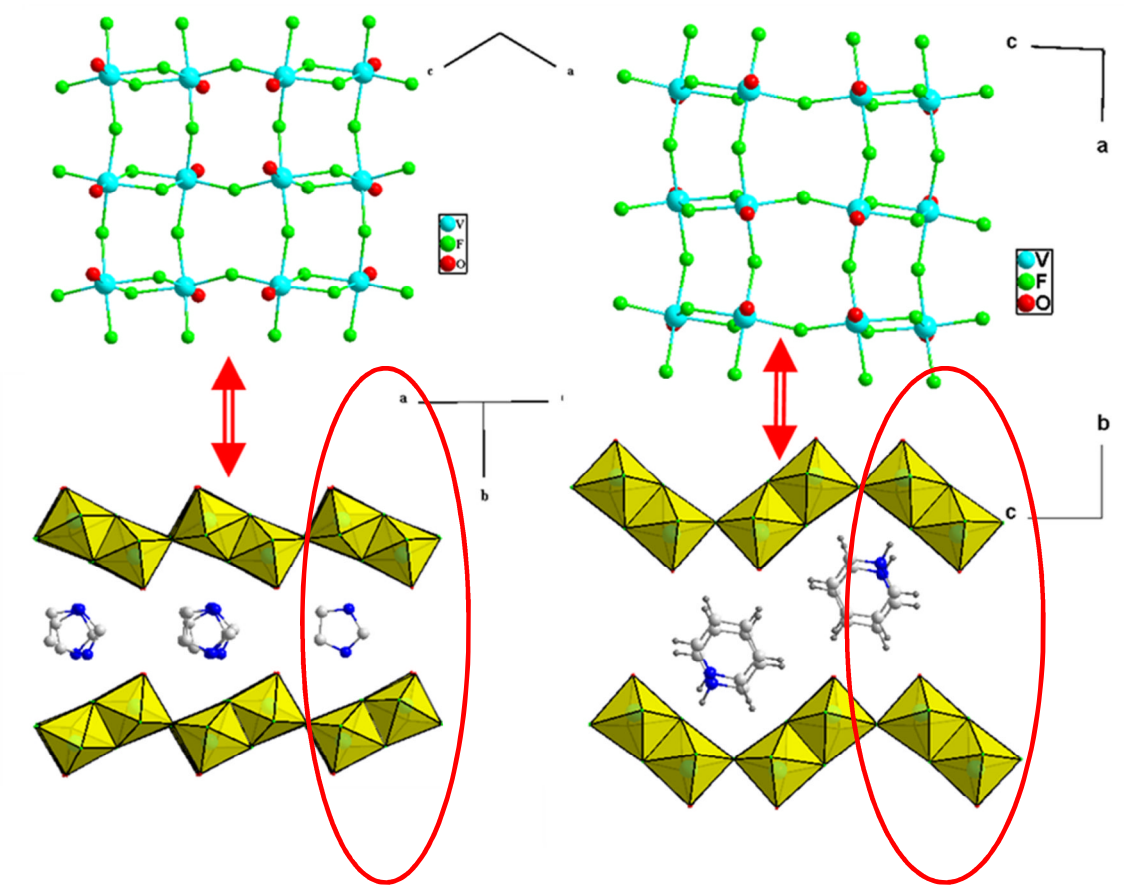

Figure 5-14. The vanadium sublatices and the layers structures found in **VF-15** (left), and **VF-14** (right).

Table 5-5. Selected bond lengths and bond valence sums for **VF-15**.

Bond	**Bond Length (Å)**	S_{ij}	**Bond**	**Bond Length (Å)**	S_{ij}
V1—O1	1.600(3)	1.644	V3—O3	1.603(3)	1.631
V1—F1	1.978 (2)	0.472	V3—F4	1.949(2)	0.513
V1—F2	1.947 (2)	0.513	V3—F3	2.139(2)	0.307
V1—F3	1.972 (2)	0.479	V3—F8	1.944(2)	0.520
V1—F4	2.105 (2)	0.335	V3—F9	1.937(2)	0.530
V1—F5^{ii}	1.933 (2)	0.533	V3—F10	1.959(2)	0.499
	∑V1= 3.976				**∑V3= 4.00**
V2—O2	1.602(3)	1.635	V4—O4	1.591(3)	1.685
V2—F5	1.937 (2)	0.527	V4—F2^{iii}	1.944(2)	0.517
V2—F10^{i}	1.965 (2)	0.489	V4—F6^{iv}	1.949(2)	0.510
V2—F6	2.135 (2)	0.309	V4—F1^{iv}	1.972(2)	0.479
V2—F7	1.967 (2)	0.486	V4—F7^{iv}	2.138(2)	0.306
V2—F8	1.961 (2)	0.494	V4—F9	1.939(2)	0.524
	∑V2= 3.94				**∑V4= 4.021**

(i) –1+x, y, –1+z; (ii) x, y, 1+z; (iii) x, y, –1+z; (iv) 1+x, y, z

CHN analysis and PXRD performed on the sample suggest the presence of another minor phase (**VF-16**) along with **VF-15** (see appendix). Unfortunately, this precludes any other measurements on the sample; *e.g*. study of its magnetic properties and comparison to **VF-14,** discussed previously. **VF-15** in a pure phase could also be studied for its SHG properties (if any) to ascertain the space group assignment.

Ladder $[HNC_3NH_4[NH_4]][(VOF_3)_2]$ (VF-16):

VF-16 presents another variation to the known ladder-type structure, previously seen in $CsVOF_3$.[7] It consists of one unique vanadium site, three fluorine atoms and one oxygen atom in the asymmetric unit. The local octahedral environment around the V atom is highly distorted (Figure 5-15) and exhibits the short V=O Vanadyl group with a distance (~1.58 Å) and the elongated *trans* F atom with a distance (~ 2.21 Å). The bond lengths are presented in Table 5-6, together with the corresponding bond valence sums, which suggest that vanadium is in the 4+ oxidation state (∑V1 = 4.02).

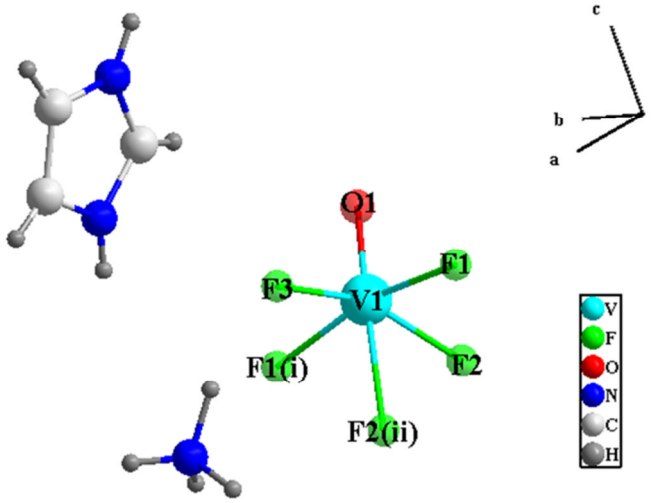

Figure 5-15. Building unit for compound **VF-16**, Symmetry operators:
(i) 1+x, y, z; (ii) x, –y, –z.

The $[VOF_1F_{4/2}]$ octahedra are edge- and corner-sharing to form ladder-like chains, these ladders are hydrogen bonded by ammonium cation to form layers as illustrated in Figure 5-16. These are further linked through protonated imidazolium cations (Figure 5-17 and 5-18).

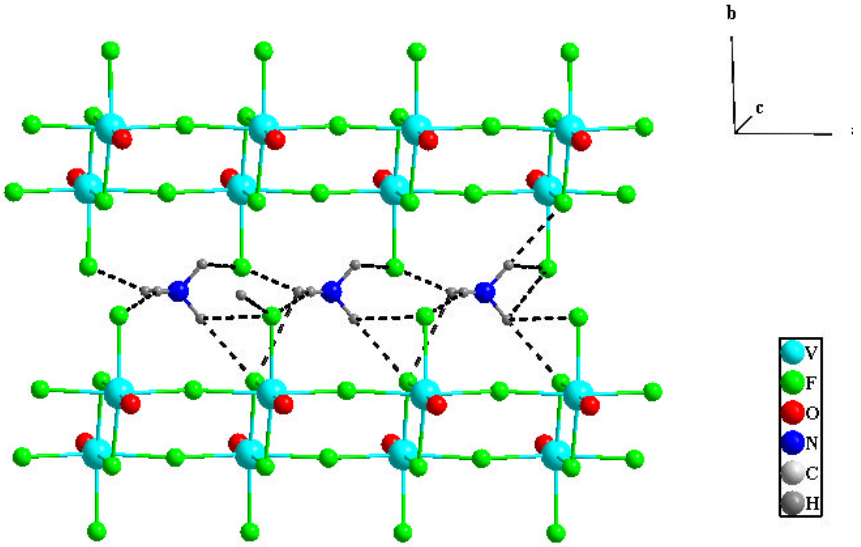

Figure 5-16. Ladder found in **VF-16** hydrogen bonded to layer by ammonium cations.

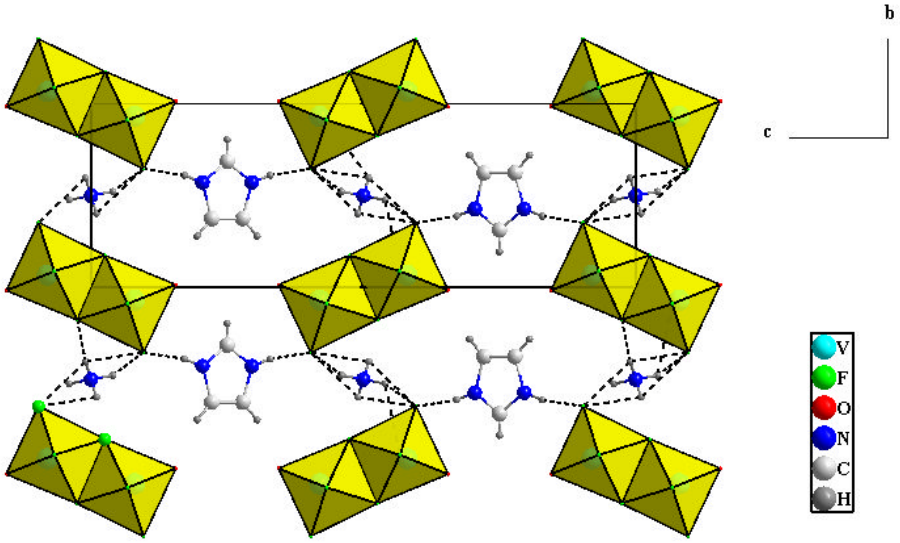

Figure 5-17. A view of **VF-16** showing how the ladders are hydrogen bonded into layers, and the layers are further hydrogen bonded to imidazolium cations.

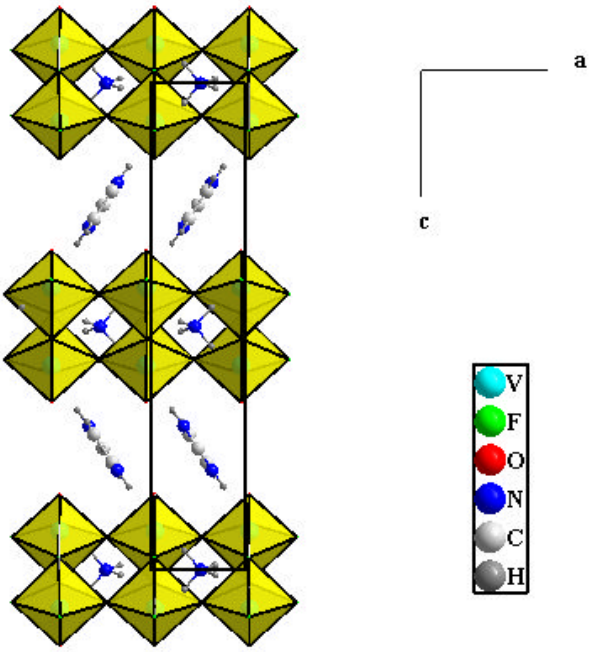

Figure 5-18. Crystal structure of **VF-16** viewed along the crystallographic *b* axis.

Table 5-6. Selected bond distances and bond valence sum calculation for **VF-16**.

Bond	**Bond Length (Å)**	S_{ij}
V1—O1	1.586(3)	1.708
V1—F1	1.961(3)	0.494
V1—F2	1.947 (2)	0.513
V1—F3	1.929 (2)	0.539
V1—F1^{i}	1.943 (3)	0.519
V1—F2^{ii}	2.214 (2)	0.249
		$\sum$V1= 4.022
(i) 1+x, y, z; (ii) x, –y, –z		

While the ladder is similar to the one seen in $CsVOF_3$, however the presence of two different templates; ammonium (probably coming from the breakdown of small amount of imidazole) and imidazole direct the structure to crystallise in a lower symmetry, a chiral space group ($P222_1$) rather that *Pbam* which was reported for $CsVOF_3$.

This structure is a very interesting candidate for SHG measurements, and it would also be interesting to measure its magnetic properties to see the differences in contrast to $CsVOF_3$. Again the sample was not pure which precluded any other measurements. Some reactions have been carried out to produce a phase pure sample without any success. The addition of alkali metals to form similar materials was also tried; the addition of KNO_3 gave an isomorphous material to **VF-16**, which will be discussed in the next section.

Ladder $[HNC_3NH_4]K[(VOF_3)_2]$ (VF-17):

VF-17 is isomorphous to **VF-16** and consists of a ladder-type structure, displaying the same features as described above for **VF-16**. Figure 5-19 shows the building unit for **VF-17**. K cations linked the ladders into layers and the layers are further linked by protonated imidazolium cations as illustrated respectively in Figures 5-20, 5-21 and 5-22. The bond lengths are presented in Table 5-7, together with the corresponding bond valence sums, which suggest that vanadium is in the 4+ oxidation state ($\sum V1 = 4.05$).

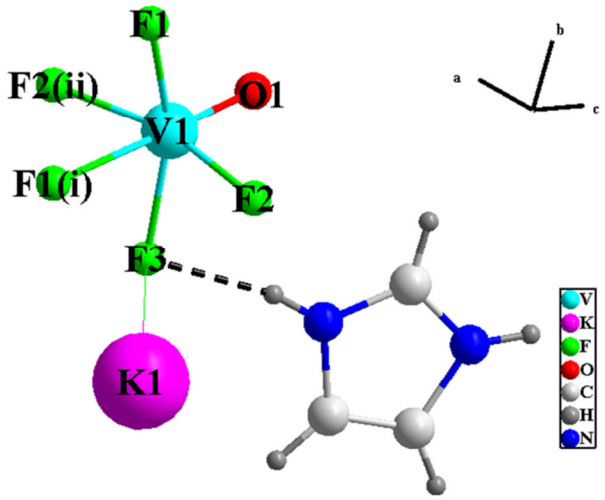

Figure 5-19. Building unit for compound Building **VF-17**, Symmetry operators: (i) 1+x, y, z; (ii) x, 1-y, -z.

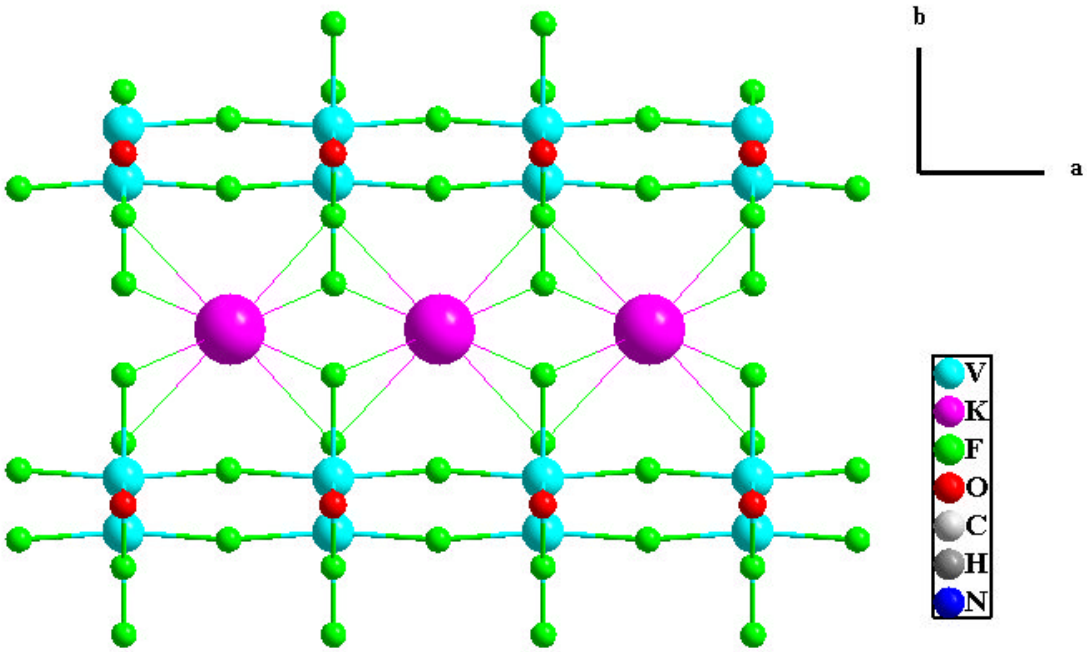

Figure 5-20. Ladder found in **VF-17** separated by K cations.

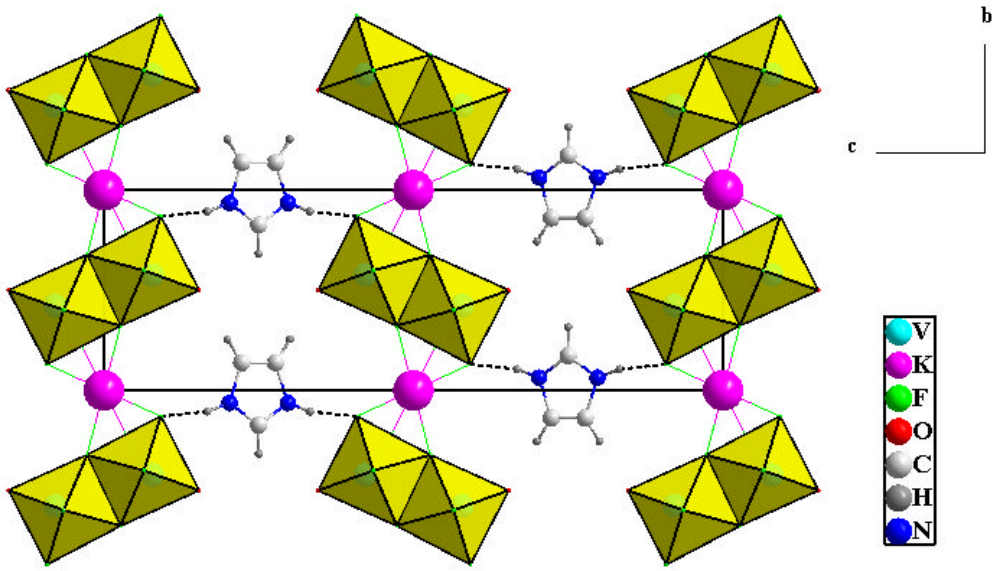

Figure 5-21. A view of **VF-17** showing how the ladders are separated by K cations and further hydrogen bonded to imidazolium cations.

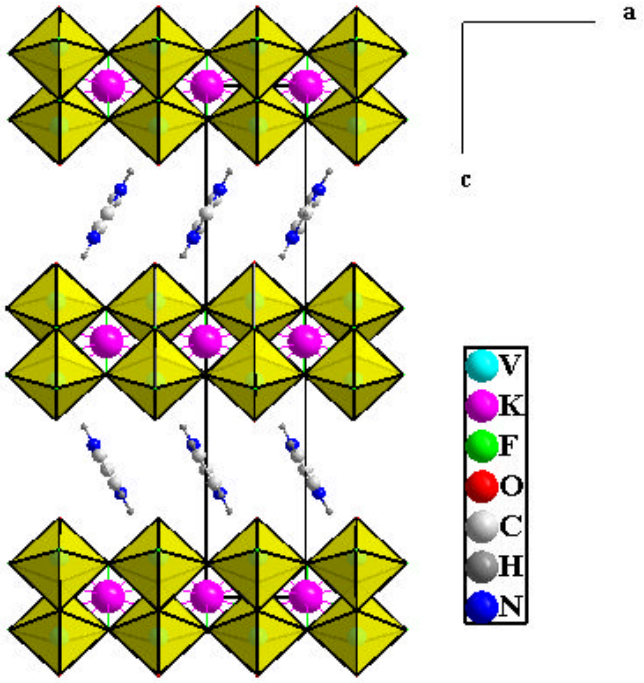

Figure 5-22. Crystal structure of **VF-16** viewed along the crystallographic *b* axis.

Table 5-7. Selected bond distances and bond valence sum calculation for **VF-17**.

Bond	**Bond Length (Å)**	S_{ij}
V1—O1	1.586 (5)	1.708
V1—F1	1.937(4)	0.527
V1—F2	1.955 (6)	0.502
V1—F3	1.917(4)	0.556
V1—F2i	1.949 (6)	0.510
V1—F1ii	2.211(4)	0.251
		∑V1= 4.054

(i) 1+x, y, z; (ii) x, 1–y, –z

VF-17 has been synthesised by the addition of KNO_3. Both templates, protonated imidazole cation and K^+ cation, are involved in the construction of this structure. It seems plausible to apply the same strategy using other alkali metals; $LiNO_3$, $NaNO_3$ and $CsNO_3$ have been used. It is interesting that in contrast to **VF-17**, the addition of $LiNO_3$ or $NaNO_3$ yielded **VF-15** containing protonated imidazole cations only, no Na or Li ions are involved in the structure (although it is not phase pure, other unidentified phase was formed with **VF-15)**. Using $CsNO_3$ yielded the known $CsVOF_3$[7] (**VF-18**) with no imidazolium in the structure. It is clear that template competition will allow the structure to crystallise or favour a template over the other.

5-5. Kagome type material $[HNC_7H_{13}][NH_4]_2[V_7O_6F_{18}]$ (VF-19)

A typical synthesis procedure was as follows: A Teflon-lined autoclave (volume 15 mL) was charged with VOF_3 (0.124 g, 1 mmol, Fluorochem) and HF (48 wt% in H_2O) (0.09 mL, 2.45 mmol, Sigma Aldrich) and then the IL EMIM Tf_2N (4 g, 10 mmol) was added along with (0.111 g, 1 mmol, Sigma aldrich) of quinuclidine. The stainless steel autoclave was then sealed and heated in an oven at 170 °C for 20 hrs yielding small blue crystals (CHN analysis: Calc: %C: 8.92, %H: 2.35, %N: 4.45; Found: %C: 10.59, %H: 2.43, %N: 4.22).

Single-crystal X-ray diffraction data for **VF-19** were collected using Mo-Kα (0.7107 Å) radiation utilising a Rigaku rotating anode single-crystal X-ray diffractometer at the University of St Andrews. The structure was solved with standard direct methods using SHELXS and refined with least-squares minimisation techniques against F^2 using SHELXL under WinGX packages. The inter-layer quinuclidine moiety was modelled in a disordered manner such that there are two equivalent, half-occupied positions relative to the 3-fold axis along *c*, and two possible positions 'head-to-tail' perpendicular to this. Hydrogen atoms were not located on this moiety, and the C and N atoms were refined isotropically (as shown in Figure 5-25). The intra-layer NH_4^+ moiety was well-behaved, and modelled with anisotropic N1, and restrained H atoms.

Crystallographic data for **VF-19** are as summarised in Table 5-8. Selected bond lengths and bond valence sums for **VF-19** are tabulated in Table 5-9.

Magnetic susceptibility data for **VF-19** were collected on a Quantum Design MPMS SQUID (Edinburgh University). Data were recorded in a 10000 Oe field while warming the sample from 2 to 300 K in 4 K steps, following consecutive zero-field cooling (ZFC) and field cooling (FC) cycles. Data were normalized to the molar quantity of the sample, and corrected for any diamagnetic contributions.

Table 5-8. Crystallographic data for compounds **VF-19**.

Compound	**VF-19**
Formula	$[HNC_7H_{13}][NH_4]_2[V_7O_6F_{18}]$
Fw (g/mol)	942.86
Space group	*R*-3*m*
a /Å	7.354(4)
b /Å	7.354(4)
c /Å	43.220(5)
α /°	90
β /°	90
γ /°	120
V / Å^3	2024.2(16)
Z	3
Crystal size /mm	0.06 × 0.03 × 0.01
Crystal shape and colour	Blue platelet
Data collection T/ K	93(2)
F(000)	1368
R_{int}	0.1679
Obsd data (I >2σ(I))	448
Data/restraints/parameters	517/3/45
GOOF on F^2	1.188
R1, *w*R2 (I >2σ(I))	0.0776, 0.1904
R1, *w*R2 (all data)	0.0877, 0.1964
Largest diff. peak / hole	1.762/–0.976
Oxidation state of V ions	4+/3+

The structure of **VF-19** (Figures 5-23, 5-24) consists of isolated pillared double layers of stoichiometry $[V_7O_6F_{18}]^{3-}$. These layers are built of two V^{4+} containing kagome sheets that are pillared by a V^{3+} ion. Within each of these layers resides the NH_4^+ cation, and between these layers along the *c*-axis lies the quinuclidinium cation, which is crystallographically disordered over two sites (Figure 5-25).

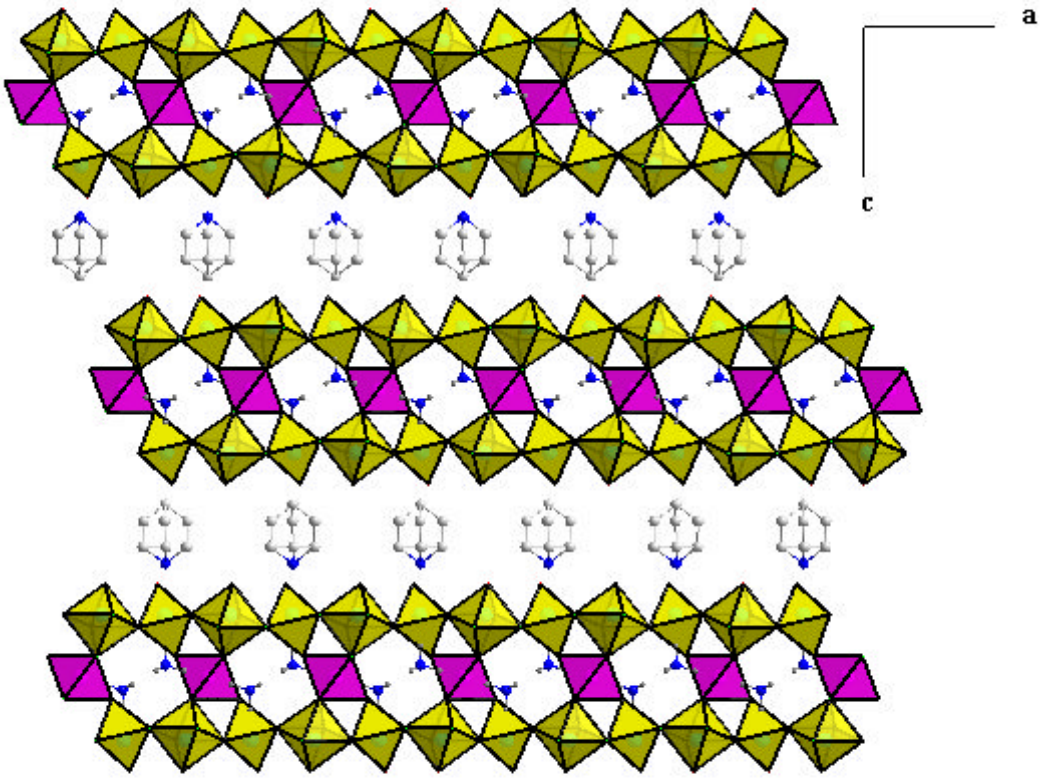

Figure 5-23. A view of **VF-19** parallel to the crystallographic *b* axis showing one of the possible orientations of the quinuclidinium cations in the interlayer space. (polyhedra that present V^{4+} are coloured yellow, the ones for V^{3+} are in pink).

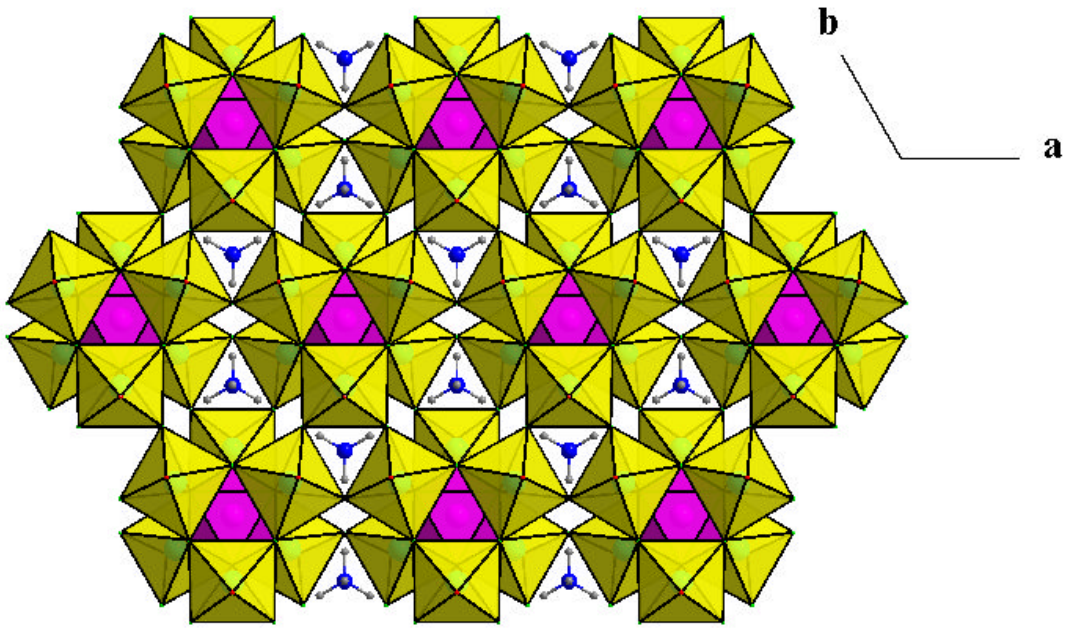

Figure 5-24. A view of the pillared double layer for **VF-19** perpendicular to the crystallographic *c*-axis.

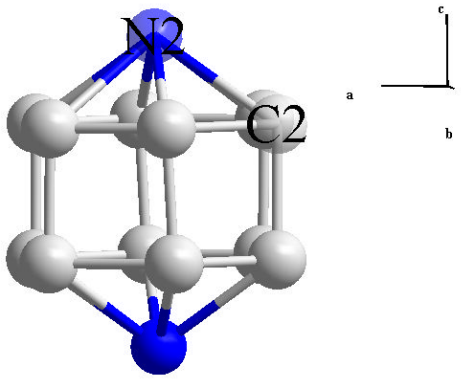

Figure 5-25. Disordered model for the quinuclidine moiety: All twelve C2 sites are equivalent and half-occupied, N2 represents 50:50 disordered C and N atoms.

There are two crystallographically distinct vanadium sites, V1 sits on a site of high symmetry (–3m), whereas V2 sits on a mirror plane: the refinement unambiguously shows O/F ordering such that each V2 has one short vanadyl (V=O) bond, whereas V1

is surrounded exclusively by F^- ligands. The building unit for **VF-19** is shown in Figure 5-26.

The structure around V2, particularly the presence of the vanadyl bond, is indicative of V^{4+}, while that around V1 suggest that this is V^{3+}. In addition to this chemical nature, bond valence sum analysis (see Table 5-9) supports this assignment of V1 as V^{3+} and V2 as V^{4+} ($\sum V1 = 3.29$, $\sum V2 = 3.97$).

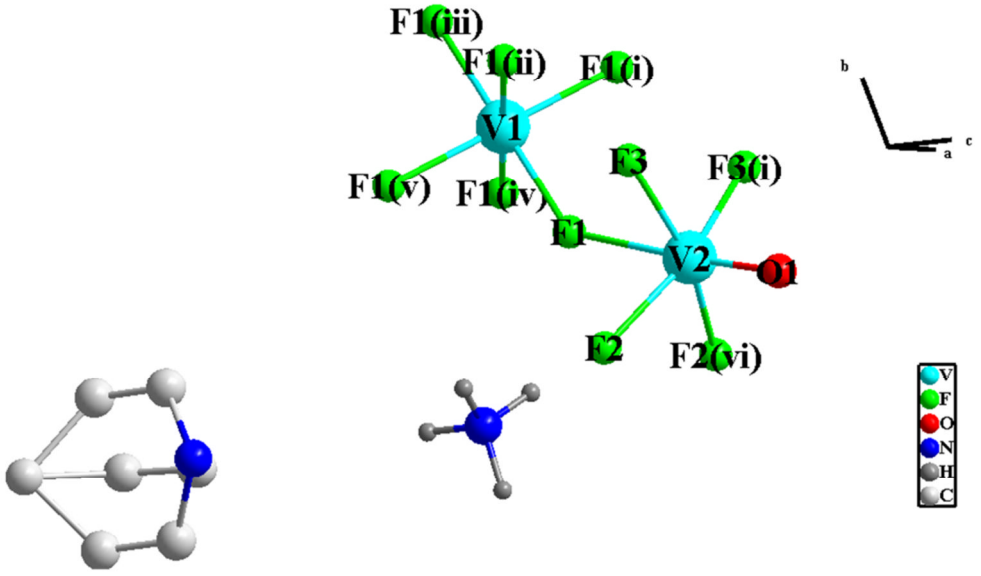

Figure 5-26. Building unit for **VF-19**. Note only one conformation of the quinuclidinium cation is shown. Symmetry operators: (i) 2–y, x–y+1, z; (ii) 1–x+y, 2–x, z; (iii) 2–x, 2–y, –z; (iv) 1+x–y, x, –z; (v) y, 1–x+y, –z; (vi) 1–x+y, 1–x, z; (vii) 1–y, x–y, z.

As we can see from Figure 5-27 V1 and V2 are connected through bridging F atoms into a heptameric, pyrochlore-like building unit consisting of two $V^{4+}{}_3O_3F_{12}$ triangles linked by a further V^{3+} ion. These heptameric building units are then connected to form the double layer (Figure 5-28).

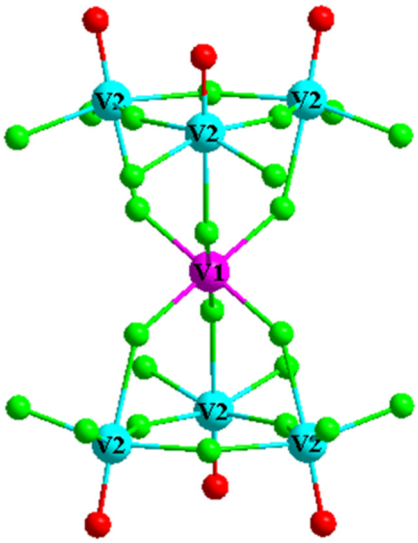

Figure 5-27. The pyrochlore-like heptameric building unit of the inorganic framework in **VF-19**.

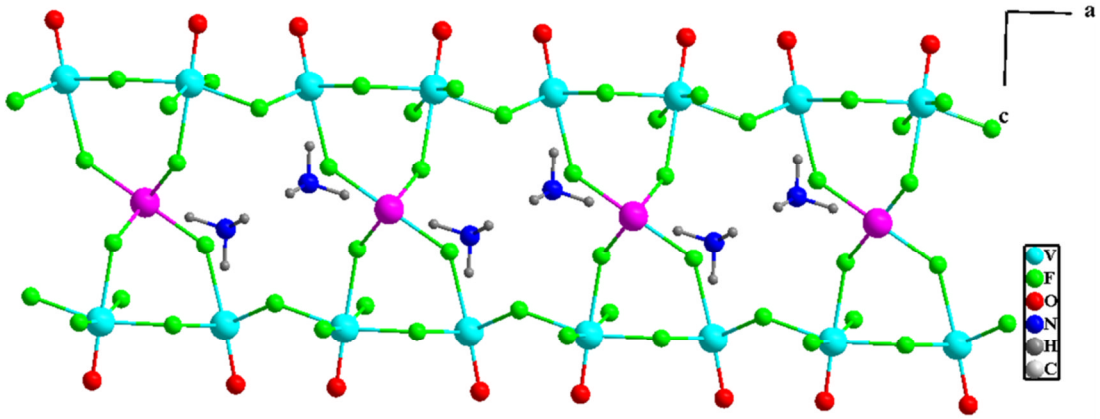

Figure 5-28. A view of the pillared double layer in **VF-19** viewed along the *b* axis.

Table 5-9. Selected bond lengths and bond valence sums for **VF-19**.

Bond	Bond length (Å)	S_{ij}	Bond	Bond length (Å)	S_{ij}
V1-F1	1.924(6)	0.549	V2-O1	1.580(8)	1.717
V1-F1^{i}	1.924(6)	0.549	V2-F1	2.153(6)	0.294
V1-F1^{ii}	1.924(6)	0.549	V2-F2	1.973(3)	0.478
V1-F1^{iii}	1.924(6)	0.549	V2-F2^{vi}	1.973(3)	0.478
V1-F1^{iv}	1.924(6)	0.549	V2-F3	1.956(6)	0.501
V1-F1^{v}	1.924(6)	0.549	V2-F3^{i}	1.956(6)	0.501
		∑V1 = 3.294			**∑V2 = 3.969**

(i) 2–y, x–y+1, z; (ii) 1–x+y, 2–x, z; (iii) 2–x, 2–y, –z; (iv) 1+x–y, x, –z; (v) y, 1–x+y, –z; (vi) 1–x+y, 1–x, z; (vii) 1–y, x–y, z.

The inverse magnetic susceptibility versus T plot (Figure 5-29) is described well by a Curie-Weiss law above 150 K. The paramagnetic moment of μ_{eff} = 5.11 μ_B derived from the slope is in excellent agreement with the value of 5.10 μ_B expected for a formula unit of six V^{4+} (S = ½) and one V^{3+} (S = 1) spin-only ions. This supports the above structural model and the assignments of V1 and V2 as V^{3+} and V^{4+} respectively.

The substantial negative Weiss constant of θ = –81 K shows that strong antiferromagnetic exchange interactions are present – this is also seen in the plot of χT versus T (Figure 5-30) which does not saturate at 300 K. However, no magnetic ordering transition (T_M) is observed down to the lowest measured temperature of 2 K.

The magnetic data suggest a spin-frustrated behaviour of **VF-19.** Ramirez has quantified the spin frustration by defining a frustration index given by the formula:

$$f = -\theta/T_M$$

(where θ is the Weiss constant and T_M represents any ordering transition temperature), with values of f greater than 10 signifies strong frustration.[12] By this definition, we can say that **VF-19** is highly frustrated, with the frustration index (*f*) having a value of at least 40.

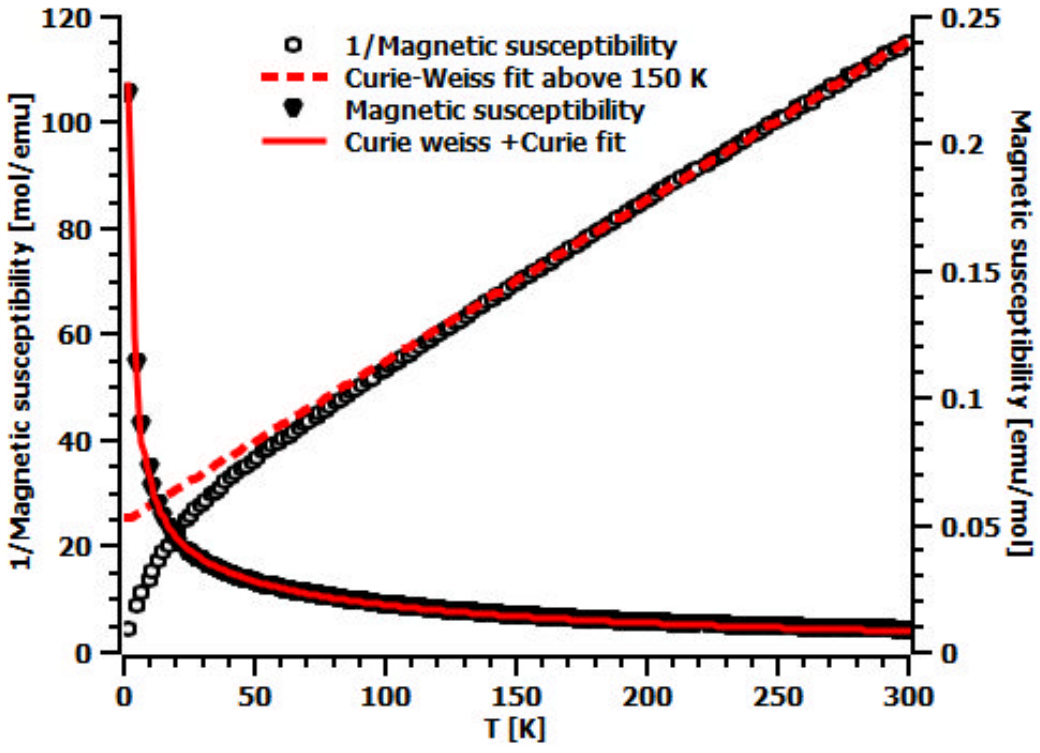

Figure 5-29. Curie-Weiss fit for 1/χ above 150 k for **VF-19**, and the Curie-Weiss + Curie fit for χ(T).

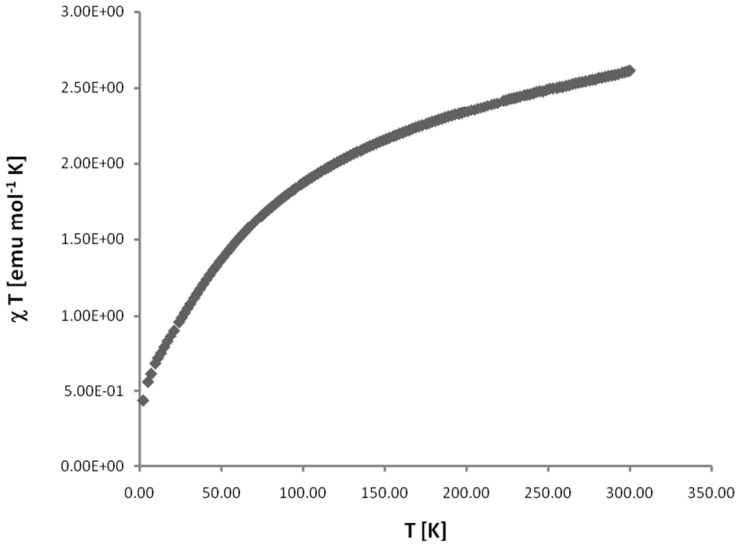

Figure 5-30. Plot of χT *versus* T for **VF-19**.

No significant divergence between zero-field (ZFC) and field (FC) cooled susceptibilities is observed (Figure 5-31), showing that no spin freezing occurs down to at least 2 K.

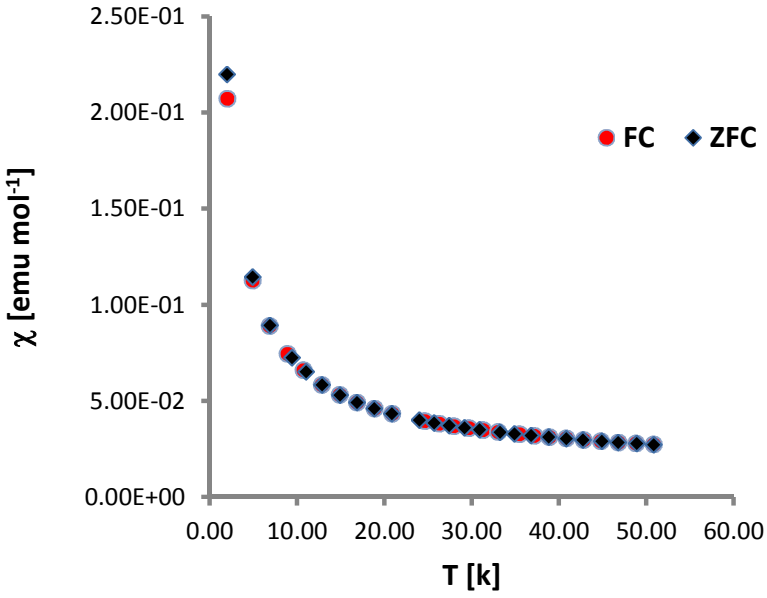

Figure 5-31. FC and ZFC plots for χ(T) from 0 to 50 K for **VF-19**.

The behaviour of the magnetic susceptibility over the whole range (2-300 K) could simply be fitted using a sum of Curie-Weiss and Curie terms ($\chi = C_1/(T-\theta)+C_2/T$) rather than Curie-Weiss (Figure 5-32).

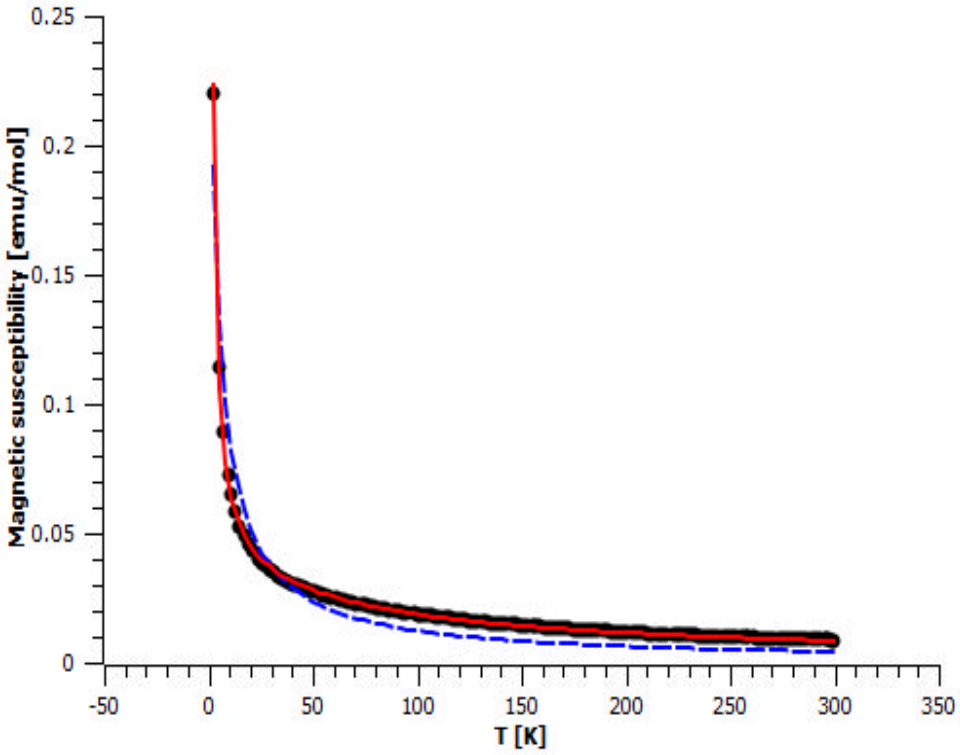

Figure 5-32. Curie-Weiss (blue lines) and Curie-Weiss + Curie (red lines) fits to $\chi(T)$ for **VF-19** from 2 to 300 K.

These results may suggest that the V1 sites are possibly decoupled from the V2 spins and behave as an additional Curie system, thus **VF-19** may present pure kagome behaviour. In order to confirm whether **VF-19** represents a pure kagome or kagome bilayer behaviour, more specific measurements are needed these may include: heat capacity and muon-spin measurements.

From the crystal structure and the magnetic properties we have presented above, it is clear that **VF-19** is a unique material in many ways and features several unusual properties that have not been seen previously in related compounds. **VF-19** stands as a new example of geometrically frustrated systems, the so called kagome lattice, in fact it represents the first d^1 and d^2 material exhibiting the kagome type within d^1 layer. In order to fully understand the importance of **VF-19**, the concepts of magnetic frustration and kagome lattice will be briefly explained, then we will review some of the popular materials exhibiting spin = ½ kagome antiferromagnet behaviour. We will then compare our system to the widely studied Herbertsmithite ($ZnCu_3(OH)_6Cl_2$) and other related materials and discern any differences and similarities.

Magnetic frustration and kagome lattice

As it was mentioned in section 3-5, antiferromagnetic interactions arise when the spins are aligned anti-parallel to each other. This can clearly be seen in a square lattice as it is illustrated in Figure 5-33(left), where all the antiferromagnetic interactions are satisfied. However for some systems due to their geometry constraints, these interactions cannot be simultaneously satisfied. This can be better understood when the lattice is based on triangles as it is highlighted in Figure 5-33(right). Three neighbouring spins cannot be pairwise anti-aligned and the system is frustrated.

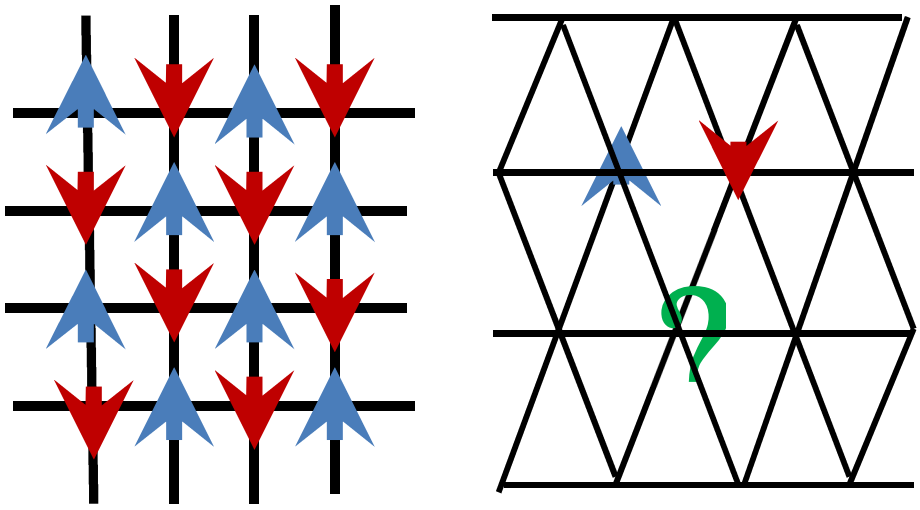

Figure 5-33. Antiferromagnetic interactions in a square lattice (left), magnetic frustration in a triangle based lattice (right).

In an antiferromagnetic system the magnetic frustration can be identified by the measure of the magnetic susceptibility as a function of the temperature in an applied magnetic field. The plot of χ versus T will show the material ordering temperature (TM) (if any). The Weiss constant can then be determined from the plot of $1/\chi$ *versus* T. In a typical case of a non-frustrated system $|\theta| \approx$ TM. For a frustrated system $|\theta|$ >> TM. This can be clearly seen in Figure 5-34.

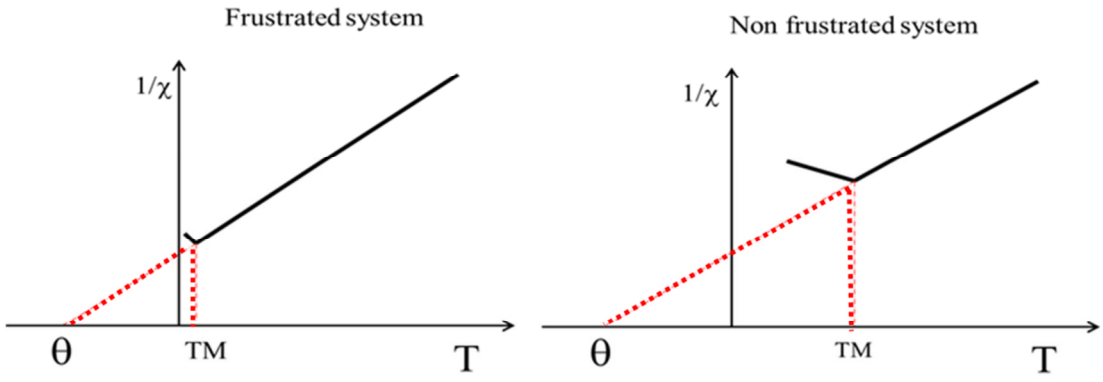

Figure 5-34. How frustration is identified in an antiferromagnetic system.[12]

The 2D lattices that represent the classic examples of geometry frustrated magnetic systems are the triangular and the kagome lattices. The triangular lattice is based on edge-shared triangles (as illustrated in Figure 5-33(right)), each site in this lattice belongs to six triangles. The FCC lattice, which may be regarded as a network of edge-sharing tetrahedra, is the three-dimensional equivalent of this. However, the kagome lattice (Figure 5-35); is based on triangles that are corner-shared, so each site belongs to only two triangles. The pyrochlore lattice contains a network of vertex-sharing tetrahedra is the three-dimensional equivalent of this. The Kagome lattice can be regarded as more frustrated than the triangular lattice.

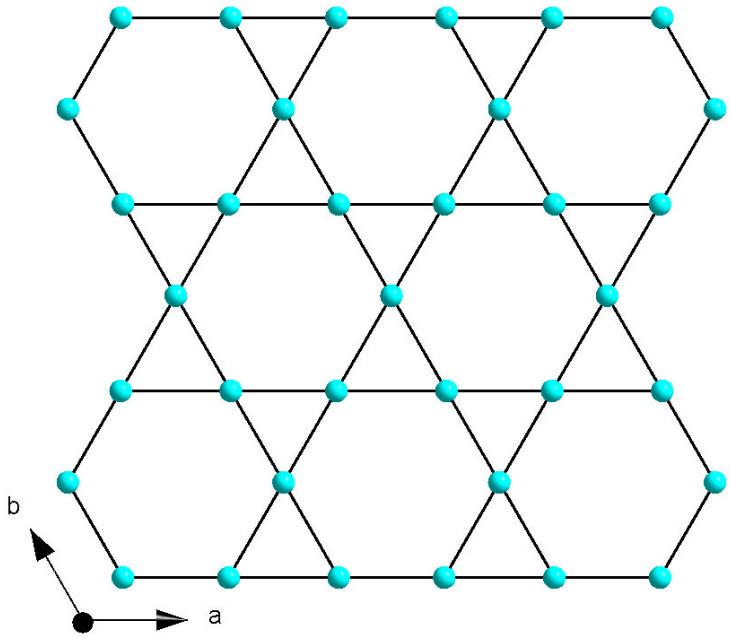

Figure 5-35. The kagome lattice.

For the purpose of this section we will be focusing (exclusively) on the kagome lattice with spin (S = ½).

Kagome antiferromagnets have been attracting considerable attention. Especially those based on S = ½ as they are the most likely candidate to display quantum spin liquid phase (QSL).[12,13] When the frustrated network is composed of magnetic spins with spin = ½ there is the possibility of strong quantum interactions between them, which should theoretically lead to a QSL. On the basis of this, most theoretical investigations of QSL have been concentrated on kagome lattices with S = ½. In practice, however, only a few materials can be regarded as perfect S = ½ kagome antiferromagnet and candidates for QSL.

Perhaps, Herbersmithite $ZnCu_3(OH)_6Cl_2$, which is a member of the parent paratacamite family of naturally occurring minerals which has the formula $Zn_xCu_{4-x}(OH)_6Cl_2$, remain, so far, a prime candidate for a QSL solid. This mineral, specially after it has been synthesised by Nocera and co workers,[14] received a huge interest and has been widely studied using a battery of techniques.[15-20] The crystal structure of the ideal Herbersmithite, $ZnCu_3(OH)_6Cl_2$ is shown in Figure 5-36, consisting of kagome planes (Figure 5-37) of hydroxide bridge S = ½ Cu^{2+} ions, the kagome layers are separated by $(Zn(OH)_6)^{4-}$ octahedral units connected to the kagome layers through the hydroxide ligand.

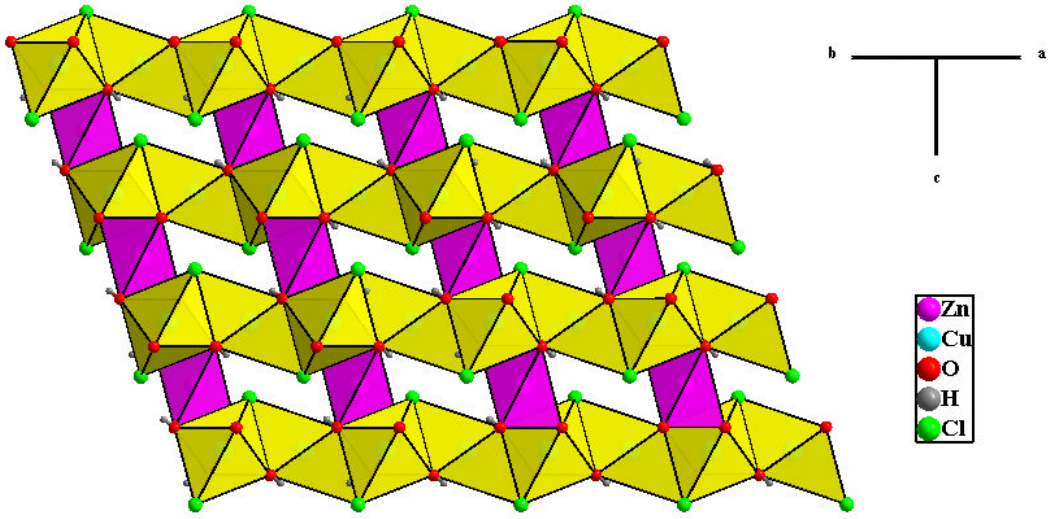

Figure 5-36. Crystal structure of the ideal Herbersmithite, showing the kagome layers separated by Zn (pink polyhedra).

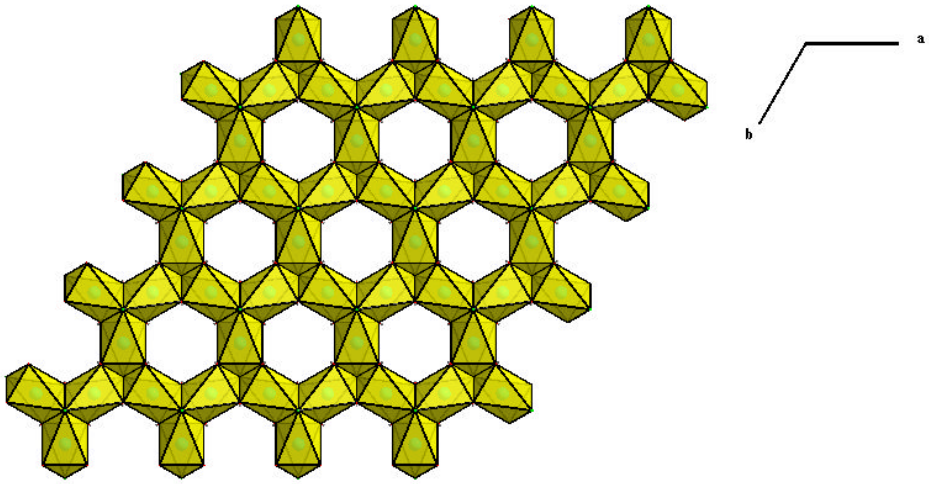

Figure 5-37. A view of the kagome layer found in the ideal Herbersmithite along the *c* axis.

However, Cu and Zn can not precisely been identified from X-ray diffraction, as their scattering factors are virtually identical. Recent studies suggest that, although there is no Cu/Zn disorder in the kagome layers (they are occupied only by Cu atoms), there is Cu/Zn disorder between the layers. Upon these studies, it was suggested that the

formula Herbersmithite would be revised to be $Zn_{0.85}Cu_{3.15}(OH)_6Cl_2$ rather than $ZnCu_3(OH)_6Cl_2$ as was thought previously.[15,16] This material is one of the most frustrated spin systems with no long-rang magnetic ordering above 50 mK, and significant antiferromagntic interactions frustration ($\theta \approx -314$ K).

Very recently the Mg analogue of Herbersmithite, Mg-Herbersmithite (γ-$MgCu_3(OH)_6Cl_2$) has been synthesised and proposed as a new, potential, candidate for QSL.[21]

There are also, various compounds formed by transition metal ions with varying spin (5/2 (Fe^{3+}), 1 (Ni^{2+}, V^{3+}), 3/2 (Co^{2+}), 2 (Fe^{2+})) and others with mixed valence ions (Fe^{2+}, Fe^{3+}), most of these material exhibit long range ordering.[22]

Similar compounds to $ZnCu_3(OH)_6Cl_2$ have been observed in the fluorides $Cs_2ZrCu_3F_{12,}$[23,24] $Cs_2LiMn_3F_{12}$[25] and related phases. In these cases, 3D *chemical* connectivity is again preserved, but magnetic connectivity is reduced to 2D by the presence of an inert 'blocking' cation in the site linking two adjacent kagome layers (analogous to Zn^{2+} in perfectly ordered $ZnCu_3(OH)_6Cl_2$). In most of these cases there is evidence of long-range magnetic ordering, perhaps caused by symmetry-lowering from the ideal kagome lattice.

Moving away from the purely inorganic kagome materials, metal-organic hybrid materials bearing the kagome structural motif are possible but are extremely rare. Although there are some reported organically template metal fluorosulfates based on

(Mn^{2+}, Ni^{2+}, Co^{2+})[22], and some metal organic framework systems based on (In, V, Zn).[26-29] However none of these materials are based on spin (S = ½), and the only hybrid kagome material with spin (S = ½) reported so far, is the Cu^{2+} based metal organic framework synthesised by Nocera and co workers.[30] This material has the formula Cu(1,3-bdc) (1,3-bdcH_2 stands for isophtalic acid), and crystallises in the hexagonal space group $P6_3/m$. Cu^{2+} ions are bridged by carboxylate groups to form a kagome lattice in the *ab* plane as it is shown in Figure 5-38. The kagome planes are linked by 1,3-bdc ligands into a three dimensional framework (Figure 5-39).

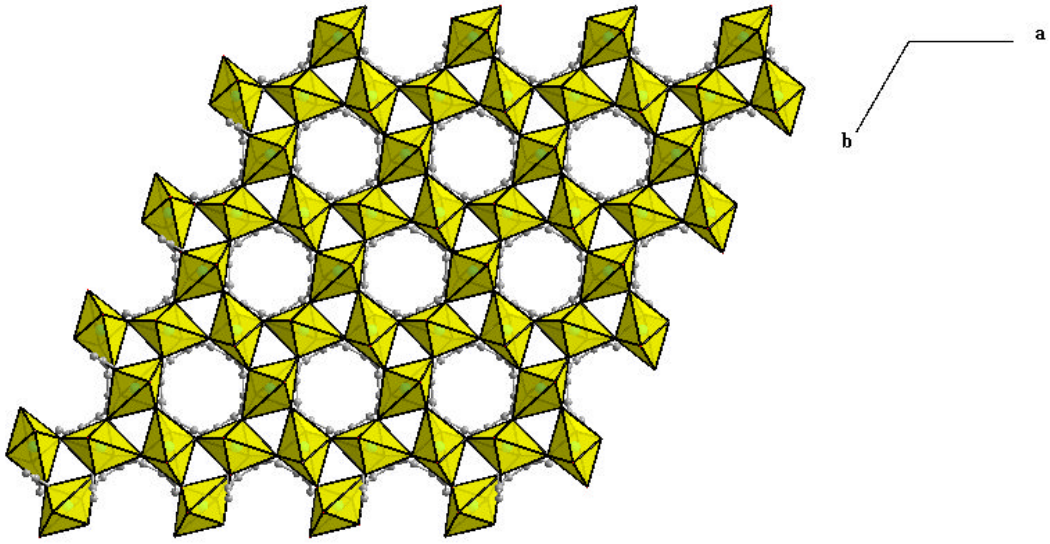

Figure 5-38. The kagome layer in Cu(1,3-bdc)

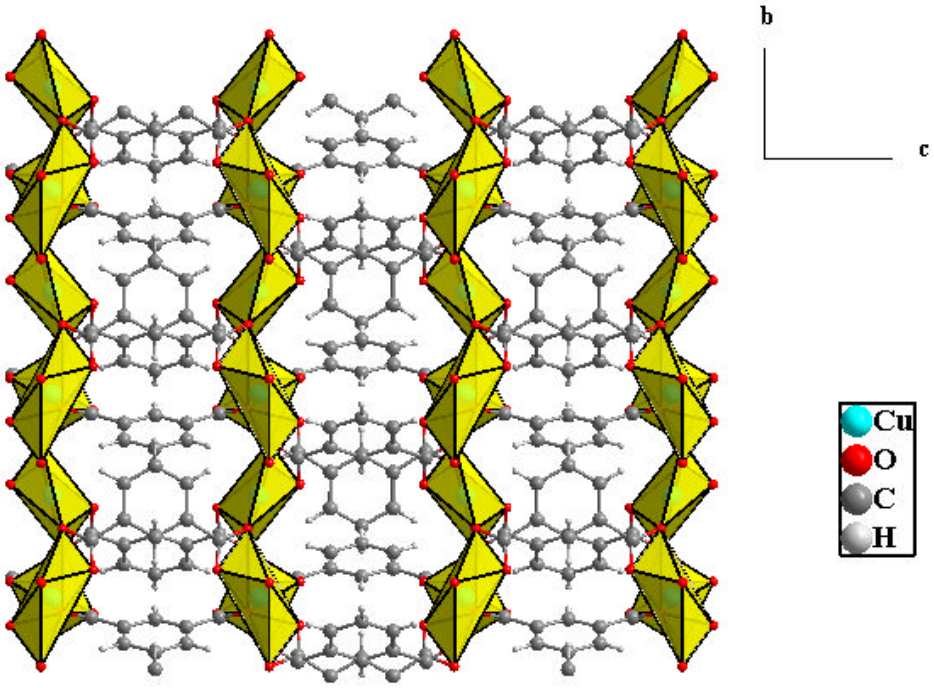

Figure 5-39. A view of Cu(1,3-bdc) along the *a* axis showing the Cu layers separated by bdc ligand.

This material exhibits spin frustration with θ = –33 K and no magnetic ordering, such that it has been proposed as a model for spin ½ kagome magnet.

It is instructive to compare the structure of **VF-19** with that of Herbertsmithite, ($ZnCu_3(OH)_6Cl_2$). The V1 sites in **VF-19** act to link adjacent kagome planes along the *c*-axis into the pillared double layer described previously. However, in the case of $ZnCu_3(OH)_6Cl_2$ this linkage is extended infinitely in this direction giving rise to overall 3D connectivity. However, in the 'perfect' Herbertsmithite structure, the kagome lattice would be separated by magnetically inert Zn^{2+} ions (which may be considered a type of 'dimensional reduction'). **VF-19** shows a different and unique kind of dimensional reduction. The double pillared layers are separated only by organic cations and are

therefore magnetically isolated. In the double layer itself the two constituent kagome nets are linked by a V^{3+} unit. Within the kagome layer itself, the detailed geometry of **VF-19** may be also be compared with that of $ZnCu_3(OH)_6Cl_2$. Firstly, unlike $ZnCu_3(OH)_6Cl_2$ where all the triangles in the kagome sheets are the same size, in **VF-19** there are two distinct near-neighbour V–V contacts of about 3.60 and 3.75 Å, which leads to two different sized equilateral triangles (marked 1 and 2 in Figure 5-40) which alternate in a periodic manner. This is easily rationalised because the VOF_5 distorted octahedra that make up the kagome net are tilted so that in one triangle all three terminal vanadyl bonds point in towards a point parallel to the 3-fold axis of the triangle, while in the adjacent triangle all three vanadyl groups point away from the 3-fold axis. This is clearly seen in Figure 5-40. This 'alternating triangle' kagome sheet is an unusual feature of compound **VF-19**, which is not seen in other kagome structures of interest.

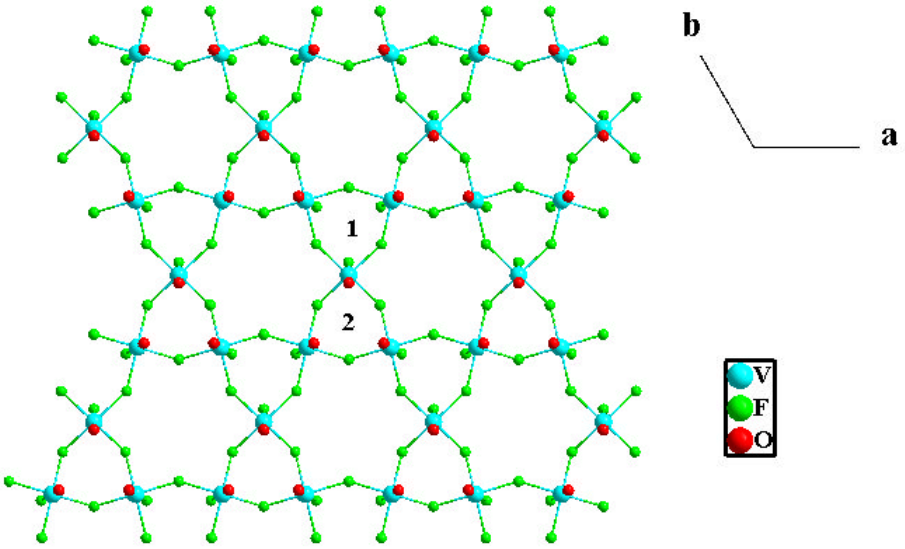

Figure 5-40. The V^{4+} containing kagome lattice found in **VF-19.**

The out-of-plane ligand distances are significantly different, due to the Cu^{2+} Jahn-Teller distortion (Cu-Cl 2.77 Å versus V-O, V-F 1.582(6), 2.150(5) Å). Note that in $ZnCu_3(OH)_6Cl_2$ the in-plane O-atoms are also coordinated to the interlayer site, whereas they are not in the case of **VF-19** and instead the apical F1 sites are bonded to V1.

5-6. Concluding remarks

The results presented in this chapter show how the careful choice of the reaction environment can yield novel materials and how accessing novel chemistry offers in turn the opportunity to discover new solids with exciting new chemical and physical properties. The foregoing results show without any doubt that the choice of EMIM Tf_2N, with its unusual properties, at high reaction temperature (170 °C) is a key for the synthesis of VOFs with extended networks.

VF-14, the first 2D VOF compound that contains only V^{4+} ions, has been prepared using EMIM Tf_2N as the solvent and HF·Pyridine as a non-aqueous form of fluoride source and also as a template. EMIM Tf_2N, although not occluded into the final structure, has a great importance in stabilising V ions at higher oxidation state at elevated temperature. While **VF-14** can be synthesised at 170 °C, this material can still be accessible at a temperature as high as 220 °C. Other reactions have been carried out by replacing the IL with other solvents (ethylene glycol, pyridine, water), none of them gave the desired material.

VF-14 can also be prepared by a slightly different procedure, with V_2O_5 being replaced by VOF_3 and HF·pyridine being replaced by using a small amount of HF (allowing the IL to still be the predominant solvent despite the presence of a small amount of water arising from the HF solution), pyridine is also added to act as a template.

Upon that, using the same procedure with imidazole as an added template afforded (**VF-15**) an imidazolium analogue of **VF-14,** despite having the same inorganic framework, these two materials exhibit interesting differences.

VF-16 exists as a minor phase with **VF-15, VF-16** in its turn presents another variation to the typical known ladder-type structures, it is template by both imidazolium moieties and NH_4^+ cations, which probably came from the partial breakdown of the imidazolium cations. However, in this work we could not get this material in a pure phase and this precluded any further analysis.

VF-17 was prepared by the addition of KNO_3 to the reaction; it is isostructural to **VF-16.** However the addition of $CsNO_3$ gave **VF-18** that contains Cs cations only as a template with no imidazolium moities**.**

The selective choice of the template used is of great importance, in an attempt to direct the structure to higher dimensionality; a bicyclic amine "quinuclidine" has been used. There is no previous report of using such template in VOFs or other metal fluorides synthesis. This has afforded a unique material (**VF-19)**. **VF-19** is a unique material in many ways: it is one of the very few organic-inorganic hybrid materials bearing the kagome structural motif with spin (S = ½), it is also the first example of a d^1 S = ½ kagome net. The double pillared layer and the "alternating kagome triangle" are also unprecedented in previous kagome-type materials. Interestingly, when EMIM Tf_2N is replaced by other ILs (EMIM Br, BMIM Br) or other solvents (ethylene glycol, pyridine, water) no solid product was formed under these conditions.

From the successful synthesis of the materials presented in this chapter, there is a great scope to apply the same strategy for the synthesis of other related or may be different materials. Definitely, by using different templates, or by slightly changing the procedure we would expect the isolation of different materials, the templates used in this chapter are mainly cyclic organic amine with one nitrogen site (pyridine, imidazole, quinuclidine), other linear or cyclic amines could be used.

There is also great scope to alter the chemistry in order to prepare other similar materials with subtle differences to **VF-19**. For instance it is perfectly plausible to imagine replacing the organic structure directing agents in **VF-19** with other inorganic or organic moieties, Similarly, studies of chemical substitutions into the kagome layers or into the V1 sites are possible targets.

The structures presented in this chapter are summarised in Table 5-10, along with their formula, dimentionality and the oxidation state of vanadium ions. References for the known structures are also given.

Table 5-10. Selected structural characteristics of VOFs structures in this chapter

Identification code	Chemical formula/Ref	Dimensionality	Structural unit	Ox. State
VF-14	$[HNC_5H_5][V_2O_2F_5]$	2D	Edge-and corner-sharing octahedra into 2D net (F bridges)	4+
VF-15	$[HNC_3NH_4][V_2O_2F_5]$	2D	Edge-and corner-sharing octahedra into 2D net (F bridges)	4+
VF-16	$[HNC_3NH_4]NH_4[V_2O_2F_6]$	1D	Ladder of corner- and edge- sharing octahedra (F bridges)	4+
VF-17	$[HNC_3NH_4]K[V_2O_2F_6]$	1D	Ladder of corner- and edge- sharing octahedra (F bridges)	4+
VF-18	$CsVOF_3$[7]	1D	Ladder of corner- and edge- sharing octahedra (F bridges)	4+
VF-19	$[HNC_7H_{13}][NH_4]_2[V_7O_6F_{18}]$	2D	Double layers of Kagome type.	4+/ 3+

5-7. References

(1) Aldous, D. W.; Stephens, N. F.; Lightfoot, P. *Dalton Trans.* **2007**, 4207.

(2) Aldous, D. W.; Stephens, N. F.; Lightfoot, P. *Dalton Trans.* **2007**, 2271.

(3) DeBurgomaster, P.; Ouellette, W.; Liu, H.; O'Connor, C. J.; Yee, G. T.; Zubieta, J. *Inorg. Chim. Acta* **2010**, *363*, 1102.

(4) Mahenthirarajah, T.; Li, Y.; Lightfoot, P. *Inorg. Chem.* **2008**, *47*, 9097.

(5) Mahenthirarajah, T.; Lightfoot, P. *Chem. Commun.* **2008**, 1401.

(6) Férey, G. *J. Fluorine Chem.* **1995**, *72*, 187.

(7) Aldous, D. W.; Goff, R. J.; Attfield, J. P.; Lightfoot, P. *Inorg. Chem.* **2007**, *46*, 1277.

(8) Carlin, R. L. *Magnetochemistry*; Springer: Berlin, 1986.

(9) Kaul, E. E.; Rosner, H.; Yushankhai, V.; Sichelschmidt, J.; Shpanchenko, R. V.; Geibel, C. *Physical Review B* **2003**, *67*, 174417.

(10) Fisher, M. E. *J.Math. Phys.* **1963**, *4*, 124.

(11) Landee, C. P.; Turnbull, M. M.; Galeriu, C.; Giantsidis, J.; Woodward, F. M. *Physical Review B* **2001**, *63*, 100402.

(12) Ramirez, A. P. *Annu. Rev. Mater. Sci.* **1994**, *24*, 453.

(13) Harrison, A. *J. Phys.: Condens. Matter* **2004**, *16*, S553.

(14) Shores, M. P.; Nytko, E. A.; Bartlett, B. M.; Nocera, D. G. *J. Am. Chem. Soc.* **2005**, *127*, 13462.

(15) de Vries, M. A.; Harrison, A. *Nature* **2010**, *468*, 908.

(16) Freedman, D. E.; Han, T. H.; Prodi, A.; Muller, P.; Huang, Q.-Z.; Chen, Y.-S.; Webb, S. M.; Lee, Y. S.; McQueen, T. M.; Nocera, D. G. *J. Am. Chem. Soc.* **2010**, *132*, 16185.

(17) Lee, S. H.; Kikuchi, H.; Qiu, Y.; Lake, B.; Huang, Q.; Habicht, K.; Kiefer, K. *Nat. Mater.* **2007**, *6*, 853.

(18) Marcipar, L.; Ofer, O.; Keren, A.; Nytko, E. A.; Nocera, D. G.; Lee, Y. S.; Helton, J. S.; Bains, C. *Physical Review B* **2009**, *80*, 132402.

(19) Mendels, P.; Bert, F.; de Vries, M. A.; Olariu, A.; Harrison, A.; Duc, F.; Trombe, J. C.; Lord, J. S.; Amato, A.; Baines, C. *Phys. Rev. Lett.* **2007**, *98*, 077204.

(20) Poilblanc, D.; Ralko, A. *Physical Review B* **2010**, *82*, 174424.

(21) Colman, R. H.; Sinclair, A.; Wills, A. S. *Chem. Mater.* **2011**, *23*, 1811.

(22) Pati, S. K.; Rao, C. N. R. *Chem. Commun.* **2008**, 4683.

(23) Ono, T.; Morita, K.; Yano, M.; Tanaka, H.; Fujii, K.; Uekusa, H.; Narumi, Y.; Kindo, K. *Physical Review B* **2009**, *79*, 174407.

(24) Yamabe, Y.; et al. *J. Phys.: Condens. Matter* **2007**, *19*, 145253.

(25) Englich, U.; Frommen, C.; Massa, W. *J. Alloys Compd.* **1997**, *246*, 155.

(26) Barthelet, K.; Marrot, J.; Ferey, G.; Riou, D. *Chem. Commun.* **2004**, 520.

(27) Chun, H.; Moon, J. *Inorg. Chem.* **2007**, *46*, 4371.

(28) Liu, Y.; Kravtsov, V. C.; Beauchamp, D. A.; Eubank, J. F.; Eddaoudi, M. *J. Am. Chem. Soc.* **2005**, *127*, 7266.

(29) Rusanov, E. B.; Ponomarova, V. V.; Komarchuk, V. V.; Stoeckli-Evans, H.; Fernandez-Ibañez, E.; Stoeckli, F.; Sieler, J.; Domasevitch, K. V. *Angew. Chem. Int. Ed.* **2003**, *42*, 2499.

(30) Nytko, E. A.; Helton, J. S.; Müller, P.; Nocera, D. G. *J. Am. Chem. Soc.* **2008**, *130*, 2922.

CHAPTER 6

SYNTHESIS OF ORGANICALLY TEMPLATED IRON FLUORIDES USING ILs AND DESs

6-1. Introduction

In the two previous Chapters (Four and Five) it has been shown that ILs and DESs are promising solvents for the synthesis of organically-templated VOFs. While there is still much scope for other potential structures to be discovered in that system, it has been decided to investigate other metal-based systems to see how this affects the resulting products. In this chapter trivalent transition metal Fe(III) has been chosen due to its role in catalytic applications and potential magnetic properties.

The few reported examples of the hydrothermally prepared organically templated iron fluorides[1-6] revealed a poor structural diversity in contrast to other trivalent elements, *e.g.* Al(III).[7] Most of the reported structures exhibit isolated monomers, dimers or chains, with iron ions adopting the most common oxidation states (3+ or 2+) and octahedral geometry.

ILs and DESs may provide interesting alternative methods to obtain new structures in iron based systems. The strategy followed here is the same as the one used in Chapters Four and Five. Different systems have been studied with the exception of using NH_4F as fluoride source, as according to the results in Chapter Four, this system was the less

interesting and it mainly produced known structures templated by ammonium cations. Three chain type materials have been synthesised and characterised by single-crystal X-ray diffraction. **FeF-1** and **FeF-2a** have been isolated when BMIM Br is the solvent. **FeF-2b** and **FeF-3** were isolated using a DES composed, respectively, of choline chloride/2-imidazolidinone and choline chloride/2,2,2-trifluoroacetamide. The crystal structure of these materials along with synthesis aspects will be discussed here.

6-2. Synthesis of ILs and DESs

The IL BMIM Br and the two DESs (choline chloride/2-imidazolidinone and choline chloride/2,2,2-trifluoroacetamide) used in this chapter were synthesised according to the literature procedure, as described in sections 4-2-2 and 4-2-7, respectively.

6-3. BMIM Br as a solvent for the synthesis of iron fluorides

6-3-1. Synthesis of $FeF_3(H_2O)\cdot H_2O$ (FeF-1)

A typical synthesis procedure was as follows: a Teflon-lined autoclave (volume 15 mL) was charged with Fe_2O_3 (0.160 g, 1 mmol, Sigma Aldrich) and HF (1 mL, 26.7 mmol, 48% in H_2O, Sigma Aldrich) and then the IL BMIM Br (2.2 g, 10 mmol) was added. The stainless steel autoclave was then sealed and heated in an oven at 170 °C for 3 days. After the autoclave had been cooled to room temperature, the product was filtered, washed with methanol and dried in air for 24 hrs. Brown needle shape crystals were collected.

X-ray diffraction data were collected at station 11.3.1 of the Advanced Light Source at Lawrence Berkeley National Laboratory using a Bruker APEX II CCD diffractometer. Structures were solved using direct methods with the program SHELXS and refined on F^2 using full-matrix least-squares with SHELXL-97 under WINGX package. All non-hydrogen atoms were refined anisotropically. Crystal data and structure refinement datails for **FeF-1** are given in Table 6-1. Selected bond lengths and bond valence sums for **FeF-1** are tabulated in Table 6-2.

Table 6-1. Crystal data and structure refinement details for **FeF-1.**

Compound	**FeF-1**
Formula	$FeF_3(H_2O)_2 \cdot H_2O$
Fw (g/mol)	166.90
Space group	*P*4/*n*
a /Å	7.822(5)
b /Å	7.822(5)
c /Å	3.884(5)
α /°	90
β /°	90
γ /°	90
V / Å^3	237.6(4)
Z	2
Crystal size /mm	0.19 × 0.1 × 0.1
Crystal shape and colour	Brown needle
Data collection T/ K	100(2)
F(000)	166
R_{int}	0.0228
Obsd data (I>2σ(I))	356
Data/restraints/parameters	361/1/35
GOOF on F^2	1.103
R1, *w*R2 (I >2σ(I))	0.0160, 0.0453
R1, *w*R2 (all data)	0.0162, 0.0453
Largest diff. peak / hole	0.315 / –0.361
Oxidation state of Fe ion	3+

The inorganic framework was initially solved with one Fe atom and two fluorine atoms in the asymmetric unit, and this resulted in ionic chains $(FeF_{2/2}F_4)^{2-}$ which requires two positively charged moieties to balance the charge. The positively charged moiety was first thought to be ammonium (with one N atom and only one H atom, that can be geometrically located without any constraint, in the asymmetric unit). Ammonium cations could be generated by the breakdown of the IL. The refinement seems fine (R1 ~ 2%) and there were no anomalies in the crystal structure. However CHN analysis (Calc (for a compound with the formula $(NH_4)_2FeF_5$): %C: 0.00; %H: 4.31; %N: 14.98; Found: %C: 0.05; %H: 2.10; %N: 0.01) did not show any nitrogen in the sample. This indicates that the tetrahedral looking molecule is not ammonium and also suggests there may be some disorder in the structure.

Changing the N site to oxygen and the non bridging fluorine to mixed F/O sites did improve the refinement. Refining 75%, 25% F/O disorder would lead to a compound with the formula $[H_3O][FeF_4(H_2O)]$. Refining 50:50 disorder led to the compound $FeF_3(H_2O)_2{\cdot}H_2O$, and this is also in agreement with the crystal structure reported for the β-form of iron fluoride hydrate; β-$FeF_3{\cdot}3H_2O$.[8] The 50:50 F/OH disorder seems to be more acceptable based on the values of R-factors. In this case it is assumed the existence of two disordered water molecules (two orientations) which generates a tetrahedral looking molecule; this requires the framework to be neutral.

The asymmetric unit contains one iron atom, one fluorine atom, one mixed site O/F and one non coordinating water molecule. The metal cations consist of slightly distorted octahedra made of 2 F^- and four O/F disordered sites (V-F/O distances: 1.896(19) -

2.000(2)). The octahedra are connected together through the non disordered F atoms to form infinite *trans*-chains as shown in Figure 6-1.

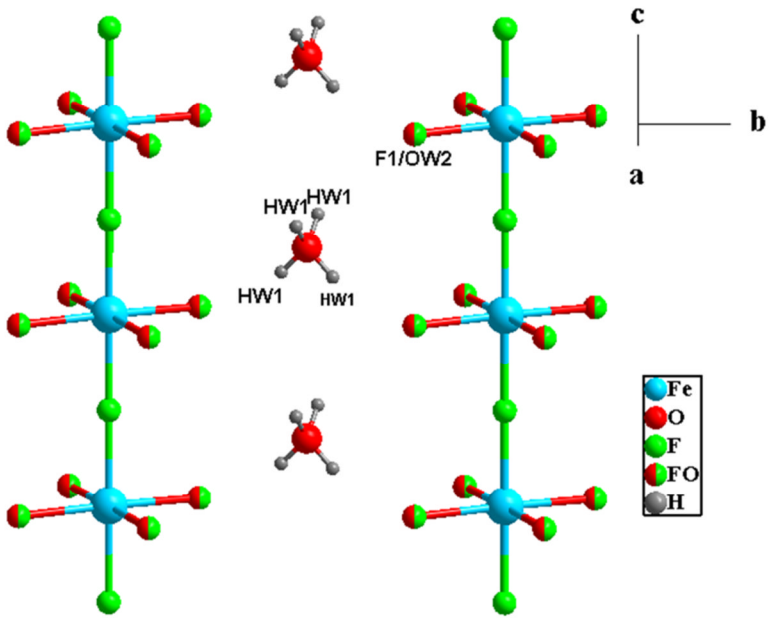

Figure 6-1: A view of **FeF-1** showing the *trans* connected chains with the four O/F disordered sites and the disordered water molecules.

The bond valence sum calculation confirmed that Fe is in the 3+ oxidation state and did not undergo any reduction during the synthesis, as shown in Table 6-2.

Table 6-2. Selected bond lengths, bond valence sums and site occupacy factors for **FeF-1**

Bond	Bond Length (Å)	S_{ij}×S.O.F	Bond	Bond Length (Å)	S_{ij}×S.O.F
Fe01—F1	1.896(19)	0.556*0.5	Fe01—OW2	2.000(20)	0.521*0.5
Fe01—F1^{i}	1.896(19)	0.556*0.5	Fe01—OW2^{i}	2.000(20)	0.521*0.5
Fe01—F1^{ii}	1.896(19)	0.556*0.5	Fe01—OW1^{ii}	2.000(20)	0.521*0.5
Fe01—F1^{iii}	1.896(19)	0.556*0.5	Fe01—OW2^{iii}	2.000(20)	0.521*0.5
Fe01—F2	1.936(3)	0.499	Fe01—F2^{iv}	1.948(3)	0.483
		∑Fe01 = 3.13			

(i) 0.5–x, 0.5–y, z; (ii) y, 0.5–x, z; (iii) 0.5–y, x, z; (iv) x, y, 1+z

The chains are connected together though H-bonding from both the coordinated and the uncoordinated water molecules as it is shown in Figure 6-2.

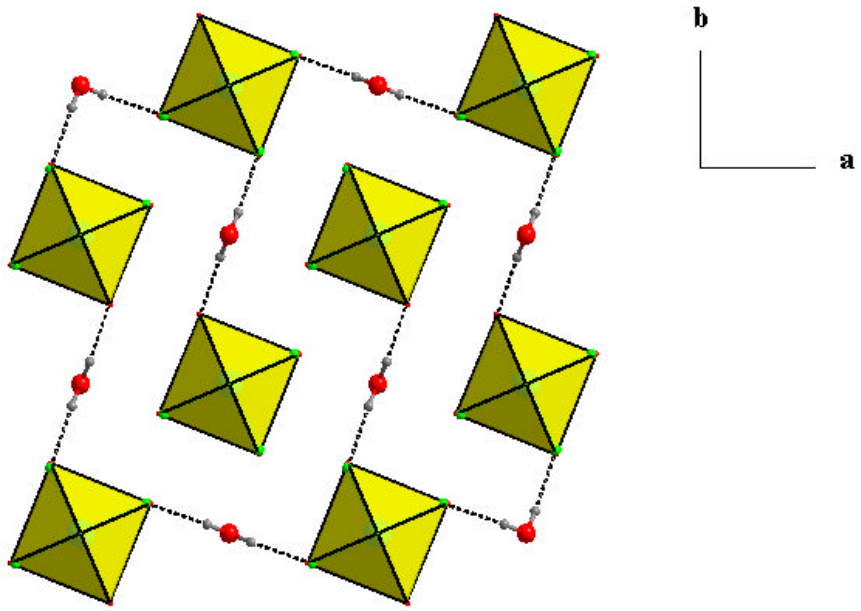

Figure 6-2: Polyhedra presentation of **FeF-1** viewed down the *c* axis**,** showing part of the hydrogen bonding, note that only one orientation of the water molecules is presented.

6-3-2. Synthesis of $[H_2NH_2(CH_2)_2NH_2][FeF_5]$ (FeF-2a)

A typical synthesis procedure was as follows: a Teflon-lined autoclave (volume 15 mL) was charged with FeF_3 (0.112 g, 1 mmol, Sigma Aldrich) and HF (0.1 mL, 2.67 mmol, 48% in H_2O, Sigma Aldrich), the IL BMIM Br (2.2 g, 10 mmol) was added and then (0.60 g, 1 mmol, Sigma Aldrich) of ethylenediamine (*en*) as an added template. The stainless steel autoclave was then sealed and heated in an oven at 170 °C for 24 hrs. After the autoclave had been cooled to room temperature, the product was filtered, washed with methanol and dried in air for 24 hrs to yield white prism shaped crystals.

Single-crystal X-ray diffraction data for **FeF-2a** were collected using Mo-Kα (0.7107 Å) radiation utilising a Rigaku rotating anode single-crystal X-ray diffractometer at the University of St Andrews. The structure was solved with standard direct methods using SHELXS and refined with least-squares minimisation techniques against F^2 using SHELXL under WinGX packages. Crystallographic data and structural refinements for **FeF-2a** are summarised in Table 6-3, selected bond lengths and bond valences are tabulated in Table 6-4.

Table 6-3. Crystallographic data and structure refinement for **FeF-2a.**

Compound	**FeF-2a**
Formula	$[H_2NH_2(CH_2)_2NH_2][FeF_5]$
Fw (g/mol)	212.97
Space group	*P*4/*ncc*
a /Å	12.8670(7)
b /Å	12.8670(7)
c /Å	7.9100(3)
α /°	90
β /°	90
γ /°	90
V / Å^3	1309.58(11)
Z	8
Crystal size /mm	0.30 × 0.03 ×0.03
Crystal shape and colour	Colourless prism
Data collection T/ K	93(2)
F(000)	856
R_{int}	0.0716
Obsd data (I >2σ(I))	555
Data/restraints/parameters	726/0/68
GOOF on F^2	1.264
R1, *w*R2 (I >2σ(I))	0.0514, 0.0964
R1, *w*R2 (all data)	0.0739, 0.1032
Largest diff. peak / hole	0.426 / –0.368
Oxidation state of Fe ion	3+

FeF-2a is isostructural with **VF-7** ([H_2en][VF_5] and **VF-12** (β-[H_2en][VOF_4]**.** The same structure type has also been reported for [H_2en][$TiOF_4$][9] and [H_2en][ScF_5].[10] It is built up from two types of infinite *trans*-connected chains of corner sharing [$FeF_{2/2}F_4$] octahedra. There are two iron atoms, four fluorine atoms and half of the ethylenediammonium cation in the asymetric unit (Figure 6-3). The F atoms bridge the neighboring octahedra into chains (Fe-F distances : 1.911(2) – 2.003(4) Å).

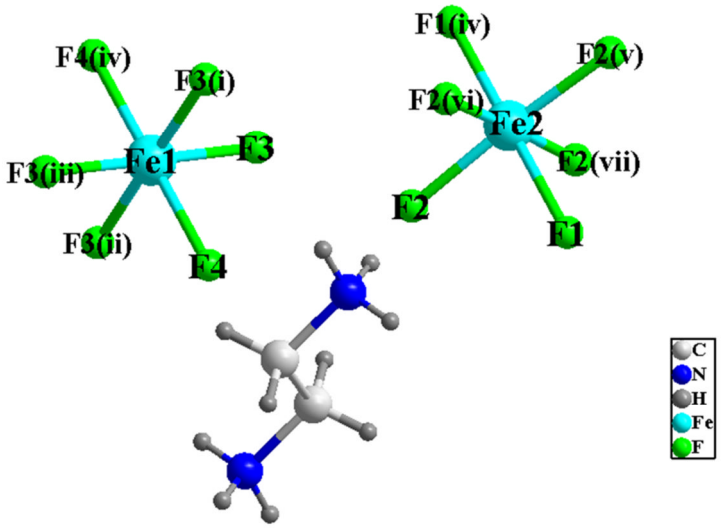

Figure 6-3. The building unit in **FeF-2a**. Symmetry operators
(i) 1–y, 1–x, 1.5–z; (ii) –0.5+y, 0.5+x, 1.5–z; (iii) 0.5–x, 1.5–y, z;
(iv) 0.5–x, y, –0.5+z; (v) 0.5–x, 0.5–y, z; (vi) y, 0.5–x, z; (vii) 0.5–y, x, z.

One chain is in an eclipsed conformation, and the other is in a staggered conformation (Figure 6-4) as occurs in **VF-7** and **VF-12.** F atoms are engaged in an extensive H-bond network (2.654(4) – 3.130(5)Å). The bond valence sum calculations (∑Fe1 = 3.04, ∑Fe2 = 3.03) (Table 6-4) indicate that both Fe ions remain in the 3+ oxidation state.

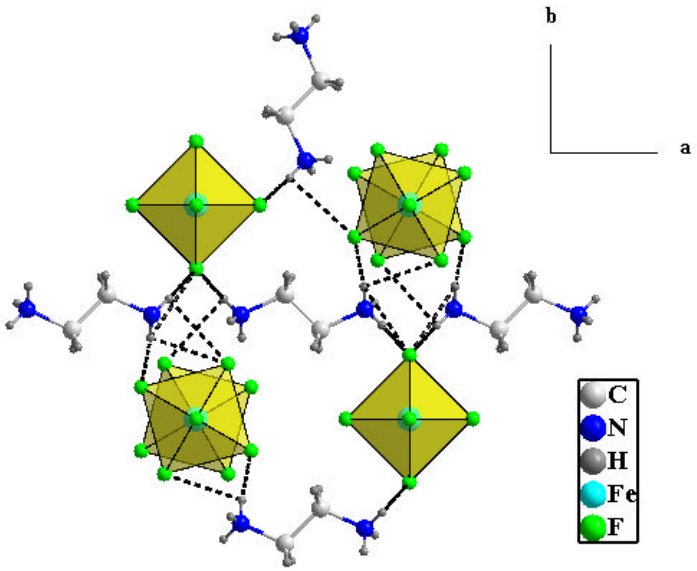

Figure 6-4. The packing of **FeF-2a** as viewed down the *c* axis showing the eclipsed and staggered chains and how they are hydrogen bonded to the ethylenediammonium cations.

Table 6-4. Selected bond lengths and bond valence for **FeF-2a.**

Bond	**Bond Length (Å)**	S_{ij}
Fe1—F3	1.909(2)	0.537
Fe1—F3^{i}	1.909(2)	0.537
Fe1—F3^{ii}	1.909(2)	0.537
Fe1—F3^{iii}	1.909(2)	0.537
Fe1—F4	1.978(1)	0.446
Fe1—F4^{iv}	1.978(1)	0.446
		∑Fe1 = 3.040
Fe2—F2	1.911(2)	0.534
Fe2—F2^{v}	1.911(2)	0.534
Fe2—F2^{vi}	1.911(2)	0.534
Fe2—F2^{vii}	1.911(2)	0.534
Fe2—F1	2.003(4)	0.417
Fe2—F1^{iv}	1.952(4)	0.478
		∑Fe2 = 3.031

(i) 1–y, 1–x, 1.5–z; (ii) –0.5+y, 0.5+x, 1.5–z; (iii) 0.5–x, 1.5–y, z; (iv) 0.5–x, y, –0.5+z; (v) 0.5–x, 0.5–y, z; (vi) y, 0.5–x, z; (vii) 0.5–y, x, z.

6-4. Iron fluoride synthesis using DESs as solvent and template delivery agents

The DESs used in this work are a mixture of choline chloride and two different urea derivatives. The reactions were carried out at low temperature (110 °C). Two chain type structures were synthesised and characterised using single crystal X-ray diffraction.

6-4-1. Chains $[H_2NH_2(CH_2)_2NH_2][FeF_5]$ (FeF-2b)

A typical synthesis procedure was as follows: a Teflon-lined autoclave (volume 15 mL) was charged with Fe_2O_3 (0.160 g, 1 mmol, Sigma Aldrich) and HF (1 mL, 26.7 mmol, 48% in H_2O, Sigma Aldrich) and then the DES choline chloride/2-imidazolidinone was added. The stainless steel autoclave was then sealed and heated in an oven at 110 °C for 24 hrs. After the autoclave had been cooled to room temperature, the product was filtered, washed with methanol and dried in air for 24 hrs. White needle shape crystals were collected.

Single-crystal X-ray diffraction data for **FeF-2b** were collected using Mo-Kα (0.7107 Å) radiation utilising a Rigaku rotating anode single-crystal X-ray diffractometer at the University of St Andrews. The structure was solved with standard direct methods using SHELXS and refined with least-squares minimisation techniques against F^2 using SHELXL under WinGX packages. Crystallographic data and structural refinements for **FeF-2b** are summarised in Table 6-5.

Table 6-5. Crystallographic data and structure refinement for **FeF-2b.**

Compound	**FeF-2b**
Formula	$[H_2NH_2(CH_2)_2NH_2][FeF_5]$
Fw (g/mol)	212.97
Space group	*P*4/*ncc*
a /Å	12.8545(6)
b /Å	12.8545(6)
c /Å	7.9200(4)
α /Å	90
β /Å	90
γ /Å	90
V / Å^3	1308.69(11)
Z	8
Crystal size /mm	0.27 × 0.03 × 0.03
Crystal shape and colour	Colourless prism
Data collection T/ K	93(2)
F(000)	856
R_{int}	0.0836
Obsd data (I >2σ(I))	426
Data/restraints/parameters	601/0/68
GOOF on F^2	0.997
R1, *w*R2 (I >2σ(I))	0.0294, 0.0681
R1, *w*R2 (all data)	0.0428, 0.0724
Largest diff. peak / hole	0.337 / –0.676
Oxidation state of Fe ion	3+

The structure of **FeF-2b** is isostructural to **FeF-2a** and consists of chain templated by protonated ethylene diammonium cations. For full structure description of **FeF-2b** refer to sub section 6-3-2.

6-4-2. Chains $(NH_4)_2FeF_5$ (FeF-3)

A typical synthesis procedure was as follows: a Teflon-lined autoclave (volume 15 mL) was charged with Fe_2O_3 (0.160 g, 1 mmol, Sigma Aldrich) and HF (1 mL, 26.7 mmol, 48% in H_2O, Sigma Aldrich) and then the DES choline chloride/2,2,2-trifluoroacetamide was added. The stainless steel autoclave was then sealed and heated in an oven at 110 °C for 24 hrs. After the autoclave had been cooled to room temperature, the product was filtered, washed with methanol and dried in air for 24 hrs. White prism shape crystals were collected.

Single-crystal X-ray diffraction data for **FeF-3** were collected using Mo-Kα (0.7107 Å) radiation utilising a Rigaku rotating anode single-crystal X-ray diffractometer at the University of St Andrews. The structure was solved with standard direct methods using SHELXS and refined with least-squares minimisation techniques against F^2 using SHELXL under WinGX packages. Crystallographic data and structural refinements for **FeF-3** are summarised in Table 6-6, selected bond lengths and bond valences are tabulated in Table 6-7.

Table 6-6. Crystallographic data and structure refinement for **FeF-3.**

Compound	**FeF-3**
Formula	$(NH_4)_2FeF_5$
Fw (g/mol)	186.93
Space group	*Pcnb*
a /Å	7.6470(2)
b /Å	10.4550(3)
c /Å	13.1710(4)
α /°	90
β /°	90
γ /°	90
V / Å^3	1053.01(4)
Z	8
Crystal size /mm	0.27 × 0.03 ×0.03
Crystal shape and colour	Colourless prism
Data collection T/ K	93(2)
F(000)	744
R_{int}	0.0725
Obsd data (I >2σ(I))	1058
Data/restraints/parameters	1140/0/108
GOOF on F^2	1.244
R1, *w*R2 (I >2σ(I))	0.0620, 0.1450
R1, *w*R2 (all data)	0.0658, 0.1467
Largest diff. peak / hole	0.825 / –0.752
Oxidation state of Fe ion	3+

The structure of **FeF-3** (Figure 6-5) consists of *cis*-connected chains templated by ammonium cations. The asymmetric unit contains one Fe atom, six fluorine atoms and three nitrogen atoms.

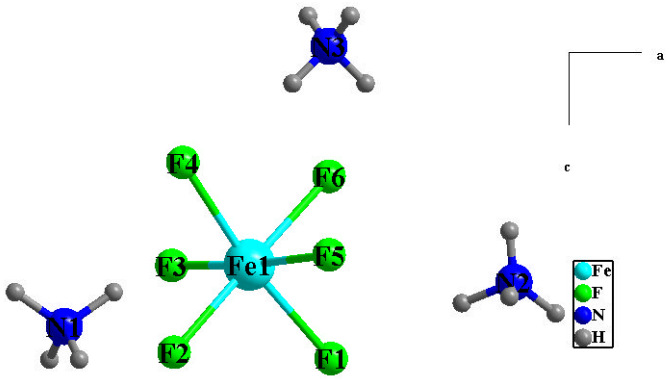

Figure 6-5. Building unit in **FeF-3**.

The octahedra are *cis*-connected together through a F atom to form infinite chains as illustrated in Figure 6-6. (Fe-F distances : 1.892(4) – 1.9968(10) Å). The bond valence sum calculations (∑Fe1 = 3.06) (Table 6-7) indicate that Fe ion remains in the 3+ oxidation state. The chains are separated by ammonium cations generated *in situ* by the partial breakdown of 2,2,2-trifluoroacetamide (Figure 6-8).

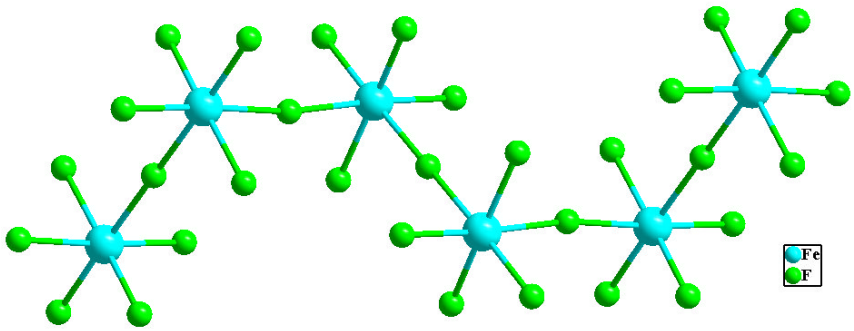

Figure 6-6. *Cis*-connected chains found in **FeF-3**.

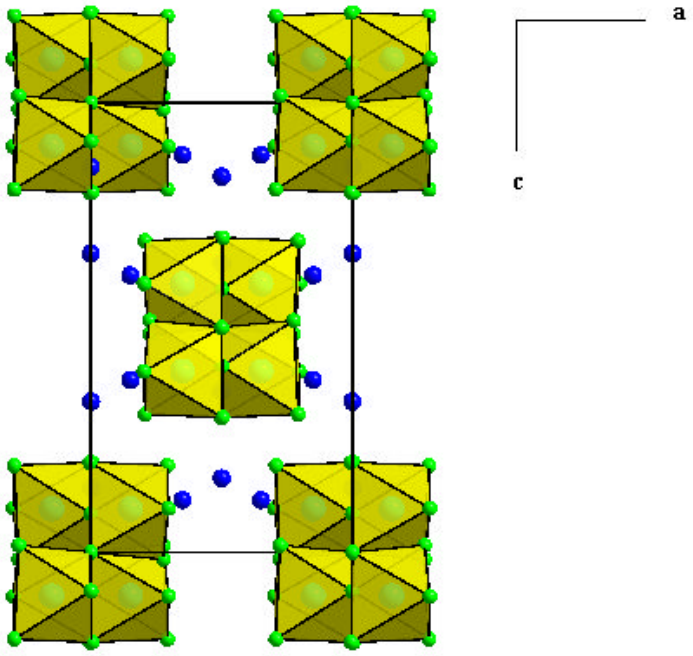

Figure 6-8. A projection of **FeF-3** along the *b* axis.

Table 6-7. Selected bond lengths and bond valence for **FeF-3.**

Bond	**Bond Length (Å)**	S_{ij}
Fe1—F1	1.905(4)	0.543
Fe1—F2	1.898(4)	0.553
Fe1—F3	1.892(4)	0.562
Fe1—F4	1.906(4)	0.541
Fe1—F5	1.9968(10)	0.423
Fe1—F6	1.9817(9)	0.441
		∑Fe1 = 3.063

6-5. Concluding remarks

Despite the large range of reactions that have been carried out, only three iron fluorides structures have been isolated and characterised. Clearly the iron based systems are different from vanadium systems studied in Chapters Four and Five and it is less productive under the reaction conditions that have been studied here. This also was observed in the hydrothermal synthesis of iron fluoride that show significant contrast compared to the aluminium based systems.[2]

The most successful system in the synthesis of organically-templated VOFs using the hydrophobic IL EMIM Tf_2N was first tried using either iron oxide or iron fluoride and HF or HF·pyridine as starting materials; this led only to the formation of mixed unidentified phases. This system has been studied by varying different parameters (addition of HF, increase the temperature, using different amines) without any success. After that other ILs and DESs have been also tried, among all the ILs used: EMIM Br, BMIM Br, EMIM BF_4, BMIM Br/Asp, BPB, HBet Tf_2N, only BMIM Br makes some difference with the isolation of the first two materials **FeF-1** and **FeF-2a**.

DESs show better results than ILs. Using a DES (choline chloride/2-imidazolidinone) provides **FeF-2b,** isostructural to **FeF-2a**. **FeF-2b** has been synthesised at low temperature (110 °C) compared to **FeF-2a** (170 °C). Ethylenediammonium cations in **FeF-2b** have been generated *in situ* by the decomposition of 2-imidazolidinone, however in **FeF-2a** ethylenediamine has been added as an additional structure directing agent.

Fluorinated urea has been used which shows the same behaviour as the other non

fluorinated urea derivative, and decomposes to ammonium to produce the ammonium templated chains **FeF-3** at 110ºC.

From these investigations the underlying reasons behind the limited structural diversity in organically-templated iron fluorides cannot yet been identified. However since DESs gave better results than ILs it is more likely to be the solubility of the precursors in the chosen solvent, as it is known that many metal salts and metal oxides show better solubility in DESs.[11]

There is still much scope for developing further the crystal chemistry of organically-templated iron fluorides, this can be achieved by: using different type of ILs that have not been used in this work like task specific ILs, using other metal sources like metal hydroxides may also provide different results, another important step is to carry out a full study of the solubility of the precursors in the corresponding IL prior to the reactions.

6-6. References

(1) Adil, K.; Saada, M. A.; Ben Ali, A.; Body, M.; Dang, M. T.; Hémon-Ribaud, A.; Leblanc, M.; Maisonneuve, V. *J. Fluorine Chem.* **2007**, *128*, 404.

(2) Ben Ali,, A.; Grenèche, J.-M.; Leblanc, M.; Maisonneuve, V. *Solid State Sci.* **2009**, *11*, 1631.

(3) Ben Ali, A.; Trang Dang, M.; Grenèche, J.-M.; Hémon-Ribaud, A.; Leblanc, M.; Maisonneuve, V. *J. Solid State Chem.* **2007**, *180*, 1911.

(4) Bentrup, U.; Feist, M.; Kemnitz, E. *Prog. Solid State Chem.* **1999**, *27*, 75.

(5) Silva, M. R.; Beja, A. M.; Costa, B. F. O.; Paixão, J. A.; da Veiga, L. A. *J. Fluorine Chem.* **2000**, *106*, 77.

(6) Zouaghi, A.; BenAli, A.; Maisonneuve, V.; Leblanc, M. *Acta Crystallogr.. E* **2010**, *66*, m702.

(7) Adil, K.; Marrot, J.; Leblanc, M.; Maisonneuve, V. *Solid State Sci.* **2007**, *9*, 531.

(8) Teufer, G. *Acta Crystallogr.* **1964**, *17*, 1480.

(9) Lhoste, J.; Gervier, R.; Maisonneuve, V.; Leblanc, M.; Adil, K. *Solid State Sci.* **2009**, *11*, 1582.

(10) Stephens, N. F.; Lightfoot, P. *Solid State Sci.* **2006**, *8*, 197.

(11) Abbott, A. P.; Capper, G.; Davies, D. L.; McKenzie, K. J.; Obi, S. U. *J. Chem. Eng. Data* **2006**, *51*, 1280.

CHAPTER 7

IONOTHERMAL SYNTHESIS OF Ln-TRIMESATE

7-1. Introduction

There has been extensive research in the ionothermal synthesis of metal organic frameworks. While this field has been well developed in transition metal based MOFs and many fascinating structures have been documented,[1-6] it is surprising that the ionothermal synthesis of lanthanide containing MOFs is virtually unexplored and only a few examples have been reported.[7] Where imidazolium based ILs are involved in the synthesis of Ln-MOFs they show exactly the same pattern previously seen in transition metal MOFs. In these cases the metal organic framework is anionic and the charge balance comes from the occluded IL cation. It was observed in general that even if a porous material can be achieved under ionothermal synthesis, the strong electrostatic interactions between the IL cation and the framework make removal of the cations to leave a true porous solid more difficult than in many other cases. This precludes most of the ionothermally prepared MOFs having a proper practical interest in gas adsorption or other applications.

DESs have been widely used in the synthesis of zeolitic materials,[8,9] and organophosphate[10-12] compounds. Among the sheer number of DESs available, the mixture of choline chloride and urea (and its derivatives) or carboxylic acid are the most used to produce crystalline materials. The use of these type of DESs has shown

that besides acting as unusual reaction media, they can serve as template-delivery agents in a controlled manner,[8] where the expected protonated amine is delivered to the reaction by *in situ* breakdown of the urea portion of the DES. DESs composed of choline chloride and carboxylic acids seems to be more stable and do not break down during the reaction, and as a result the corresponding materials are not templated by any of the DES components.[11] This demonstrates that DESs can provide totally different synthetic processes and structural features. Subsequently in this chapter, and following the interest in extending ionothermal synthesis, preliminary investigations have been carried out in the synthesis of Ln- MOFs using DESs.

The ionothermal synthesis of the lanthanide salt and TMA-H_3 in a deep eutectic mixture of choline chloride/1,3-dimethylurea produced three isostructural lanthanide trimesate materials with the formula Ln(TMA)$(DMU)_2$ (Ln: La (**LnMOF-1)**, Nd (**LnMOF-2)**, Eu (**LnMOF-3**)). Changing only the second component of the DES from dimethylurea to ethylene glycol afforded a new material **LnMOF-4**. The crystal structures of these materials will be discussed in detail, solid state NMR and thermal analysis results will also be presented.

7-2. Synthesis of the DESs

The DES choline chloride/1,3-dimethylurea was synthesised as described in section 4-2-7 to give white solid.[8] The DES choline chloride/ethylene glycol was synthesised by mixing choline chloride and ethylene glycol in 1:2 molar ratio in a flask and then heating it until a colourless homogenous liquid formed. This mixture was cooled to RT forming a colourless liquid.[13]

7-3. Synthesis of $Ln(C_6O_9H_3)_3(CO(NH)_2(CH_3)_2)_2$ (Ln = La, Nd, Eu) (LnMOF-1, LnMOF-2 and LnMOF-3.

A typical synthesis procedure was as follows: a Teflon-lined autoclave (volume 15 mL) was charged with the appropriate Ln (III) salt, TMA-H_3 and a DES (choline chloride/DMU) in the molar ratio of (1:1:5:10), exact amounts used are as detailed in Table 7-1. The reaction vessel was sealed and placed in an oven at 110 ^oC for 6 days for **LnMOF-1, LnMOF-2** and 5 days for **LnMOF-3**. For **LnMOF-1** the addition of 0.05 ml of HF (48% in water) increases the crystallinity of the product but has no effect on the resulting materials. Upon cooling to room temperature, the products were filtered, washed with methanol and dried in air for 24 hrs to give colourless prism-like crystals for **LnMOF-1** and **LnMOF-3** and light pink prism-like crystals for **LnMOF-2**.

CHN analyses:

LnMOF-1: Calc: %C: 34.48; %H: 3.64; %N: 10.72.
Found: %C: 34.38; %H: 3.28; %N: 10.21.

LnMOF-2: Calc: %C: 34.14; %H: 3.60; %N: 10.62.
Found: %C: 33.76; %H: 3.31; %N**:** 10.12.

LnMOF-3: Calc: %C: 33.64; %H: 3.55; %N: 10.70.
Found: %C: 33.80; %H: 3.43; %N: 10.70.

Table 7-1. Lanthanide salts used and the exact amounts of other reagents added in the ionothermal synthesis of compounds **LnMOF-n (**n = 1-3).

Product	**Ln salt: g (mmol)**	**TMA g (mol)**	**Choline chloride g (mmol)**	**DMU g (mmol)**
LnMOF-1	$La(NO_3)_3 \cdot 6H_2O$: 0.43 (1)	0.210 (1)	0.70 (5)	0.82 (10)
LnMOF-2	$NdCl_3 \cdot 6H_2O$: 0.36 (1)	0.210 (1)	0.70 (5)	0.82 (10)
LnMOF-3	$Eu(NO_3)_3 \cdot 5H_2O$: 0.43 (1)	0.210 (1)	0.70 (5)	0.82 (10)

Single-crystal X-ray diffraction data for **LnMOF-1, LnMOF-2** and **LnMOF-3** were collected using Mo-Kα (0.7107 Å) radiation using a Rigaku rotating anode single-crystal X-ray diffractometer at the University of St Andrews.

The structures of **LnMOF-1** and **LnMOF-3** were solved with standard direct methods using SHELXS and refined with least-squares minimisation techniques against F^2 using SHELXL under WinGX packages. All non-hydrogen atoms have been anisotropically refined. Hydrogen atoms for the methyl group and the N-H were fixed using the commands HFIX 137 and HFIX43 respectively. Crystal data and structure refinement details for **LnMOF-1** and **LnMOF-3** along with crystal data for **LnMOF-2** are given in Table 7-2. Selected bond lengths are tabulated in Table 7-3.

^{13}C CP MAS NMR spectrum for **LnMOF-1** was acquired using a Bruker Avance III spectrometer equipped with a 9.4 T wide-bore superconducting magnet at the University of St Andrews. The MOF was packed in a standard 4 mm outer diameter ZrO_2 rotor and rotated at 10 or 12.5 kHz using a standard Bruker 4 mm double-resonance MAS probe.

A simulated NMR spectrum for **LnMOF-1** was obtained using the structural model obtained by single-crystal diffraction after optimisation of H atomic positions, calculations were carried out using the CASTEP density functional theory (DFT) code, with NMR parameters calculated using the GIPAW algorithm.

^{13}C MAS NMR spectrum for **LnMOF-2** was acquired using a Bruker Avance III spectrometer equipped with a 14.1 T wide-bore superconducting magnet. The MOF was packed in a standard 1.3 mm outer diameter ZrO_2 rotor and rotated at 60 kHz using a standard Bruker 1.3 mm double-resonance MAS probe.

Thermal analyses experiments on **LnMOF-n** (n = 1-3) were carried out at the university of St Andrews using a TA Instruments 2960 TGA analyser. The samples were heated under argon uo to 600 °C.

Single crystal X-ray diffraction confirmed that the unit cell of **LnMOF-2** is almost the same as **LnMOF-1** and **LnMOF-3 (**Table 7-2), and powder X-ray diffraction confirms the isostructural nature of the three materials. The structure of **LnMOF-2** could not be

solved from single-crystal data, and so for this reason the Rietveld method was used to refine the experimental PXRD using the crystal structure of **LnMOF-1** as a model, a good refinement was obtained with agreement factors; wRp = 0.0389, Rp = 0.0303, Chi^2 = 1.991). The Rietveld refinement plot for **LnMOF-2** is illustrated in Figure 7-1.

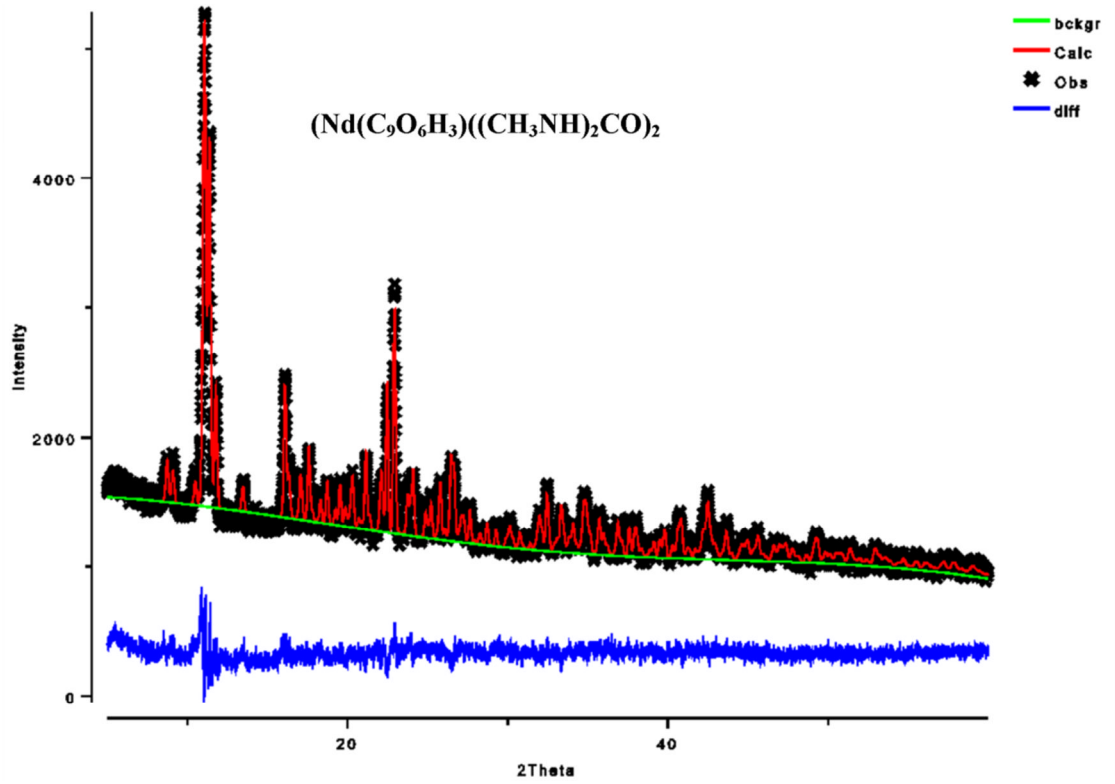

Figure 7-1. The Rietveld refinement of **LnMOF-2** (black crosses indicate experimental data, the red line is the calculated data, the blue line is the difference profile between them and the green line is the background).

Table 7-2. Crystallographic data for **LnMOF-1**, **LnMOF-2** and **LnMOF-3.**

Compound	**LnMOF-1**	**LnMOF-2**	**LnMOF-3**
Formula	$LaTMA(DMU)_2$	$NdTMA(DMU)_2$	$EuTMA(DMU)_2$
Fw (g/mol)	522.24	527.6	535.30
Space group	$P\bar{1}$	$P\bar{1}$	$P\bar{1}$
a /Å	9.4558(4)	9.729(3)	9.5970(40)
b /Å	10.8193(7)	11.0461(52)	10.3970(40)
c /Å	11.2293(6)	11.3065(90)	10.9840(40)
α /°	74.432(16)	78.88(13)	74.017(3)
β /°	65.817(14)	70.69(10)	65.569(3)
γ /°	66.449(14)	64.705(91)	66.357(3)
V / Å^3	953.15(9)	1034.92(10)	906.18(18)
Z	2	2	2
Crystal size /mm	0.1× 0.1 × 0.1	0.09 × 0.09 × 0.06	0.03 × 0.03 × 0.03
Crystal shape and colour	Colourless prism	Pink prism	Colourless prism
Data collection T/ K	293(2)	125(2)	293(2)
F(000)	516		528
R_{int}	0.0883		0.0645
Obsd data (I >2σ(I))	3120		2686
Data/restraints/parameters	3534/0/269		3307/0/269
GOOF on F^2	1.190		1.133
R1, *w*R2 (I >2σ(I))	0.0589, 0.1439		0.0657, 0.1592
R1, *w*R2 (all data)	0.0763, 0.1722		0.0852, 0.1727
Largest diff. peak / hole	0.277/–4.289		2.256/–2.201

As the three materials are isostructural, as an example, the crystal structure of **LnMOF-1** will be discussed in detail.

LnMOF-1 is composed of one La(III) ion, one TMA and two DMU molecules (see Figure 7-2). The coordination environment around each central atom can be regarded as a distorted square antiprism, made up from two carboxylate groups from two different bidentate chelating TMA ions, two carboxylate oxygen atoms from two different bridging TMA and two DMU oxygens, as illustrated in Figure 7-3. It is worth noting that in the structure the DMU molecules remain intact and adopt two different orientations (*cis*/*trans*) with respect to the carbonyl (C=O) group.

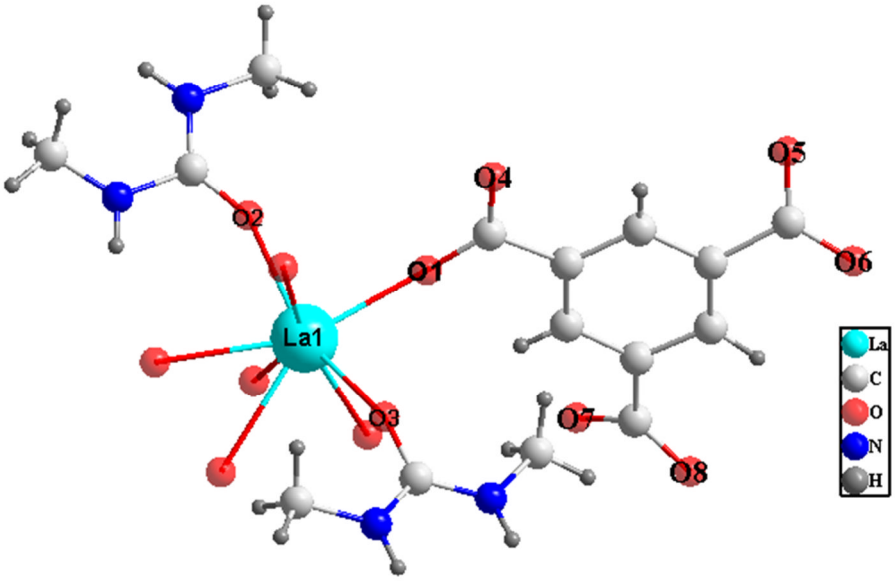

Figure 7-2. Building unit found in **LnMOF-1**.

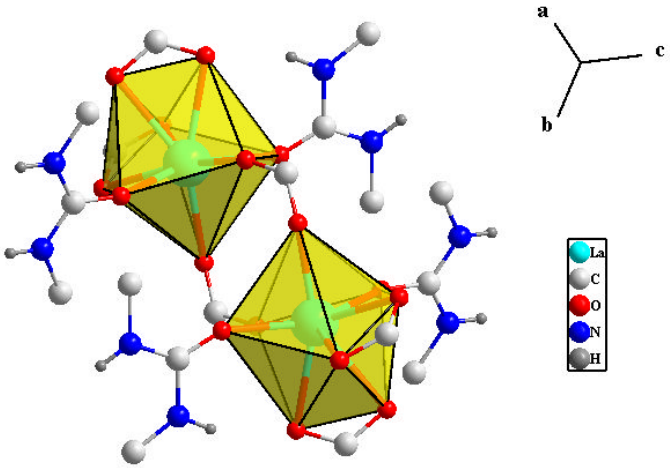

Figure 7-3. Coordination sphere of the metal ions in **LnMOF-1** and the two different orientations of the intact DMU molecules and how they are coordinated to the metal centre.

The La–O distances range from 2.406(6) to 2.644(8) Å (Eu-O distances ranges from 2.284(8) to 2.526(8) Å) (Table 7-3). In the structure, two of the COO^- groups of the TMA are acting as bidentate ligands to chelate two different lanthanum ions, the remaining COO^- group is acting as a bridging group between two further lanthanum ions. Thus one TMA is connecting four different lanthanum ions, the coordination behaviour of TMA is presented in Figure 7-4.

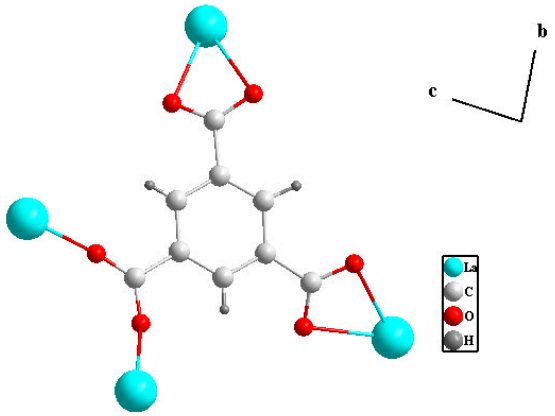

Figure 7-4. Coordination behaviour of TMA in **LnMOF-1**.

The structure consists of an infinite network spreading along the *a* axis, where the TMA acts as the linking agent between the neighbouring La atoms. Furthermore, one can observe that the basic unit is the centrosymmetric dimer, consisting of two La atoms with two TMA acting as bridges between them (Figure 7-5). The distance between two La atoms belonging to the same dimer is 5.295(2) Å. The infinite network is assembled by the coordination of the free carboxylate groups of the dimer to the neighbouring La atoms.

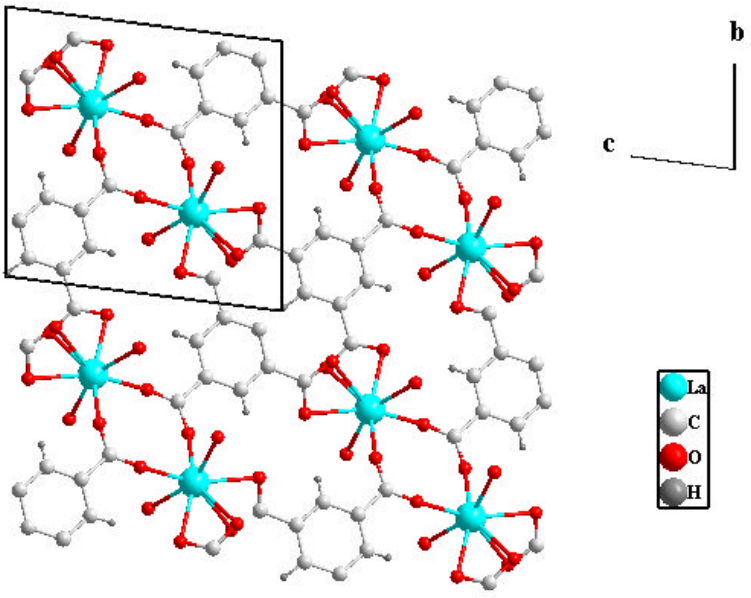

Figure 7-5. Crystal structure of **LnMOF-1** viewed along the *a* axis, DMU molecules have been omitted for clarity.

Table 7-3. Selected bond lengths and bond valence for **LnMOF-1** and **LnMOF-3.**

LnMOF-1		**LnMOF-3**	
Bond	**Bond Length (Å)**	**Bond**	**Bond Length (Å)**
La1—O1	2.406(6)	Eu1—O1	2.301(8)
La1—O2	2.422(7)	Eu1—O2	2.313(8)
La1—O3	2.426(7)	Eu1—O3	2.284(8)
La1—O4^{i}	2.420(8)	Eu1—O4^{i}	2. 289(9)
La1—O5^{ii}	2.570(6)	Eu1—O5^{ii}	2.466(8)
La1—O6^{ii}	2.636(7)	Eu1—O6^{ii}	2.526(8)
La1—O7^{iii}	2.573(6)	Eu1—O7^{iii}	2.449(8)
La1—O8^{iii}	2.644(8)	Eu1—O8^{iii}	2.516(8)

(i) 1–x, 1–y, 1–z; (ii) 1+x, –1+y, z; (iii) 1–x, 1–y, –z

DMU contains both an efficient coordination site and two hydrogen-bonding functionalities. Interestingly, in **LnMOF-1** the DMU is directly coordinated to the lanthanum through the oxygen atom and also provides a hydrogen bonding donor site where all the NH groups participate in H-bonding. Therefore a 3D supramolecular framework is achieved by the formation of hydrogen bridges between the DMU molecules and the nearest carboxylic groups of the two separate dimers. An interesting feature of the present structure is the formation of distinct layers containing either the europium atoms or the DMU molecules, resulting from the presence of both the above-mentioned carboxylic bridges and hydrogen bonds (Figure 7-6 and Figure 7-7).

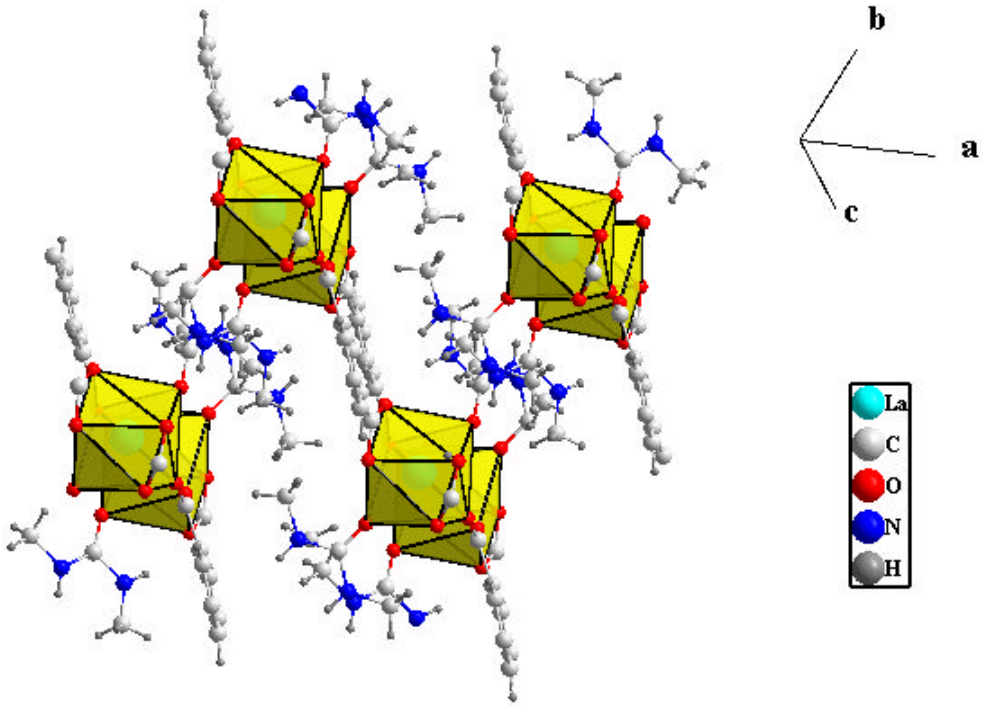

Figure 7-6. Structure of **LnMOF-1** showing the distinct layers of the lanthanium atoms and DMU.

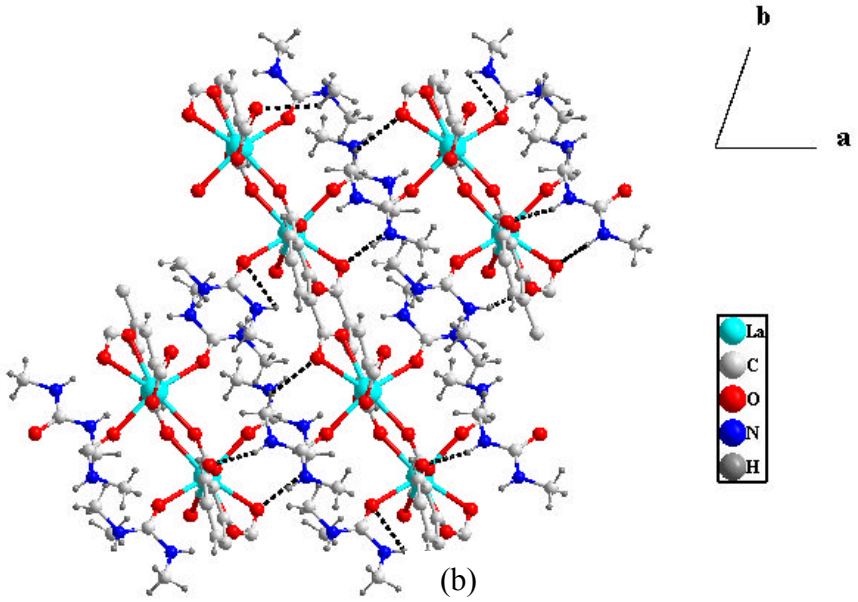

(b)

Figure 7-7. Structure of **LnMOF-1** viewed along the *c* axis showing how the DMU molecules connect the layers through hydrogen bonds (broken lines).

^{13}C NMR for LnMOF-1 and LnMOF-2

In order to confirm the presence of the intact DMU molecules in the structure, ^{13}C MAS NMR was carried out on the powder samples for **LnMOF-1** and **LnMOF-2**.

The experimental spectrum for **LnMOF-1** shows both the methyl groups in the expected region (25-28 ppm) and the carbonyl group at the expected region (160-162 ppm) as it is illustrated in Figure 7-8. Using the structural model described above for **LnMOF-1** and after optimisation of H atomic positions, relatively good agreement between calculated and experimental spectra is achieved (Figure 7-8). Resonances are separated into broadly the right regions, as summarised in Table 7-4. Two additional resonances are observed in the experimental spectrum of **LnMOF-1**, at 55 and 68 ppm. These cannot be assigned based on the crystal structure, but may arise from an impurity (solvent).

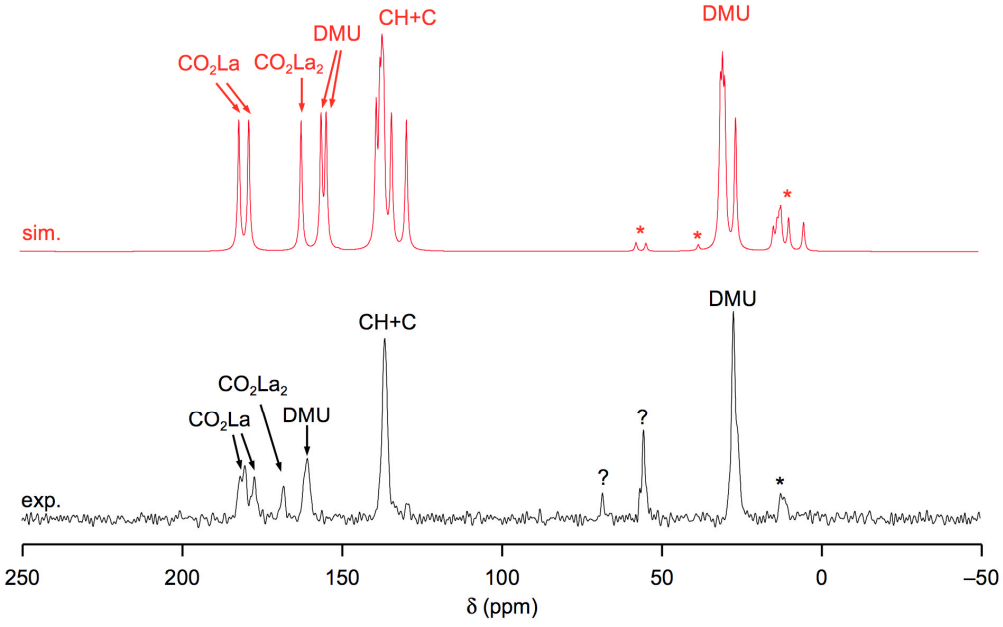

Figure 7-8. Experimental ^{13}C CP MAS NMR spectrum (9.4 T, 12.5 kHz) (below) and simulated ^{13}C MAS NMR spectrum (9.4 T, 12.5 kHz) (above) for **LnMOF-1**. The simulated spectrum is based on NMR parameters calculated for the structure of **LnMOF-1** determined by single-crystal diffraction after optimisation of H atom positions. Spinning sidebands in both spectra are marked *.

Table 7-4. Comparison of calculated and experimental shifts for **LnMOF-1**.

Site(s)	Calculated shift range (ppm)	Experimental shift range (ppm)
DMU methyl	26-31	25-28
aromatics	129, 134-139	129, 134-138
DMU carbonyl	154-156	160-162
Bridging carboxylate	162	168
Non-bridging carboxylate	178-181	180, 181

The plot of the experimental spectrum for **LnMOF-2** is illustrated in Figure 7-9 shows broad peaks compared to those seen in **LnMOF-1.** The spectrum suggests the presence of DMU molecules, however the assignment has not been completed yet due to the difficulty in assigning the peaks because of the paramagnetic shift contribution of Nd.

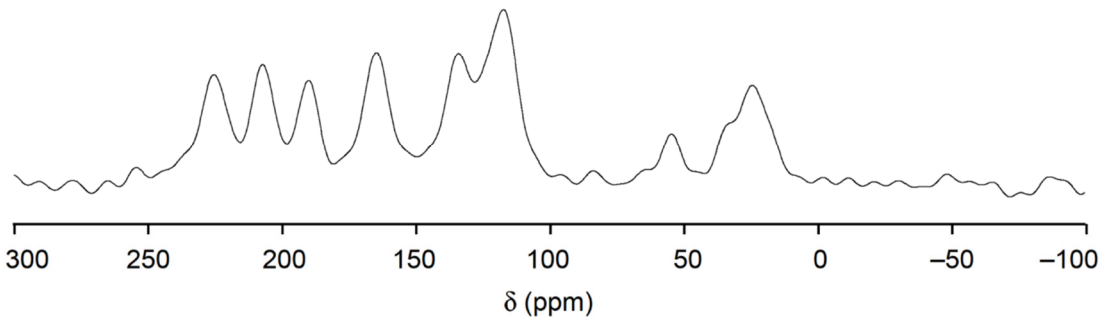

Figure 7-9. Experimental ^{13}C MAS NMR spectrum (14.1 T) for **Ln-MOF-2**.

Thermogravimetric analysis

Thermogravimetric analyses carried out on the three materials **LnMOF-n** (n = 1-3) show the same pattern. As it is illustrated in Figure 7.10 (only the plot for **LnMOF-1** is shown here), there are three distinct weight losses, the first two are identical (~ 17 %) these are likely due to the successively loss of the two DMU molecules, this is in agreement with the calculated weight change due to the loss of DMU (16.66 %). Followed the collapse of the material by the breakdown of the organic linker (TMA) (~40 %), is again in agreement with the calculated (40.30 %).

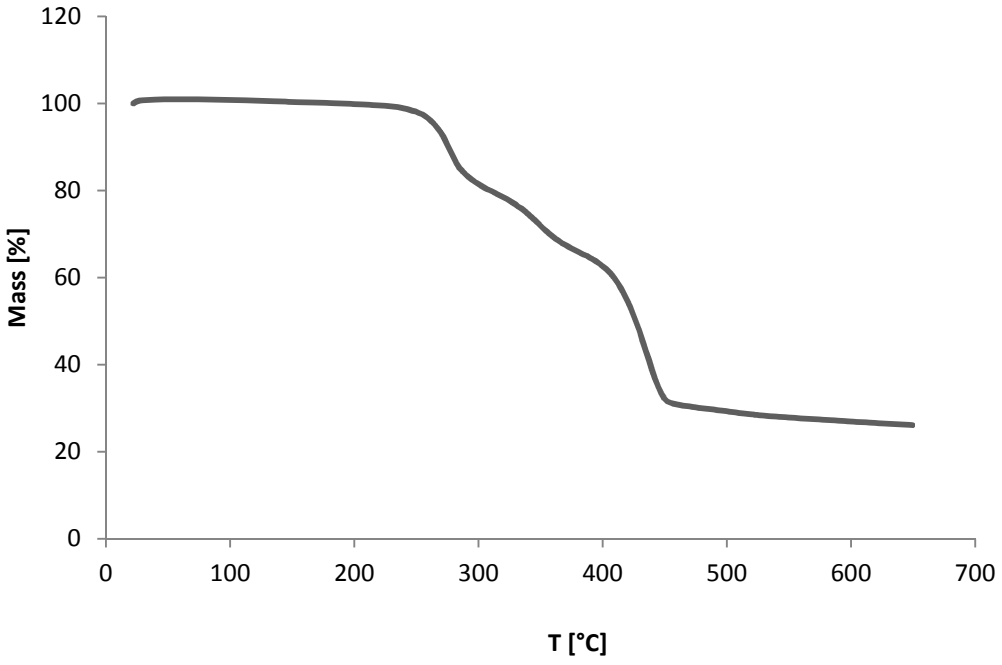

Figure 7-10. TGA plot for **LnMOF-1.**

7-4. La($C_6O_9H_3$) (LnMOF-4)

A typical synthesis procedure was as follows: a Teflon-lined autoclave (volume 15 mL) was charged with $La(NO_3)_3 \cdot 6H_2O$ (0.436 g, 1 mmol, Alfa Aesar) and TMA-H_3 (0.210 g, 1 mmol, Sigma Aldrich) and then the DES (choline chloride (0.70 g, 5 mmol, Sigma Aldrich) and ethylene glycol (6.20 g, 10 mmol, Fluka) was added. The stainless steel autoclave was then sealed and heated in an oven at 110 °C for 6 days. Upon cooling to room temperature, the product was filtered, washed with methanol and dried in air for 24 hrs to give colourless prism-like crystals.

Single-crystal X-ray diffraction data for **LnMOF-4** were collected using Mo-Kα (0.7107 Å) radiation utilising a Rigaku rotating anode single-crystal X-ray diffractometer at the University of St Andrews. The structure was solved with standard direct methods using SHELXS and refined with least-squares minimisation techniques against F^2 using SHELXL under WinGX packages. The refinement ambiguously suggested the chiral space group $P4_12_12$, with the flack parameter (0.0775 (esd 0.0722)). A run of PLATON suggested there are large solvent accessible voids, for that reason the SQUEEZE program was used which excludes electron density in the pores; this resulted in an improved refinement.

Crystallographic data and structural refinements for **LnMOF-4** are summarised in Table 7-5. Selected bond lengths are tabulated in Table 7-6.

Table 7-5. Crystal data and structure refinement details for **LnMOF-4.**

Compound	**LnMOF-4**
Formula	$La(C_6H_3(CO_2)_3$
Fw (g/mol)	346.02
Space group	$P4_12_12$
a /Å	14.7900(4)
b /Å	14.7900(4)
c /Å	14.1680(3)
α /°	90
β /°	90
γ /°	90
V / Å^3	3099.17(14)
Z	8
Crystal size /mm	0.15 × 0.03 × 0.03
Crystal shape and colour	Colourless prism
Data collection T/ K	93(2)
F(000)	1296
R_{int}	0.0644
Obsd data ($I > 2\sigma(I)$)	2815
Data/restraints/parameters	3279/0/145
GOOF on F^2	1.126
R1, *w*R2 ($I > 2\sigma(I)$)	0.0655, 0.1561
R1, *w*R2 (all data)	0.0784, 0.1561
Largest diff. peak / hole	2.270/ –0.749

LnMOF-4 features a three dimensional structure which presents some similarities and many differences with the lanthanide trimesate MIL-78.[14] They both have the same formula $MC_6H_3(CO_2)_3$: (M = Y, Ln) and are based on edge-shared 1D inorganic chains connected through trimesate ions into a 3D open framework. However **LnMOF-4** crystallises in a chiral tetragonal space group ($P4_12_12$), while MIL-78 crystallises in the monoclinic space group $C2/m$.

Both **LnMOF-4** and MIL-78 are built up from eight coordinated Ln(III) and trimesate ions. TMA in both structures presents the same coordination behaviour with two tridentate (bridging/chelating) carboxylates and one bidentate bridging as it is illustrated in Figure 7-11 .

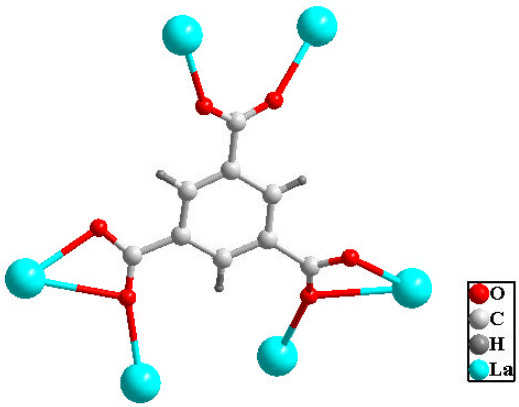

Figure 7- 10. Coordination behaviour of TMA in **LnMOF-4**.

While the Ln(III) ions in both cases adopt an eight coordination polyhedra made up of six oxygens from four different tridendate (bridging/chelating) COO^- groups and two oxygens from two different bidentate bridging COO^- group, thus each Ln(II) ion is connected to six TMA ions. However they show different connection modes as is

illustrated in Figure 7-12. In **LnMOF-4** all the eight oxygens connect the metal centre to two other adjacent Ln(III). In contrast to MIL-78 the metal centre is connected to two adjacent La(III) ions through the six oxygens coming from the bridging/chelating caboxylates and the remaining two (coming from the bridging carboxylates) connect it further to a fourth Ln(III) ion.

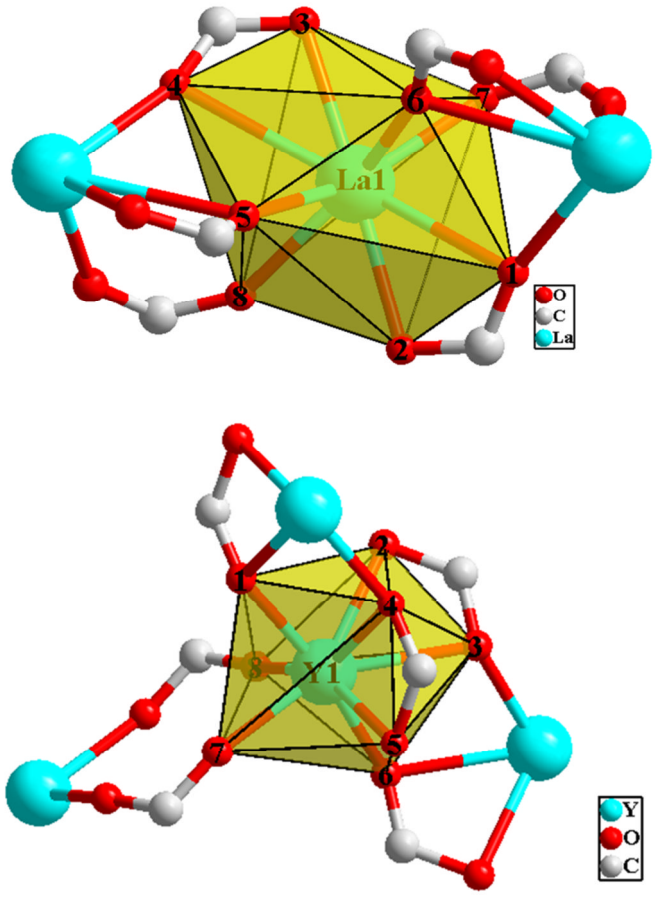

Figure 7-12. Coordination environment of the Ln ions respectively in **LnMOF-4 (**top**)** and MIL-78 (below) showing the different type of carboxylate groups**,** oxygen atoms are arbitrary numbered.

The difference in the polyhedra connection modes will generate two different styles of edge-sharing chains as illustrated in Figure 7-13.

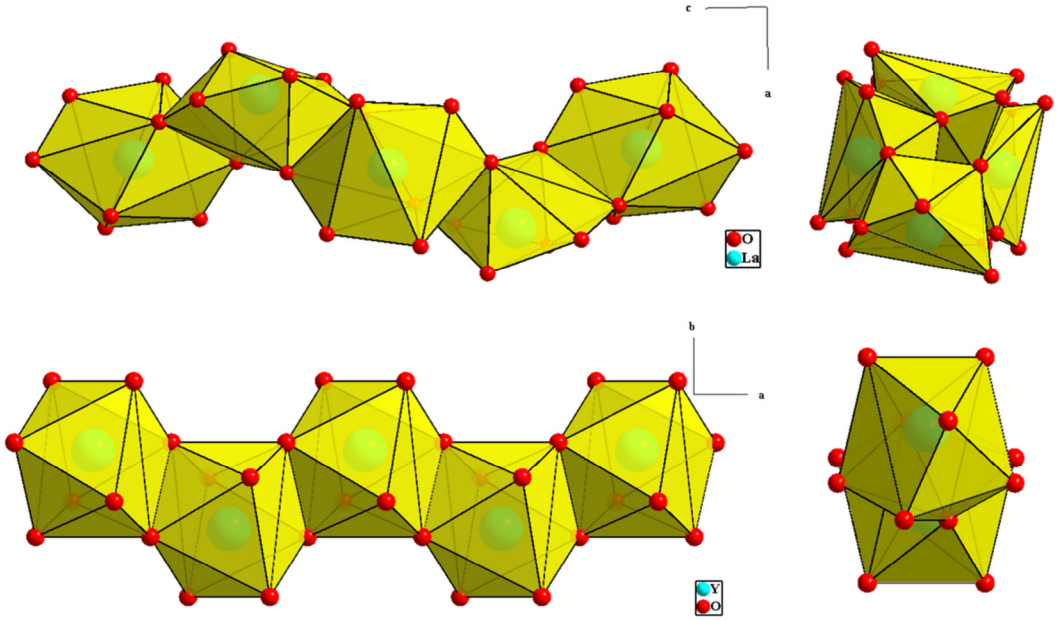

Figure 7-13. Inorganic chains found respectively; in **LnMOF-4** viewed along the *b*-axis (leftt top) with a projection along the *c*- axis (right top), in MIL-78 viewed along the c axis (left below) with a projection along the *a* axis (right below).

The La–O distances range from 2.406(10) to 2.935(9) Å (see Table 7-6). TMA moities connect the inorganic chain into 3D open framework as it is illustrated in Figure 7-14 and Figure 7-15.

Table 7-6. Selected bond lengths for **LnMOF-4**.

Bond	**Bond Length (Å)**	**Bond**	**Bond Length (Å)**
La1—O1	2.499(11)	La1—O5	2.406(10)
La1—O2	2.521(9)	La1—O6	2.426(10)
La1—O3	2.507(7)	La1—O4^{i}	2.892(8)
La1—O4	2.539(9)	La1—O2^{ii}	2.935(9)
(i) –0.5+y, 0.5–x, –0.25+z; (ii) 0.5–y, 0.5+x, 0.25+z			

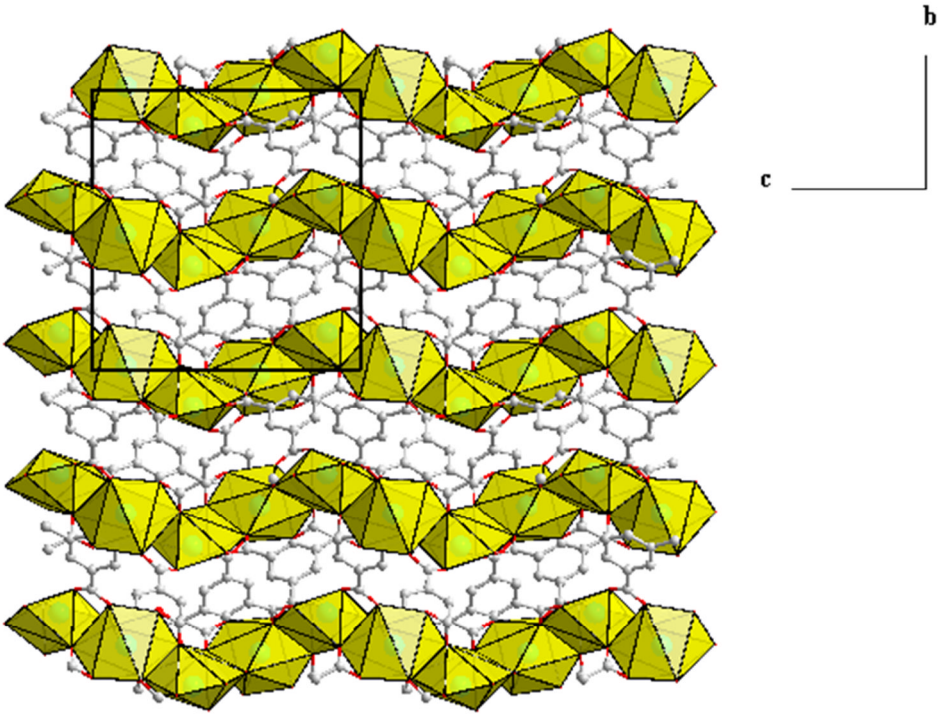

Figure 7-14. A view of **LnMOF-4** along the *a*-axis, showing how the inorganic chains are connected through the TMA.

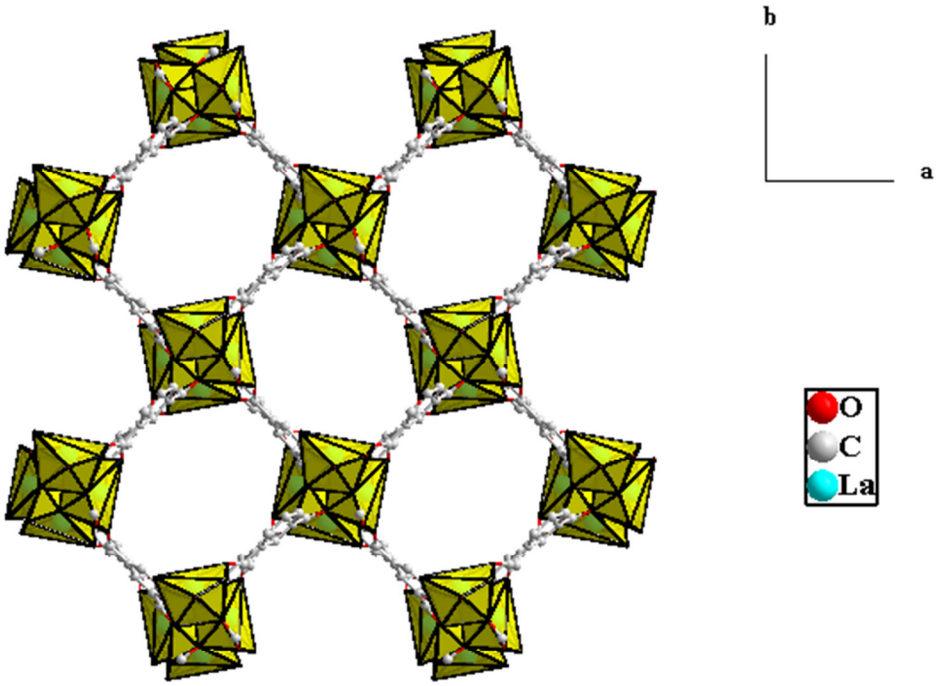

Figure 7-15. A view of **LnMOF-4** along the *c*-axis.

LnMOF-4 and MIL-78 are based on the same building unit composed of one Ln and one TMA ions and the TMA follows exactly the same coordination behaviour in both materials. However, the differences occur in the inorganic chains connectivities and also in how they are further connected through TMA ions, yielding two completely different materials. Figure 7-16 below shows how the inorganic sub-network is related *via* TMA in MIL-78.

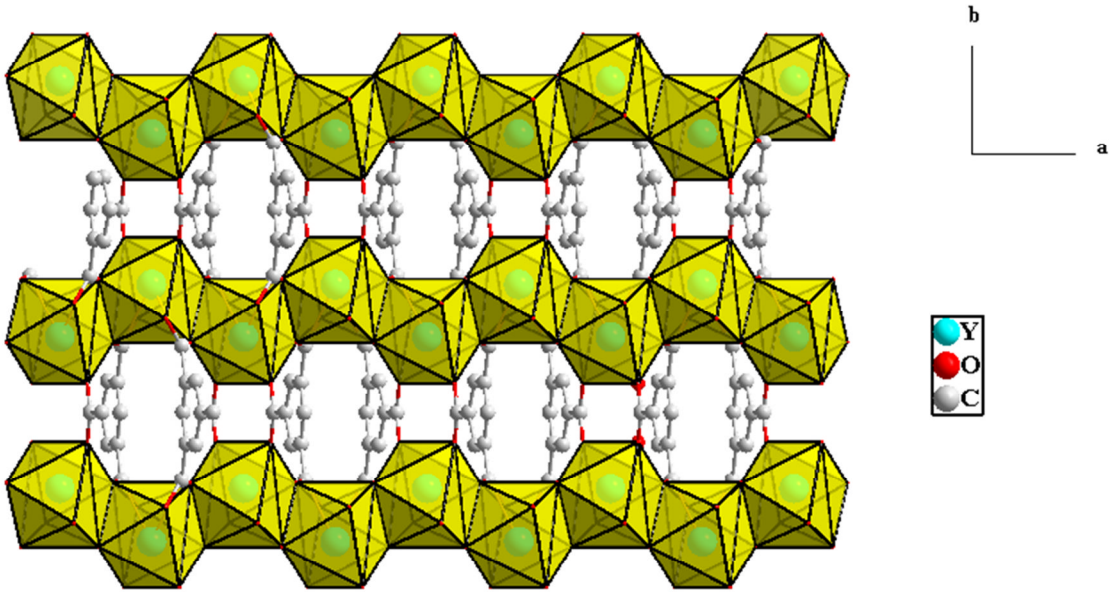

Figure 7-16. A view of MIL-78 along the *c*-axis, showing how the inorganic chains are connected through the TMA.

7-5. Concluding remarks

The work undertaken in this chapter concerns the ionothermal synthesis of Ln containing MOFs using DESs. Two different DESs based on choline chloride have been used; choline chloride/1,3-dimethylurea and choline chloride/ethylene glycol. While DMU has been used as a mixture with choline chloride for the synthesis of zeolites and other MOFs, however it is the first time ethylne glycol is used as the second component of the DES for the preparation of crystalline materials. It is interesting to note the two DESs behave in completely different ways, choline chloride/DMU acts as a solvent and a reactant (co-ligand) however choline chloride/ ethylene glycol acts as a solvent only and neither the choline component or the ethylene glycol appear in the structure.

In the vast majority of synthetic procedures using urea-containing DESs as the solvent in ionothermal synthesis, including the preparations of both zeolites and metal organic frameworks, the urea component of the DES has broken down to ammonium or alkyl ammonium cations (depending on the exact nature of the urea derivative used). These ammonium compounds are excellent structure directing agents and are almost always incorporated into the final materials. In the synthesis of **LnMOF-n** (n = 1–3), however, the occluded compound is the intact DMU molecule. Of course, this does not preclude the possibility of there being some breakdown of the urea component under the synthesis conditions, but it does indicate that the urea itself can also act as a ligand in such ionothermal preparations. This opens up new possibilities for the use of urea components of DESs in ionothermal synthesis that have not been seen before. The three compounds are all prepared in the presence of a small amount of water, emanating from

the lanthanide salts used and, in the case of **LnMOF-1**, the aqueous HF. In ionothermal synthesis water can act as a very important reactant, increasing the rate of ionothermal reactions[15] and improving the crystallinity of the products. Similarly, fluoride ions are extremely well-known mineralisers in both hydrothermal[16] and ionothermal reactions,[17,18] again increasing the rate of reaction and improving crystallinity of the products. However, when using DESs as the solvent the addition of too much water or fluoride increases the likelihood of breakdown of the urea component.[8] This also was observed in the synthesis of organically templated vanadium and iron (oxy)fluorides presented in this work (chapter four and chapter six).

It is interesting to mention that similar work has now been published by Bu *et al*.,[19] which support the forgoing results, where the three DESs composed of choline chloride and three urea derivatives (urea, 1,3-dimethylurea and imidazolidinone) were used to produce different MOFs. All urea derivatives did not decompose and remain intact, however the resulting materials are templated in different ways. In terms of MOFs application it seems that the most promising results in *Bu et al*. work is when only the unstable urea derivative coordinate to the metal centre or template the resulting MOF (this is also the case in **LnMOF-n** (n = 1 – 3)). As this characteristic can be used for the creation of porosity and open metal sites in ionothermally prepared MOFs, since the urea derivatives, in general, are unstable and upon heating they will be the first to decompose. This will lead to the formation of unsaturated metal sites that might be of special interest. After the removal of the urea, the material can be studied for any potential applications especially if it retains its crystallinity. These types of materials

may also provide interesting candidates for the *in situ* X-ray diffraction studies in MOFs.

For **LnMOF-4**, the DES is not occluded within the structure but interesting points can be raised here. Choline chloride/ethylene glycol seems to be an excellent solvent as the material can be synthesised in a single crystal form at 110 °C in contrast to some other Ln-MOFs *e.g*. MIL-78 was synthesised at 220 °C and only micro-crystalline powder sample was obtained whatever the synthesis conditions.[14] The low-temperature synthesis route probably has an effect to produce large pores as it is known that high temperature will increase the propensity of the material to have a dense structure. For now the material is not pure phase so no further experimental work has been carried out on **LnMOF-4**. Further work needs to be carried out in order to get **LnMOF-4** as pure phase, after which any potential applications can be studied, *e.g*. gas adsorption properties. Also the thermal analysis of **LnMOF-n** (n = 1-3) can be studied after each step of their weight loss as shown in the TGA plot (Figure 7-11) in order to see if these materials remain crystalline after heating.

The promising results of these preliminary investigations need more attention and extensive research on ionothermal synthesis of Ln-MOFs using different DESs, especially those based on urea derivatives and alcohol, needs to be undertaken. As it appears that the ionothermal synthesis of Ln-MOFs using DESs presents an excellent alternative route for the creation of open metal organic frameworks.

7-6. References

(1) Ji, W.-J.; Zhai, Q.-G.; Li, S.-N.; Jiang, Y.-C.; Hu, M.-C. *Chem. Commun.* **2011**, *47*, 3834.

(2) Jin, K.; Huang, X.; Pang, L.; Li, J.; Appel, A.; Wherland, S. *Chem. Commun.* **2002**, 2872.

(3) Lin, Z.; Slawin, A. M. Z.; Morris, R. E. *J. Am. Chem. Soc.* **2007**, *129*, 4880.

(4) Lin, Z.; Wragg, D. S.; Morris, R. E. *Chem. Commun.* **2006**, 2021.

(5) Lin, Z.; Wragg, D. S.; Warren, J. E.; Morris, R. E. *J. Am. Chem. Soc.* **2007**, *129*, 10334.

(6) Wu, Z.-F.; Hu, B.; Feng, M.-L.; Huang, X.-Y.; Zhao, Y.-B. *Inorg. Chem. Commun.* **2011**, *14*, 1132.

(7) Chen, W.-X.; Ren, Y.-P.; Long, L.-S.; Huang, R.-B.; Zheng, L.-S. *Cryst. Eng. Comm* **2009**, *11*, 1522.

(8) Parnham, E. R.; Drylie, E. A.; Wheatley, P. S.; Slawin, A. M. Z.; Morris, R. E. *Angew. Chem. Int. Ed.* **2006**, *45*, 4962.

(9) Drylie, E. A.; Wragg, D. S.; Parnham, E. R.; Wheatley, P. S.; Slawin, A. M. Z.; Warren, J. E.; Morris, R. E. *Angew. Chem. Int. Ed.* **2007**, *119*, 7985.

(10) Liao, J.-H.; Wu, P.-C.; Bai, Y.-H. *Inorg. Chem. Commun.* **2005**, *8*, 390.

(11) Sheu, C.-Y.; Lee, S.-F.; Lii, K.-H. *Inorg. Chem.* **2006**, *45*, 1891.

(12) Tsao, C.-P.; Sheu, C.-Y.; Nguyen, N.; Lii, K.-H. *Inorg. Chem.* **2006**, *45*, 6361.

(13) Abbott, A. P.; Capper, G.; Davies, D. L.; McKenzie, K. J.; Obi, S. U. *J Chem. Eng. Data* **2006**, *51*, 1280.

(14) Serre, C.; Millange, F.; Thouvenot, C.; Gardant, N.; Pelle, F.; Ferey, G. *J. Mater. Chem.* **2004**, *14*, 1540.

(15) Wragg, D. S.; Slawin, A. M. Z.; Morris, R. E. *Solid State Sci.* **2009**, *11*, 411.

(16) Morris, R. E.; Burton, A.; Bull, L. M.; Zones, S. I. *Chem. Mater.* **2004**, *16*, 2844.

(17) Cooper, E. R.; Andrews, C. D.; Wheatley, P. S.; Webb, P. B.; Wormald, P.; Morris, R. E. *Nature* **2004**, *430*, 1012.

(18) Morris, R. E. *Chem. Commun.* **2009**, 2990.

(19) Zhang, J.; Wu, T.; Chen, S.; Feng, P.; Bu, X. *Angew. Chem. Int. Ed.***2009**, *48*, 3486.

CHAPTER 8

SUMMARY, CONCLUSIONS AND FURTHER WORK

8-1. Summary and Conclusions

Hybrid organic-inorganic transition-metal fluorides, such as vanadium and iron fluorides and oxyfluorides, are a class of materials that have received a great deal of interest recently. This is due to their potential useful properties that might realise their usefulness in diverse applications: *e.g.* magnetism, catalysis. Organically templated VOFs have been well studied and a wide range of materials displaying rich and interesting structural diversity have been prepared.[1] However, in this system, it was noted the absence of extended structures and most VOFs are only extended as far as 1D chains. In contrast, iron-based systems are relatively less studied than their vanadium counterpart and the few reported structures show poor structural diversity.[2] Ionothermal synthesis,[3] a relatively new synthesis method that utilises IL as the solvent and possibly as a template in material synthesis, has shown great initial success for the synthesis of zeolites and metal organic frameworks. This then has been extended to the synthesis of other type of materials. The exploration of the ionothermal synthesis of MOFs has mainly focused on transition metals,[4] lanthanide metals are largely absent, even though they have the potential to create fascinating MOFs.

Using ionothermal as the synthesis method often results in new materials with characteristic that can be traced back to the specific IL used. One of the main properties that differentiate the ionothermal synthesis method from the other synthesis techniques is the unique reaction environment dictated by the IL. Other studies also have shown that ILs are highly structured,[5] this is also a major advantage over molecular solvents.

Consequently, it is of particular interest to embark on an extensive investigation into the synthesis of vanadium- and iron-based metal fluoride and lanthanide containing MOFs using ILs and DESs as the solvent. The work involves following simple constructive steps in an attempt to answer many raised questions. These questions may be summarised in three major points:

(1) Can the ionothermal approach be applied to the synthesis of organically templated metal fluorides and lanthanide containing MOFs?

(2) Will this make a difference in terms of the structures dimensionality, properties and functionality?

(3) Does the synthesis of these types of materials offer in turn an opportunity to further extend the ionothermal synthesis beyond what has been already known?

The use of ILs and DESs for the synthesis of VOFs initially produced 13 different materials including eight new materials. Typical ILs used in ionothermal synthesis act as excellent solvents for the synthesis of VOFs, however no templating effect was observed in these systems. Consequently, organic amines are added to the reaction to act as a template, which proved to be successful with the isolation of organically templated VOFs under different conditions. DESs can also been used for the synthesis

of VOFs, they act as solvent and provide the template to the reaction. Basically the DESs used in this work are those composed of choline chloride and urea derivatives. In the synthesis of VOFs the urea portion of the DES decomposed *in situ* and provided the resultant template to the reaction. A similar behaviour was also observed when a chiral IL was used where it decomposed to ammonium. Another interesting point in the synthesis of VOFs using ILs and DESs is the versatility of the synthesis routes can target the same framework topology. A good example can be found in $[H_2en][VF_5]$ which can be synthesised using IL as the solvent and ethylenediamine as an added structure directing agent or template; if no template was added, $VF_3(H_2O)_2$, a non template vanadium fluoride hydrated resulted. The synthesis of $[H_2en][VF_5]$ can also be achieved by using a DES composed of choline chloride and 2-imidazolidinone (decomposing to give ethylenediamine as the template) as the solvent without adding any other templating source. These results demonstrate that some degree of taking control of the out come of the reaction in these systems would be achievable by carefully choosing the components of the solvent, whether it be an IL or DES.

To increase the dimensionality of the materials beyond 1D, it is of key importance to find the right system composed of the correct combination of: vanadium source, fluorine source, ionic liquid and organic amine. The system V_2O_5/HF·pyridine/EMIM Tf_2N produced the first VOF material with two dimensionality containing vanadium exclusively in the 4+ oxidation state, **VF-14**. This structure can be regarded as the fusion of the previously known ladder-type structure into a continuous sheet. **VF-14** showed antiferromagnetic ordering. The successful synthesis of **VF-14** was followed by the synthesis of **VF-15**, a related material also displaying two dimensionality. **VF-15**

was synthesised when imidazole was used as an added template with the system VOF_3/HF/EMIM Tf_2N. Three other phases **VF-16**, **VF-17** and **VF-18** displaying ladder-type were also prepared from the same system. Interestingly, vanadium ions in all these materials are in the 4+ oxidation despite the high reaction temperature used for the synthesis (170 °C) and there were no signs of possible F/O disorder in these structures. This characteristic is unprecedented in the hydrothermal synthesis of VOFs, as raising the reaction temperature above 150 °C would often result in further reduction of V^{4+} to V^{3+}.[6] This is therefore a major advantage of using the ionothermal synthesis method and precisely utilising the hydrophobic IL EMIM Tf_2N for the synthesis of VOFs.

After the synthesis of layered organic-inorganic hybrid VOFs, an important question to answer is would a dimensionality greater that 2-D possible to achieve in this system? One of the main variables in the reaction is the added organic amine that acts as the structure directing agent, combining this system with the right structure directing agent would potentially lead to a more extended network. Ultimately, the use of quinuclidine afforded **VF-19**, a novel material displaying unique double layered topology featuring S = ½ kagome type lattice. **VF-19** is the first example of a d^1, S = ½ kagome lattice and among the very few examples of S = ½ materials bearing the kagome lattice. **VF-19** is a highly frustrated material, with Weiss constant of θ = -81 K and no sign of any magnetic ordering transition temperature, thus it represents an excellent candidate for realising QSL.

The use of BMIM Br as the solvent for the synthesis of the iron-based metal fluorides resulted in **FeF-1**, adding ethylenediamine gave a novel material **FeF-2** which can also be prepared using DES composed of choline chloride and 2-imidazolidinone as the solvent, where ethylenediamonium cations generated *in situ* by the partial breakdown of 2-imidazolidinone. This behaviour is mirrored in the synthesis of VOFs mentioned above. However, it should be noted that the iron-based system is less productive when compared to the vanadium-based system despite the large number of synthetic preparations studied, only three phases based on iron have been synthesised and characterised.

The ionothermal synthesis of Ln-containing MOFs yielded four different materials. **LnMOF-n** (n = 1-3) are isostructural and were prepared from a DES composed of choline chloride and 1,3-dimethylurea. Interestingly, the DES in this system behaved differently from the other systems described above, as the urea derivative portion did not decompose as before but remained intact and included in the final structure as a ligand and coordinated to the metal centre. **LnMOF-4** was synthesised from the DES composed of choline chloride and ethylene glycol. None of the DES components appeared in the final structure, however the low temperature synthesis of this MOF with its interesting structural features, chirality and high porosity, would suggest that this synthetic route may be particularly useful for targeting MOFs with similar properties as **LnMOF-4**.

8-2. Further work

The applicability of the ionothermal synthetic route for the synthesis of vanadium and iron based metal fluoride and Ln-MOFs has been discussed. Besides from confirming the feasibility and versatility of their synthesis using ILs and DESs, it demonstrated how the choice of the ionothermal method can yield novel materials and novel functionalities. It has also shown for the first time that the ionothemal synthetic route can be extended to include control over oxidation state that is difficult to achieve using other synthesis methods. The results that have been summarised here and discussed in full details in chapters 4 through 7 would pave the way for this work to be developed further and offer the possibility for many research investigations.

It would be of particular research interest if the outcomes presented in this present work were complemented by the following:

- Obtaining better quality data to allow for higher resolution structure solution that would aid in the structural characterisations (*e.g*. the use of synchrotron radiation); this could be applied to the perovskite VOF, **VF-13,** and to the alternating ladder-type structure, **VF-6**, in order to confirm the space group choice and for better refinement.

- Some other materials of interest, while there is no ambiguity in the crystal structure, they are synthesised as mixed phases which hinders the study of their potential properties or applications. It is therefore essential to perform further

exploration on these systems in order to make these materials phase pure. Primarily, the system that allowed the synthesis of the chiral porous MOF, **LnMOF-4**, is an ideal candidate that needs to be investigated further. This may initially involve changing the reaction time or temperature, it would also be worth changing the reactant stoichiometry in an attempt to enhance selectivity to produce the desired compound phase pure. The 2D VOF material **VF-15** which is present as mixed phases with **VF-16** also deserves additional investigations to obtain phase pure materials.

- The use of microwave as an alternative heating method could also be carried out. However, this method typically uses glass vials that are not convenient for the synthesis of metal fluorides so Teflon-lined vials are preferred to perform this type of reactions.

This work can be further developed in many ways and directed into many areas of interest, a selection of ideas for possible future work include:

- Further exploration of the system VOF_3/HF/EMIM Tf_2N by using other bicyclic amines; as the successful synthesis of the kagome type material **VF-19** suggested that these amines potentially are good SDAs for targeting this type of materials.

- Another interesting point can also be investigated in the VOF_3/HF/EMIM Tf_2N system is the use of chiral amines, from the results obtained from that system,

vanadium mainly remained in the 4+ oxidation state and all synthesised structures do not show any F/O disorder. In an attempt to direct the whole structure towards non centrosymmetric packing it could be useful to include chiral amines within this system.

- In order to further develop the area of organically templated iron fluorides, it is useful to try other type of ILs, task specific ILs (TSILs) may make a difference to these systems, also including various iron sources would be worth trying. An important part is to carry out full solubility measurements of the precursors in different ILs in order to establish the general trends, and this may potentially allow the selection of the right system.

  There is also much scope to develop the area of porous lanthanide containing MOFs using the ionothermal approach, in particular when DESs are used as the solvent. The type of DESs that may present great interest are those composed of quaternary ammonium salt and urea derivatives, where the urea derivative portion plays a great role in achieving porous materials, work in this direction has already been reported by Bu *et al*.[7] but there is much more scope to develop it further. The other important DES is the one composed of choline chloride and ethylene glycol, it is extremely important to investigate if this synthetic route may be generalised to include other metals. Similarly, other DESs composed of quaternary ammonium salts and alcohols could also be studied as potential useful solvents for targeting porous MOFs.

8-3. References

(1) Aldous, D. W.; Goff, R. J.; Attfield, J. P.; Lightfoot, P. *Inorg. Chem.* **2007**, *46*, 1277.

(2) Ali, A. B.; Grenèche, J.-M.; Leblanc, M.; Maisonneuve, V. *Solid State Sci.* **2009**, *11*, 1631.

(3) Cooper, E. R.; Andrews, C. D.; Wheatley, P. S.; Webb, P. B.; Wormald, P.; Morris, R. E. *Nature* **2004**, *430*, 1012.

(4) Lin, Z.; Wragg, D. S.; Warren, J. E.; Morris, R. E. *J. Am. Chem. Soc.* **2007**, *129*, 10334.

(5) Mele, A.; Romanò, G.; Giannone, M.; Ragg, E.; Fronza, G.; Raos, G.; Marcon, V. *Angew. Chem.* **2006**, *118*, 1141.

(6) Adil, K.; Leblanc, M.; Maisonneuve, V.; Lightfoot, P. *Dalton. Trans.* **2010**, *39*, 5983.

(7) Zhang, J.; Wu, T.; Chen, S.; Feng, P.; Bu, X. *Angew. Chem. Int.Ed.* **2009**, *48*, 3486.

APPENDIX

A1. PXRD for VF-13 and VF-1c

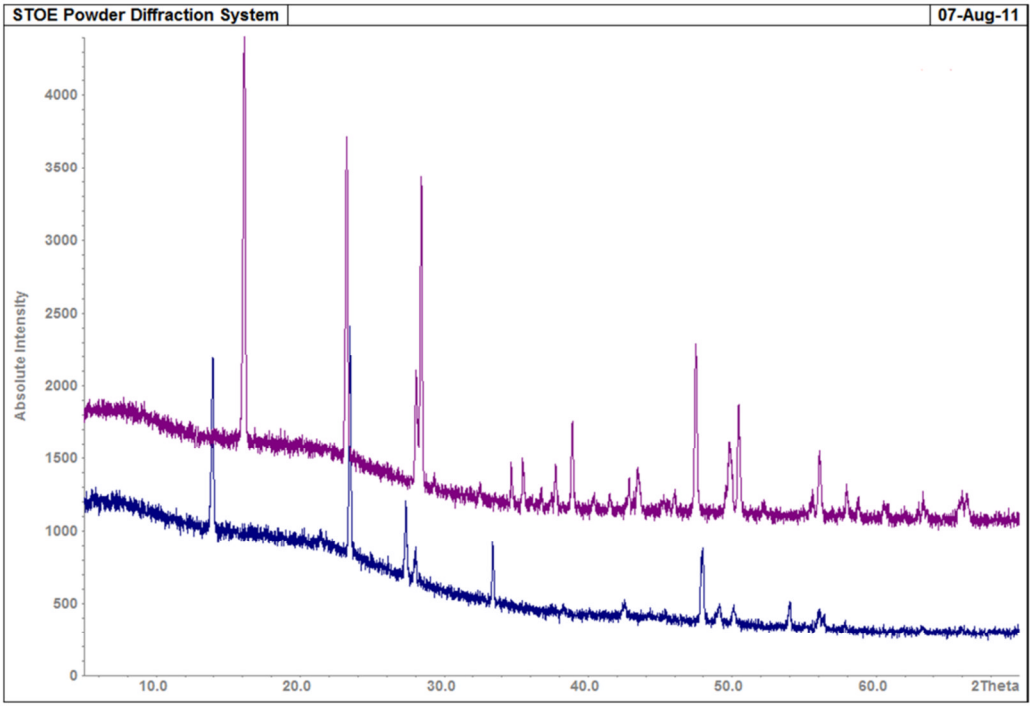

Figure A1. PXRD for **VF-13** and **VF-1c**.

A2. PXRD and CHN analysis for VF-15.

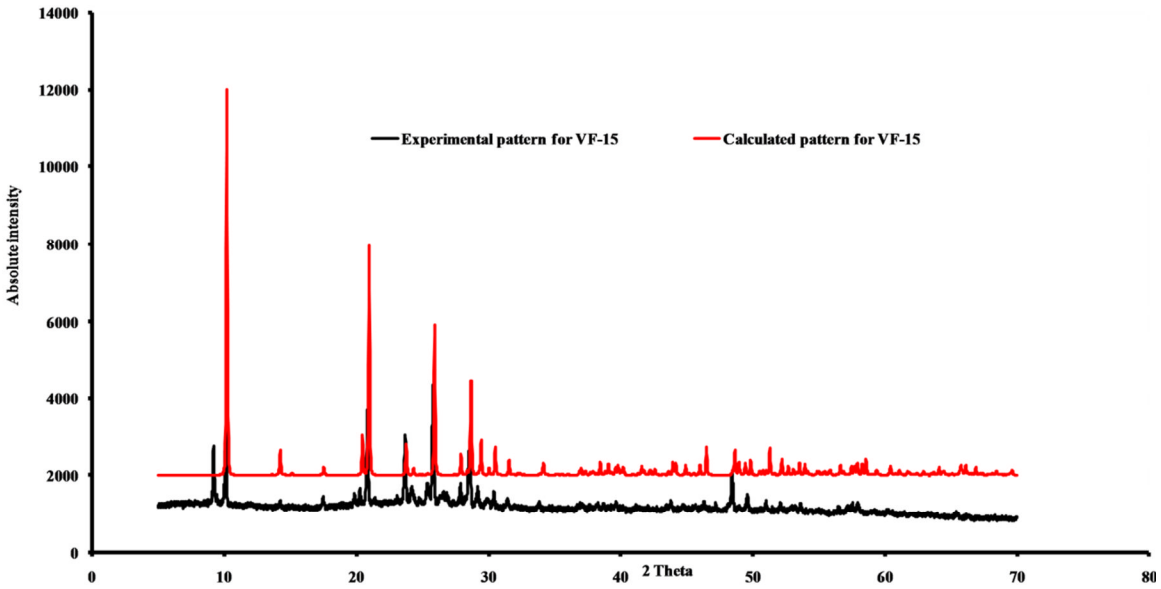

Figure A2. Simulated PXRD (above) and experimental (below) for **VF-15**.

CHN analysis for **VF-15**:

Calc: %C: 11.37, %H: 1.57, %N: 8.84.

Found: %C: 12.93, %H: 1.23, %N: 8.57.

The CHN analysis indicates the presence of another minor phase.